DNA Directed Self-assembly of Plasmonic Nanoparticles

by

Suchetan Pal

A Dissertation Presented in Partial Fulfillment
of the Requirements for the Degree
Doctor of Philosophy

Approved November 2012 by the
Graduate Supervisory Committee:

Yan Liu, Co-Chair
Hao Yan, Co-Chair
Ian Gould
Stuart Lindsay

ARIZONA STATE UNIVERSITY

December 2012

ABSTRACT

Deoxyribonucleic acid (DNA), a biopolymer well known for its role in preserving genetic information in biology, is now drawing great deal of interest from material scientists. Ease of synthesis, predictable molecular recognition via Watson-Crick base pairing, vast numbers of available chemical modifications, and intrinsic nanoscale size makes DNA a suitable material for the construction of a plethora of nanostructures that can be used as scaffold to organize functional molecules with nanometer precision. This dissertation focuses on DNA-directed organization of metallic nanoparticles into well-defined, discrete structures and using them to study photonic interaction between fluorophore and metal particle.

Presented here are a series of studies toward this goal. First, a novel and robust strategy of DNA functionalized silver nanoparticles (AgNPs) was developed and DNA functionalized AgNPs were employed for the organization of discrete well-defined dimeric and trimeric structures using a DNA triangular origami scaffold. Assembly of 1:1 silver nanoparticle and gold nanoparticle heterodimer has also been demonstrated using the same approach. Next, the triangular origami structures were used to co-assemble gold nanoparticles (AuNPs) and fluorophores to study the distance dependent and nanogap dependencies of the photonic interactions between them. These interactions were found to be consistent with the full electrodynamic simulations. Further, a gold nanorod (AuNR), an anisotropic nanoparticle was assembled into well-defined dimeric structures with predefined inter-rod angles. These dimeric structures exhibited unique optical properties compared to single AuNR that was consistent

with the theoretical calculations. Fabrication of otherwise difficult to achieve 1:1 AuNP- AuNR hetero dimer, where the AuNP can be selectively placed at the end-on or side-on positions of anisotropic AuNR has also been shown. Finally, a click chemistry based approach was developed to organize sugar modified DNA on a particular arm of a DNA origami triangle and used them for site-selective immobilization of small AgNPs.

ACKNOWLEDGEMENTS

First and foremost, I would like to thank God for his showers of blessings throughout my research work that helped me to complete this research successfully.

I would like to express my deep and sincere gratitude to my advisors, Dr. Yan Liu and Dr. Hao Yan for giving me an opportunity to work in their esteemed lab and providing invaluable guidance throughout this research. Their dedication, passion, and incredible drive are truly inspires me to carry research as my career. It was a great privilege and honor to carry out research under their guidance. I am also grateful to the members of my committee, Dr. Ian Gould and Dr. Stuart Lindsay, for their valuable time and useful suggestions to my research.

I am indebted to my fiancée Tatini for the unconditional love and support she gave me in all these years. I would like to thank my parents for their love, upbringing and care. I thank my sister for standing by my mother in my absence at home. Without the support of my family, my research would not have been possible.

Finally, I want to thank all the past and present graduate students, postdocs in the lab, who I have interacted with in these years. Their advice and support have been instrumental to my success. My special thanks goes to Dongran Han, one of the brilliant minds I have ever met, for the successful collaborations we had over the years. I would like to thank Dr. Su Lin, Dr. Gerdenis Kodis, Dr. Zhengtao Deng, Dr. Barun Das, David Lowry, Dr. Shengli Zou(UCF), Dr. Debin Wang (UCB) for the collaboration and stimulating discussions. I also specially

thank Dr. Jeanette Nangreave, Chad Simmons, Dr. Rahul Chhabra and Dr. Jaswinder Sharma for standing by me in some rough time. I would like to Angela Edwards for proofreading my dissertation.

TABLE OF CONTENTS

Page

LIST OF TABLES xi

LIST OF FIGURES xii

CHAPTER

1. DNA NANOTECHNOLOGY AND DNA DIRECTED ASSEMBLY OF NANOPARTICLES 1

1.1. Introduction 1

1.1.1. DNA Nanotechnology 2

1.1.2. Branched DNA Structures 5

1.1.3. DNA Origami 7

1.2. Organization of Nanomaterials onto DNA Scaffolds 9

1.2.1. Organization of Nanomaterials into 2D and 3D Assembly 9

1.2.2. Organization of Nanomaterials into Discrete Assembly: Using DNA Origami Structures 11

1.2.3. Metallic Nanoparticles 12

1.2.4. DNA Functionaliozation of Metallic Nanoparticles 14

1.2.5. DNA Origami Directed Assembly of Plasmonic Nanoparticles into Discrete Structures 15

1.3. Radiative Decay Engineering (RDE) of Fluorophores Using Plasmonic particles 19

1.4. Projects 23

CHAPTER Page

1.4.1. DNA Functionalization of Silver Nanoparticles and DNA Origami Directed Organization of such DNA Functionalized Nanoparticles into Discrete Structures 23

1.4.2. Quantum Efficiency Modification of Organic Fluorophores Using Gold Nanoparticles on DNA Origami Scaffolds 23

1.4.3. DNA Directed Self-assembly of Anisotropic Nanoparticles 24

1.4.4. Site specific synthesis and *in-situ* immobilization of fluorescent silver nanoclusters on DNA nanoscaffolds using Tollens' reaction 25

1.5. References 25

2. DNA DIRECTED SELF-ASSEMBLY OF STABLE SILVER NANOPARTICLE STRUCTURES 29

2.1. Abstract 29

2.2. Introduction 29

2.3. Materials and Methods 33

2.4. Results and Discussion 33

2.4.1. Silver Nanoparticle Functionalization with ps-po Chimeric DNA 33

2.4.2. Optimization of Number ps Moiety on the Stability of AgNPs 34

CHAPTER Page

2.4.3. Optimization of Number ps Moiety on the Stability of Silver Nanoparticles 35

2.4.4. Colorimetric Assay to Confirm the Successful DNA Functionalization…….38

2.4.5. Immobilization Efficiency of 20 nm ps-po DNA Modified AgNPs on DNA Origami Platform…….40

2.4.6. Organization and Characterization of 20 nm ps-po DNA Modified AgNPs into Discrete Dimeric and Trimeric Structures on DNA Origami Platform ……42

2.4.7. Fabrication of 1:1 20 nm AgNP and 5 nm AuNP Hetero Dimeric Structures……...45

2.5. Conclusion.....47

2.6. References 47

3. QUANTUM EFFICIENCY MODIFICATION OF ORGANIC FLUOROPHORES USING GOLD NANOPARTICLES ON DNA ORIGAMI SCAFFOLDS 49

3.1. Abstract 49

3.2. Introduction 49

3.3. Materials and Methods 53

3.3.1. Materials.....53

3.3.2. Phosphination of AuNPs 53

CHAPTER Page

3.3.3. DNA Functionalization of AuNPs 54

3.3.4. Formation of Origami Structures 55

3.3.5. Immobilization of AuNPs on DNA Origami and Electrophoretic Gel Purification.....55

3.3.6. TEM Imaging of the Origami Triangles with the AuNP.....56

3.4. Results and Discussion.....57

3.4.1. Fabrication of 1:1 Fluorophore-AuNP Constructs Using DNA Origami Directed Assembly 57

3.4.2. Steady State Measurements.....59

3.4.3. Fluorescence Lifetime Measurements.....65

3.4.4. Theoretical Calculations.....66

3.4.5. Fabrication of Dimeric AuNP Structures with a Fluorophore in the Gap 68

3.4.6. Photonic Interaction of Cy3 and 20 nm AuNP Dimer 71

3.4.7. Photonic Interaction of Cy3 and 30 nm AuNP Dimer 74

3.5. Conclusions 75

3.6. References 76

4. DNA DRECTED SELF-ASSEMBLY OF ANISOTROPIC PLASMONIC NANOSTRUCTURES 79

4.1. Abstract 79

4.2. Introduction 80

4.3. Materials and Methods 81

CHAPTER Page

4.4. Results and Discussion 81

4.4.1. Fabrication of DNA Origami 81

4.4.2. Immobilization Efficiency of Single Nanorod on DNA Origami Platform 82

4.4.2. Fabrication of Dimeric AuNR Structures on DNA Origami Platform 85

4.4.3. Optical Measurements and Theoretical Calculations Dimeric AuNR Structures on DNA Origami Platform 89

4.4.4. Fabrication of 1:1 AuNP-AuNR Structures on DNA Origami Platform 91

4.5. Conclusions 93

4.6. References 94

5. SITE-SPECIFIC SYNTHESIS AND IN-SITU IMMOBILIZATION OF FLUORESCENT SILVER NANOCLUSTERS ON DNA NANOSCAFFOLDS USING TOLLENS REACTION 95

5.1. Abstract 95

5.2. Introduction 96

5.3. Materials and Methods 97

5.4. Results and Discussion 98

5.4.1. DNA Directed Synthesis of Ag-NCs 98

CHAPTER Page

5.4.2. Site-Specific Immobilization of Ag-NCs on Triangular Origami....100

5.4.3. AFM Characterization of Site-Specific Immobilization of Ag-NCs on Triangular Origami....101

5.4.4. HRTEM Characterization of Site-Specific Immobilization of Ag-NCs on Triangular Origami....103

4.5. Conclusions....106

4.6. References....106

6. SUMMARY AND OUTLOOK....109

6.1. Conclusions....109

6.2. Future Directions....111

6.3. References....115

BIBLIOGRAPHY....116

APPENDIX

A. SUPPLEMENTAL INFORMATION FOR CHAPTER 2....125

B. SUPPLEMENTAL INFORMATION FOR CHAPTER 3....169

C. SUPPLEMENTAL INFORMATION FOR CHAPTER 4....201

D. SUPPLEMENTAL INFORMATION FOR CHAPTER 5....233

F. CO-AUTHOR APPROVAL....269

LIST OF TABLES

Table Page

4.1 Assembly yields after purification, designed and the observed angles of the different dimeric structures 89

LIST OF FIGURES

Figure Page

1.1 Watson-Crick base pair of double helical DNA 2

1.2 Cartoon representation of DNA self-assembly 4

1.3 Self-assembled 2D and 3D DNA structures 6

1.4 2D DNA origami.....8

1.5 DNA-directed assembly of plasonic nanoparticles using multicomponent nanoarrays 10

1.6 Schematic representation of spherical nucleic acid nanostructure self-assembly.....13

1.7 Schematic representation of SNA nanostructures.....15

1.8 Examples of nanoparticle assembly using 17

1.9 Examples of functional DNA origami templated nanoparticle assembly.....19

1.10 Jablonski diagram of a fluorophore in absence and in the presence of metallic nanoparticle.....22

2.1 Schematic representation of the functionalization of AgNPs with ps-DNA 31

2.2 Schematic representation of the fabrication of discrete AgNP architectures by DNA-origami-directed assembly 32

2.3 UV-Vis absorbance of DTT assay 35

Figure Page

2.4 TEM images, UV-Vis, DLS of 32 nm Ag-core-5 nm Au satellite cluster 36

2.5 UV-vis spectra of the aggregates and free silver nanoparticles.....39

2.6 Negatively stained TEM image of the triangular DNA origami and origami attached to one silver nanoparticle 41

2.7 Illustration of individual designs I–IV with different center-to-center distances.....44

2.8 Schematic view of the fabrication of 5 nm AuNP and 20 nm AgNP dimer structure.....46

3.1 Schematic representation of the formation of a triangular origami structure with a gold nanoparticle and a fluorophore molecule at the predetermined locations. 52

3.2 Schematic representations and corresponding negatively stained TEM images of monomeric constructs 60

3.3 Schematic representation of sample and the corresponding control.....64

3.4 Schematic representations of top view, side view and the corresponding negatively stained TEM images of the 20 nm or 30 nm dimeric constructs 70

3.5 The fluorescence intensity ratios of the sample and control of 20 nm AuNP dimers.....73

Figure Page

3.6 Normalized fluorescence emission spectra (excited at 525 nm) of 30 nm dimeric structures.....75

4.1 Schematic representation of the formation of triangular origami structures and Schematic representation of four different dimeric structures displaying different angles between the AuNRs 81

4.2 Negatively stained TEM image of single AuNR immobilized on specific orientation of one arm of triangular origami.....84

4.3 Schematic representation of different dimer constructs, TEM images, UV-Vis spectra with inter-rod angles indicated.....87

4.4 Scheme of formation and TEM images of side-on and end-on AuNR-AuNP hetero dimers.....92

5.1 Schematic representation of the site specific immobilization of fluorescent Ag-NCs on a triangular-shaped DNA origami scaffold 96

5.2 TEM and STEM images of excitation and emission spectra of Ag-NCs synthesized after the treatment of tollens reagent.....100

5.3 AFM images of the site specific incorporation of DNA and the subsequent *in-situ* synthesis and site specific immobilization of Ag-NCs on a particular arm of the triangular shaped DNA origami scaffold. 103

5.4 TEM image of the origami structure after the treatment with Tollens reagent.....105

6.1 Binary assembly of spherical nanoparticles and anisotropic nanoparticles in 3D using DNA origami as linker 113

Figure Page

6.2 Fabrication of Bowtie antenna structures 114

Chapter 1

DNA Nanotechnology and DNA Directed Assembly of Nanoparticles

1.1. Introduction

Deoxyribonucleic acid or DNA is by far the most important molecule in biology as it performs the storage and transmission of genetic information from one generation to next.[1] The pioneering work of Watson and Crick helped elucidate the structure of the DNA double helix in the 1953. DNA is aptly referred to as the 'blue-print' of life, as it encodes the biological evolution and fate of almost the entire living world. Interestingly DNA has been shown to be an exquisite material for nanoscale construction due to the predictability of the interaction between two nucleobases. In a typical B form of double-stranded DNA, adenine(A) always binds with thymine(T) and guanine(G) always binds with cytosine(C). The highly predictable interaction of single nucleotides allows precise engineering of DNA structures with the use of single-stranded overhangs called sticky ends, which will selectively recognize their complementary strands to form DNA structures. The B form of double helical DNA structure is a nanoscale material that has a 3.4 nm helical repeat and diameter of ~ 2 nm. In addition, immense advancement in solid-state synthesis chemistry has made the cost of synthetic oligonucleotides lower and modifiable at desired location using small molecules, such as biotin and fluorophores. These unique features of DNA make it a very useful tool for bottom-up assembly in nanotechnology.

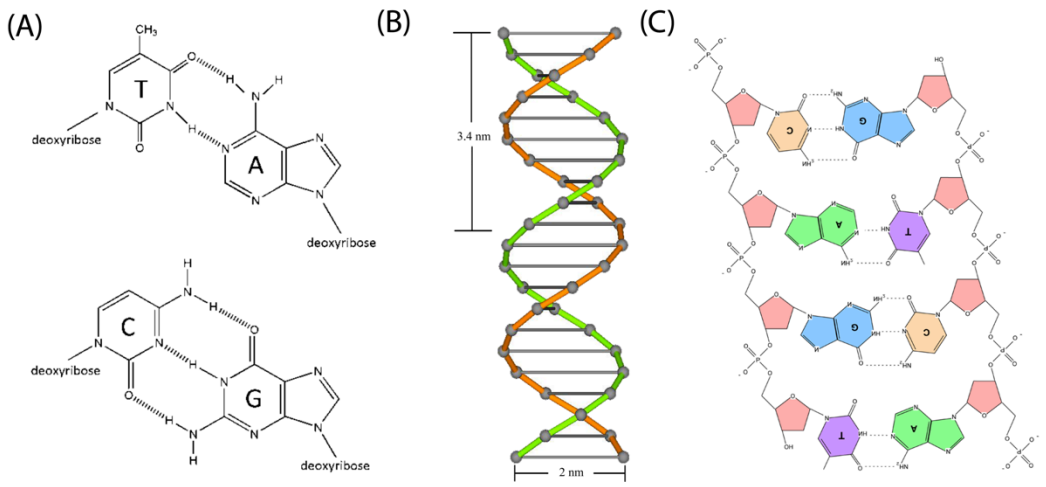

Figure 1.1. (A) The structure of Watson-Crick base pairs between A with T and G with C (B) Double stranded of DNA with a helical turn every 10.5 bases or 3.4 nm and a diameter of 2 nm. (C) Chemical structure of two DNA strands coming together to form the double helix, A with T and G with C.

1.1.1. DNA Nanotechnology. Despite these amenable features, however, DNA double helix molecules possess linear topologies that will only promote one-dimensional linear structures shown in figure 1.2 (A). In his seminal paper in the year 1982,[2] Prof. Nadrian Seeman proposed that by specifically determining ss-DNA sequences and considering complementarities in the sequences of the other strand, it is possible to design stable branched DNA molecules and expand the DNA structures in 2D and in turn in 3D. The fore-mentioned branched DNA motifs are equivalent to "lego" bricks in toys, and often referred to as 'tiles', and can be potentially used as the basic building blocks of almost all DNA nanostructures. However, without a robust way to self-assemble these building blocks, a well-defined higher order structures could not be formed; attaching single stranded "sticky ends" that can act as smart molecular glue in between

tiles, to provide a robust and consistent method for inter-tile association. The ultimate goal of this proposed idea is to co-organize proteins in 3D as illustrated in figure 1.2 which will aid in elucidating the molecular structures of proteins with unknown structures.

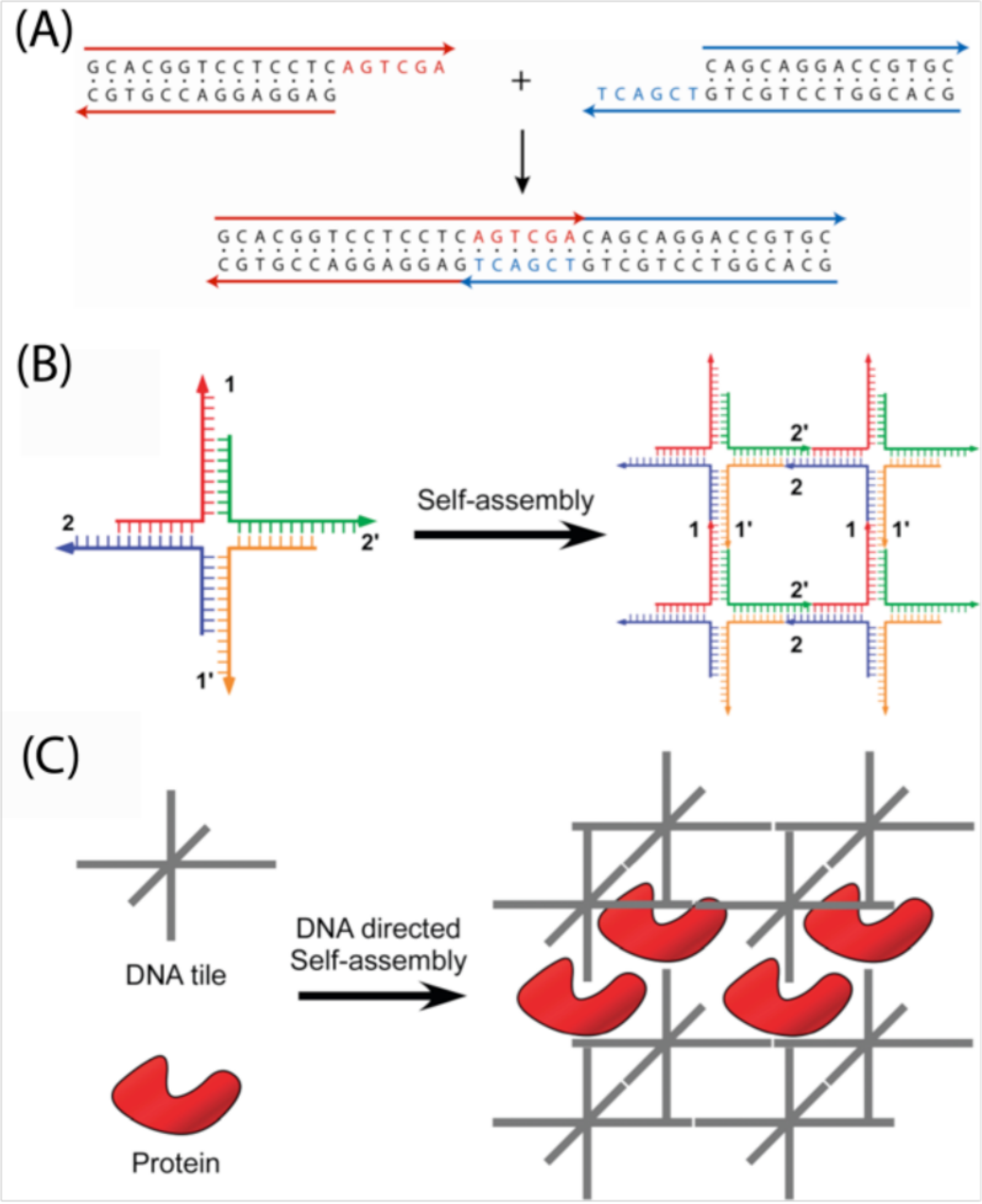

Figure 1.2. (A) 1D organization of two double helical DNA molecules. (B) Principle of DNA self-assembly organizing branched DNA nanostructures with single stranded overhangs to form 2D arrays. Arabic numbers indicate base pairing strategies between sticky ends (1 is complementary to 1', etc.). (C) Cartoon representation of protein crystallization templated by 3D DNA self-assembled structures as originally proposed by Seeman.

1.1.2. Branched DNA Structures: From 2D Array to Discrete 3D Structures.

The intrinsic flexibility of Holliday junction DNA tile motifs with a single crossover point did not form higher order structures mainly due to thermodynamic constrains. The problem was alleviated when multiple crossovers between helices was introduced thus decreasing the flexibility in the tiles. The double crossover motif was first developed in 1993. [3] Researchers developed branched DNA tiles for the synthesis of periodic structures[4-6] as well as a variety of rigid, multiple-crossover building blocks such as triple crossover molecules, multi-helical planar and bundled helix molecules, and several types of one and two dimensional periodic networks were constructed.[7-11] These structures are reviewed in reference 11. A number of novel self-assembled 3D DNA structures were constructed using these rigid branched DNA molecules. Turberfield's group reported a series of tetrahedra with different arm length. [12] Later the same group successfully encapsulated a protein, cytochrome *c,* inside a tetrahedron cage.[13] Joyce and coworkers assembled a DNA octahedron by folding a ssDNA 1.7 kb long with five short DNA strands.[14] The assembled structures were visualized using cryo-electron microscopy showing exotic 3D shapes formed in very good yield. In 2008 Mao's group reported the hierarchical assembly of tetrahedra, dodecahedra, and buckyball structures. [15]

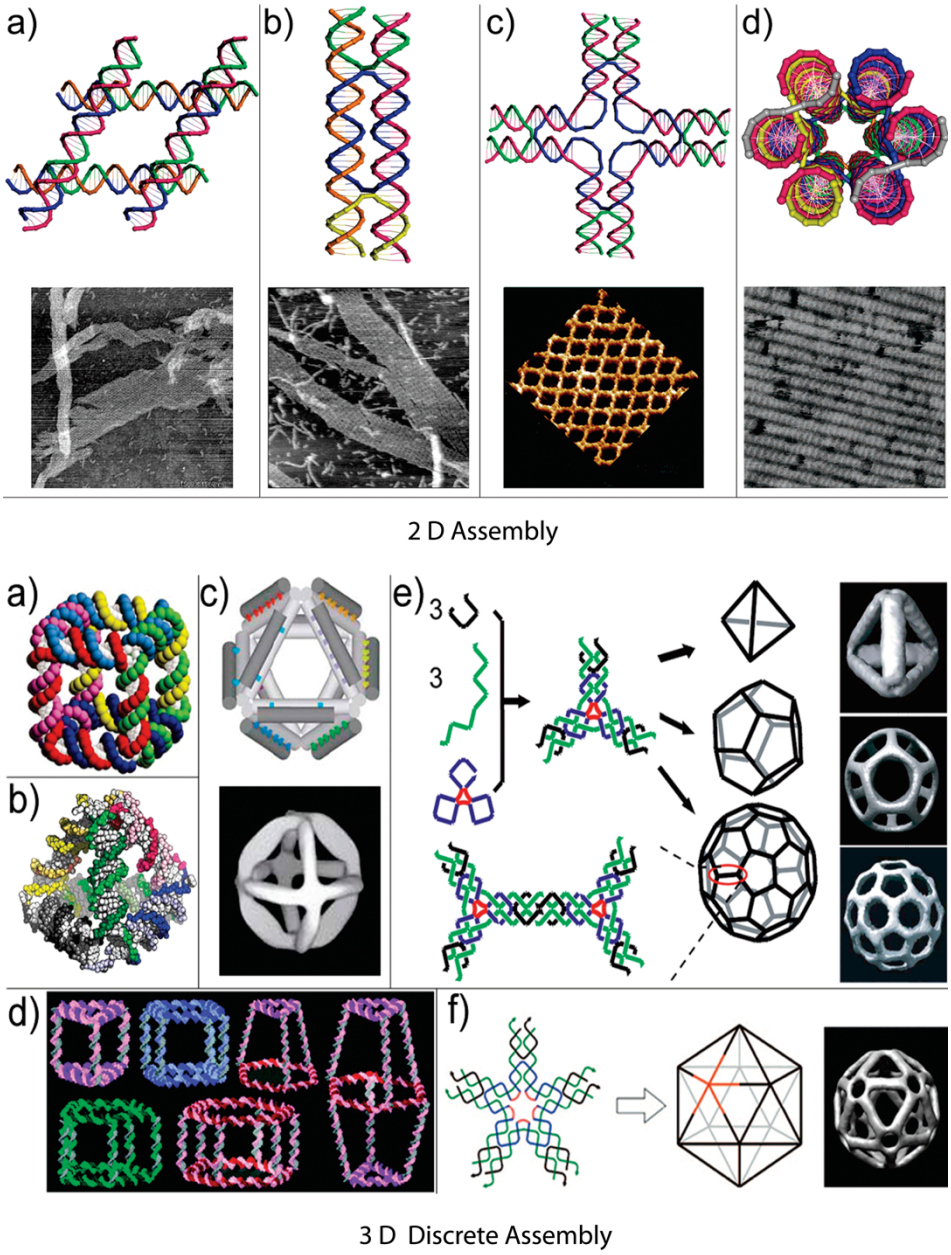

Figure 1.3. Computer aided models of some representative DNA tiles (A) Parallelogram DNA tile constructed by four Holliday junctions. (B) Double-crossover (DX) tile (C) A 4-way junction tile. (D) Six-helix bundle tube tile viewed from the top. Image below of each model is self-assembled 2D structures viewed using a atomic force microscope (AFM). Discrete 3D DNA structures from crossover molecules (E) DNA cube. (F) DNA tetrahedron. (G) Model (top)

and cryo-EM image (bottom) of a DNA octahedron. (H) 3D prisms and cubes are assembled from cyclic and single-stranded DNA molecules with vertices made of organic molecules. (I) Models and cryo-EM images of DNA tetrahedron, dodecahedron, and Bucky ball self-assembled from a single symmetric three-point star tile. (J) Cryo-EM image DNA icosahedron self-assembled from a five-point star tile.

1.1.3. DNA Origami. The arsenal of self-assembled DNA nanostructures was significantly enriched after the publication of a groundbreaking work by Rothemund in 2006,[16] in which the concept of DNA origami method was first introduced. The word "origami" refers to the ancient Japanese art of folding a sheet of paper into arbitrarily shaped structures without cutting or gluing. DNA origami technique uses a long single-stranded circular viral DNA and folds it into arbitrary shapes by several hundreds of short, custom made oligonucleotides (30-50 bases long) are named "staple strands". Each of the staple strands consists of a sequence that can recognize and bind using hydrogen bonding interactions to different places of the DNA scaffold, thus bringing these distant points into close proximity. The sequences of the collection of staple strands determine the final size and shape of different discrete origami structures. In the figure 1.4, the versatility of the concept can be underlined by designing a number of different 2D DNA origami structures.

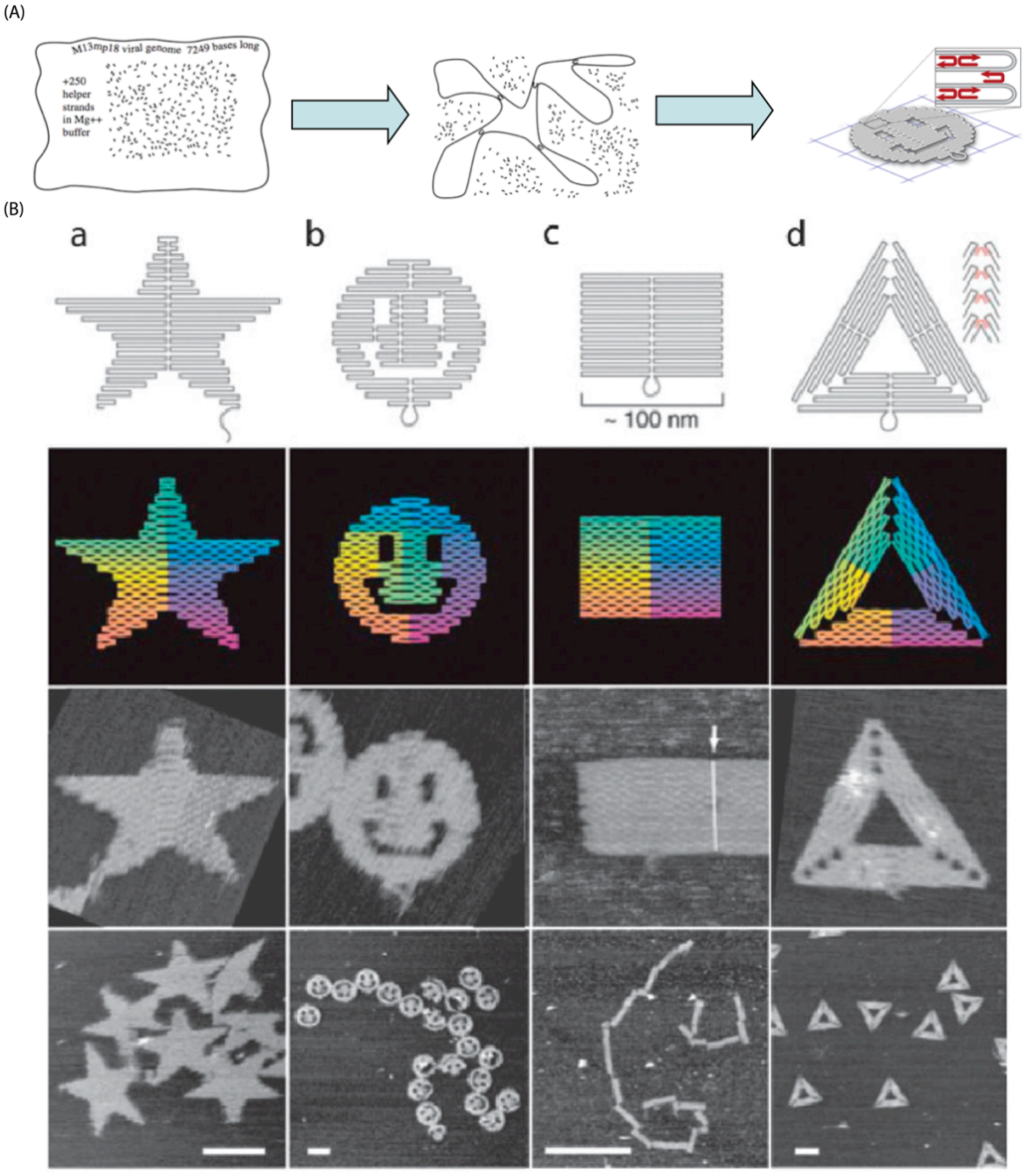

Figure 1.4. (A) Schematic diagram of DNA origami formation. (B) The first examples of the versatile DNA Origami technique. The upper panel illustrates the designs and the lower panels contain the resulting DNA structures as imaged by AFM. Scale bars are 100 nm for a, b, d and 1 mm for c. Reproduced with permission from 21.

1.2. Organization of Nanomaterials onto DNA Scaffolds.

1.2.1. Organization of Nanomaterials into 2D AND 3D Assembly.

These 2D and 2D DNA nanoarchitectures provide great opportunities to be utilized as scaffolds for organizing other nanomaterials with well-controlled inter-molecular distances. This in turn opens up exciting avenues for studies of distance-dependent molecular interactions, biosensing, DNA-templated chemistry, drug delivery and crystallization of biomolecules. Researchers have extensively investigated the assembly of inorganic nanomaterials (carbon nanotubes, metallic and semiconducting nanoparticles) and biomacromolecules (DNA, proteins, enzymes, antibodies) on DNA scaffolds because they have interesting optical, electrical and biological properties. For example, gold nanoparticles (AuNP) fuctionalized with multiple copies of ssDNA or a single copy of DNA were organized on the surface of periodic DNA array made of DX tiles or 4 arm cross tiles.[17-19] In 2009, Yan *et. al.* demonstrated the formation of exquisite nanotubules of various architectures, ranging in shape from stacked rings to single spirals, double spirals, and nested spirals using nanoparticles as a driving agent for the 3-D structure formation.[20] The organization of other biomolecules using DNA scaffold has been reviewed in reference 21.

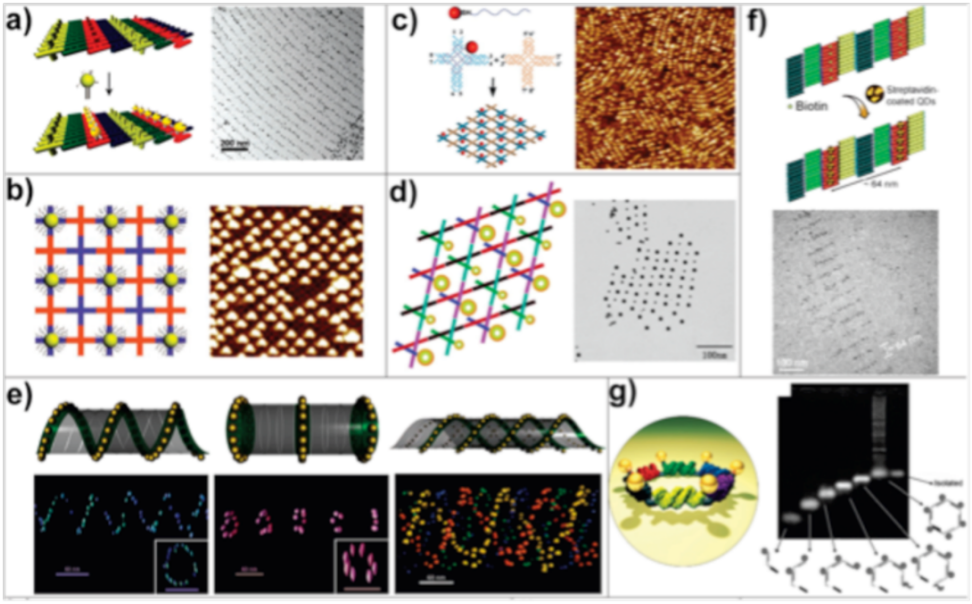

Figure 1.5. DNA-directed assembly of plasonic nanoparticles using multicomponent nanoarrays. (a) Organization of 5 nm AuNPs on DNA DX lattices. (b) Periodic 5 nm AuNP nanoarrays with well-controlled interparticle distances templated by 2D DNA nanogrids. (c) Single DNA modified 5 nm AuNPs directly participate in the self-assembly process and yield periodic nanoparticle arrays. (d) 2D periodic array of 5 and 10 nm AuNPs generated by incorporating DNA monomodified AuNPs into robust triangle-shaped DNA motifs. (e) Controlled self-assembly of DNA tubules through integration of AuNPs. The assembly results in 3D nanoparticle architectures such as a single-spiral tube (left), a stacking ring tube (middle), and an interlocking double-spiral tube (right). The schematic views are placed above corresponding electron tomographic images. (f) Quantum dots organized on DNA DX lattices through biotin-streptavidin interaction. (g) Discrete hexagonal AuNP array displayed on a DNA hexagon consisting of six non-identical molecules each with two ssDNA arms linked by an organic molecule. Reproduced with permission from 20.

1.2.2. Organization of Nanomaterials into Discrete Assembly: Using DNA Origami Structures.

Since the introduction of DNA origami in the field of DNA nanotechnology, DNA origami has become a very popular platform for patterning different biomolecules and inorganic nanomaterials in nanometer scale precision into discrete structures. Below are a few examples demonstrating such organization capabilities of DNA origami. Single-walled carbon nanotubes (SWNT) gained a lot of attention due to interesting electrical electronic properties and have been used in nanoelectronic devices. However, it remains a challenge to organize multiple SWNTs in different orientations. Recently, Maune et al. reported an elegant strategy to arrange SWNT in different orientation using a rectangular DNA origami template,[22] in which SWNT were first functionalized with a ssDNA complementary to capture strands extended from the surface of the rectangular origami. AFM imaging confirmed that the SWNTs attached to the templates with good efficiency and intended orientation with respect to each other. Recently, assembly of quantum dots have been achieved using streptavidin biotin interaction and DNA hybridization on DNA origami scaffold.[23, 24] Assembly of plasmonic nanoparticles will be discussed later. DNA origami has also been used in the organization of protein, enzymes and other molecules and to investigate chemical reactions at a single molecule level and is reviewed in reference 25.

1.2.3. Metallic nanoparticles. Methods have long been known to make elegantly colored glass by adding gold colloids to the glass. As the size or shape of a metallic nanoparticle changes, the color observed from the particle solution also changes. Gold nanoparticles have a characteristic red color, while silver spheres are yellow. More recent treatments have shown that the color is because of the collective oscillation of the loose electrons in the conduction band, termed as the surface plasmon oscillation. For the gold and silver nanoparticles the oscillation frequency is usually in the visible region of the electromagnetic spectrum, giving rise to the strong surface plasmon resonance absorption and hence the color. When metallic nanospheres increases in size, there is minimal change in their optical properties. However, for anisotropic nanoparticles (such as nanorods, nanobones, etc.) the optical properties of the nanoparticles change dramatically with a variation in the aspect ratio. Many applications have become feasible due to the large enhancement of the surface electric field very close to surface of the metal nanoparticle Moreover, plasmon resonance absorption has an absorption coefficient orders of magnitude higher than strongly absorbing organic fluorophores, making them ideal candidates for analyte detection and optical microscopy purposes. Furthermore, anisotropic metallic nanoparticles have even stronger plasmon resonance with increased detection sensitivity. Metal nanoparticles generate enhanced electromagnetic fields that affect only the local field. This enhanced electric field can enhance the fluorescence of a fluorophore and the Raman signal of a molecule situated very close to the metal surface. The optical properties of noble metal nanoparticles have been utilized to many uses as

sensing and imaging techniques. Chad Mirkin's group have pioneered the use of DNA in assembling and studying their interaction and their application in colorimetric detection of targets.[41]

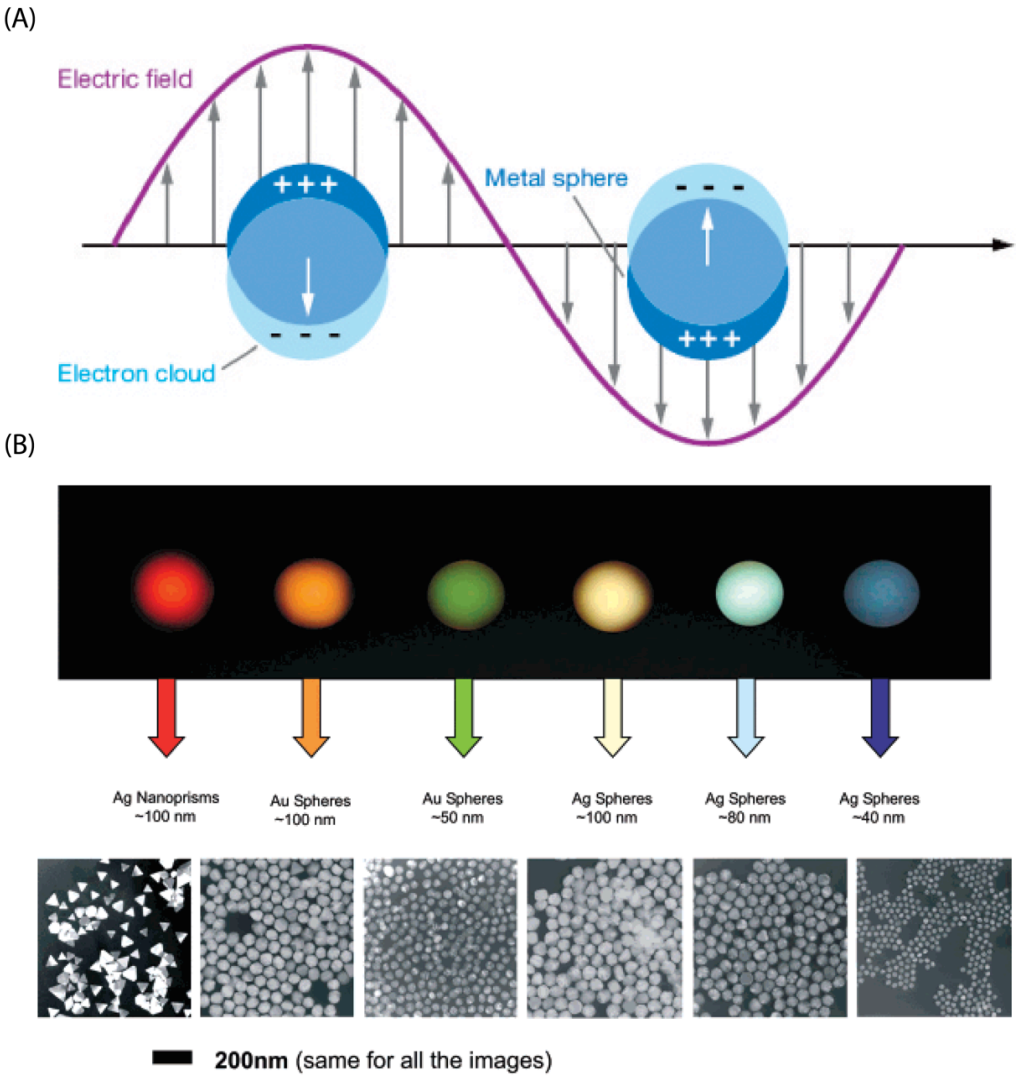

Figure 1.6. (A) Schematic diagram of the interaction of an electromagnetic field of light with an electron cloud of metallic nanoparticles. (B) Sizes, shapes, and compositions of metal nanoparticles can be systematically varied to produce materials with distinct light-scattering properties. Reproduced with permission from 41.

1.2.4. DNA Functionalization of Metallic Nanoparticles. The ligand shell corona around the nanoparticle surface is responsible for its colloidal stability (to remain well dispersed in a solvent) and reactivity. These ligands consist of a "head group" moiety that is attached to the surface of the nanoparticles and a "tail group" that extends into the surrounding solution to maintain the solubility. Major advancement in the field occurred when Mirkin and coworkers in their seminal paper described using thiolated DNA as a protecting surface ligand.[26] This gave rise to a new nucleic acid paradigm recently termed as spherical nucleic acid (SNA),[27] which are dense, oriented spherical arrays of short oligonucleotides. The most important feature of the DNA ligands is the capability of forming very specific Watson–Crick base pairing with complimentary DNA. With stringent designing the structure and sequence of DNA corona of SNAs, 'artificial bonds' between different elementary nanoparticles can be created and engineered.

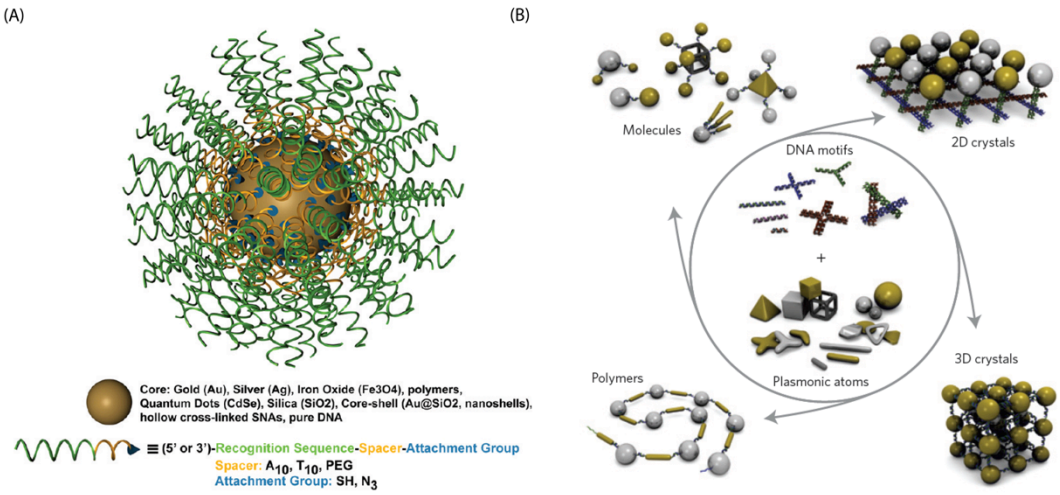

Figure 1.7. (A) Schematic representation of SNA nanostructures. An inorganic core is densely functionalized with oligonucleotides containing three segments: a recognition sequence, a spacer segment, and a chemical-attachment group. Additionally, other functional groups such as dye molecules, quenchers, modified bases, and drugs can be attached along any segment of the oligonucleotide. (B) A vast library of plasmonic atoms can be synthesized using wet-chemistry approaches. Various DNA motifs can be created using DNA nanostructures and the plasmonic atoms and DNA can then be used to rationally design and synthesize a range of plasmonic nanostructures. Reproduced with permission from 27,42.

1.2.5. DNA Origami Directed Assembly of Plasmonic Nanoparticles into Discrete Structures. Assemblies of well-defined plasmonic SNAs have gained a lot of interest due to the high local electric field enhancement generated when the assembly is excited at their plasmon resonance frequency. To maximize the enhancement it is crucial to fabricate materials with inter-particle spacing less than 10 nanometers, which is very expensive to achieve using electron beam

lithography techniques. Advancement DNA nanotechnology and DNA origami technology has seen a burst in the field of nanoparticle self-assembly. A few examples of DNA based nanoparticle assembly are discussed here.

In 1996, Alivisatos and co-workers first established a protocol to functionalize 1.4-nm gold nanoparticle with a single copy of ss DNA strand. [28] These monofunctionalized nanoparticles were then assembled into discrete dimeric and trimeric nanoparticle molecules through selective recognition of the ssDNA strand. However this strategy becomes significantly less realistic as the sizes and surface areas of the nanoparticles increase. Multiparticle dimeric systems have also been shown to be assembled using two different kind of particles.[29] More complex plasmonic systems, for instance, chiral pyramidal nanoparticles assembly have also been fabricated.[30] Satellite-like particle assembly, consisting of a large gold nanoparticle (31 nm) surrounded by a number of smaller 8-nm gold nanoparticles were experimentally observed by hybridizing DNA sequences on the particles.[31] Despite this observation, the lack of spatially directed organization often resulted in the formation of binary nanoparticle aggregates rather than discrete nanostructures. To circumvent this problem Oleg Gang's group reported a stepwise high-throughput strategy for assembling nanoparticle molecules from anisotropically functionalized DNA–gold nanoparticle conjugates based on the geometric restrictions imposed by a solid substrate. Most importantly, this approach is modular and scalable thus can produce dimers or Janus nanoparticle assemblies in high yield for plasmonic applications.

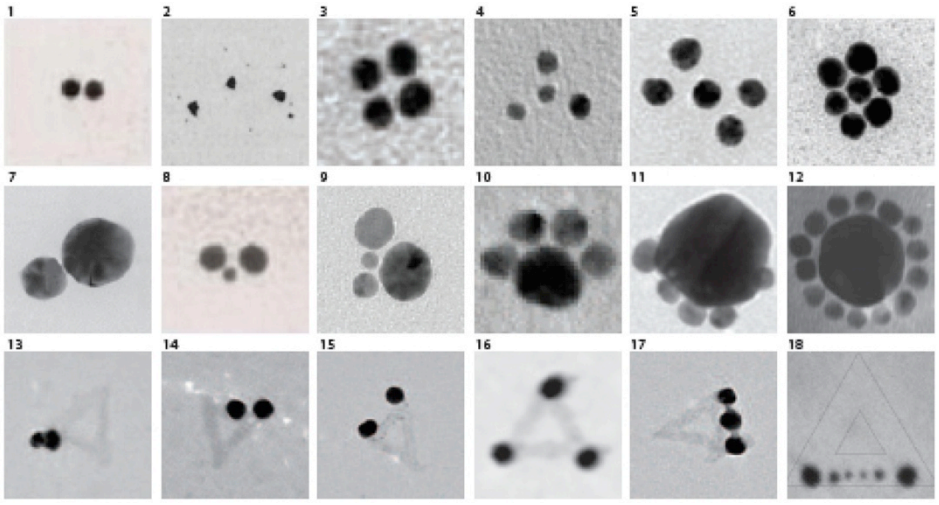

Figure 1.8. Examples of nanoparticle assembly using dsDNA (1-2) dimeric structures. (3-9) multimeric structures. (10,11) Janus assembly (12) core satellite structures. (13-18) Examples of nanoparticle assembly using triangular DNA origami. Reproduced with permission from 42.

A key parameter that can dictate plasmonic properties of nanoparticle assembly is the interparticle spacing, which in turn can be rationally controlled by the length of dsDNA. However, in reality there is often an ambiguity due to the deformation of DNA molecules under various conditions. Rigid DNA scaffolds can reliably be constructed by the use of DNA origami structures. DNA origami also provides an efficient template for organizing metallic nanoparticles into discrete multimeric plasmonic molecules. Sharma et al. used a rectangular origami structure to organize 10 nm gold nanoparticles with highly specific between two particles characterized by atomic force microscopy. [33] Chain of gold nanoparticles which has been shown to generate very high local field.[34]Three different gold nanoparticles were functionalized with DNA having complimentary

sequences displayed on the surface of origami triangle along one edge. Scanning electron microscopy technique revealed the patterning Recently Ding et al. used a triangular DNA origami platform to organize a self-similar of the gold nanoparticles with the desired inter-particle spacing had really been achieved. Later, Zhao et al. reported successful assembly of 5 nm and 10 nm gold nanoparticle inside the cavity of a DNA origami and surrounded the origami with 1,2 or 3 particles. This strategy potentially diminishes the isotropic coating of DNA on gold nanoparticles and can create site selective biding of other particles.[35]

The bottom-up approach of DNA origami formation process has also been combined with top-down lithography approach, enabling not only large area fabrication but also control over the orientation of the nanoparticle assemblies.[36] These self-assembled plasmonic nanostructures on DNA origami have been utilized for different purposes. For example, Pilo-Pais *et. al.* reported that the particles on the origami structures can be fused using metal deposition after the assembly to form arbitrarilyshaped metallic rods.[27] There are few reports on the organization of those nanoparticles into spiral orientation give rise to unique optically active nanoparticle assembly which can interact with circularly polarized light and vice-versa.[38,39] Recently Acuna *et al.* used DNA origami as a platform to vary the distance between an organic fluorophore and AuNPs to investigate the distance dependent interaction on the fluorescence. [40]

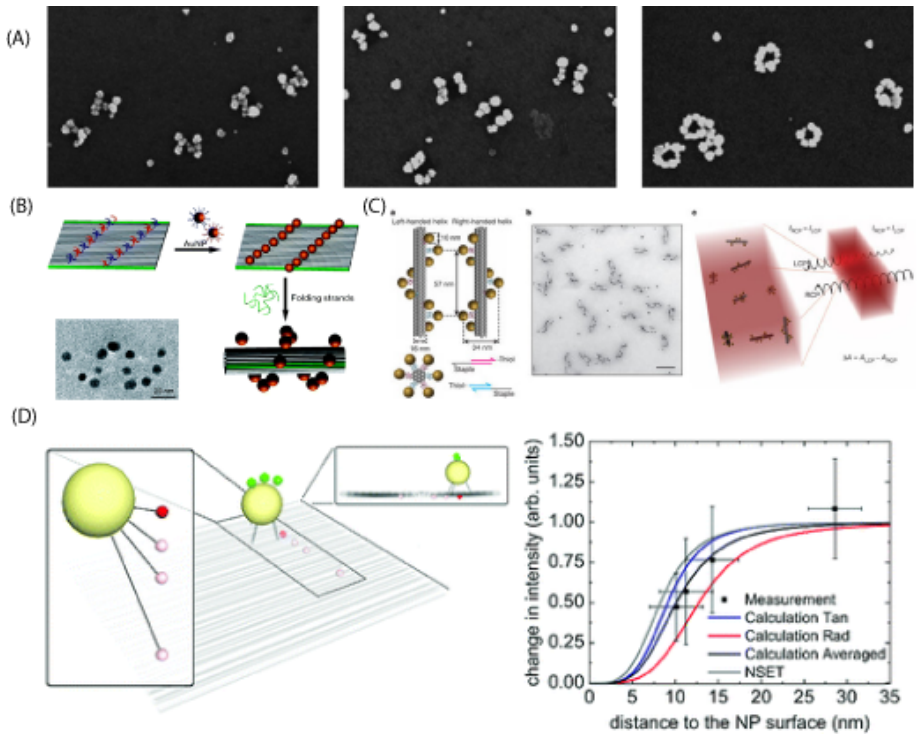

Figure 1.9. Examples of functional DNA origami templated nanoparticle assembly. (A) Formation of different nanoparticle shapes teplated on rectangular DNA origami after the metal deposition on seed nanoparticles. (B,C) Fabrication of spiral gold nanoparticles into spiral orientation on an origami platform. (D) Distance dependent fluorescence quenching of a dye using origami as a scaffold.

1.3. Radiative Decay Engineering (RDE) of Fluorophores Using Plasmonic Particles

Typically a solution of fluorophore is transparent to emitted radiation or there may be changes in refractive index (for example a fluorophore in a lipid bilayer membrane) but such changes have minimal effect on the fluorescence spectral properties. In such nearly homogeneous solution, the fluorophores emit into free space and are observed in the far field. Local effects are not usually observed because the size of the fluorophore is miniscule with respect to the

experimental chamber. In these cases the spectral properties are described by Maxwell's equations for an oscillating dipole radiating into free space. However the situation of a fluorophore, which is an oscillating dipole, nearby a metal surface is more complicated. The metal surface can respond to the oscillating dipole and modify the rate of emission and the spatial distribution of the radiated energy. The electric field felt by the fluorophore is not only affected by the interactions of the incident electromagnetic wave with the nearby metal surface, but also by the interaction of the fluorophore oscillating dipole with the metal surface. Additionally, the fluorophore-oscillating dipole induces a electric field in the metal. These interactions can in turn increase or decrease the field incident on the fluorophore and increase or decrease the radiative decay rate. These interactions provide more radiative decay pathways and faster radiative decay rates.

The theory for such effects can be complex, but people have described these effects in an intuitive manner. Much of my knowledge and insight about optical spectroscopy is based on measurements on fluorophores, which radiate into free space. However, there are several important exceptions to the free space condition, which result in dramatic spectral changes in different aspects of spectroscopy. Depending upon the distance and geometry, metal surfaces or particles can result in quenching of fluorescence or enhancement of fluorescence. The effects of metallic surfaces on fluorophores can be attributed to at least three mechanisms. The first is energy transfer to the metals with a d^3 dependence (d represents the distance of florophore from metal surface) that causes quenching,

which can be understood by damping of the dipole oscillators by the nearby metal. The second mechanism is an increase in intensity due to the metal enhances the incident electric field. These effects of quenching and enhancing the local fields are important. However, another more important effect of metal surfaces and particles is possible that the nearby metal can increase the intrinsic radiative decay rate of the fluorophore. This is a highly unusual effect. In fluorescence spectroscopy there is usually have no significant control over the radiative rate (k_r). The spectral observables of quantum yields and lifetimes are governed by the magnitudes of the radiative rate k_r and the sum of the nonradiative decay rates (k_{nr}). To understand the value of controlling the radiative decay rate (k_r), it is informative to consider how this rate affects the quantum yield Q_0 and lifetime τ_0 of a fluorophore in the absence of a metal surface. Consider the Jablonski diagram in figure 1.10. The quantum yield of the fluorophore in the absence of other quenching interactions is given by $QE = k_r/(k_r + k_{nr})$.Radiative decay rate k_r is essentially constant for any given fluorophore. Hence, decreasing the nonradiative rate k_{nr}, which usually occurs at lower temperatures, can increase the quantum yield. The lifetime of a fluorophore is determined by the sum of the rates, which depopulate the excited state. In the absence of other quenching interactions the lifetime is given by $\tau_{av}= 1 / (k_r+k_{nr})$.

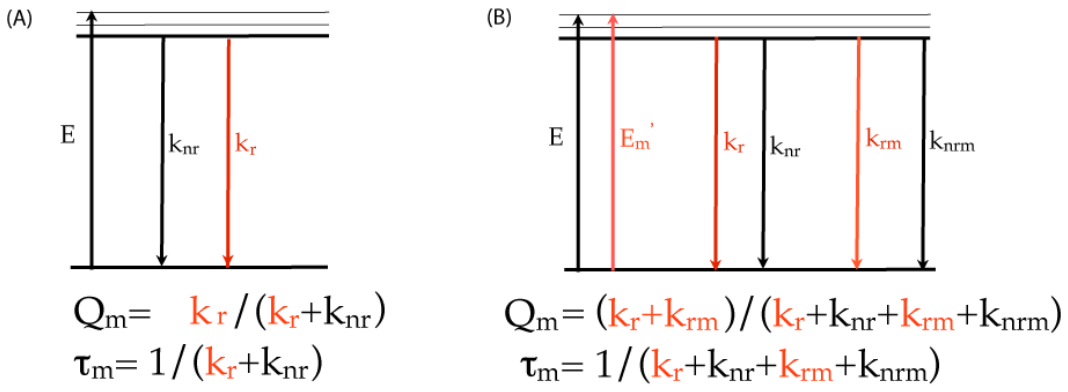

Figure 1.10. Jablonski diagram of a fluorophore in absence (A) and in the presence of (B) metallic nanoparticle.

The concept of modifying the radiative decay rate is relatively new to fluorescence spectroscopy. It is informative to consider the novel spectral effects expected by increasing the radiative rate. Assume the presence of a nearby metal (m) surface increases the radiative rate by addition of a new rates k_{rm} and k_{nrm}. In this case the quantum yield and lifetime of the fluorophore near the metal surface are given by, $QE_m = (k_r+k_{rm}) / (k_r+k_{nr}+k_{rm}+k_{nrm})$ and $\tau_{av} = 1 / (k_r+k_{nr}+k_{rm}+k_{nrm})$. These equations result in unusual predictions for a fluorophore near a metal surface: as the value of k_{rm} increases, the quantum yield increases while the lifetime decreases. DNA nanotechnology in general provides excellent opportunity to investigate these kind of interactions as we can reliably place a fluorophore and metallic nanoparticles and control their distances precisely.

1.4. Projects.

1.4.1. DNA Functionalization of Silver Nanoparticles and DNA Origami Directed Organization of Such DNA Functionalized Nanoparticles into Discrete Structures.

In this project we developed a novel strategy to functionalize silver nanoparticles with chimeric phosphorothioate DNA (ps-po-DNA) and these functionalized nanoparticles are used for the fabrication of bimetallic core-satellite nanoclusters that each contain a silver core of 32 nm diameter surrounded by 5 nm gold NPs. Then we also demonstrate a bottom-up method for the fabrication of discrete, well-ordered silver nanoparticle structures on self-assembled DNA origami structures of triangular shape. The results demonstrate that the center-to-center distance between adjacent nanoparticles can be precisely tuned from 94 to 29 nm, whereby the distance distribution is limited by the size distribution of the nanoparticles. We also fabricated 1:1 gold nanoparticle and silver nanoparticle heterodimeric structures using two-step bottom up self-assembly method. This work is described in chapter 2.

1.4.2. Quantum Efficiency Modification of Organic Fluorophores Using Gold Nanoparticles on DNA Origami Scaffolds.

We have used DNA origami as the platform to create different distances between a 20 nm gold nanoparticle (AuNP) and an organic fluorophore (TAMRA) and studied the distance dependent plasmonic interactions between the particle and the florescence of the dye using both steady state and lifetime fluorescence measurements. More fluorescence quenching was found at lower distances, which was accompanied with an enhancement of the nonradiative decay rate. Then we

fabricated both 20 nm and 30 nm AuNP homodimers using DNA origami as scaffold and placed a Cy3 fluorophore in the middle position of the two particles. Two different distances between the dimers were investigated. Up to 50% enhancement of the Cy3 fluorescence quantum efficiency for the dye in between the 30 nm AuNP dimers was observed, which was accompanied with over a significant enhancement of the radiative decay rate. These results are in good agreement with the theoretical simulations predicted by FTDT calculations. These results are included in chapter 3.

1.4.3. DNA Directed Self-assembly of Anisotropic Nanoparticles.

Anisotropic nanomaterials such as gold nanorods possess unique optical properties, including high optical extinction in the range of visible and near-infrared (NIR) wavelengths, and strong localized plasmonic fields at the tips of the materials. Due to these unique optoelectronic properties, AuNRs have been used for cellular imaging, cancer therapy and biosensing. Higher order assembly of AuNRs may lead to new optical properties depending on the ensuing geometric properties including size, distance, and orientation, as proposed by theory and verified by experiment. Most recent attempts to create high order AuNR nanostructures have focused on the use of top-down electron beam lithography to pattern or manipulate the materials in a serial fashion. New strategies are needed to deterministically position these anisotropic nanostructures in a massively parallel fashion, within complex multi-component architectures. In this work a DNA origami based strategy of fabricating discrete dimers of AuNRs with predetermined angle resulted in different shift in longitudinal surface plasmonic

band (LSPR) has been shown. Precise positioning of 0 dimensional nanomaterials with respect to anisotropic AuNRs have also been demonstrated in this project. These results are included in chapter 4.

1.4.4. Site-specific synthesis and *in-situ* immobilization of fluorescent silver nanoclusters on DNA nanoscaffolds using Tollens' reaction. In this work DNA strands with specific sequences and covalently attached sugar moieties using click chemistry approach. These sugar-modified DNA strands were shown to act as a seed for small silver nanoparticle formation, and were employed for the site-specific incorporation of the sugar units on a DNA origami scaffold. This approach enabled the subsequent site-specific synthesis and in situ immobilization of fluorescent Ag clusters at predefined positions on the DNA nanoscaffold by treatment with the Tollens reagent. These results are included in chapter 5.

1.5. References

(1) Watson, J. D.; Crick, F. H. C. *Nature.* **1953**, 171, 737-738.

(2) Seeman, N. C. *J. Theor. Biol.* **1982**, 99, 237-247.

(3) Fu, T. J.; Seeman, N. C. *Biochemistry.* **1993**, 32, 3211-3220.

(4) Chen, J. H.; Kallenbach, N. R.; Seeman, N. C. *J. Am. Chem. Soc.* **1989**, 111, 6402-6407.

(5) Chen, J. H.; Seeman, N. C. *Nature.* **1991**, 350, 631-633.

(6) Zhang, Y.; Seeman, N. C. *J. Am. Chem. Soc.* **1994**, 116, 1661-1669.

(7) Li, X. J.; Yang, X. P.; Qi, J.; Seeman, N.C. *J. Am. Chem. Soc.* **1996**, 118, 6131-6140.

(8) LaBean, T. H.; Yan, H.; Kopatsch, J.; Liu, F. R.; Winfree, E.; Reif, J. H.; Seeman, N. C. *J. Am. Chem. Soc.* **2000**, 122, 1848-1860.

(9) Winfree, E.; Liu, F.; Wenzler, L. A.; Seeman, N. C. *Nature.* **1998**, 394, 539-544.

(10) Liu, Y.; Lin, C.; Li, H.; Yan, H. *Angew. Chem. Int. Ed.* **2005**, 44, 4333-4338.

(11) Lin, C.; Liu, Y.; Rinker, S.; Yan, H. *ChemPhysChem.* **2006**, 7, 1641-1647.

(12) Goodman, R. P.; Schaap, I. A. T.; Tardin; C. F.; Erben, C. M.;Berry, R. M.; Schmidt, C. F.; and Turberfield, A. J. *Science.* **2005,** *310*, 1661–1665.

(13) Erben, C. M.; Goodman, R. P.; and Turberfield, A. J. *Angew. Chem., Int. Ed.* **2006,** *45*, 7414–7417.

(14) Shih, W. M.; Quispe, J. D.; Joyce, G. F. *Nature.* **2004,** *427*, 618–621.

(15) He, Y.; Ye, T.; Su, M.; Zhang, C.; Ribbe, A. E.; Jiang, W.; Mao, C. *Nature.* **2008,** *452*, 198–202.

(16) Le, J. D., Pinto, Y.; Seeman, N. C.; Musier-Forsyth, K.; Taton, T. A.; Kiehl, R. A. *Nano Lett.* **2004,** *4*, 2343–2347.

(17) Zhang, J.; Liu, Y.; Ke, Y.; and Yan, H. *Nano Lett.* **2006,** *6*, 248–251.

(18) Sharma, J.; Chhabra, R.; Liu, Y.; Ke, Y.; Yan, H. *Angew. Chem., Int. Ed.* **2006,** *45*, 730–735.

(19) Sharma, J.; Chhabra, R.; Cheng, A.; Brownell, J.; Liu, Y., Yan, H. *Science.* **2005,** *323*, 112–116.

(20) Lin, C.; Liu, Y.; Yan, H. *Biochemistry.* **2009**, 48, 1663.

(21) Rothemund, P. W. K. *Nature.* **2006**, 440, 297– 302.

(22) Maune, H.T.; Han, S.P.; Barish, R.D.; Bockrath, M.; Goddard, W.A.; Rothemund, P.W.K.; Winfree, E. *Nat. Nanotechnol.* **2010**, 5, 61-66.

(23) Bui, H.; Onodera, C.; Kidwell, C.; Tan, Y.,Graugnard, E.; Kuang, W.; Lee, J.; Knowlton, W. B.; Yurke, B.; Hughes, W. L. *Nano Lett.* **2010**, 10, 3367.

(24) Deng, Z. T.; Samanta, A.; Nangreave, J.; Yan, H.; Liu, Y . *J. Am. Chem. Soc.* 2012, Article ASAP DOI: 10.1021/ja3081023.

(25) Nangreave, J. ;Han, D.; Liu, Y.; Yan, H. *Curr. Opin. Chem. Biol.* **2010**,14, 608-615.

(26) Mirkin, C. A.; Letsinger, R. L.; Mucic, R. C.; Storhoff, J. J. Nature **1996**, 382, 607−609.

(27) Cutler, J. I.; Auyeung, E; Mirkin, C. A. *J. Am. Chem. Soc.*, **2012**, *134*, 1376-1391.

(28) Alivisatos, A. P. *et al. Nature* **1996***,* 382**,** 609–611.

(29) Loweth, C. J.; Caldwell, W. B.; Peng, X.; Alivisatos, A. P.; Schultz, P. G. *Angew. Chem. Int. Ed.* **1999***,* 38**,** 1808–1812.

(30) Mastroianni, A. J.; Claridge, S. A.; Alivisatos; A. P. *J. Am. Chem. Soc.* **2009,** 131**,** 8455–8459.

(31) Mucic, R. C.; Storhoff, J. J.; Mirkin, C. A.; Letsinger, R. L. *J. Am. Chem. Soc.* **1998***,* 120**,** 12674–12675.

(32) Maye, M. M.; Nykypanchuk, D.; Cuisinier, M.; van der Lelie, D.; Gang, O. *Nature Mater.* **2009***,* 8**,** 388–391.

(33) Sharma, J.; Chhabra, R.; Andersen, C. S.; Gothelf, K. V.; Yan, H.; Liu, Y. *J. Am. Chem. Soc.*, **2008**, 130, 7820.

(34) Ding, B.; Deng, Z.; Yan, H.; Cabrini, S.; Zuckermann, R.N.; Bokor, J. *J. Am. Chem. Soc.* **2010**, 132, 3248-3249.

(35) Zhao, Z.; Jacovetty, E. L.; Liu, Y.; Yan, H. *Angew. Chem., Int. Ed.*, **2011**, 50, 2041.

(36) Kershner, R. J. *et al. Nature Nanotech.***2009**, 4**,** 557–561.

(37) Pilo-Pais, M.; Goldberg, S.; Samano, E.; Labean, T. H.; Finkelstein, G. *Nano Lett.* **2011**, 11,3489.

(38) Shen, X. B.; Song, C.; Wang, J. Y.; Shi, D. W.; Wang, Z. A.; Liu,N.; Ding, B. Q. *J. Am. Chem. Soc.* **2012**, 134, 146−149.

(39) Kuzyk, A.; Schreiber, R.; Fan, Z.; Pardatscher, G.; Roller, E.;Högele, A.; Simmel, F.; Govorov, A. O.; Liedl, T. *Nature* **2012**, 483, 311–314.

(40) Acuna, G. P.; Bucher, M.; Stein, I. H.; Steinhauer, C.; Kuzyk, A.; Holzmeister, P.; Schreiber, R.; Moroz, A.; Stefani, F. D.; Liedl, T.*et al ACS Nano* **2012**, 6,3189– 3195.

(41) Rosi, N. L.; Mirkin, C. A. *Chem. Rev.* **2005**, 105, 1547–1562.

(42) Tan, S. J.; Campolongo, M. J.; Luo, D.; Cheng, W. *Nat. Nanotechnol.* **2011**, 6, 268–276.

(43) Principles of Fluorescence Spectroscopy, J. R. Lakowicz, Third edition.

Chapter 2

DNA Directed Self-assembly of Stable Silver Nanoparticle Structures

Adapted with permission from Chem Commun (Camb). 2009, 40, 6059-6061.

2.1. Abstract

In this chapter we report a novel strategy to functionalize silver nanoparticles with chimeric phosphorothioate modified DNA (ps-po-DNA) and these functionalized nanoparticles are used for the fabrication of bimetallic core-satellite nanoclusters that each contain a silver core of 32 nm diameter surrounded by 5 nm gold NPs. Then we demonstrate a bottom-up method for the fabrication of discrete, well-ordered silver nanoparticle structures on self-assembled DNA origami structures of triangular shape. The results demonstrate that the center-to-center distance between adjacent nanoparticles can be precisely tuned from 94 to 29 nm, whereby the distance distribution is limited by the size distribution of the nanoparticles. We also fabricated 1:1 gold nanoparticle and silver nanoparticle hetero dimeric structures using two-step bottom up self-assembly methods.

2.2. Introduction

The past two decades have seen increased use of nano-scale materials for bio-sensing, diagnostics and therapeutics. Noble metal nanoparticles have been used extensively for these applications due to their biocompatibility, rich optoelectronic properties.[1] Metal nanoparticles conjugated with oligonucleotide have potentials in bio-detection for targets as oligonucleotides, proteins and

peptides, colorimetric detection of pH changes and in studying real-time molecular interactions.[2] The sequence specificity of Watson-Crick base pairing between two single stranded oligonucleotides allows the use of metal nanoparticle DNA conjugates as building blocks for bottom up nanotechnolology.[3]

Bottom-up organization of noble metal nanoparticles (NPs) with nanometer scale precision is an important goal in nanotechnology.[1]DNA-guided self-assembly of these nanoparticles has shown significant progress to meet this challenge.[2] Past years have seen enormous progress in DNA guided organization of nanoparticles in discrete,[3-5] one-dimensional,[6-9] two-dimensional[10-12] and three-dimensional architectures.[13-15] Facile DNA-functionalization strategies for gold nanoparticles (AuNPs) are available now, making AuNPs preferred (easier) candidates for subsequent self-assembly to form higher order structures. In contrast, assembly of silver nanoparticles (AgNPs) mediated by DNA self-assembly into higher order, well-defined discrete nanoarchitectures has not been well explored. This is mainly due to the relatively unstable chemistry of Ag (easy to be oxidized compared to Au) that makes the conjugated ligands on AgNP surface more labile, and AgNPs tend to aggregate irreversibly in solutions at high salt concentration, which is the most crucial condition for efficient DNA self-assembly. However Recently, AgNPs have gained much interest due to their high extinction coefficients compared to AuNPs, inherent catalytic properties and propensity to enhance Raman scattering. Thus efficient DNA functionalization strategy of AgNPs can alleviate the limitations to use these particles for the above-mentioned studies. Researchers have started to address this problem by

introducing multiple sulfur moieties on DNA to achieve stable AgNP-DNA conjugates that resist aggregation in high salt concentration buffers. [16,17] It has been demonstrated that increasing the number of sulfur moieties in the capping ligands resulted in enhanced stability of the AgNPs in high salt concentrations. Despite this advancement, the synthesis of oligonucleotides labeled with multiple thiol groups remains cumbersome and involves special purification steps.

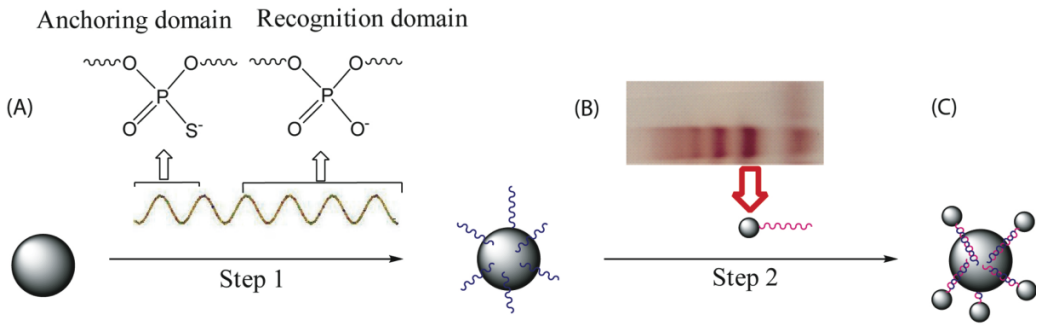

Figure 2.1. Schematic representation of the functionalization of AgNPs with ps-DNA, and subsequent fabrication of Ag-core–Au-satellite nanoclusters. (A) The oligonucleotide contains tandem sequence of an anchoring domain that consists of nucleotides with phosphorothioate groups in the backbone and a recognition domain with the normal phosphate backbone. (B) 1:1 conjugation of 5 nm AuNP with oligo of the complementary sequence of the recognition domain is prepared and purified by agarose gel electrophoresis. (C) The fabrication of the bimetallic nanocluster: the first step is conjugation of ps-DNA to the surface of 32 nm AgNP. The second step is hybridization of the complimentary DNA conjugated to 5 nm AuNP to the DNA anchored on the surface of the 32 nm AgNP.

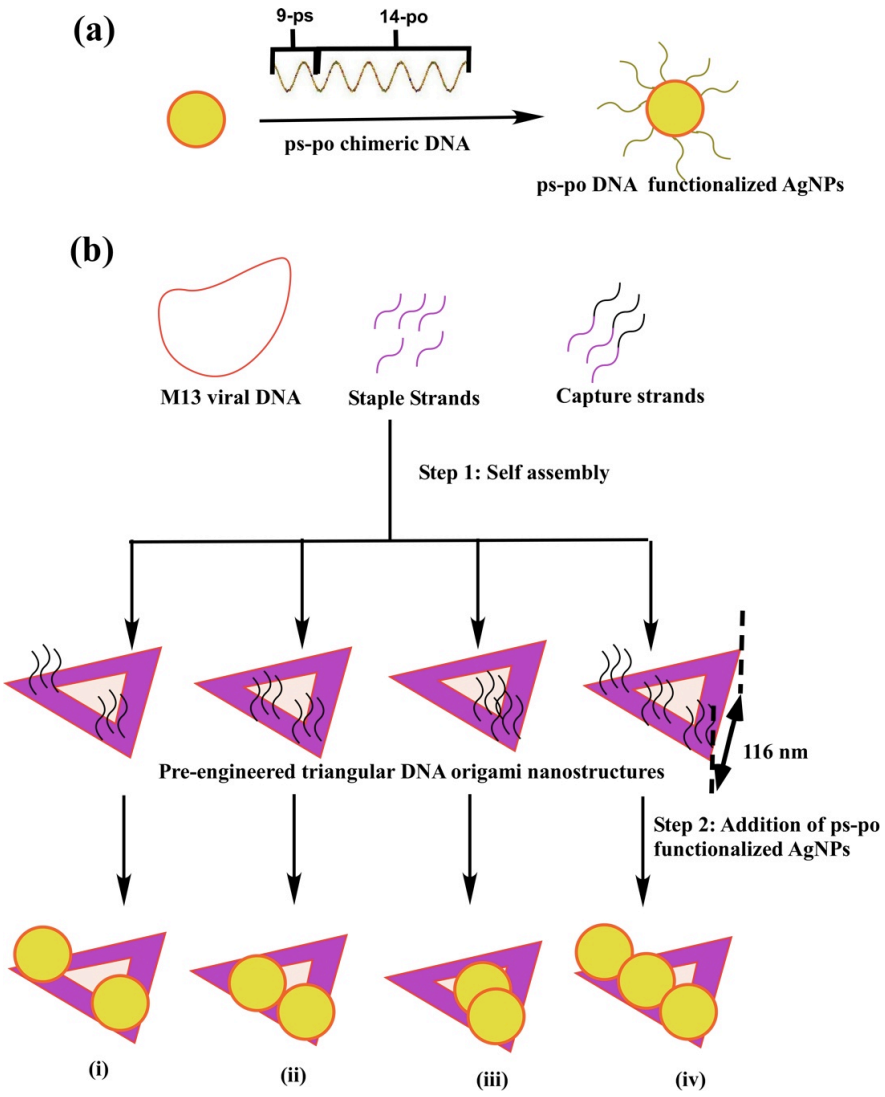

Figure 2.2. Schematic representation of the fabrication of discrete AgNP architectures by DNA-origami-directed assembly. a) Functionalization of the**.** AgNP with ps-po chimeric DNA. b) Step 1: preparation of preengineered triangular-shaped DNA origami displaying capture strands at predetermined locations on the structure; step 2: hybridization of AgNPs conjugated to ps-po chimeric DNA with capture strands on the DNA origami to form discrete dimeric AgNP architectures (I–III) with different interparticle distances as well as a trimeric architecture (IV).

2.3. Materials and Methods

See APPENDIX A

2.4. Results and Discussion

2.4.1. Silver Nanoparticle Functionalization with ps-po Chimeric DNA.

Our strategy (shown figure 2.1.) involves the use of oligonucleotides containing multiple consecutive phosphorothioate linkages (ps-linkages), in which a sulfur atom replaces a non-bridging oxygen in the phosphate backbone of the oligo (figure 2.1.A). These phosphorothioated oligos can be custom designed and commercially synthesized (www.idtdna.com) at relatively low cost. The sequence, the number of ps units and their positions in the oligos can be arbitrarily assigned. The presences of sulfur atoms on the backbone not only make the oligo nuclease resistant but also sulfur atoms are also available for coordination with metal ions or metal surfaces. We expect that multivalent Ag–S interactions between the AgNP's surface and the ps-domain of the DNA will result in the anchoring of the DNA to the metal nanoparticle surface. The remainder of the DNA sequence containing a recognition sequence with a normal phosphate backbone will point away from the surface and it can be hybridized with its complimentary DNA (figure 2.1.B). Then, when a 5 nm AuNP is pre-linked to the end of the complimentary sequence through Au–thiol bond, DNA hybridization will bring the AuNPs onto the surface of the AgNPs to make a core-satellite structure.

2.4.2. Optimization of Number ps Moiety on the Stability of AgNPs.

The effect of the number of ps-linkages in the oligonucleotides on the stability of AgNPs was examined by a DTT-displacement experiment (figure 2.3.), monitored by UV-vis spectroscopy. DTT is a reducing agent that is known to cleave the Ag–S bond and displace the thiol modified ligands from the AgNP surface, thus resulting in irreversible aggregation of the nanoparticles in a high salt condition. 4a,5b It is expected that the more stable the capping ligand is on the surface of the AgNPs, the slower the aggregation is in the presence of DTT. Three DNA strands, ps-3, ps-6 and ps-9, were used to functionalize the AgNPs, each contains 3, 6 or 9 ps groups close to the 5' end, respectively, and they share a same 56 nucleotide recognition domain. Upon addition of DTT, all samples showed a decrease of the absorbance at 400 nm and a red shift of the absorbance peak, indicating growing size of the aggregates with time. The AgNPs functionalized with ps-3 showed the lowest stability with a decay half life of only 6 min, and within 20 min extensive aggregation was already observed from broadening of the absorbance peak. The AgNPs functionalized with ps-9 showed the highest stability with a half time of longer than 1 h. Even at 4 h after addition of DTT, the particle solution still remained clear and some degree of aggregation started to appear, evidenced by the UV-Vis spectral shift from 400 nm to 460 nm. Comparing the changes of the UV-Vis spectra of the ps-3 and ps-9 modified AgNPs, significant differences were observed. For the ps-3 sample, a very small shift of the plasmon resonance peak at 400 nm was observed as the absorbance intensity dropped by two folds. However for the ps-6 and ps-9 samples, the drop of the absorbance intensity at 400 nm was

accompanied by a dramatic spectral shift of the peak from 400 nm to 490 nm along with a significant broadening. From this DTT displacement experiment we can conclude nthat the ps-DNA is specifically bound to the surface of the AgNPs and function as a protection layer against particle aggregation. The longer ps-domain of the DNA provides a stronger binding affinity to the AgNP surface, which is more difficult to be displaced by DTT. Three ps groups are not enough for the stabilization of the AgNPs. We choose to use 9-ps in the formation of the core-satellite structures.

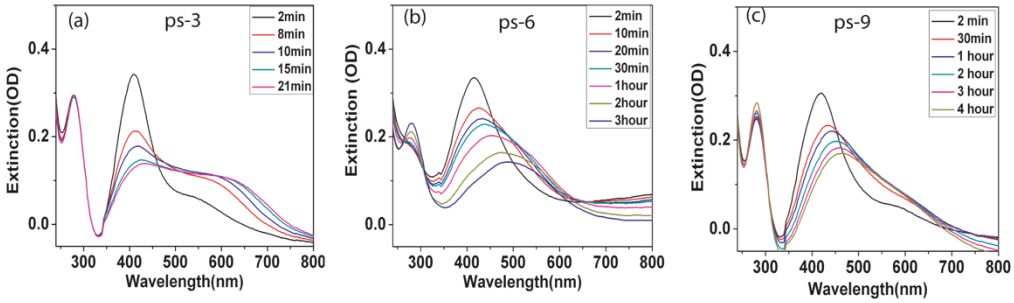

Figure 2.3. UV-Vis absorbance assay after 15 mM DTT was added to the same concentration of ps-3, ps-6 and ps-9 functionalized AgNPs.

2.4.3. Fabrication and Characterizations of 32 nm AgNP Core- 5 nm AuNP Satellite Structures. We prepared a 1 : 1 conjugate of a 5 nm AuNP with the DNA sequence that is complementary to the recognition domain of the DNA on the AgNP .Upon hybridization with the AgNPs at a 10 : 1 ratio (10 of 5 nm AuNP per 32 nm AgNP), satellite nanoclusters that each contains a 32 nm AgNP core surrounded by 5 nm AuNPs were self-assembled, as shown in the transmission electron microscopy (TEM) images (figure 2.4.).

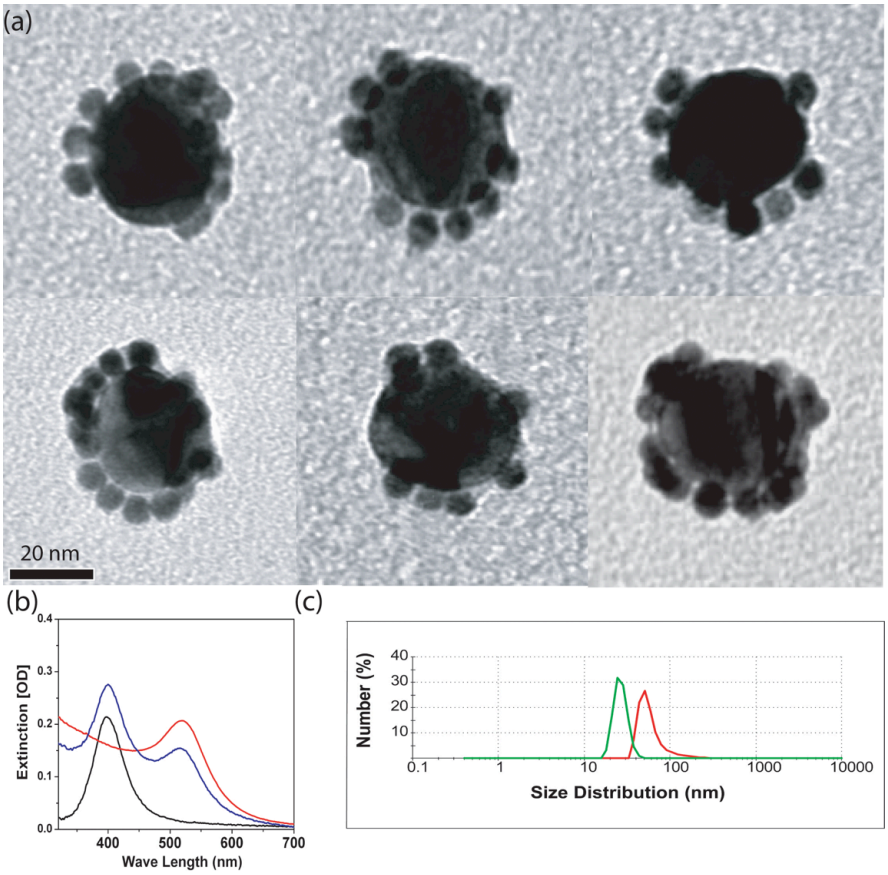

Figure 2.4. (A) Representative TEM images of 32 nm Ag-core-5 nm Au satellite cluster. The scale bar for each image is 20 nm. (B) UV-vis spectra of 32 nm AgNP with ps-9 (black), 5 nm AuNP with a single DNA (red), AgNP core-AuNP satellite (blue). (C) DLS shows the hydrodynamic radius for the AgNP and AgNP core-AuNP satellite ~24 nm (green) and ~50 nm (red), respectively.

UV-Vis spectroscopy (2.4.B) and dynamic light scattering (DLS) (figure 2.4.C) were employed to further characterize these bimetallic nanoclusters. The UV-Vis spectra of the nanoclusters indicated the presence of the plasmonic absorption peaks for both AuNPs and AgNPs. Compared to the spectra of AgNP alone and AuNP alone that were each modified by the corresponding DNA sequences, the plasmonic peaks for the Ag–Au nanoclusters each showed a slight red shift ~2–3 nm, from 398 nm to 400 nm and 516 to 519 nm, respectively (figure 2.4.B). DLS studies showed a significant size difference between the ps-DNA functionalized AgNPs and the Ag–Au core-satellite structure. The hydrodynamic radius for the ps-9 DNA modified AgNP is ~ 24 ± 5 nm (green), which is larger than the radius measured from TEM, 16 ± 3 nm. In TEM imaging, the DNA surface modification cannot be observed due to significant lower electron density of DNA compared to that of the AgNPs. But DLS measures the size by means of diffusion correlation in aqueous solution. The loose layer of ssDNA strands (56mers extending from the surface) on the AgNP surface if assume a random coiled conformation in aqueous solution would increase the hydrodynamic radius of the particle by ~ 8–10 nm. On the other hand, the hydrodynamic radius of the bimetallic nanocluster measured by DLS is ~50 ±29 nm. From the 16 nm (radius) AgNP core, 5 nm (diameter) AuNP satellite, and the length of a 56 bp dsDNA linker (~19 nm when fully extended away from the surface), a radius of ~45 nm of the satellite cluster can be expected. The wide distribution of the hydrodynamic radius reflects the heterogeneity of the sample, consistent with the TEM images that there is a wide distribution of the number of

AuNPs surrounding each AgNP core, ranging from 6–16. The distance between the AuNPs and AgNP measured by the TEM does not reflect the distance in solution, because the DNA linkers cannot be observed in the TEM images, and the drying conditions before imaging caused the collapse of the AuNPs to the surface of the AgNP.

2.4.4. Colorimetric Assay to Confirm the Successful DNA Functionalization.

We also carried out a colorimetric assay using two sets of AgNPs, each functionalized with an oligonucleotide that contains a ps-9 domain and a recognition domain complementary to each other. When the two sets of functionalized AgNPs were mixed together, they formed aggregates due to hybridization of the complimentary recognition domains of the DNAs. This aggregation resulted in a characteristic broadening of the peaks and dampening of the silver plasmonic resonance absorbance peak (blue trace in figure. 2.5.). When the aggregates were heated to 70 degree C, the absorption profile of dispersed AgNPs was recovered (black trace in figure 2.5.), suggesting the reversibility of DNA mediated aggregation. This melting and aggregation with temperature change was cycled three times to confirm the reversibility of the aggregation (inset in fig. 2.5.).

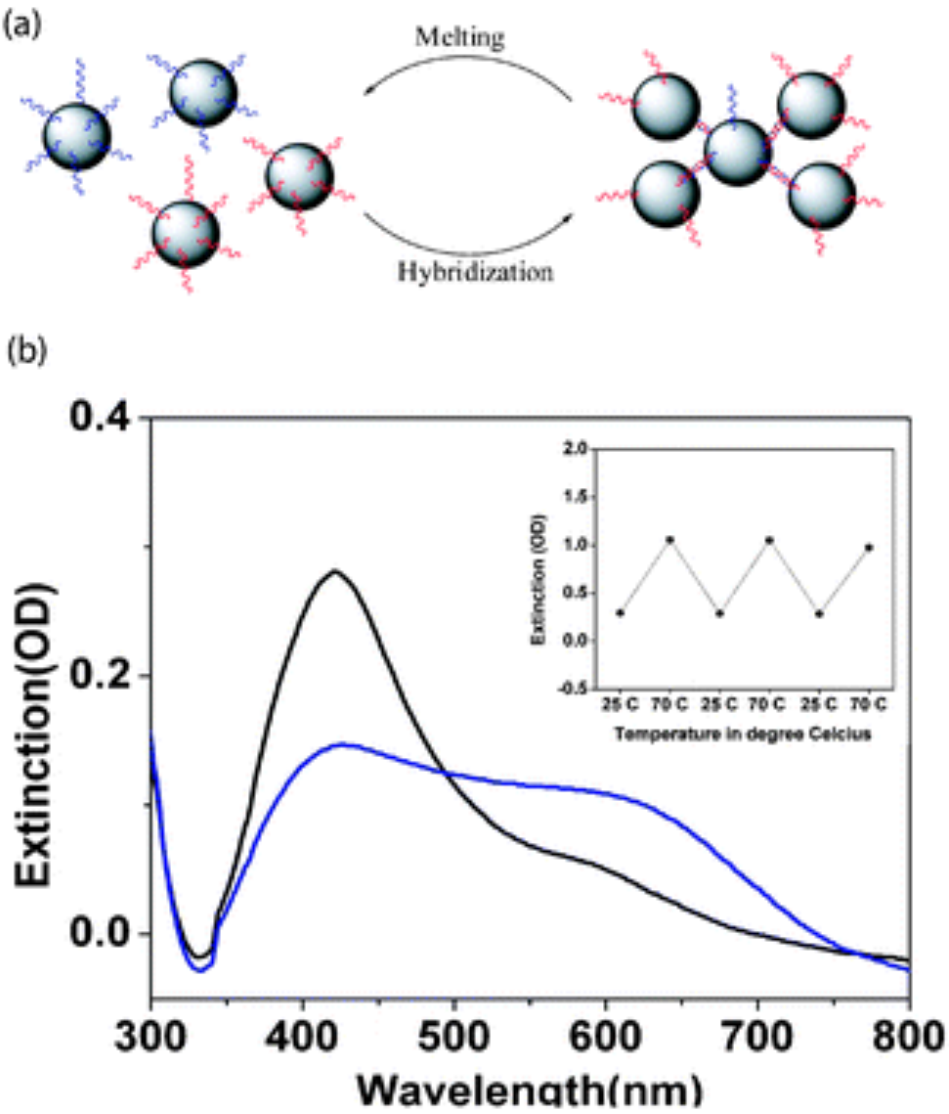

Figure 2.5. (a) The reaction scheme showing hybridization of the complementary DNA (red and blue) on the two sets of AgNPs causes the aggregation of the nanoparticles, while melting at higher temperature will separate the aggregates into individual particles. (b) UV-vis spectra of the aggregates (blue) and resulting spectra after heating at 70 °C for 5 min (black). Inset: The absorbance change with temperature shows excellent reversibility after three cycles from 25 °C to 70 °C.

2.4.5. Immobilization Efficiency of 20 nm ps-po DNA Modified AgNPs on DNA Origami Platform. The assembly of discrete AgNP architectures was then achieved in a two-step protocol as illustrated in figure 2.2.b. In the first step, a triangular shaped DNA origami structure was assembled with the required number of staple strands mixed with 3, 6 or 9 capture strands that each has ~15 bases single stranded overhangs, which are complementary to the DNA strands on the AgNPs. It was determined that the linkage provided by one 15 base-paired DNA hybridization was not strong enough to hold one particle with ~ 20 nm diameter on the origami surface (data not shown). We therefore designed a group of three capture strands, arranged in a nearly equilateral triangle ~ 6 nm apart from one another, to capture each particle though three complementary strand hybridizations. It is also noted that more than three capturing strands in each cluster or other arrangements may create much greater positional uncertainty. Here we used A_{15} as the capture sequence pointing out from the origami surface and T_{15} as the sequence on the po portion of the chimeric DNA on the AgNP. This choice of sequence ensures a greater degree of freedom for strand hybridization, allowing possible sliding of one single strand against the other to provide enough flexibility for all three capture strands to bind with a single 20 nm AgNP simultaneously. In the second step, pre-engineered DNA origami in different equivalent molar ratios was added to the DNA-functionalized AgNP in 1xTBE, 350 mM NaCl buffer to form the desired structures In addition, 1xTAE-Mg buffer was added to ensure that the mixture solution was sufficiently diluted to reduce undesired crosslinking among the discrete structures. The mixture was

then annealed from 40 ^{o}C to 4 ^{o}C to complete the assembly process (see Supplemental Information for experimental details). Formation of the triangular shaped DNA origami structures was first verified by Transmission Electron Microscope imaging (TEM) of negatively stained samples (figure 2.5.a). The length of each arm of the origami was observed to be ~114±2 nm, which is consistent with the designed length. High fidelity hybridization between capture strands and DNA strands on the AgNP was first verified using the triangular DNA origami with three capture strands that was designed to capture only one AgNP (figure 2.5.b). Over ~95 % of the triangle DNA origami structures in this sample display a single AgNP at one corner (see more images in Supplemental Information). Energy dispersive X-ray spectroscopy (EDS) of these structures shows the presence of Silver from the AgNP and Uranium from the negative stain (figure 2.5. c).

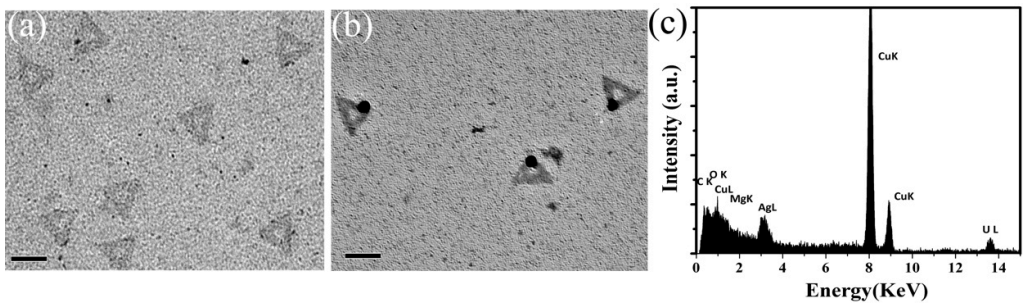

Figure 2.6. (a) TEM image of the triangular DNA origami negatively stained with Uranyl formate shows the triangular shape with an average arm length of 114±2 nm. (b) Hybridization of origami with one AgNP shows high efficiency of attachment. (c) EDS spectrum of the sample in (b) shows the presence of Silver from AgNP, Uranium from negative staining. Cu is from TEM grid. Scale bars of TEM images: 100 nm.

2.4.6. Organization and Characterization of 20 nm ps-po DNA Modified AgNPs into Discrete Dimeric and Trimeric Structures on DNA Origami Platform.

To demonstrate the organizational power of using my method to create complex AgNP patterns, we further prepared triangular shaped DNA origami structures displaying capture strands at unique positions to control the assembly of discrete AgNP nanoarchitectures. These include three different dimeric AgNP structures each having well-defined inter-particle separations and an asymmetric trimeric AgNP structure (figure 2.2). Design (i) contains two particles at the two corners of a single arm in the triangular DNA origami with a center-to-center distance of ~94 nm. The average distance measured from TEM images of over 100 of these dimers was ~90±3 nm, which is consistent with the designed parameters. The formation of the correct dimmer AgNP structure was dominant with a yield of dimers ~81%. Since we used two equivalents of AgNPs to origami structure, a small population of monomeric (12.6%) and cross-linked structures (7.4%) were also observed. Design (ii) has an inter-paticle center-to-center distance of ~52 nm by design, with a measured distance of ~49±2 nm and similar high yield (~81%) of the designed dimer structure. Design (iii) has the shortest center-to-center distance of 29 nm between the two particles by design and a measured distance of ~24 ± 2 nm. TEM images of this dimer showed a decreased yield as compared to the other dimer structures of larger inter-particle distances. It has ~57% yield of dimers and ~40% yield of monomers. It is noted that the AgNPs have a diameter of ~20±2 nm, the measured distance of ~24 ± 2 nm indicated that the edge-to-edge distance between the particles is ~4±4 nm. It is

possible that the relative low yield of dimers obtained for design (iii) at such close distance may be caused by the stronger electrostatic repulsion between the two particles and also the steric hindrance between the DNA strands covering the surfaces of the two approaching particles. Another possibility is that as the diameter of the particle is comparable to the distance between the two groups of capture strands, one particle might occupy the space between the two groups thus preventing the second particle to bind.

We also used a triangular shaped origami structure with three groups of capture strands on one arm having two different center-to-center distances between neighbouring particles, 42 nm and 52 nm. Addition of three equivalents of 9ps-T15 DNA-functionalized AgNPs formed the desired assembly with ~62.5% yield of correctly formed trimers. It is observed that the middle nanoparticle is situated asymmetrically in between the other two particles. The center-to-center distances were measured to be ~37 ± 2 nm and ~45 ± 2 nm, which are ~12% less than the designed distances. From the TEM images it is also found that the arm of the triangle origami holding the three AgNPs is ~10% shorter than the other two arms. We speculate that structural strains caused by the assembly of the three particles on the DNA structure might have caused some distortion of the underlining DNA structure, resulting in the observed shortening of the triangle arm with the particles attached. In addition, the drying condition in preparing the samples for the TEM imaging may also contribute to the shortening of the distance between the particles where there might be larger capillary forces between particles of closer spacing.

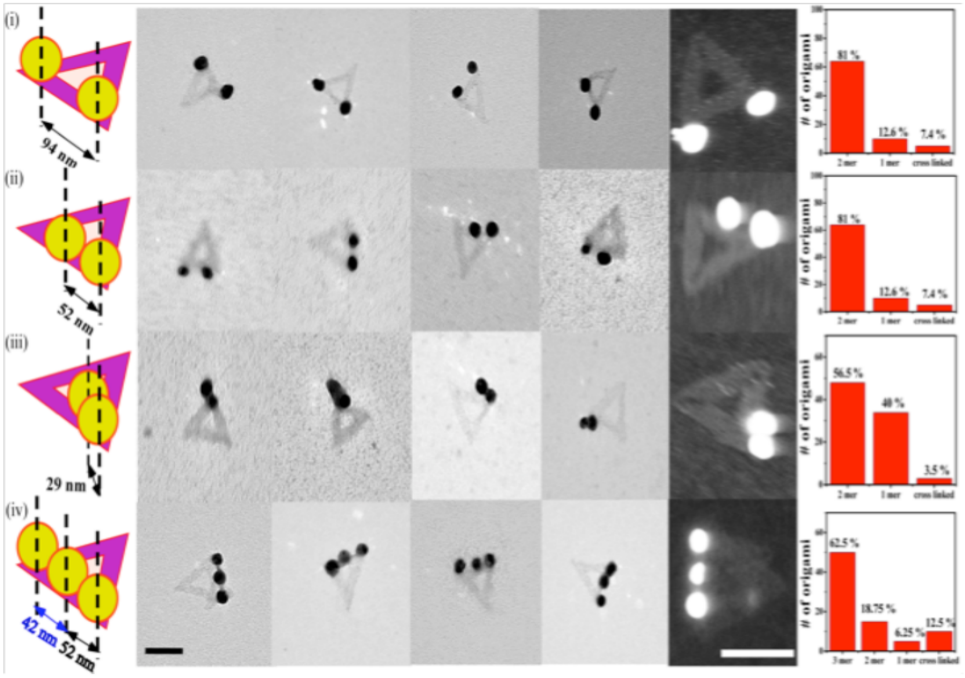

Figure 2.7. Left: Illustration of individual designs I–IV with different center-to-center distances. Middle: In the first four columns are enlarged TEM images of individual structures after negative staining of the samples with uranyl formate. The shape of the triangular DNA origami can be clearly seen; the dark balls are the AgNPs. The fifth column shows STEM images of the samples without staining. Again, the shape of the triangular DNA origami is clearly visible; the AgNPs appear as bright spots. Scale bars: 100 nm. Right: Yield distribution of the formed structures.

For the designs shown in figure 2.6.,we also used scanning transmission electron microscope (STEM) to image the structure. STEM provides a convenient way to visualize the AgNP decorated DNA origami samples with high contrast and without any staining. This provided us further direct evidence of the assembled structures, showing clearly the AgNPs and the underlining triangular shaped DNA origami nanostructures.

2.4.7. Fabrication of 1:1 20 nm AgNP and 5 nm AuNP Hetero Dimeric Structures. Organizing different types of noble metal nanoparticles with defined spatial distance and stoichiometry control remains a challenge for bottom up nanotechnology. Here we demonstrated that DNA origami structures can act as spatial templates to organize two different types of nanoparticles (AgNP and AuNP). We demonstrate that a stoichiometrically controlled hetero dimer of AuNP and AgNP can be easily assembled. The assembly scheme is shown in figure 2.7.a. First, we selectively modified a staple strand with a 5 nm AuNP. The 5 nm AuNP was first attached to a specific position on the DNA origami structure, in close proximity to the position at which three capture strands (A15) were designed to bind a AgNP. Second, 9ps-T15 DNA functionalized AgNP was added in a 1:1 ratio to fabricate the final bimetallic discrete structure. TEM (figure 2.7.b) and STEM images (figure 2.7.c) clearly demonstrated the formation of the designed hetero dimer structure with an average center-to-center distance of ~13±2 nm. EDS analysis (figure 2.7.d) from the STEM imaging of the sample confirmed the presence of both silver and gold elements. The low abundance of Au relative to that of Ag is consistent with the smaller sizes of the AuNP.

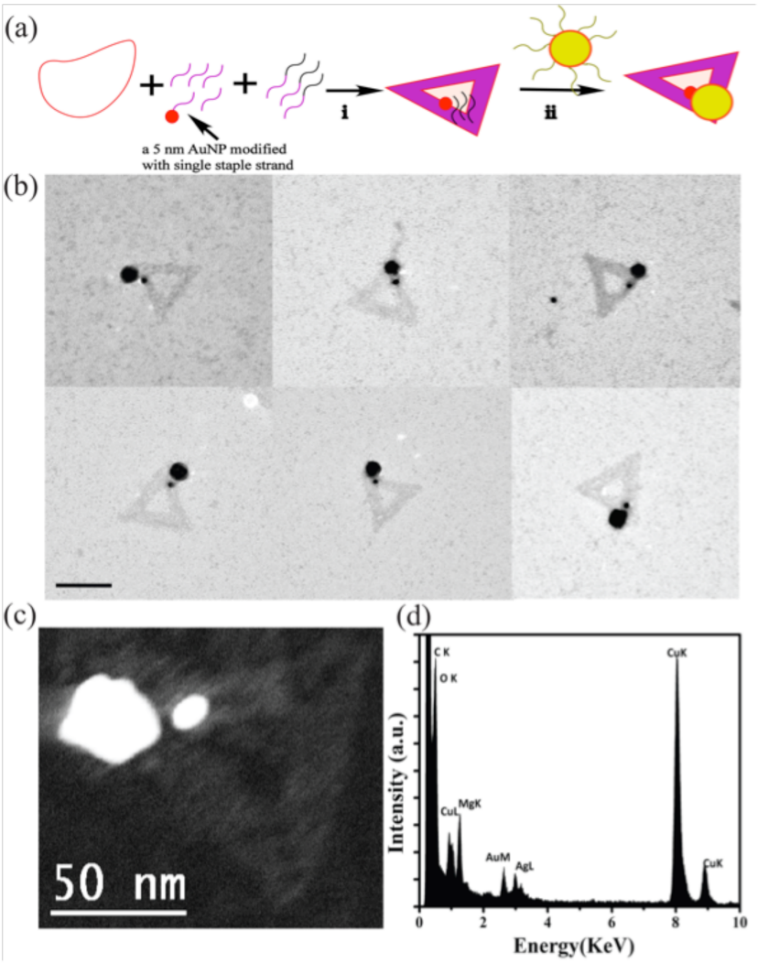

Figure 2.8. **a)** Schematic view of the fabrication of 5 nm AuNP and 20 nm AgNP dimer structure. (i) self-assembly of M13 DNA, staple strands, staple strand modified with 5 nm AuNP and capture strands to form origami DNA structure carrying a single 5nm AuNP. (ii) Attachment of ps-po chimeric DNA functionalized AgNP to the AuNP carrying DNA origami to form the bimetallic hetero dimer. **b)** TEM images show organization of AgNP-AuNP dimeric structure with average center to center distance of ~15 nm. Scale bar:100 nm. **c)** STEM image of the AgNP-AuNP dimeric structure. Scale bar: 50 nm. **d)** EDS analysis of the AgNP-AuNP hetero dimer on the DNA origami structure.

2.5. Conclusion

In summary, we have developed an easy to use and robust strategy to achieve AgNP and DNA conjugates that are stable in buffer conditions that are amenable to DNA hybridization. Such AgNP–DNA conjugates open up opportunities to assemble hierarchical nanostructures that may find use in nanophotonics and biosensing application.Then we have demonstrated the self-assembly of a discrete number of AgNP and AgNP-AuNP nanoarchitectures using DNA as rationally designed templates allowed us to have control of some of the properties that are essential for hierarchical nanoparticle assembly, which include but not limited to the spatial relationship between the particles and the identity of the particles. The system demonstrated here could potentially be used to gain better insight of particle-particle interactions. Systematic studies in this direction are underway. Although much more systematic efforts (e.g. spectroscopic studies combined with theoretical simulation of the assembled structures) are needed to investigate the photonic properties of the spatially controlled AgNP architectures, we see not fundamental limitation now to make the target structures, as demonstrated in this work.

2.6. References

(1) Stewart, M. E.; Anderton, C. R.; Thompson, L. B. ; Maria, J.; Gray, S. K Rogers, J. A.; Nuzzo, R. G. *Chem. Rev.* **2008**, 108, 494 – 521.

(2) Lin, C.; Liu, Y. ; Yan, H.*Biochemistry* **2009**, 48, 1663 – 1674.

(3) Loweth, C. J.; Caldwell, W. B.; Peng, X.; Alivisatos, A. P.; Schultz, P. G.; *Angew. Chem.* **1999**, 111, 1925 – 1929; *Angew. Chem. Int. Ed.* **1999**, 38, 1808 – 1812.

(4) Aldaye, F. A.; Sleiman, H. F.; Angew. *Chem.***2006**, 118, 2262 – 2267; *Angew.Chem. Int. Ed.* **2006**, 45, 2204 – 2209.

(5) Sharma, J.; Chhabra, R.; Andersen, C. S.; Gothelf, K. V.; Yan, H.; Liu, Y. **2008**, 130, 7820 – 7821.

(6) Deng, Z. X. ; Tian, Y.; Lee, S. H.; Ribbe, A. E.; Mao, C. D. *Angew. Chem.* **2005**, 117, 3648 – 3651; *Angew. Chem. Int. Ed.* **2005**, 44, 3582 – 3585.

(7) Beyer, S.; Nickels, P.; P. Simmel, P. *Nano Lett.* **2005**, 5, 719 – 722.

(8) Lee, J. H.; Wernette, D. P.; Yigit, M. V.; Liu, J.; Wang, Z.; Lu, Y. *Angew. Chem.* **2007**, 119, 9164 –9168; *Angew. Chem. Int. Ed.* **2007**, 46, 9006 – 9010.

(9) Niemeyer, C. M.; Brger, W.; Peplies, J. *Angew. Chem.* **1998**, 110, 2391 – 2395; *Angew. Chem. Int. Ed.* **1998**, 37, 2265 – 2268.

(10) Le, J.; Pinto, Y.; Seeman, N. C.; MusierForsyth, K.; Taton, T. A.; Kiehl, R. A.; *Nano Lett.* **2004**, 4, 2343 – 2347.

(11) Zhang, J.; Liu, Y.; Ke, Y.; Yan, H. *Nano Lett.* **2006**, 6, 248 – 251.

(12) Zheng, J. ; Constantinou, P. E.; Micheel, C.; Alivisatos, A. P.; Kiehl, R. A.; Seeman, N. C. *Nano Lett.* **2006**, 6, 1502 – 1504.

(13) Nykypanchuk, D.; Maye, M. M.; Van derLelie, D.; Gang, O. *Nature* **2008**, 451, 549 – 552.

(14) Park, S. Y. et al.,*Nature* **2008**, 451, 553 – 556.

(15) Sharma, J.; Chhabra, R.; Cheng, A.; Brownell, J.; Liu, Y., Yan, H. *Science.* **2005,** *323*, 112–116.

(16) Lee, J.-S.; Lytton-Jean, A. K. R.; Hurst, S. J.; Mirkin, C. A.; *Nano Lett.* **2007**, 7, 2112 – 2115.

(17) Pal, S.; Sharma, J.; Yan, H.; Liu, Y.; *Chem. Commun.* **2009**, 6059 – 6061.

Chapter 3

Quantum Efficiency Modification of Organic Fluorophores Using Gold Nanoparticles on DNA Origami Scaffolds

3.1. Abstract

We have used DNA origami as the platform to create different separation between a 20 nm gold nanoparticle (AuNP) and an organic fluorophore (TAMRA) and studied the distance dependent plasmonic interactions between the particle and the florescence of the dye using both steady state fluorescence and lifetime measurements. Greater fluorescence quenching was found at smaller distances, which was accompanied with an enhancement of the decay rate. We then fabricated both 20 nm and 30 nm AuNP homodimers using DNA origami as a molecular scaffold and placed a Cy3 fluorophore in the middle position of the AuNP dimer. Two different distances between the dimers were investigated. Up to 50% enhancement of the Cy3 fluorescence quantum efficiency was observed for the dye placed in between the 30 nm AuNP dimers. These results are in good agreement with the theoretical simulations.

3.2. Introduction

Bottom-up DNA directed self-assembly has been a robust and reliable approach to organize nanomaterials into discrete, 1-dimensional, 2-dimesional, 3-dimensional architechtures.[1]-DNA origami has recently emerged as the peak of complexity in the field of nucleic acid nanostructures, providing a method for facile formation of a 30-100 nm length platform with near unity yield, which can

act as a scaffold to have different functional moieties site-specifically placed on the surface with 4-6 nm spatial resolutions. DNA origami has attracted a great deal of attention for organizing nanomaterials due to the discrete structure, remarkable high yield of formation, structural rigidity and high density of modifiable DNA sequences on the surface.[2-4] Researchers have shown reliable organization of quantum dots, carbon nanotubes, virus capsids, proteins, enzymes and aptamers on DNA origami.[5-11]

Deterministic positioning of noble metal nanoparticles (NPs) using DNA origami [12-18] has also attracted a lot of interest due to their unique distance and geometry dependent optoelectronic properties.[19]Recently two efforts on organization of gold NPs into unique chiral spiral arrangements have been reported, which give rise to a unique response to circularly polarized light. [20,21] Noble metal NPs are also known to have influences on the quantum efficiency and life times of organic fluorophores placed within close proximity from the metallic particles. Due to high rigidity and structural predictability of dsDNA and DNA origami structures, these structures can be used as a nanometer scale ruler to control the distances between two photonic elements (e.g. nanoparticle-organic fluorophores or nanoparticle-nanoparticle). Recently, dsDNA has been employed to systematically change the distanece between fluorophores and metallic nanoparticles.[22,23] Acuna *et. al* reported distance dependent fluorescence quenching of organic fluorophores using DNA origami as a nanoscale molecular pegboard. [24] Due to the high modularity of the organization of nanoparticles on a DNA origami platform, there are far more opportunities to systematically

investigate effects of the distance dependent photonic interactions between the NPs (with different size and noble metal) and fluorophores. It is easy to create a nanogap between a particle dimer on the DNA origami, simply by selectively changing a few DNA sequences out of the hundreds of origami staple strands to incorporate the immobilization sites of the nanoparticles. Organic fluorophores can then be precisely attached at the center of the structure, yielding the desired distance and orientation relative to the bound NP. In this way, diverse, discrete nanoparticle assemblies can be created to study the distance or nanogap dependent local electric field enhancement of both monomeric and dimeric AuNP structures, as well as the photophysics of the fluorophores in close distance and their interactions with the AuNPs.

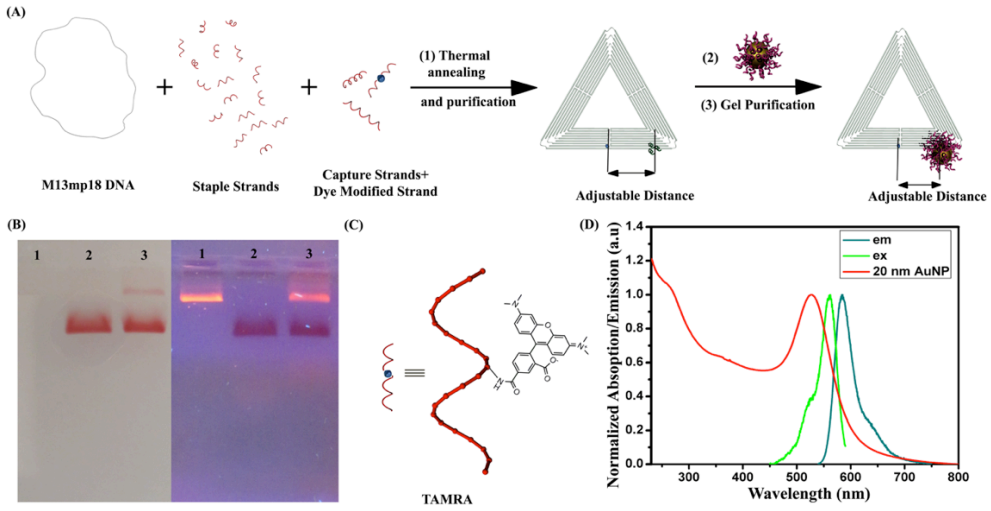

Figure 3.1. (A) Schematic representation of the formation of a triangular origami structure with a gold nanoparticle and a fluorophore molecule at the predetermined locations. The first step is to do a thermal annealing of the mixture of the long circular single stranded M13 DNA, the staple strands, the capture strands that carry single stranded extensions (probes) and the fluorophore-modified strand with the defined molar ratios, and then purify the DNA origami to get rid of extra short strands. The second step is the hybridization of the DNA functionalized AuNPs and the probe strands on the origami surface. The third step involves purification of origami with nanoparticles from the free nanoparticles using native agarose gel electrophoresis (B) White light (left) and UV light illuminated (right) native agerose gel for the purification of structures. Lane 1: origami triangles. Lane 2: 20 nm DNA functionalized AuNPs. Lane 3: origami structures with a single 20 nm gold nanoparticle attached per origami. In Lane 3, the fastest band (thick band) corresponds to the excess unbound nanoparticles. The second band (thin band) corresponds to the structure with a 20 nm

nanoparticles immobilized on specific site of the origami (C) Molecular structure of internally TAMRA modified DNA. This particular strand acts as a staple strand and hybridizes into a specific location of the DNA origami and hence has a fixed position in the structure. The orientation of the dye is expected to be random if it points outward from the DNA origami or be more parallel to the nanoparticle surface if the dye got intercalated between the nearby DNA base-pairs. (D) Excitation (green) and emission spectra (olive) of TAMRA dsDNA plotted with the AuNP plasmon band.

3.3. Materials and Methods

3.3.1. Materials All unmodified staple strands were purchased from Integrated DNA Technologies Inc. (www.idtdna.com) in a 96-well plate format (200 uM/well) and mixed according to the different designs. All disulfide-functionalized DNA strands were also purchased from IDTDNA and purified using denaturing PAGE gel electrophoresis. Tris-(carboxyethyl)phosphine hydrochloride (T-CEP), and Sodium Chloride (NaCl) were purchased from Sigma-Aldrich, USA. Bis(p-sulfonatophenyl)phenylphosphine dihydrate dipotassium salt (BSPP) was purchased from Strem Chemicals Inc.. Colloidal solution of 20 nm and 30 nm AuNPs were purchased from Ted Pella Inc.

3.3.2. Phosphination of AuNPs. The original citrate ligands on the surface of AuNPs (20 and 30 nm) were replaced by the BSPP ligands, in order to enhance the colloidal stability. Solid BSPP (20 mg for the 20 nm particle or 30 mg for the 30 nm particles) was added to a 50 mL solution of the colloidal nanoparticles (particle density 7 $x10^{11}$/mL for the 20 nm or 2 $x10^{11}$/mL for the 30

nm particles) and the mixture was stirred for 16-20 hours at room temperature in the dark. 2-5 mg NaCl was added at a time to this mixture while shaking until the color changed from red to purple. The resulting solution was subjected to centrifugation (3000 rpm for 30 min) and the supernatant carefully removed with a pipette to eliminate excess BSPP and NaCl. AuNPs were with a pipette, AuNPs were then resuspended in 1 mL BSPP (2.5 mM) solution. 2 mL of methanol was added to the solution to aggregate the particles again and another centrifugation was used to remove any residual salt in the solution. The AuNP pellet at the bottom of the centrifuge tube was resuspended in 1 mL 2.5 mM BSPP solution. The concentration of the AuNPs was estimated from the optical absorbance at ~ 520 nm using the extinction coefficient of 8.8 $x10^8$ $M^{-1}cm^{-1}$ for the 20 nm particles and 6 $x10^9$ $M^{-1}cm^{-1}$ for the 30 nm particle. Phosphine coating increases the negative charge on the particle surface and consequently stabilizes the AuNPs in a high salt concentration at a higher particle density.

3.3.3. DNA Functionalization of AuNPs. The disulfide bond in the thiol-modified oligonucleotides was reduced to monothiol using TCEP (1:200 molar ratio of DNA:TCEP, overnight) in water. The oligonucleotides were purified using G-25 size exclusion columns (GE Healthcare) to remove the small molecules. The purified monothiolmodified oligonucleotides were incubated with phosphinated AuNPs in 1:500 ratio for the 20 nm AuNPs and 1:1000 ratio for the 30 nm AuNPs in 0.5 × TBE buffer (44 mM Tris, 44 mM boric acid, 1 mM EDTA, pH 8.0). The NaCl concentration was gradually increased to 350 mM over 36 hours at room temperature to ensure the full coverage of the AuNPs by the

thiolated DNA. The AuNP-DNA conjugates were washed 3 times using Microcon centrifugal devices (100 kD MWCO membrane filters, Millipore) to get rid of excess oligonucleotides and resuspended in 0.5 × TAE-Mg^{2+} buffer (20 mM Tris, 10 mM Acetic acid, 1 mM EDTA and 6.25 mM Magnesium acetate, pH 8.0) after the final centrifugation. The concentration of these AuNP-DNA conjugates was estimated from the optical absorbance at ~ 520 nm.

3.3.4. Formation of Origami Structures. To assemble the triangular shaped DNA origami, 3 nM single stranded M13mp18 DNA (New England Biolabs, 7,249 nt-length) was mixed in 0.5 × TAE-Mg^{2+} buffer with unpurified staple strands and the required numbers of capture strands (sequences detailed later) in a 1:5:10 molar ratio, following the original triangular origami design outlined by Rothemund.[2(a)] The resulting solution was cooled from 95 ^{o}C to 4 ^{o}C to form the DNA origami structure. It was subsequently purified three times by Microcon centrifugal filtration devices (100 kD MWCO filters, Millipore, Bedford, MA) to remove the excess staple strands.

3.3.5. Immobilization of AuNPs on DNA Origami and Electrophoretic Gel Purification. The DNA functionalized NP solution was added to a 3 nM DNA origami solution in 0.5 × TAE-Mg^{2+}, with a molar ratio of 2:1 for the monomeric structures and 1: 5 for the dimeric structures (2-2.5 fold excess of the AuNPs were added to ensure higher yields of the desired structure). The concentration of NaCl was raised to 300 mM by adding 5 M NaCl solution. The mixture was then cycled 25 times between 45 ^{o}C and 30 ^{o}C in a PCR thermocycler for 24 hours to promote hybridization of the DNA on the AuNPs

with the complementary capture strands on the DNA origami. The resulting mixture was subjected to 1% agarose gel electrophoresis for 40 minutes at a constant 80 V. The band containing the desired structure was cut out from the gel, extracted using a freeze-n-squeeze column (Biorad) and concentrated by centrifugation at 6000 rpm for 10 minutes and redispersed in 0.5xTAE-Mg^{2+} buffer.

3.3.6. TEM Imaging of the Origami Triangles with the AuNP. TEM samples were prepared by dropping 2 μL of the purified sample solution on a carbon-coated grid (400 mesh, Ted Pella) that was previously negative glow discharged using an Emitech K100X instrument. After 1 minute, the sample drop was wicked from the grid by absorption into a filter paper. A drop of water was added to the grid to remove the excess salt, and the excess water was again wicked away by the filter paper. To stain, the grid was treated with a drop of 0.7 % uranyl formate solution for 2 seconds and the excess solution was wicked away with a filter paper. The grid was then treated with a second drop of uranyl formate solution for 12 seconds, and the excess solution was removed by the filter paper. Finally, the grid was kept at room temperature to allow drying. Staining allowed us to observed the underlining DNA origami together with the AuNPs under TEM. Low-resolution TEM studies were conducted using a Philips CM12 transmission electron microscope, operated at 80 kV in bright field mode.

3.4. Results and Discussions

3.4.1. Fabrication of 1:1 Fluorophore-AuNP Constructs Using DNA Origami Directed Assembly

Construction of DNA origami uses ~200 short DNA staple strands to fold single-stranded genomic DNA (e.g., DNA of M13mp18) into geometrically well-defined nanopatterns, which are fully addressable, with a spatial resolution determined by the distance between each staple strand. Figure 3.1A illustrates our strategy of creating different distances between an organic fluorophore and a metal nanoparticle. Automated solid-state chemical synthesis of DNA enables incorporation of a fluorophores at any predetermined position of any DNA sequence. In this experiment, we internally modified a DNA staple strand with a TAMRA fluorophore. The molecular structure of TAMRA is shown in Figure 3.1C. The internal modification of a staple strand ensures that the fluorophore molecule is fixed at a specific location on the origami surface. We also modified three of the staple strands with a 15 nucleotide extended sequence, complimentary to the DNA sequence conjugated on the AuNPs (capture strand) for the site-specific immobilization of AuNPs on the DNA origami platform, following Ding et al. [13] We fixed the position of the fluorophore by using the same TAMRA modified staple strand for all the constructs, and by changing the positions of the three capture strands, we created different distances between the particle and the fluorophores. The final construct fabrication process was comprised of two steps. The first step was mixing of M13mp18 DNA, the fluorophore modified strand, and the staple strands

(including the capture strands), and the mixture was annealed from 90 °C to 25 °C over 12 hours. The excess short DNA strands were removed using a Microcon centrifugal device (MWCO 100kD). In the second step, AuNPs were mixed with the purified DNA origami solution and then subjected to another annealing step and native agarose gel purification. Figure 3.1B shows the white light and UV-light illuminated image of a typical purification gel. The fastest bands in both lane 2 and 3 are the free AuNP, and the second band in lane 3 is the desired AuNP monomeric structure on DNA origami. This particular band was excised and extracted to obtain the desired structures for further measurements.

The fluorophore we chose has well-characterized photophysical properties. The optical properties of the TAMRA-modified single stranded DNA is depicted in the Figure 3.1D, with absorbance maximum at ~ 559 nm and emission maximum at ~ 580 nm. The lifetime of the fluorophore is ~ 2.8 ns. No changes in the photophysical properties were observed when the strand was incorporated into DNA origami. Figure 3.2 shows the schematic drawing of different distances from the particle surface to the fluorophore. These distances were calculated using the known distance parameter of triangular origami (114 nm for each arm) and the length of double stranded DNA (3.4 nm/10.5 base pairs). The corresponding TEM images shown in the panels below the schematic diagrams show very efficient positioning of the 20 nm AuNPs at the predetermined positions. All the samples were found to have more than ~95 % yield of the correct structures.

It is noted that the three capture strands chosen were arranged in a triangle, and if assuming all three strands were fully hybridized to the corresponding three DNA strands on the same AuNP, the AuNP should have little freedom to move its position except some flexibility provided by a 5-nt single stranded linker region between the hybridization region and the underlining DNA origami. So that the uncertainty of the center of the AuNP positioning relative to the position of the fluorophore is expected to be less than 1.5 nm. The diameter distribution of the 20 nm AuNP was determined from TEM images to be ~ 2 nm. Therefore the distance between the particle surface to dye has uncertainty roughly ~ 2 nm.

3.4.2. Distance Dependent Photonic Interaction of TAMRA and 20 nm AuNPs; Steady State Measurements. A control sample of each construct was generated by disrupting the structures through adding ~ 100 folds ssDNA with fully complimentary sequence to the fluorophore modified DNA, then heating to 80 °C and quickly cooling to room temperature. The process is schematically described in Figure 3.3A. The complete dismantled structure was verified using TEM imaging, which showed no sign of perfectly formed structures in the controls (see SI Figure S22 for details). The addition of the displacement strands and the subsequent heating did not result in any change in the gold nanoparticle plasmon band, as shown in Figure 3.3B. Due to addition of the single DNA strand and disruption of DNA structures, the DNA signature peak at 260 nm increased. This strategy enables us to measure the fluorescence intensities of the sample and the corresponding control sample with the same optical density (OD) at the excitation wavelength, so that the measured steady state fluorescence intensities

can be directly compared, and any difference observed would reveal the distance dependent plasmonic effect.

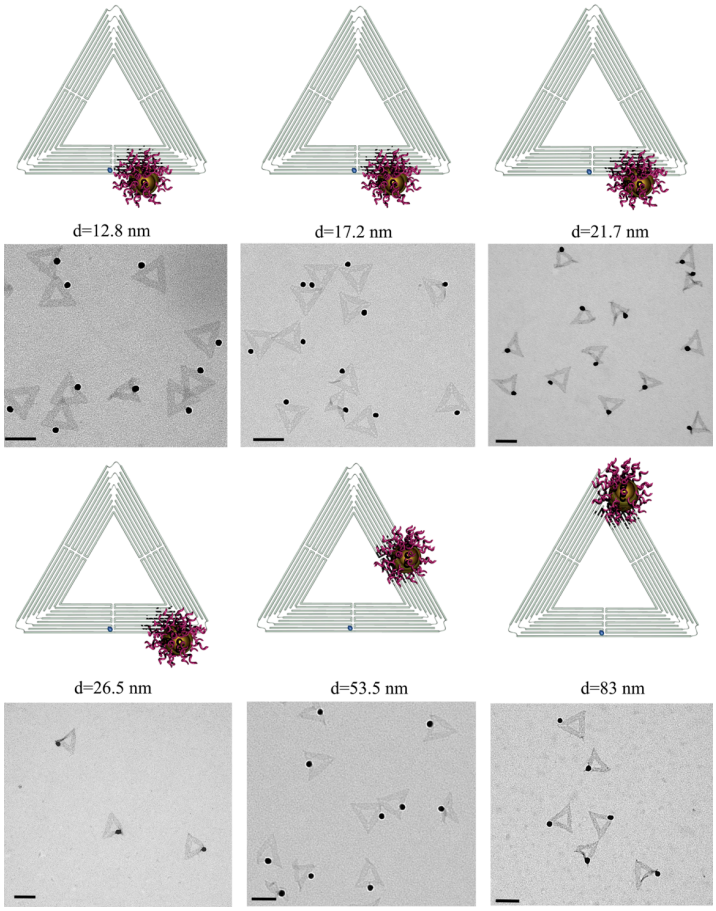

Figure 3.2. Schematic representations and corresponding negatively stained TEM images of monomeric constructs with different AuNP positions on the origami (thus different distances between the fluorophore and the AuNP). Nearly 100% yield of each construct is observed. Some distortions of the DNA origami scaffold were observed, which most likely resulted from imperfect attachment of the structure to the TEM grid surface during the deposition of the sample on the TEM grid, or the vacuum TEM imaging conditions, which may cause shrinking of DNA. The scale bar is 100 nm.

We have taken the fluorescence emission spectra of each sample and the corresponding control with excitation wavelength at 525 nm under the same experimental conditions. The normalized spectra with respect to control samples are shown in Figure 3.3C. The intensity of the emission spectra decreases with decreasing separations. To illustrate this effect we plotted the ratio of the fluorescence intensities for the sample and the control against the respective distance in Figure 3.3D. The ratios essentially reflected fluoresecence quenching effect due to the presence of the AuNP in the vicinity, with higher quenching at lower distances. The quenching effect was significant between 10-30 nm and diminishes beyond ~ 60 nm.

Förster resonance energy transfer (FRET) is commonly employed to describe the energy transfer between two fluorophores, which can be approximated as discrete dipoles. FRET occurs through electromagnetic coupling of two dipoles and the rate of energy transfer is shown to be proportional to $1/d^6$ where d is the distance between the dipoles.[25] FRET effects are detectable over very short distances and active up to 1-10 nm distances. Clearly the interaction between a fluorophore and an AuNP is detectable at much greater than 10 nm distance and cannot be modeled with FRET mechanism. To address the interactions of molecules with nanoparticles over distances more than 10 nm, nano-surface energy transfer (NSET) had been proposed.[23] The quenching behavior is proportional to $\frac{1}{d^n}$, where d is the distance between the fluorophore and the nanoparticle surface, and the index n is expected to be 4 in NSET instead of 6 in FRET. The quenching (Q) vs. distance was fitted (grey plot in Figure

3.3C) with a typical equation:

$$Q = \frac{1}{[1 + (\frac{d}{d_0})^n]} \qquad (1)$$

as reported in previous literatues,[22,23] where d_0 is the distance at which the quenching becomes 50%. The d_0 and n values were found to be 16.5 nm and 2.4, respectively for the 20 nm AuNP. The value of n is significantly lower than the values observed for small sized particles (5 nm and 10 nm AuNPs).[22] This demonstrates the long-range quenching behavior for larger particles and necessary for the development of more rigorous theoretical models.

To understand this behavior in more details, we made electrodynamics calculations of the quenching. The quenching effect of Au nanoparticles on fluorophore molecules can be modeled with a rigorous electrodynamics method developed by Zou *et al*.[22,26,27] In this theoretical modeling method, the fluorophore molecule is treated as a radiating dipole. When the molecule is situated close to an AuNP, the emitted fluorescence signal from the molecule may be amplified due to the enhanced local electric field near the metal nanoparticle, at both the excitation wavelength and the emission wavelength. On the other hand, the signal will also be quenched due to the non-radiative energy transfer between the molecule and the metal nanoparticle at the emission wavelength. The measured fluorescence signal of the system, including a molecule and a metal nanoparticle, as compared to that of an isolated molecule, can be calculated with:

$$f = f_{ex} \times f_{em} \times q_{em} \qquad (2)$$

Where f_{ex} is the enhancement factor at the excitation wavelength, which is proportional to the enhanced local electric field, $|E|^2$, of the metal nanoparticle at the position of the molecule at the excitation wavelength; f_{em} is the enhancement factor at the emission wavelength, which is also proportional to the enhanced local electric field, $|E|^2$, at the emission wavelength; and q_{em} is the quenching factor due to the nonradiative energy transfer between the molecule and the metal nanoparticle at the emission wavelength. The q_{em} can be obtained by $\frac{1}{f_t \times \eta + 1 - \eta}$ where η is the quantum efficiency (QE) of an isolated dye molecule and f_t can be calculated by dividing the emission intensity of an isolated molecular dipole. The electric field around a metal NP was calculated using the Mie theory and averaged over different orientations. The coupling between the molecular dipole and the AuNPs is treated with the coupled dipole method.

The theoretical quenching curves for different orientations of the fluorophore respect to the AuNP surface were plotted together with the experimental data points in Figure 3.3E, all of which agree very well with the experimental points in the range of distance examined.

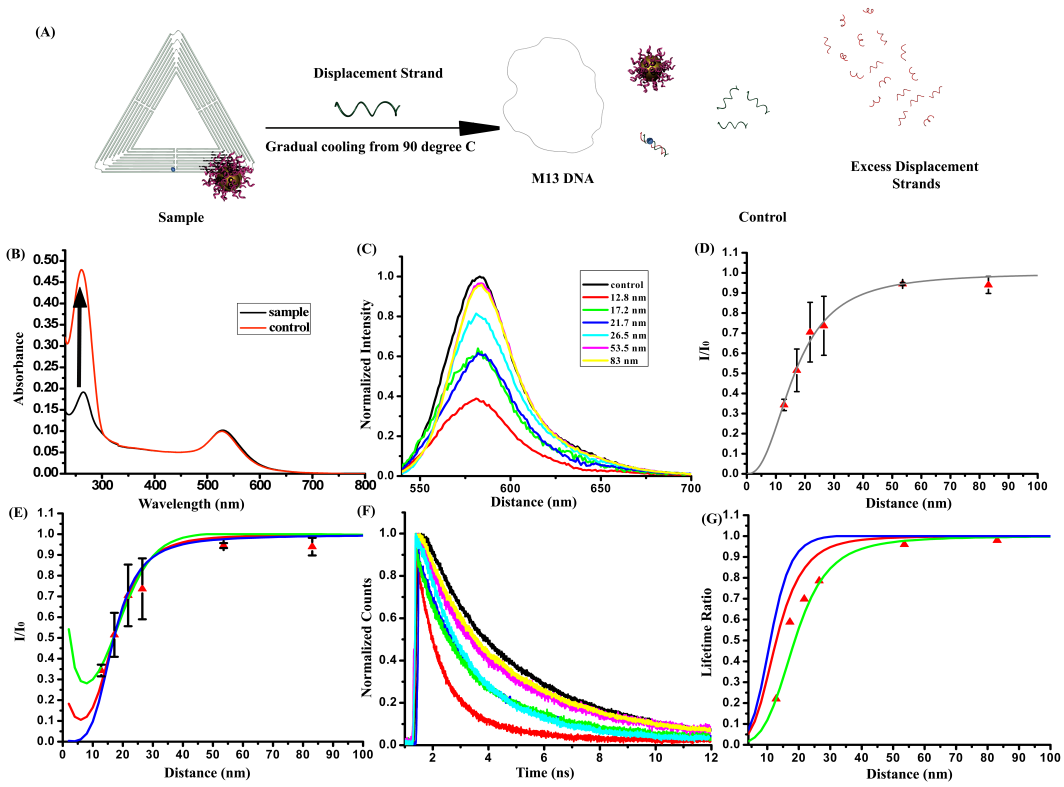

Figure 3.3. (A) Schematic representations of sample and the corresponding control. (B) The UV-Vis spectra of one representative sample (black) and its control (red). The absorbance at 260 nm increases due to addition of the displacement strand, but the absorbance peak at ~520 nm due to the surface plasmon of AuNP remains unchanged. (C) The normalized emission spectra of different monomeric constructs where all the samples are excited at 525 nm. Control (black), 83 nm (yellow), 53.6 nm (pink), 26.5 nm (cyan), 21.7 nm (blue), 17.3 nm (green) and 12.8 nm (red). (D) The fluorescence intensity ratios of the sample and control at 580 nm for different fluorophore-particle distances plotted together with the fitting curve using equation (4). (E) The same ratios are plotted with the theoretical prediction for different orientations of the fluorophores with respect to the particle surface: average orientation (red), perpendicular orientation

(green) and parallel orientation (blue). (F) Fluorescence lifetime decay curves for different distances, TAMRA internally labeled in dsDNA, with no AuNP (black), 83 nm (yellow), 53.6 nm (pink), 26.5 nm (cyan), 21.7 nm (blue), 17.3 nm (green) and 12.8 nm (red). (G) The ratio of the average fluorescence lifetime of the sample and control for different distances is plotted with the theoretical prediction for the different orientations of the fluorophores with respect to the particle: average orientation (red), perpendicular orientation (green) and parallel orientation (blue).

3.4.3. Fluorescence Lifetime Measurements. The lifetime of the excited state of a fluorophores is also influenced when a metal nanoparticle is placed near to the fluorophore. We used time correlated single photon counting technique (TCSPC) to measure the fluoresecence decay lifetimes of the different constructs with varying fluorophore-AuNP distance (Figure 3.3F). The TCSPC decay kinetics were analyzed with a home-written software package ASUFIT (www.public.asu.edu/~laserweb/asufit/asufit.html), fitted with a sum of multiple exponential decay model according to:

$$f(t) = \sum a_n \exp(-t/\tau_n) \qquad (3)$$

$f(t)$ is the measured experimental kinetic decay curve, a_n is the amplitude for the n th exponential component,τ_n is the corresponding lifetime. Numerically averaged lifetime was calculated according to equation (4).

$$\tau_{av} = \sum a_n \tau_n \qquad (4)$$

As shown in Figure 3.3F, the decay becomes faster with decreasing distance. In Figure 3.3G, the ratio of the average lifetime of the different constructs with that of TAMRA internally modified on double stranded DNA was plotted against the distance and overlayed with the theoretically predicted lifetime ratio. The experimental data show very good agreement with the theoretical predictions.

3.4.4. Theoretical Calculations.

We simulate the energy transfer between a dye molecule and nearby metal nanoparticles using a coupled dipole method similar to the method described in the reference. "Distance-dependent interactions between gold nanoparticles and fluorescent molecules with DNA as tunable spacers" Rahul Chhabra, Jaswinder Sharma, Haining Wang, Shengli Zou, Su Lin, Hao Yan, Stuart Lindsay, Yan Liu, ***Nanotechnology*** (2009) 20(48) 485201].

The excitation rate of the molecule at the excitation frequency is proportional to the enhanced local electric field $|E|^2$ at the position of the dye molecule due to the presence of nearby metal nanoparticles. At the emission frequency, the energy transfer between the dye molecule and the metal nanoparticle depends on the size and composition of the metal nanoparticle, the distance between the dye and the surface of metal nanoparticle. The quantum yield of the dye molecule will also have an effect to the energy transfer. For a dye molecule molecule with radiative and non-radiative rate constants, k_r and k_{nr}, its quantum yield, η,

$$\eta = \frac{k_r}{k_r + k_{nr}} \qquad (5)$$

when one or more metal nanoparticles are placed near a dye molecule, the energy transfer between the dye molecule and the nanoparticles will change the radiative decay rate of the dye molecule. We represent the new radiative rate constant of the dye molecule as k_t. Please note that part of the radiated energy from the dye molecule will be re-absorbed by the metal nanoparticle and become non-radiative, and only part will be emitted eventually. The modified quantum yield η',

$$\eta' = \frac{k_r'}{k_t + k_{nr}} = \frac{f_r \times k_r}{f_t \times k + k_{nr}} \qquad (6)$$

where k_r' is the radiative rate constant of the total system including the dye molecule and metal nanoparticles.

Since the total energy is conserved, the enhancement or quenching factor of the fluorescence of the dye molecule due to the presence of nearby metal nanoparticles becomes

$$\frac{\eta'}{\eta} = \frac{f_r \times (k_r + k_{nr})}{f_t \times k_r + k_{nr}} = \frac{f_r}{f_t \times \eta + 1 - \eta} \qquad (7)$$

If including the enhancement at the excitation frequency, the measured fluorescence signal relative to the original one can be calculated using

$$\frac{I'}{I_0} = \frac{|E|^2 f_r}{f_t \times \eta + 1 - \eta} \qquad (8),$$

where I_0 and I' are the fluorescence intensities of an isolated dye molecule and a dye molecule surrounded with metal nanoparticle, respectively. $|E|^2$ is the enhanced local electric field at the position of the dye molecule at the excitation frequency due the nearby metal nanoparticles.

In the coupled dipole method, we illuminate only the dye molecule and leave the metal nanoparticles in the dark. $f_r = \frac{k_r'}{k_r}$ is the enhancement of the radiative rate constant of the system due to the presence of nearby metal nanoparticles relative to an isolated dye molecule, which is proportional to the enhanced electric field $|E|^2$ of nearby metal nanoparticle at the position of the dye molecule.[Kerker, M.; Wang, D. S.; Chew, H. *Appl. Opt.* **1980**, *19*, 3373.]. $f_t = \frac{k_t}{k_r}$ is the enhancement factor of the radiative constant of the dye molecule itself, which is partially re-absorbed by the nearby metal nanoparticle and becomes non-radiative decay. f_t can be calculated by subtracting the extinction cross section of the dye molecule and its absorption cross section.

The lifetime, τ, change of the dye molecule can be calculated using equation

$$\frac{\tau'}{\tau} = \frac{k_r + k_{nr}}{k_t + k_{nr}} = \frac{k_r + k_{nr}}{f_t \times k_r + k_{nr}} = \frac{1}{f_t \times \eta + 1 - \eta} \quad (9)$$

3.4.5. Fabrication of Dimeric AuNP Structures with a Fluorophore in the Gap. Then we moved on to prepare the dimeric nanoparticle structures, which have greatly higher electric field in between the two particles (see Figure S21 for the example of E field enhancement comparison for the dimer and monomer structures), in order to study the effect of the higher E field on a fluorophore molecule placed in the center of the gap. Recently, Busson *et al.* specifically placed a single fluorophore in between two 36 nm AuNPs and demonstrated an accelerated single photon emission compared to monomers.[28]However DNA

origami method gives us unique opportunity to change the nanogap by not only changing the distance but also changing the particle size. To demonstrate that, we carefully chose and extended two different sets of staple strands (three in each set), which were expected to protrude in the two opposite sides of the origami plane (see SI for detailed sequences). The fluorophore-modified strand was kept the same as in the monomer constructs. In this way, we have ensured the correct placement of the fluorophore in the middle of the two nanoparticles as shown schematically in Figure 3.4. For the proof of concept that these constructs can eventually lead to QE enhancement, we chose Cy3 as the fluorophore. This particular fluorophore has very similar emission and excitation maxima (550 nm excitation, and 565 emission) as that of TAMRA, shown in figure 3.5A. The intrinsic QE of Cy3 is 28%, significantly lower than that of TAMRA (see Figure S23 for the excitation and emission spectra of Cy3). For this reason Cy3 might have higher chance to display a QE enhancement.

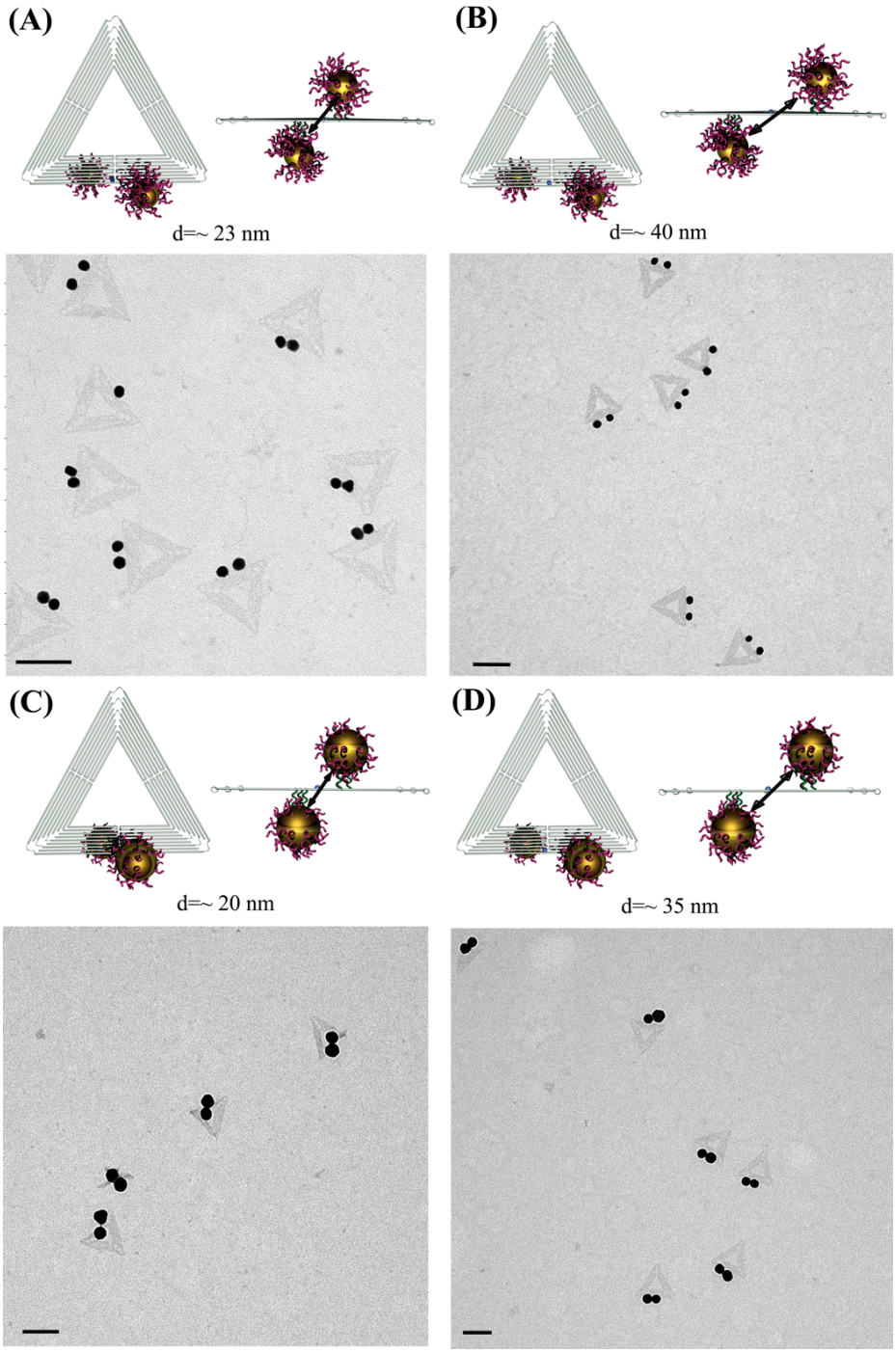

Figure 3.4. Schematic representations of top view, side view and the corresponding negatively stained TEM images of the 20 nm (A and B) or 30 nm (C and D) dimeric constructs with two different interparticle distances (surface to surface): 23 nm and 40 nm or 20 nm and 35 nm.

3.4.6. Photonic Interaction of Cy3 and 20 nm AuNP Dimer. We have designed four different AuNP dimer constructs with two different inter-particle distances from the surface of one NP to the surface of the other: ~ 23 nm and ~ 40 nm for the 20 nm AuNPs and ~20 nm and 35 nm for the 30 nm AuNPs . The constructs were purified using agarose gel electrophoresis and characterized using TEM after purification. From the TEM images the formation yield of the dimer after the purification was 90-95% (Figure 3.4A and B). The observed interparticle gap is generally smaller than the designed gap. This can be attributed to the fact that the DNA origami scaffolds underlining the dimers, when deposited on the TEM grid surface, are expected to adhere to the surface of the grid. Thus in the TEM imaging the dimers are seen from a top view rather than a side view. This will decrease the apparent distance observed. In addition, the vacuum condition during TEM imaging and the air-drying condition used to prepare the sample for TEM can cause shrinking in the interparticle distance. However, this shrinking in the interparticle distance should not be the case in the solution phase used for all the optical measurements. Therefore the interparticle distances for the dimers were chosen to be calculated from the design based on the DNA structural characteristics rather than determined from experimental means. Again the uncertainty of the interparticle distances is limited by the diameter distribution of the AuNPs rather than structural uncertainty of the DNA hybridization.

The high yield of formation enables us to investigate the effect of the nanoparticle dimers on the fluorescence of the fluorophores by using the same bulk measurements as for the monomeric structures. Initially we carried out the

steady state fluorescence measurements of the 20 nm dimer samples and the corresponding control samples with excitation at 525 nm (emission spectra shown in Figure S23). Figure 3.5B shows the ratio of fluorescence intensity of the sample and the control at the emission maxima, 565 nm. At the large gap distance of 40 nm, we observed a quenching of ~ 38%. Interestingly, when the gap distance was decreased to 23 nm, the fluorescence intensity ratio became ~ 1, comparable with the control. In Figure 3.5A these two data points are plotted with the theoretical simulations and they track very well with the theoretical calculations. Remarkably, at the closer distance, the data seems to follow the trend with the dye orientation perpendicular to the gold nanoparticle surface. This is possibly because the internally labeled Cy3 has its dipole moment fixed along the backbone of the DNA, and when the dye labeled DNA strand binds inside the DNA origami, the orientation of the dye is fixed with orientation close to parallel to the center line of the dimer. This relative orientation would change with variation in the positions of the nanoparticles with the dye position fixed.

We also carried out TCSPC measurements of the fluorophore emission for the individual dimer constructs. The average lifetimes were calculated in the same way as described before. The lifetime decay curves for the individual constructs are plotted in Figure 5.5C. The lifetime of Cy3 modified dsDNA is ~ 1.3 ns. However for the dimer construct with a 40 nm gap, the lifetime is shortened to ~ 0.75 ns and for the dimer with a 23 nm gap, the lifetime is dramatically reduced to ~ 0.11 ns. The ratios of the lifetimes for the dimers of the two distances with that of the Cy3 labeled dsDNA were plotted together with the distance dependence of

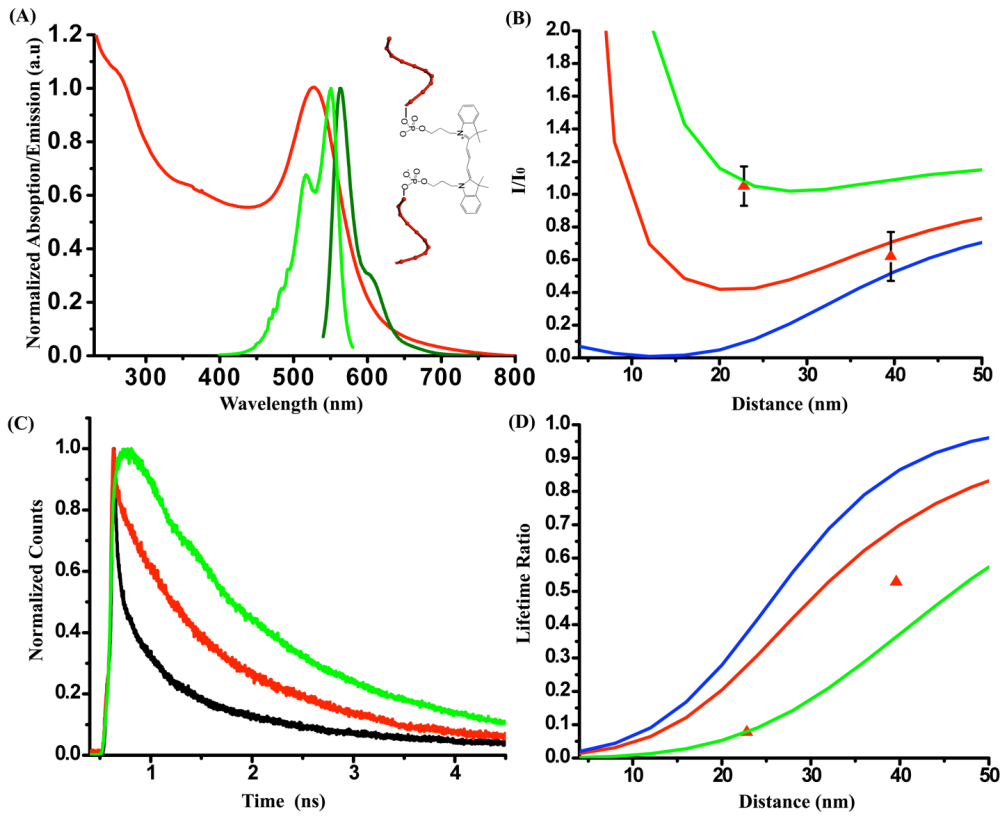

Figure 3.5. (A) Excitation (green) and emission spectra (olive) of Cy3 on dsDNA plotted with the AuNP plasmon band. Inset: Structure of internal Cy3 modified DNA (B) The fluorescence intensity ratios of the sample and control of 20 nm AuNP dimers at 565 nm for both interparticle distances are plotted with the theoretical prediction for different orientations of the dye with respect to the particle: average orientation (red), perpendicular orientation (green) and parallel orientation (blue). (B) Fluorescence lifetime decay curves for different distances: Cy3 labeled dsDNA (green), 40 nm gap (red) and 23 nm gap (black). (C) The average lifetime ratio of the sample and control fluorescence for different interparticle distances is plotted with the theoretical prediction for different orientation of the dye with respect to the particle: average orientation (red), perpendicular orientation (green) and parallel orientation (blue).

the theoretical simulated lifetime ratio in Figure 5.5D. The experimental data are in accordance with the theoretical predictions. Similarly, the shorter distance one agrees with the dye orientation perpendicular to the particle surface.

3.4.7. Photonic Interaction of Cy3 and 30 nm AuNP Dimer. To observe higher E field enhancement, we created dimers of AuNPs with a larger diameter of 30 nm. The 30 nm AuNP dimers were constructed with two different gaps (20 and 35 nm) and characterized using TEM, as shown in Figure 3.4 C and D, which displayed excellent formation yield (~90%). The apparent size of the gap is smaller than the designed gap due to the reasons mentioned before. We then proceeded to the steady state and lifetime fluorescence measurements. Figure 3.6A shows the emission spectrum of two different dimeric constructs excited at 525 nm. From the emission spectra we observed ~ 50% enhancement of QE for both the constructs. Figure 3.6B shows the intensity ratio of sample with respect to the corresponding control plotted together with the theoretical simulation. The observed results track very well with the theory, which predicts little or no difference for the QE with a change in the gap distances within the range of this study. The TCSPC measurements did not produce very reliable information about the lifetimes, as the decay lifetime was shortened below the time resolution of the instrument, which has an instrument response time of ~ 60 ps. Nonetheless, the measured lifetime indicated very short lifetime, as predicted by the theory shown in Figure S24.

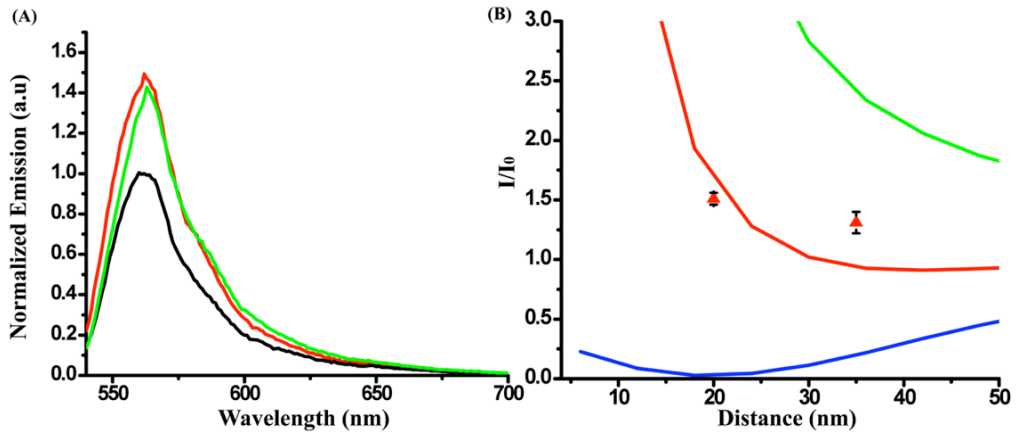

Figure 3.6. (A) Normalized fluorescence emission spectra (excited at 525 nm) of 30 nm dimeric structures with 26 nm gap (red) and 35 nm gap (green) with respect to the control (black). (B) The fluorescence intensity ratios of the sample and control of the 30 nm AuNP dimers at 565 nm for different interparticle distances are plotted with the theoretical prediction for the different orientation of the dye with respect to the particle: average orientation (red), perpendicular orientation (green) and parallel orientation(blue).

3.5. Conclusions

In summary, we have developed a robust strategy to create different distances between an organic fluorophore with a monomeric metallic nanoparticle or in the gap between a metallic nanoparticle dimer using DNA origami as the scaffold and distance ruler. We have demonstrated the increased quenching of fluorescence intensity with decreased distance to the monomeric AuNP by both steady state measurements and lifetime measurements and compared the results with existing empirical models and rigorous electrodynamics theory. The lifetime measurements combined with the steady state measurements indicated that the higher nonradiative rate enhancement at shorter distances gives rise to the higher

overall quenching at shorter distances, as observed in the experiments. We further constructed dimeric AuNP structures of different separations with a fluorophore of lower QE in the center of the gap. For the 30 nm dimer with both 26 and 35 nm gap distances, we observed 50% enhancement in QE, which is supported by theoretical simulation. The enhancement is accompanied with a significantly faster fluorescence decay rate, indicating a higher enhancement for the radiative decay rate than the non-radiative decay rate inside the dimer gap.

The same DNA directed self-assembly method can potentially be used to construct nanoparticle assemblies with very high field enhancements, such as gold nanorod dimers and silver nanoparticle dimers, which can possibly lead to much higher enhancements in fluorescence of fluorophores or photo-emission of quantum dots. These structures, which are demonstrated to form with unprecedented control of yield and inter-particle distance, if coupled with single molecule measurements can ensure reliable observation of the photonic interaction between nanoparticles and fluorophores or quantum dots.

3.6. References

(1) Aldaye, F. A. Palmer, A. L. Sleiman,H. F. *Science*. **2008**, 321, 1795-1799.

(2) Rothemund, P. W. K. *Nature,***2006,** 440, 297-302.

(3) Ke, Y. *et al. J. Am. Chem. Soc.* **2009,** 131, 15903.

(4) Han, D.; Pal, S.; Nangreave, J.; Deng, Z.; Liu, Y.; Yan, H. *Science* **2011**, 332, 342−346.

(5) Deng, Z.; Samanta, A.; Nangreave, J.; Yan, H.; Liu, Y. *J. Am. Chem. Soc.*, 2012, *134* (42), 17424–17427.

(6) Maune, H. T.; Han, S.-p.; Barish, R. D.; Bockrath, M.; Goddard III, W. A.; Rothemund, P. W. K.; Winfree, E. *Nat. Nanotech.* **2009**, 4, 61−66.

(7) Stephanopoulos, N.; Liu, M.; Tong, G. J.; Li, Z.; Liu, Y.; Yan, H.; Francis, M. B. *Nano Lett*. **2010**, 10, 2714–2720.

(8) Numajiri, K.; Yamazaki, T.; Kimura, M.; Kuzuya, A.; Komiyama, M. *J. Am. Chem. Soc*. **2010**, 132, 9937–9939.

(9) B Sacca, B.; Meyer, R.; Erkelenz, M.; Kiko, K. ; Arndt, A.; Schroeder, H.; Rabe, K. S.; Niemeyer, C. M. *Angew. Chem. Int. Ed.* **2010**, 49, 9378 –9383.

(10) Chhabra, R.; Sharma, J. ; Ke, Y.; Liu, Y.; Rinker, S.; Lindsay, S.; Yan, H. *J. Am. Chem. Soc.* **2007**, 129, 10304–10305.

(11) Rinker, S.; Ke, Y.; Liu, Y.; Chhabra, R.; Yan, H. *Nat. Nanotech.* **2008**, 3, 418−422.

(12) Sharma, J.; Chhabra, R.; Andersen, C. S.; Gothelf, K. V.; Yan, H.; Liu, Y. *J. Am. Chem. Soc.* **2008**, 130, 7820–7821.

(13) Ding, B.; Deng, Z.; Yan, H.; Cabrini, S.; Zuckermann, R. N.; Bokor, J. *J. Am. Chem. Soc*. **2010**, 132, 3248–3249.

(14) Hung, A. M.; Micheel, C. M.; Bozano, L. D.; Osterbur, L. W.; Wallraff, G. M.; Cha, J. N. *Nat.Nanotech.* **2010**, 5, 121−126.

(15) Stearns, L. A., Chhabra, R., Sharma, J., Liu, Y.; Petuskey, W. T.; Yan, H.; Chaput, J.C. *Angew. Chem. Int. Ed.* **2009**, 45, 8494−8496.

(16) Kuzuya, A.; Koshi, N.; Kimura, M.; Numajiri, K.; Yamazaki, T.; Ohnishi, T.; Okada, F.; Komiyama, M. *Small.* **2010,** *6*, 2664–2667.

(17) Pal, S.; Deng, Z.; Ding, B.; Yan, H.; Liu, Y. *Angew. Chem. Int. Ed.* **2010***,* 49*,* 2700 –2704.

(18) Pal, S.; Deng, Z.; Wang, H.; Zou, S.; Liu, Y.; Yan, H. *J. Am. Chem. Soc.* 2011, 133, 17606−17609.

(19) Stewart, M. E.; Anderton, C. R.; Thompson, L. B. ; Maria, J.; Gray, S. K.; Rogers, J. A.; Nuzzo, R. G. *Chem. Rev.* **2008**, 108, 494 – 521.

(20) Shen, X. B.; Song, C.; Wang, J. Y.; Shi, D. W.; Wang, Z. A.; Liu,N.; Ding, B. Q. *J. Am. Chem. Soc.* **2012**, 134, 146−149.

(21) Kuzyk, A.; Schreiber, R.; Fan, Z.; Pardatscher, G.; Roller, E.;Högele, A.; Simmel, F.; Govorov, A. O.; Liedl, T. *Nature*. **2012**, 483, 311–314.

(22) Chhabra, R.; Sharma, J.; Wang, H. N.; Zou, S. L.; Lin, S.; Yan, H.; Lindsay, S.; Liu, Y. *Nanotechnology* 2009, 20, 485201-485201.

(23) Yun, C. S.; Javier ,A.; Jennings, T.; Fisher, M.; Hira, S.; Peterson, S.; Hopkins, B.; Reich, N. O.; Strouse, G. F. *J. Am. Chem. Soc.* **2005**, 127, 3115–3119.

(24) Acuna, G. P.; Bucher, M.; Stein, I. H.; Steinhauer, C.; Kuzyk, A.; Holzmeister, P.; Schreiber, R.; Moroz, A.; Stefani, F. D.; Liedl, T.*et al ACS Nano* **2012**, 6, 3189– 3195.

(25) Lakowicz J R 1999 Principles of Fluorescence Spectroscopy 2nd edition (New York: Kluwer Academic Plenum)

(26) Zou, S.; Schatz, G. C. *Chem. Phys. Lett.* **2005**, 403, 62–67.

(27) Zou, S.; Schatz, G. C. *Phys. Rev. B,* **2006***,* 74, 125111.

(28) Busson, M. P.; Rolly, B.; Stout, B.; Bonod, N.; Bidault, S. *Nat. Commun.* **2012**, 3, 962.

Chapter 4

DNA Directed Self-assembly of Anisotropic Plasmonic Nanostructures

Adapted with permission from *J. Am. Chem. Soc.* **2011**, *133*, 17606-17609.

4.1. Abstract

A DNA based strategy of programmable positioning of one-dimensional (1D) gold nanorods (AuNRs) by DNA directed self-assembly has been demonstrated. AuNR dimer structures with various predetermined inter-rod angles and relative distances were constructed with high efficiency. These discrete anisotropic metallic nanoparticle assemblies exhibit unique optoelectronic properties, as measured experimentally and simulated by discrete dipole approximation methods. Further, Precise positioning of zero dimensional nanomaterials with respect to anisotropic AuNRs have also been demonstrated.

4.2. Introduction

Anisotropic nanomaterials such as gold nanorods possess unique optical properties, including high optical extinction in the range of visible and near-infrared (NIR) wavelengths, and strong localized plasmonic fields at the tips of the materials.[1,2] Due to these unique optoelectronic properties, AuNRs have been used for cellular imaging, cancer therapy and biosensing.[3] Higher order assembly of AuNRs may lead to new optical properties depending on the ensuing geometric properties including size, distance, and orientation, as proposed by theory and verified by experiment.[4] Most recent attempts to create high order AuNR nanostructures have focused on the use of top-down e-beam lithography to pattern or manipulate the materials in a serial fashion.[5] New strategies are needed to deterministically position these anisotropic nanostructures in a massively parallel fashion, within complex multi-component architectures.

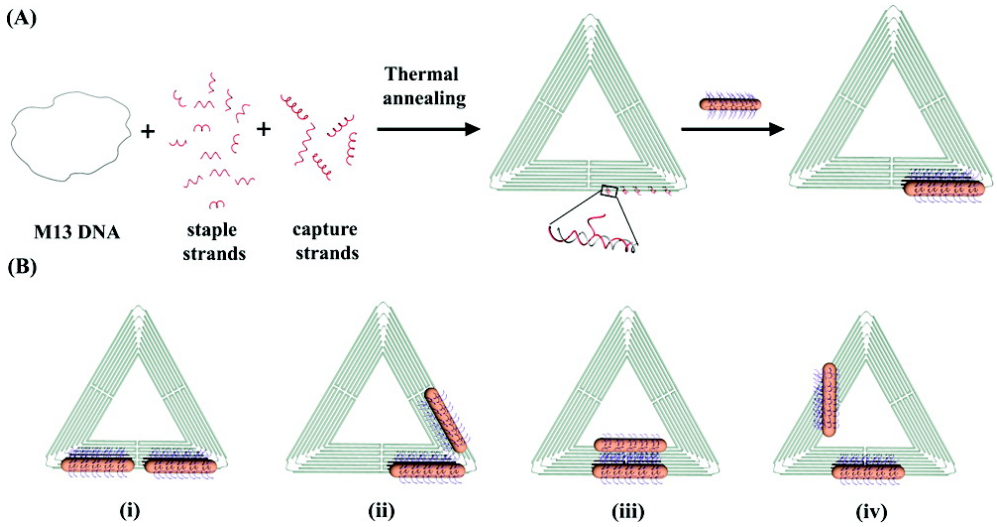

Figure 4.1. (A) Schematic representation of the formation of triangular origami structures. First step isthermal annealing of M13 DNA with staple and capture strand carrying single stranded extensions (probes) at desired positions. Second step is the hybridization of the DNA functionalized on the AuNR surface and the probe strands on the origami surface to obtain site-specific immobilization of the AuNR. (B) Schematic representation of four different dimeric structures displaying different angles between the AuNRs (i)180^{o} (ii)60^{o} (iii)0^{o} (iv) 90^{o} respectively.

4.3. Materials and Methods

See APPENDIX C

4.4. Results and Discussion

4.4.1. Fabrication of DNA Origami. DNA origami technology[6] is a method to create spatially fully addressable DNA nanostructures using ~200 short staple DNA strands to fold a single stranded genomic DNA (e.g. DNA of M13mp18, 7249 nucleotides long) into geometrically defined nanopatterns[7,8]. The schematic figure 4.1. illustrates the process of fabricating discrete AuNRs dimeric

structures using an equilateral triangular origami structure (~116 nm length of each arm) as a scaffold. The AuNRs were synthesized using the reported seed mediated method,[9] functionalized with desired DNA sequences (thiolated T_{15} or a random sequence, see SI for detailed information) using previously described method[10] and characterized by Transmission Electron Microscopy (TEM) imaging. They had aspect ratio of ~4 with average diameter 12±3.5 nm, average length 42.5±6.5 nm, and exhibited a longitudinal plasmonic band at ~785 nm and a transverse plasmonic band at ~520 nm (figure S1). To allow the AuNRs to be positioned onto the DNA nanostructures with precision, the DNA origami was modified at selective positions with corresponding staple strands extending out with single strand regions to complement the DNA displayed on the AuNR surface.

4.4.2. Immobilization Efficiency of Single Nanorod on DNA Origami Platform. We first tested the efficiency of immobilizing a single AuNR on the DNA origami to optimize the assembly process. In this case, five of the staple strands in the triangular origami was extended with a A_{15} sequence in the 5'end (capture probes), which are aligned linearly along one arm of the triangle (figure4.1.A) with the inter-probe distance ~ 10.4 nm (separated by 32 bps). The formation of the desired triangular origami structures was verified by TEM (figure S1) and purified by Microcon centrifugal device with 100 kD molecular cutoff filter. A 1:2 molar ratio of the DNA origami:AuNRs was used and the temperature was cycled 4 times from 45ºC to 30ºC at 0.1ºC/min to ensure complete hybridization of the DNA on the AuNRs to the capture probe strands

displayed on the DNA origami templates. The resultant mixture consists of extra un-hybridized AuNRs, one DNA origami associated with one AuNR (the desired structure), and some cross-linked structures (one AuNR associated with more than one DNA origami). The sample was then subject to agarose gel-electrophoresis to separate the different products (see figure S2). Triangular shaped DNA origami with a single AuNR has lower mobility than the free origami in a 1% native agarose gel. The fastest moving origami band was excised and extracted from the gel using Freeze-n-squeeze column (Biorad Inc.), and imaged by TEM. The samples were negatively stained with 0.7% Uranyl formate on the TEM grid before imaging.

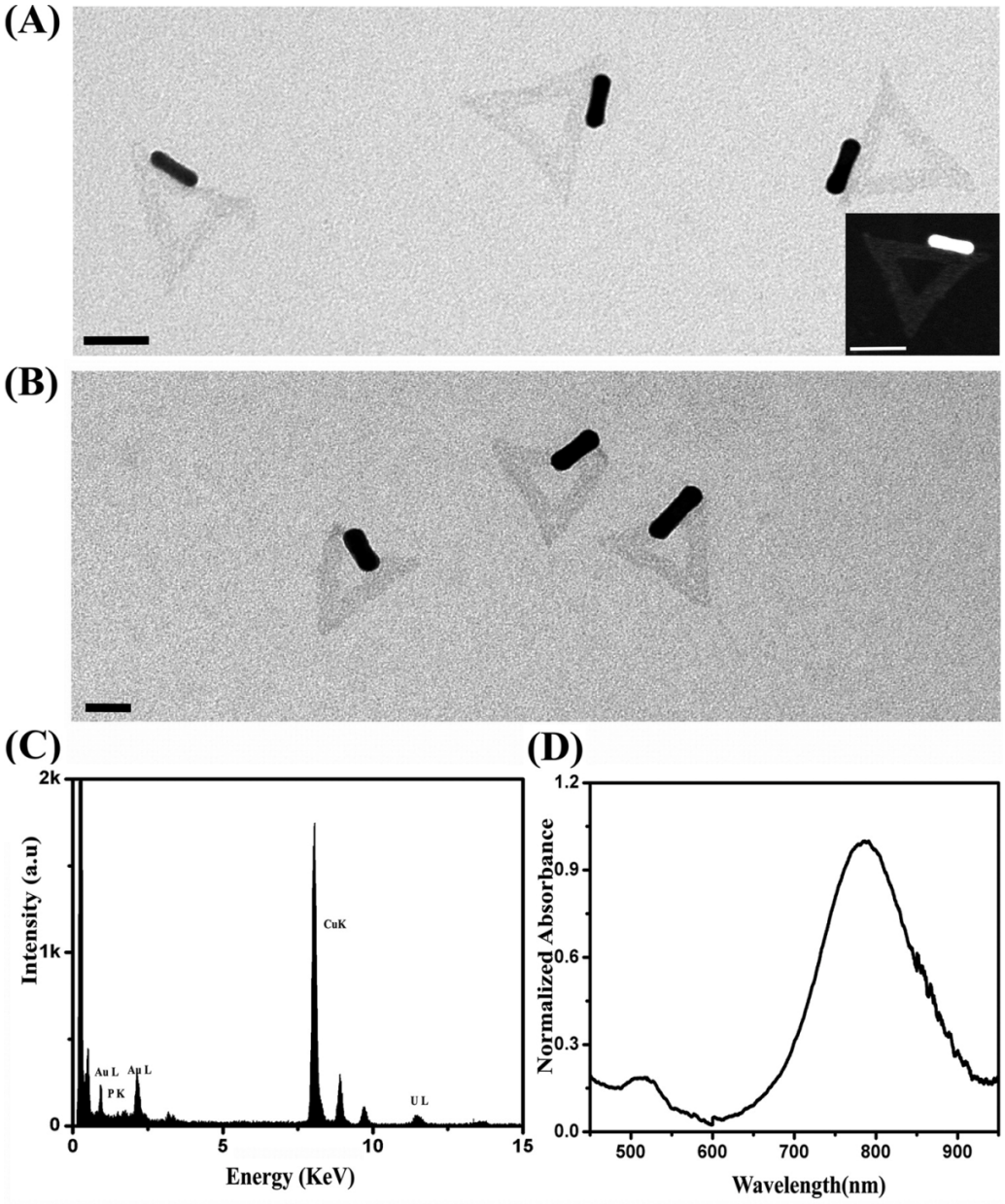

Figure 4.2. (A) Negatively stained TEM image of single AuNR immobilized on specific site parallel to one arm of triangular origami. (B) STEM image of the same sample. (C) Negatively stained TEM image of single AuNR immobilized on specific site making 30° angle to one arm of triangular origami. Scale bar is 50 nm.(D)EDS spectra of the structure. Au signal comes from AuNR and P signal comes from DNA origami. U signal is from uranyl formate staining and copper is

from the TEM grid. (E) UV-Vis-NIR spectra of monomeric structure showing longitudinal plasmon resonance at ~788 nm and transverse plasmon resonance at ~520 nm.

TEM images in 4.2. demonstrate that almost all DNA origami display one AuNR parallel to one of the triangle arms. The AuNRs are aligned precisely to the direction of capture strands as expected. The five captures strands spanning a distance of ~42 nm are enough to fix the AuNR's translational and rotational freedom with respect to the origami template. The assembly was further characterized using high-angle annular dark field-scanning Transmission Electron Microscopy (HAADF-STEM), which has the advantage of no requirement of heavy metal staining and high image contrast and resolution. STEM in combination with Energy Dispersive X-Ray Spectroscopy (EDS) analysis confirmed the elemental composition of the nanostructures.

We also verified that the AuNRs can be immobilized at arbitrary direction with respect to the triangular origami by simply redesigning the capture probe positions. For example, when the five capture strands were positioned to form a line that made a ~ 30º angle with the helix axis, we observed all the AuNRs attached on the DNA origami with the angle controlled about 30º±7º with respect to one arm of the triangle origami (see figure 2C and figure S5).

4.4.2. Fabrication of Dimeric AuNR Structures on DNA Origami Platform. Motivated by the high efficiency and precise control of the position and angle of a singular AuNR on the DNA origami, we further designed several discrete dimeric structures (figure 4.1.B) that have different angles between the

two AuNRs to increase the complexity of the assembly. To fabricate the dimeric assemblies, we designed two different sets ($C_1$and C_2) of five capture strands. One set (C_1) has the A_{15} sequence, same as that used for the monomeric structures. The other set (C_2) has a random probe sequence (12 nt long, see SI for details), complementary to the DNA sequence (C_2') functionalized on the other batch of AuNRs. Four different angles between the two probestrand sets were designed, 180° (end to end), 0° (side by side), 90°, and 60°, respectively (figure 4.1.B). The preassembled triangular origami was purified to remove extra staple strands, and then mixed with the two batches of AuNRs that were functionalized with sequences T_{15} and C_2', respectively, in a molar ratio of 1:2:2 in 0.5xTAE-Mg buffer (see SI for experimental details). Reduced buffer ions and Mg^{2+}concentration were used to minimize any cross-linking or aggregation of DNA origami. The mixture was then cycled between 45°C to 30°C four times at a rate of 0.1°C/min. Then the resultant solution was loaded onto a 1% agarose gel and electrophoresis was run for 45 min. The band corresponding to dimeric structure runs slower than the monomeric structure (see figure S2) and was carefully excised and extracted from the gel using previously described protocol.

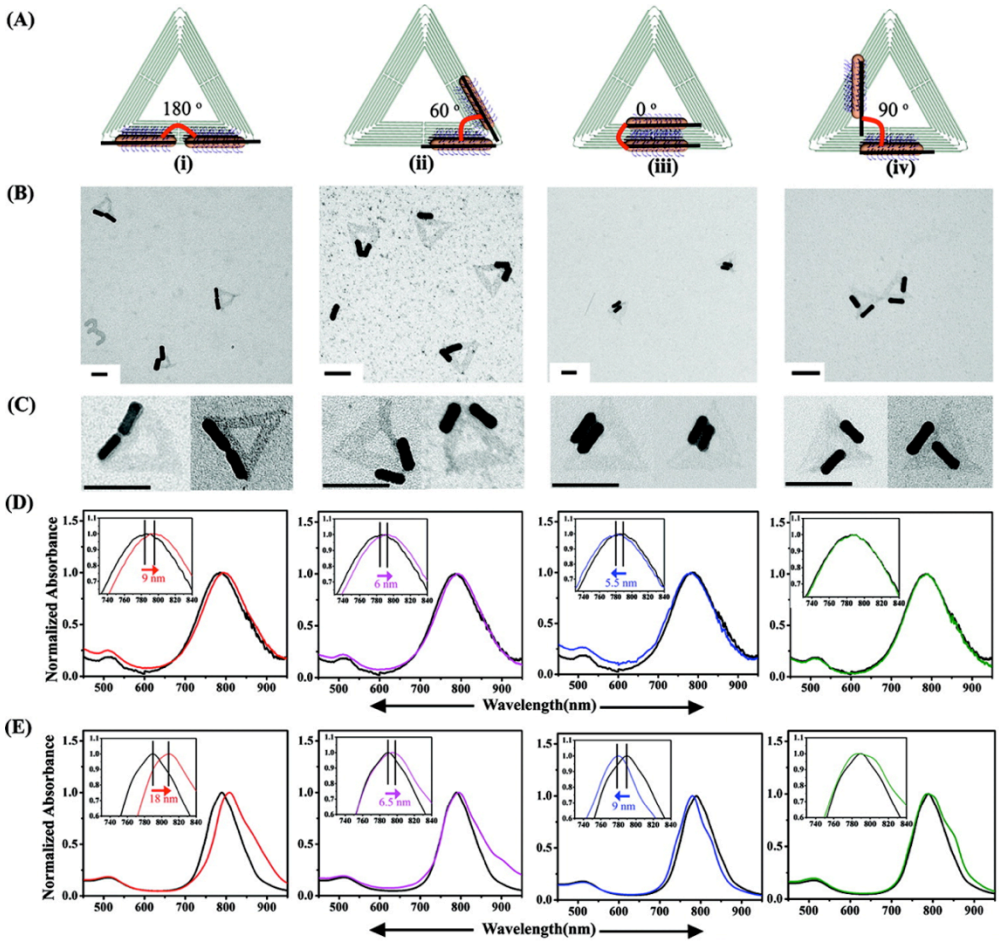

Figure 4.3. (A) (i)-(iv) Schematic representation of different dimer constructs having different inter-rod angles indicated. (B) Representative zoom-out TEM images of different dimer constructs. The samples were stained with 0.7% Uranyl Formate solution. (C) Representative zoom-in images showing dimer formation scaffolded by triangular origami structure. All scale bars are 100 nm. (D) UV-Vis spectrum of the purified dimeric constructs compared with monomeric construct (black curve). Construct (i) red curve and (ii) pink curve is red-shifted 9 and 6 nm respectively. Construct (iii) is blue-shifted by 5.5 nm. (iv) has no shift with respect to the monomeric construct. (E) Simulated UV-Vis spectrum corresponding the constructs of (i) to (iv) and the spectrum shown in D.

The formation and the angle distribution of the AuNR dimers were examined by TEM imaging (figure 4.3.B). The yields of all of the four different dimeric structures were in the range of 70-80% (summarized in Table 4.1). The rest of the structure were either de-formed or aggregated, probably due to damaging effect of the multiple centrifugation steps used in the purification procedure. The observed angles between the longigudal axis of the two nanorods were close to the designed angles. The observed angles were measured from 100 structured from TEM images. Some deviations of the observed angles from the designed angles were observed (Table 4.1). The deviation may be caused by two factors. One comes from the DNA origami that has some inherent local curvature although it is designed to be flat. Another possible reason is that the surface of the TEM grid may not be perfectly flat or the origami might not be deposited in flat orientation so that each individual origami may not be deposited on the TEM grid to be perpendicular to the electron beam during imaging, which could distort the observed angles.

Sample	Yield (%)	Designed angle	Observed angle	Designed distance(nm)	Observed distance(nm)
(i)	72	180	180±5	5.2	6.1±4.5
(ii)	77	60	63±9	3	5.0±3.5
(iii)	74	0	2±2	6	8.0±6.0
(iv)	81	90	87±8	15	16.0±7.0

Table 4.1. Assembly yields after purification, designed and the observed angles of the different dimeric structures. Sample size is 100 and ± represents standard deviation of the measured parameters.

4.4.3. Optical Measurements and Theoretical Calculations Dimeric AuNR Structures on DNA Origami Platform. We carried out UV-Vis spectra measurements of different gel purified samples of the above discrete structures. Monomeric constructs shows longitudinal plasmonic resonance (LSPR) peak at 786 nm. In contrast, we observed a bathochromic shift of LSPR for construct (i) and (ii) by ~9 nm and ~6 nm respectively (figure 4.3.D). Interestingly, we observed ~ 5.5 nm hypsochromic shift for construct (iii) and almost no shift for construct (iv).

Theoretical simulations by discrete dipole approximation (DDA) method[11] were performed for the optical spectra of the above AuNR dimers. In the simulation, we set both the length and diameter of the Au rod the same as those in

the experiments. The distances between two rods in the dimer were also from the experimental data. We considered size distribution and random orientation of single rod and dimer in the solution. The dielectric constants of Au are from Palik's handbook[12].

The first panel (leftmost) of figure 4.3.E shows the simulated extinction spectrum of two parallel Au rods with 180° angle and 6 nm end to end distance between the two rods in comparison with that of single AuNR construct. The resonance peak appears at 790 nm for the single rod and 808 nm for the dimer, which shows a red-shift of 18 nm. The shift is slightly larger than that of 9 nm obtained in the experiment. The difference might be from the smaller size distribution in the simulations in which only three different lengths and three diameters (total of 9 different sizes for the single rod) were carried out. When the inter-rod angle is 60° and distance is 5 nm, as the second panel in figure 4.3.E shows, the simulated resonance peak red shifted 5 nm to 795 nm, which is close to the experimentally measured 6 nm shift. The third panel of figure 4.3.D shows the simulated extinction spectrum of Au nanorod dimer of 0° angle and 8 nm distance. The resonance wavelength is at 780 nm with a blue-shift of 10 nm in comparison to that of the single rod. When the two rods in the dimer were arranged in a 90° angle and separated with a 16 nm distance, the resonance peak of the dimer appears at 787 nm, as shown in the fourth panel of figure 4.3.E, which is close to that of single rod but has a slight blue shift. All the peaks around 520 nm don't change much in comparison with that of single rod. Overall, the trend and the range of the spectrum shift matches well with the experimentally

measured spectrum from the DNA origami directed AuNR dimer samples. The slight discrepancy could come from the less than 100% yield the assembly and possible degradation/distortion of the structures after the purification. Future single particle spectroscopy and imaging (ideally topographical imaging combined with simultaneous spectrum measurement) may correspond more accurately between experiments and simulation. Nevertheless, the directed self-assembly strategy demonstrated here is promising in constructing and studying higher order metallic nanostructures with high programmability.

4.4.4. Fabrication of 1:1 AuNP-AuNR Structures on DNA Origami Platform. One of the potential applications of DNA directed AuNR assembly is to precisely position other molecules or particles such as fluorescent dyes or nanoparticles relative to the assembled AuNR so their interactions corresponding due to the structural anisotropy of AuNRs and the predicted non-uniform distribution of electric fields around it can be investigated. To explore the possibility to selectively position nanoparticles at unique positions around the nanorod, we constructed a series of hetero-dimer formation by placing a 10 nm AuNP relative to the AuNR on the triangular shaped DNA origami and demonstrated the excellent programmability of using DNA directed assembly to create asymmetric metallic nanoarchitectures.

The positioning of AuNPs with respect to the AuNR (side-on or end-on) was pre-determined by selectively modifying a corresponding staple strand at the desired location on the origami with a thiol group (figure 4.4.A). The 10 nm AuNP was attached to this staple strand in a 1:1 ratio[13]. Then it was mixed with

the M13 scaffold DNA and all the other staple strands including five capture strands extended with A_{15} for immobilizing the AuNR, at 1:1:5 ratio. After annealing, the origami structure that each contained a single AuNP at the desired location was obtained with a very high yield ~ 95% (see figuresS15-16 and 19-20). The construct was purified using Microcon 100 kD MWCO centrifugal device to get rid of extra staple strands, then it was mixed with the T_{15} DNA functionalized AuNRs in a 1:2 ratio, slowly annealed and gel purified for TEM imaging.

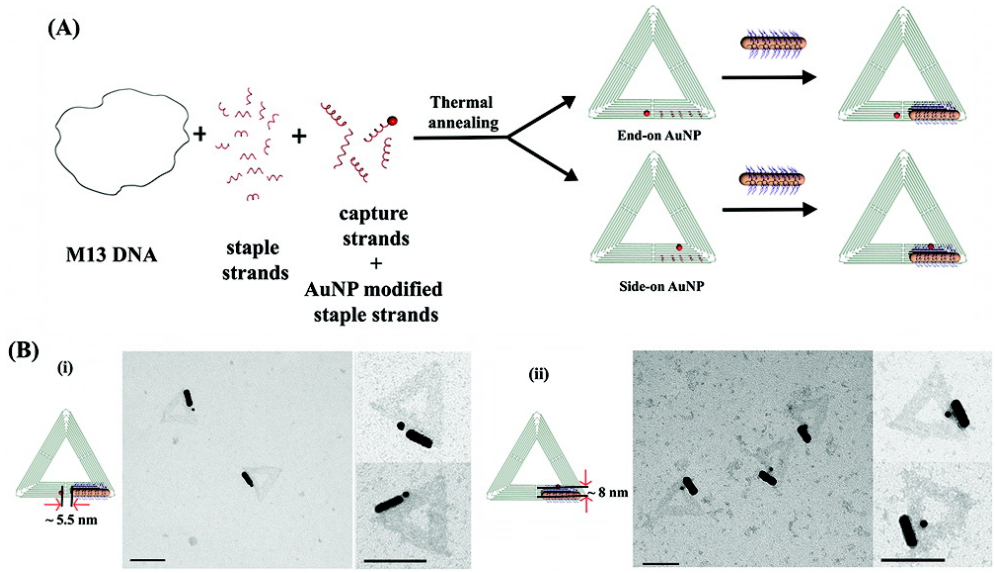

Figure 4.4. (A) Scheme of formation of side-on and end-on AuNR-AuNP hetero dimers. (B) Schematic diagrams and TEM images of end-on and side-on AuNR-AuNP hetero dimmers. Scales bars are100 nm.

Figure 4.4. B shows the representative images of the end-on and side-on hetero-dimeric constructs, respectively. It is clear that both the orientation and the distances of the 10 nm AuNPs relative to the AuNR can be dictated and controlled precisely using the DNA origami scaffold. For example, the designed distance of

the end-on AuNP from the tip of the AuNR was expected to be ~5.5 nm (design shown in SI). The measured distance was 8±4 nm. Similarly the distance of the side on dimer was expected to be ~ 8 nm, and the measured distance was 10±5 nm. The small deviation of the measured distance from the designed distance can be attributed to the size uncertainty of the AuNRs (~10% variance in both dimensions), and the flexibility of the 15 base pair capture strand region, which may have a maximum ~ 5 nm spatial range on the surface of the origami.

4.5. Conclusions. In summary, we have introduced a robust and programmable strategy to immobilize AuNR (12x42 nm) at specific positions and orientations on a DNA origami scaffold. This method was extended to assemble a number of different AuNR dimeric structures with predefined angles. We have also demonstrated that using the DNA origami as molecular scaffold, we can break the spatial symmetry of the nanoparticle and nanorods by placing a 10 nm AuNP on the end or side position of a single AuNR reliably with controlled distances. This strategy overcomes the challenging problem of site-specific placement of a single particle or molecule close to a single AuNR, and it will open new avenues to characterize the distance, and geometry dependent photonic interactions of AuNR with other nanophotonic elements, such as molecular fluorophores, quantum dots, and other plasmonic nanoparticles.

4.6. References.

(1) Burda, C.; Chen, X. B.; Narayanan, R.; El-Sayed, *M. A. Chem. Rev.* **2005**, 105, 1025–1102.

(2) Huang, X. H.; Neretina, S.; El-Sayed, M. A. *Adv. Mater.* **2009**, 21, 4880–4910.

(3) (a) Yu, C.; Irudayaraj, J. *Biophys. J.* **2007**, 93, 3684–3692. (b) Yu, C.; Nakshatri, H; Irudayaraj, J. *Nano Lett.* **2007**, 7 (8), 2300–2306. (c) Wang, L.; Zhu, Y.; Xu, L.; Chen, W.; Kuang, H.; Liu, L.; Agarwal, A.; Xu, C.; Kotov, N. A. *Angew. Chem., Int. Ed.* **2010**, 49 (32), 5472–5475. (d) Dickerson, E. B.; Dreaden, E. C.; Huang, X.; El-Sayed, I. H.; Chu, H.; Pushpanketh, S.; McDonald, J. F.; El-Sayed, M. A. *Cancer Lett.* **2008**,269, 57–66.

(4) Li, Y.; Qian, F.; Xiang, J.; Lieber, C. M. *Mater. Today* **2006**, 9, 18–27.

(5) Lu, W.; Lieber, C. M. J. Phys. D: *Appl. Phys.* **2006**, 39, R387–R406.

(6) Rothemund, P. W. K. *Nature* **2006**, 440, 297–302.

(7) Nangreave, J.; Han, D.; Liu, Y.; Yan, H. *Curr. Opin. Chem. Biol.* **2010**, 14, 608–615.

(8) Shih, W. M.; Lin, C. *Curr. Opin. Struct. Biol.* **2010**, 20, 276–282.

(9) Tan, S. J.; Campolongo, M. J.; Luo, D.; Cheng, W. *Nat. Nanotechnol.* **2011**, 6, 268–276.

(10) Nikoobakht, B.; El-Sayed, M. A. *Chem. Mater.* **2003**,15, 1957–1962.

(11) Jones, M. R.; Macfarlane, R. J.; Lee, B.; Zhang, J. A.; Young, K. L.; Senesi, A. J.; Mirkin, C. A. *Nat. Mater.* **2010**, 9, 913–917.

(12) (a) Purcell, E. M.; PennyPacker, C. R. *Astrophys. J.* **1973**, 186, 705–714. (b) Draine, B. T. *Astrophys. J.* **1988**, 333, 848–872.

(13) Palik, E. D. Handbook of Optical Constants of Solids; Academic Press: New York, **1985**.

(14) Sharma, J.; Chhabra, R.; Anderson, C. S.; Gothelf, K. V.; Yan, H.; Liu, Y. *J. Am. Chem. Soc.* **2008**, 130, 7820–2821.

Chapter 5

Site-Specific Synthesis and *in-situ* Immobilization of Fluorescent Silver Nanoclusters on DNA Nanoscaffolds using Tollens Reaction

Adapted with permission from Angew. Chem. Int. Ed. 2011, 50, 4176-4179. Wiley-VCH Verlag GmbH & Co. KGaA. 2011.

5.1. Abstract

In this work DNA strands with specific sequences and covalently attached sugar moieties were used for the site-specific incorporation of the sugar units on a DNA origami scaffold. This approach enabled the subsequent site-specific synthesis and in situ immobilization of fluorescent Ag clusters at predefined positions on the DNA nanoscaffold by treatment with the Tollens reagent.

5.2. Introduction

Fluorescent silver nanoclusters (Ag-NCs) of less than 2 nm in diameter have recently been emerged as a new class of nanomaterials that may find potential applications in nanosciences and nanotechnology.[1] A variety of methods have been demonstrated in recent years for the synthesis of fluorescent Ag-NCs,[2-14] among which the DNA templated synthesis of Ag-NCs[15,16] is particularly attractive, due to the low toxicity, good biocompatibility and unique optical properties of the Ag-NCs obtained. DNA nanostructures also has been envisoned as template for metallization such as gold or silver to create nanowires with desired patterns or junctions for nanoelectronics[17]. However, site specificity and uniform distribution of the metal NCs along the DNA templates remained a

challenge, which is crucial for the homogeneity and the efficiency of the subsequent metallization.

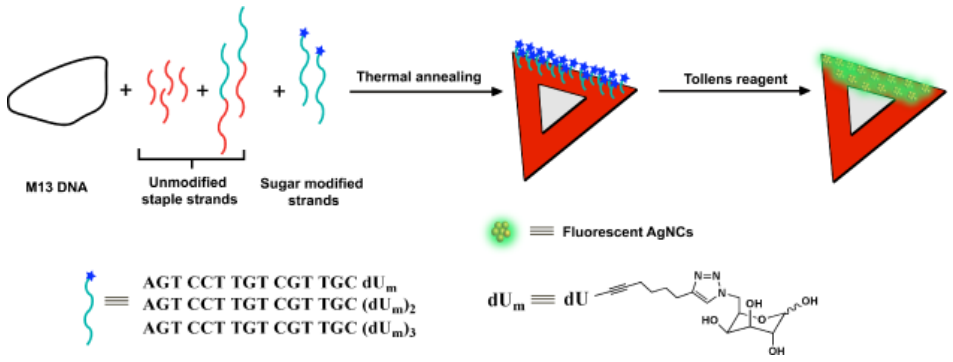

Figure 5.1. Schematic representation of the site specific immobilization of fluorescent Ag-NCs on a triangular-shaped DNA origami scaffold and the corresponding sequences of the probe DNAs used in this study (Sequences are shown from 3′→5′).

Here we describe a new DNA based method for the synthesis of water soluble fluorescent Ag-NCs with narrow size distribution using the well-known Tollens' reaction scheme, which is commonly employed in carbohydrate chemistry to test aldehyde structure of reducing sugars.[17f] We covalently incorporated discrete numbers of sugar moieties into a DNA sequence at adjacent positions and hoped this would enable synthesis of Ag-NCs by the specific stoichiometry of the Tollens' reaction, i.e. one aldehyde sugar molecule can reduce two Ag^+ into $Ag(0)_2$. These Ag-clusters can then act as nucleation sites for further Ag deposition under a mild reductive condition. Tethering the sugar functional groups to DNA offers stabilization of the Ag-NCs synthesized[15] while the DNA strands can still serves as addressable points for further sequence-specific DNA hybridization. "DNA Origami"[18] have become a superior nanoscale

scaffold for the organization of various classes of functional materials.[19] Herein we demonstrate the site-specific synthesis and *in-situ* immobilization of Ag-NCs on a triangular shaped 'DNA-origami'[18] (Scheme 1). The addressability of DNA origami allows the site- specific synthesis and *in-situ* incorporation of fluorescent Ag-NCs on the pre-defined DNA scaffolds with nano-meter scale spatial resolution.

5.3. Materials and Method

See APPENDIX D

5.4. Results and Discussion

5.4.1. DNA Directed Synthesis of Ag-NCs. We first synthesized sugar (galactose) modified DNA strands, DNA1, DNA2 and DNA3, each contains 15 nucleotides and 1, 2 or 3 consecutive modified deoxyurinidine (dU_m) units, respectively, that each dU_m carries a sugar unit, following a reported synthetic strategy.[20] Details on the synthesis and structural characterization of DNA1−DNA3 are shown in the Supporting Information. Tollens' reagent $[Ag(NH_3)_2^+]$ was first prepared by adding NH_4OH (28%) to a solution of $AgNO_3$ in 1 × TAE-Mg^{2+} buffer (40 mM Tris base, 20 mM acetic acid, 2 mM EDTA and 12.5 mM Mg acetate) in dark, followed by addition of excess NH_4OH to dissolve the precipitated Ag(OH). The Tollens' reagent was filtered and then added to the sugar modified DNAs (DNA1, DNA2 or DNA3) in 1 × TAE-Mg^{2+} buffer and incubated overnight in dark at room temperature.

The reaction product with DNA1 exhibits a fluorescence emission maximum at 412 nm and an excitation maximum at 337 nm. The corresponding products with

DNA2 and DNA3 exhibit similar emission maxima at 411 nm ($\lambda_{ex,max}$ = 337 nm) and 420 nm ($\lambda_{ex,max}$ = 337 nm), respectively (figure. 1a). The fluorescence spectra clearly indicate formation of similar sized emissive Ag-NCs using the DNA strands carrying different number of sugar units. This observation is not as expected based on the simple stoichiometry of the Tollen' reaction. We propose that the further growth of silver cluster occurs following the formation of the initial $Ag(0)_n$ (n=2, 4 or 6) seed created by the Tollens' reaction, and the particle size finally obtained depends on Ag^+/DNA ratio irrespective of sugar units present on the DNA. No significant change to the emission of NCs was observed even after several days of incubation, indicating excellent photo-stability of the Ag-NCs under these conditions. For all of the three reaction products, the characteristic Ag plasmon absorption band at around 400-450 nm was not observed, indicating no formation of larger sized Ag nanoparticles (NPs). Transmission electron microscope (TEM) and scanning transmission electron microscope (STEM) images (figure. 1c, d) show the NCs are nearly mono-dispersive with an average size ~ 2 nm. TEM image analysis for the NCs obtained using DNA1 and DNA2 also confirmed these NCs had similar sizes (see SI), consistent with the similar optical properties of the NCs observed. The mechanism for the formation of Ag-NCs is speculated that the initial reduction of Ag^+ by the sugar units was followed by the further reduction of extra Ag^+ ions by the presence of tris(hydroxymethyl)-aminomethane (Tris) in the 1 × TAE buffer solution and the further growth of the cluster size would maximize based on the initial molar ratio of Ag^+ to the sugar modified DNA. The kinetic evidences

supporting this proposed mechanism with varying Tris concentration are shown in the SI. It is estimated that a 2 nm diameter Ag-NC contains ~ 200 Ag atoms. In our experiment, 200 fold excess of Ag^{+} relative to the concentration of DNA was used and hence the expected size of ~ 2 nm for the NCs is in good agreement with our hypothesis.

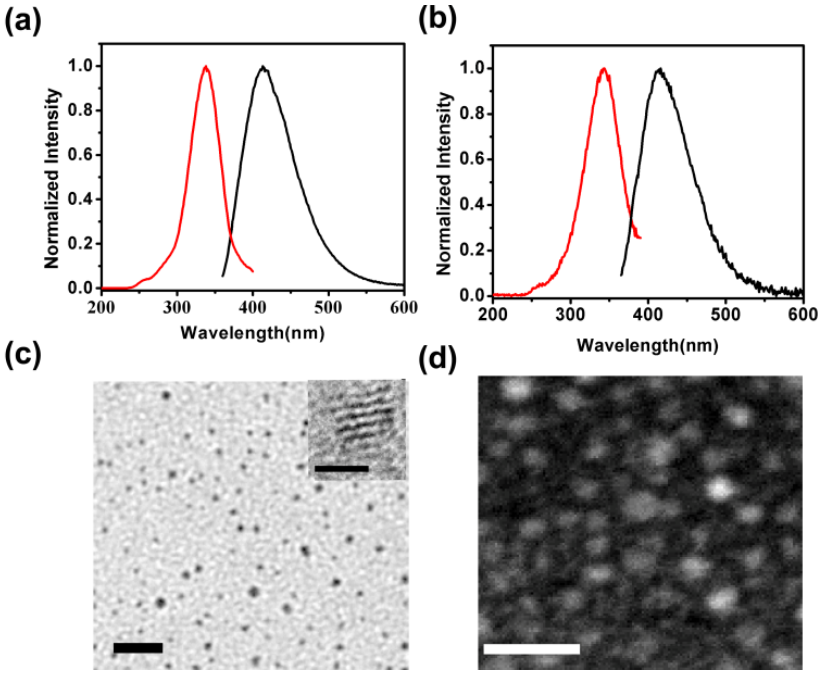

Figure 5.2. Excitation (black) and emission (red) spectra of Ag-NCs synthesized after the treatment of Tollens' reagent with a) free **DNA3**, and b) on DNA origami. c) TEM and d) STEM images of NCs synthesized using free **DNA3**. The inset in c) represents a high resolution TEM image of the nanocluster. Scale bars: 10 nm (c and d), and 2 nm (c, inset).

5.4.2. Site-Specific Immobilization of Ag-NCs on Triangular Origami.

We further carried out experiments to immobilize these fluorescent NCs site specifically onto a triangular-shaped DNA origami. The DNA M13mp18 (7249 nt) scaffold strand was mixed with 5-fold helper strands (total 205 helper strands) and 650 fold of DNA3 in 1xTAE-Mg^{2+} buffer. Roughly one third of the total helper strands (65 out of 205) located on one arm of the triangle were extended on the 3′ end to carry an additional 15 base segment of DNA sequence complementary to that of DNA3 (figure 5.1.). Therefore after annealing, the sugar modified strands hybridize with these probe strands to form DNA duplexes each carrying three sugar moieties, that are displayed on the surface of the triangle DNA origami along one of the three arms (see Supporting Information for details). The assembled DNA origami was purified by agarose gel electrophoresis to get rid of excess helper strands and excess DNA3 to prevent non-site-specific Ag-NC formation.

5.4.3. **AFM Characterization of Site-Specific Immobilization of Ag-NCs on Triangular Origami:** AFM analysis of the purified sample shows the formation of designed shape of the triangle origami, in which each arm has a length of ~ 114 nm, in good agreement with the calculated length (~115 nm) of the design (figure. 2a). The site specific display of protruding duplex of helper strands and **DNA3** along one arm of the triangle produces a bright topographical feature in the AFM image that is higher than the other two bare arms (figure. 2a). AFM cross-section analysis shows an average height of ~ 3.4 nm for this arm, which almost doubles the height of the bare arms of the triangular-origami

(figure. 2c). This indicates that the duplexes are likely lying flat rather than standing up on the origami surface under the tapping mode AFM. We performed the Tollens' reaction on the DNA origami scaffold under the same experimental conditions as that for the free **DNA3** in solution with the same molar ratio of Ag^+ to sugar modified DNA of 200. Fluorescence spectrum of such prepared sample revealed an emission maximum at 418 nm and an excitation maximum at 340 nm (figure. 5.2.b). This indicates the fluorescent Ag-NCs grown *in-situ* on the origami scaffold have optical characteristics that are similar to the NCs obtained using free **DNA3**. Similarly, no Ag-NP formation with measureable surface plasmon resonance is observed even after several days of incubation. AFM analysis of the DNA origami sample after the Tollens' reaction reveals a brighter strip on one arm of the triangle compared to the other two arms (figure. 5.3. b), with a mean height of ~ 5.5 nm. This is due to the site specific immobilization of Ag-NCs along this arm. The ~ 2.1 nm height difference before and after the Tollens' reaction could be the apparent diameter of the Ag-NCs synthesized and deposited in-situ (figure. 5.3.d). No NCs deposition was observed in other regions of the triangle origami scaffold, which demonstrates the excellent site specificity of our DNA templated approach. The sugar units act as the nucleation sites for the Ag-NC formation. DNA scaffold here don't play any reactive role for reducing Ag^+ ions, but only act as structural scaffold. TEM image analysis further confirmed the site specific immobilization of Ag-NCs on the DNA origami nanostructure (figure. 5.4.). The sample was stained using uranyl formate, so that the DNA origami scaffold was also visible along with the Ag-NCs in the TEM

images. A significant contrast difference is observed in one arm of the triangle compared with the other two arms (figure. 5.4.a). Same as the result by AFM analysis, no NC deposition was observed in any other part of the triangle structure.

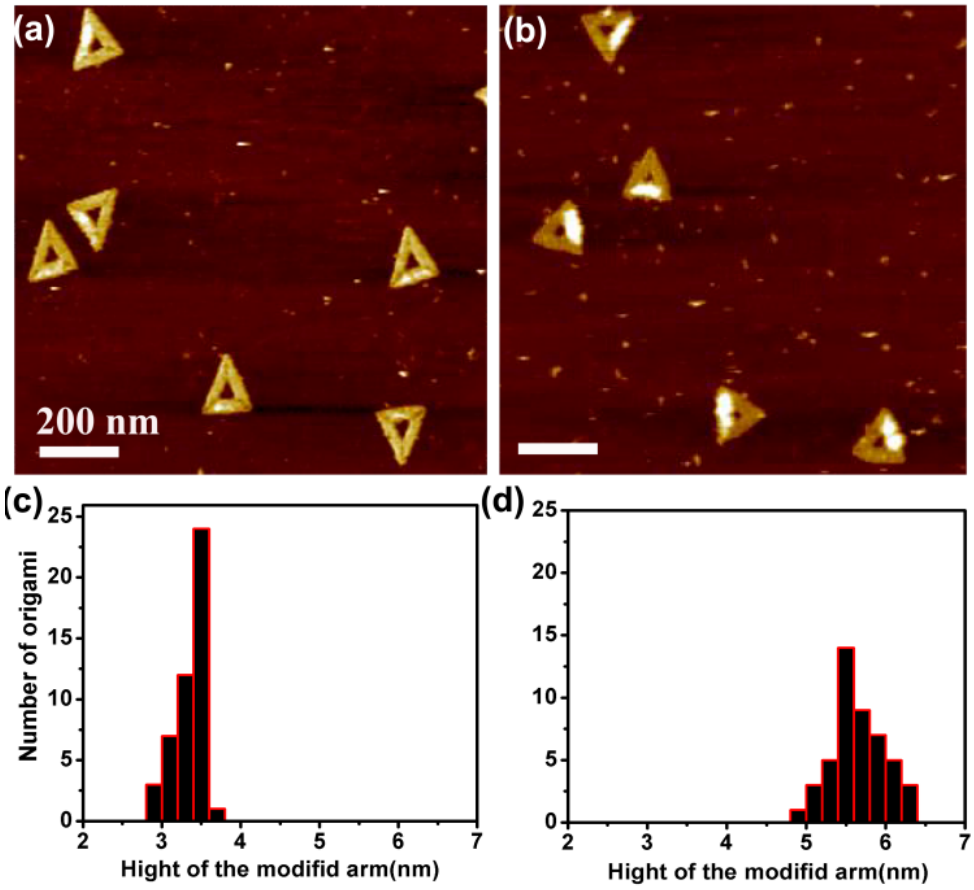

Figure 5.3. AFM images show the site specific incorporation of **DNA3** and the subsequent *in-situ* synthesis and site specific immobilization of Ag-NCs on a particular arm of the triangular shaped DNA origami scaffold. AFM images a) before and b) after the treatment with Tollens reagent (z-scale = 10 nm) and the corresponding histograms showing the height of the bright feature on the origami c) before and d) after the treatment with Tollens reagent.

5.4.4. HRTEM Characterization of Site-Specific Immobilization of Ag-NCs on Triangular Origami:

High resolution-TEM (HR-TEM) image shows a nearly uniform distribution of Ag-NCs with a diameter of ~ 2 nm (figure. 5.4.b), which is the same as the size of NCs obtained with free **DNA3** in solution. The density of the NC per unit area is consistent with the density of the DNA probe strands distributed along the arm of the DNA origami. Since the estimated yield of the hybridization between the probes and the **DNA3** is 100%, this result reveals that each DNA molecule carrying three consecutive sugar moieties in close positions actually acts as one unique nucleation site in the Ag-NC deposition. Furthermore, energy-dispersive X-ray spectroscopy (EDX) of these structures confirmed the presence of silver element on the DNA scaffold (5.4.c).

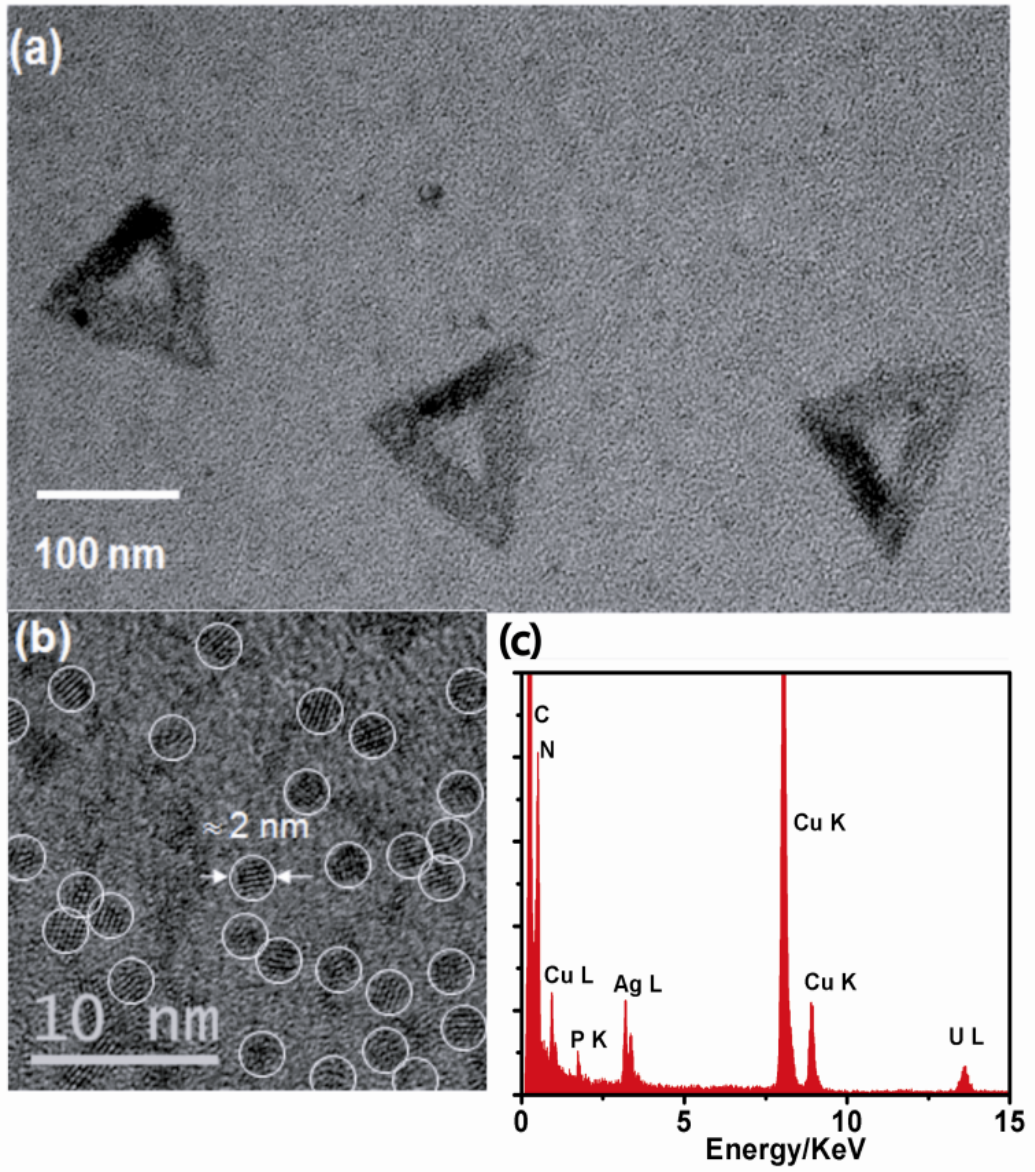

Figure 5.3. a) TEM image of the origami structure after the treatment with Tollens' reagent (sample is negative stained with uranyl formate) and b) the corresponding high resolution TEM image of the NCs immobilized on this arm. c) EDX spectrum of the Ag-NCs on the DNA origami structure.

5.5. Conclusions

In summary, I have demonstrated a new DNA based method for the synthesis of water soluble fluorescent Ag-NCs using the well known Tollens' reaction. The sugar moieties covalently attached on DNA of specific sequences have been successfully employed for site specific incorporation of the sugar units on a triangular shaped DNA origami scaffold that allows the subsequent site-specific synthesis and *in-situ* immobilization of Ag-NCs at the pre-defined positions on the DNA nanoscaffold. The high density array of emissive NCs obtained may have potential applications in many fields, such as the fabrication of semiconductor nanostructures.[21] Our new approach has excellent site specific control of NC nucleation and yields uniform sized high density arrays of Ag-NCs, thus offers a unique platform for the subsequent site specific deposition of other metals, such as gold, which may lead to future advances in DNA based nanoelectronics.

5.6 References

(1) a) Peyser, L. A.; Vinson, A. E.; Bartko, A. P.; Dickson, R. M. *Science* **2001**, 291, 103 – 106; b) Palmer, R. E.; Pratontep, S.; Boyen, H.-G. *Nat. Mater.* **2003**, 2, 443 – 448; c) Lee, T.-H.; Gonzalez, J. I.; Zheng, J.; Dickson, R. M. *Acc. Chem. Res.* **2005**, 38, 534 – 541; d) Lesniak, W.; Bielinska, A. U.; Sun, K.; Janczak, K. W.; Shi, X.; Baker, Jr., J. R.; Balogh, L. P. *Nano Lett.* **2005**, 5, 2123 – 2130.

(2) Zheng, J.; Dickson, R. M. *J. Am. Chem. Soc.* **2002**, 124, 13982 –13983.

(3) Zhang, J.; Xu, S.; Kemacheva, E. *Adv. Mater.* **2005**, 17, 2336 – 2340.

(4) Branham, M. R.; Douglas, A. D.; Mills, A. J.; Tracy, J. B.; White, P. S.; Murray, R. W. *Langmuir* **2006**, 22, 11376 – 11383.

(5) Yu, J.; Patel, S. A.; Dickson, R. M. *Angew. Chem*. **2007**, 119, 2074 – 2076; *Angew. Chem. Int. Ed.* **2007**, 46, 2028 – 2030.

(6) Nishida, N.; Yao, H.; Ueda, T.; Sasaki, A.; Kimura, K. *Chem. Mater.* **2007**, 19, 2831 – 2841.

(7) Shen, Z.; Duan, H.; Frey, H. *Adv. Mater.* **2007**, 19, 349 – 352.

(8) Narayanan, S. S.; Pal, S. K. *J. Phys. Chem. C* **2008**, 112, 4874 –4879.

(9) Shang, L.; Dong, S. *Chem. Commun.* 2008, 1088 – 1090.

(10) Anson, C. E.; Eichh, AIssac, .; I.; Fenske, D.; Fuhr, O.; Sevillano, P.; Persau, C.; Stalke, D.; Zhang, J. *Angew. Chem*. **2008**,120, 1346 – 1351; *Angew. Chem. Int. Ed.* **2008**, 47, 1326 – 1331.

(11) Yu, J.; Choi, S.; Dickson, R. M. *Angew. Chem.* **2009**, 121, 324 –326; *Angew. Chem. Int. Ed.* **2009**, 48, 318 – 320.

(12) Wu, Z.; Lanni, E.; Chen, W.; Bier, M. E.; Ly, D.; Jin, R. *J. Am. Chem. Soc.* **2009**, 131, 16672–16674.

(13) H. Xu, K. S. Suslick, *Adv. Mater.* **2010**, 22, 1078–1082.

(14) Rao, T. U. B.; Pradeep, T. *Angew. Chem.* **2010**, *122*,4017 – 4021; *Angew. Chem. Int. Ed.* **2010**, 49, 3925 – 3929.

(15) a) Petty, J. T.; Zheng, J.; Hud, N. V.; Dickson, R. M. *J. Am. Chem. Soc.* **2004**, 126, 5207 – 5212; b) Richards, C. I.; Choi, S.; Hsiang, J.-C.; Antoku, Y.; Vosch, T.; Bongiorno, A.; Tzeng, Y.-L.; Dickson, R. M. *J. Am. Chem. Soc.* **2008**, 130, 5038 – 5039; c) Petty, J. T.; Fan, C.; Story, S. P.; Sengupta, B.; Iyer, A. S. J.; Prudowsky, Z.; Dickson, R. M. J. *Phys. Chem. Lett.* **2010**, 1, 2524 – 2529.

(16) a) Sengupta, B.; Ritchie, C. M.; Buckman, J. G.; Johnsen, K. R.; Goodwin, P. M.; Petty, J. T.; *J. Phys. Chem. C* **2008**, 112, 18776 –18782; b) Sengupta, B.; Springer, K.; Buckman, J. G.; Story, S. P.; Henry Abe, O.; Hasan, Z. W.; Prudowsky, Z. D.; Rudisill, S. E.; Degtyareva, N. N.; Petty, J. T. *J. Phys. Chem. C* **2009**, 113, 19518 –19524; c) Gwinn, E. G.; ONeill, P.; Guerrero, A. J.; Bouwmeester, D.; Fygenson, D. K. *Adv. Mater.* **2008**, 20, 279 – 283; d) Guo, W.; Yuan, J. ; Wang, E. *Chem. Commun.* **2009**, 3395 – 3397;e) ONeill, P. R.; Velazquez, L. R.; Dunn, D. G.; Gwinn, E. G.; Fygenson, D. K. *J. Phys. Chem. C* **2009**, 113, 4229 – 4233; f) Sharma, J.; Yeh, H.-C.; Yoo, H.; Werner, J. H.; Martinez, J. S. *Chem.Commun.* **2010**, 46, 3280 – 3282; g) Guo, W.; Yuan, J.; Dong, Q.; Wang, E. *J. Am. Chem. Soc.* **2010**, 132, 932 – 934; h) Molotsky, T.; Tamarin, T.; Moshe, A. B.; Markovich, G; Kotlyar, A. B. *J. Phys.Chem. C* **2010**, 114, 15951 – 15954.

(17) a) Braun, E.; Eichen, Y.; Sivan, U.; Ben-Yoseph, G. *Nature* **1998**,391, 775 – 778; b) Richter, J.; Seidel, R.; Kirsch, R.; Mertig, M.; Pompe, W.; Plaschke, J.; Schackert, H. K. *Adv. Mater.* **2000**, 12, 507 –510; c) Weizmann, Y.; Patolsky, F.; Popov, I.; Willner, I. *Nano Lett.* **2004**, 4, 787 – 792; d) Berti, L.; Alessandrini, A.; Facci, P.; *J. Am.Chem. Soc.* **2005**, 127, 11216 – 11217; e) Fischler, M.; Simon, U.; Nir, H.; Eichen, Y.; Burley, G. A.; Gierlich, J.; Gramlich, P. M. E.; Carell, T. *Small* **2007**, 3, 1049 – 1055; f) Wirges, C. T.; Timper, J.; Fischler, M.; Sologubenko, A. S.; Mayer, J.; Simon, U.; Carell, T. *Angew. Chem.* **2009**, 121, 225 – 229; *Angew. Chem. Int. Ed.* **2009**,48, 219 – 223.

(18) P. W. K. Rothemund, *Nature* **2006**, 440, 297 – 302.

(19) a) Sharma, J.; Chhabra, R.; Andersen, C. S.; Gothelf, K. V.; Yan, H.; Liu, Y. *J. Am. Chem. Soc.* **2008**, 130, 7820 – 7821; b) Pal, S.; Deng, Z.; Ding, B.; Yan, H.; Liu, Y. *Angew. Chem.* **2010**, 122, 2760;*Angew. Chem. Int. Ed.* **2010**, 49, 2700 – 2704; c) Hung, A. M.; Micheel, C. M.; Bozano, L. D.; Osterbur, L. W.; Wallraff, G. M.; Cha, J. N. *Nat. Nanotechnol.* **2010**, 5, 121 – 126; d) Bui, H.; Onodera, C.; Kidwell, C.; Tan, Y.,Graugnard, E.; Kuang,W.; Lee, J.; Knowlton, W. B.; Yurke, B.; Hughes, W. L. *Nano Lett.* **2010**, 10, 3367; e) Maune, H. T.; Han, S.-p.; Barish, R. D.; Bockrath, M.; Goddard III, W. A.; Rothemund, P. W. K.; Winfree, E. *Nat. Nanotechnol.* **2009**, 4, 61 – 66; f) Numajiri, K.; Yamazaki, T.; Kimura, M.; Kuzuya, A.; Komiyama, M. *J. Am. Chem. Soc.* **2010**, 132, 9937 – 9939; g) Sacca, B.; Meyer, R.; Erkelenz, M.; Kiko, K. ; Arndt, A.; Schroeder, H.; Rabe, K. S.; Niemeyer, C. M. *Angew. Chem.* **2010**, 122, 9568; *Angew. Chem. Int. Ed.* **2010**, 49, 9378 – 9383; h) Voigt, N. V.; Tørring, T.; Rotaru, A.; Jacobsen, M. F.; Ravnsbæk, J. B.; Subramani, R.; Mamdouh, W.; Kjems, J ; Mokhir, A.; Besenbacher, F.; Gothelf, K. V. *Nat. Nanotechnol.* **2010**, 5, 200 –203; i) Sannohe, Y.; Endo, M.; Katsuda, Y.; Hidaka, K.; Sugiyama, H. *J. Am. Chem. Soc.* **2010**, 132, 16311 – 16313.

(20) Burley, G. A.; Gierlich, J.; Mofid, M. R.; Nir, H.; Tal, S.; Eichen, Y.; Carell, T. *J. Am. Chem. Soc.* 2006, 128, 1398 – 1399.

Chapter 6

Summary and Outlook

6.1. Conclusions

DNA-templated plasmonic nanostructures has experienced significant maturation, along with the continuous advancements in the nanoparticle synthesis, surface modification chemistry, structural DNA nanotechnology and nanoscale lithographic techniques. This development will ultimately lead to the realization of real-world applications, such as wave guiding, energy harvesting, sensing, etc. Dimeric structures of gold and silver nanoparticles held by DNA scaffold have already been demonstrated as robust molecular rulers for extended real-time monitoring of single-DNA hybridization events.[1] Such plasmon rulers are advantageous over traditional FRET-based molecular beacons because they are not limited by photobleaching, inherent signal fluctuations, or a low distance limit (~ 10 nm). Interparticle nanogaps between dimeric gold nanoparticles have been used to develop highly sensitive single-molecule detection based on strong surface enhanced Raman scattering (SERS) effects.[2] The DNA-directed self-assembly of metallic nanoparticles has been also extended to other nanomaterials, for examples carbon nanotubes, graphene, quantum dots, magnetic nanoparticles and other molecules. For example, a network of fluorophores was created to setup a complex four color FRET system in order to monitor and control the energy transfer paths on a DNA origami.[3]

In this thesis, I have successfully demonstrated the versatility of DNA directed self-assembly of metallic nanoparticles and solved a few challenging

problems in this field. As described in chapter 2, I developed an easy to use and robust strategy to achieve DNA functionalized AgNP that are stable in high salt conditions and then have demonstrated the self-assembly of discrete numbers of AgNP and AgNP-AuNP nano architectures using rationally designed DNA origami template. In chapter 3, I have developed a robust strategy to create different distances between a fluorophore and metallic nanoparticles using DNA origami as a distance ruler. We observed 50% enhancement in QE with both 26 and 35 nm gap distances for the 30 nm AuNP dimer, which is supported by theory. This work can potentially open up the possibility of creating nanoparticle assemblies with very high field enhancements (using gold nanorod dimer or silver nanoparticle dimer, etc.), which can possibly lead to much higher enhancements in fluorescence. In chapter 4, I have introduced a robust and programmable strategy to immobilize anisotropic Au nanorods at specific positions and orientations on a DNA origami scaffold. This method was extended to assemble a number of different AuNR dimeric structures with predefined angles. In chapter 5, I demonstrated a new DNA based method for the *in-situ* site-specific synthesis of water soluble fluorescent Ag nanocrystals. The sugar moieties covalently attached on DNA of specific sequences have been successfully employed for site specific incorporation of multiple sugar units on a triangular shaped DNA origami scaffold, and a localized Tollens reaction (quantitative reduction of Ag^{+} by sugar) allows the subsequent site-specific synthesis and *in-situ* immobilization of fluorescent Ag-NCs on the DNA origami scaffold.

6.2. Future Directions

Engineering the shapes and sizes of individual plasmonic nanoparticles, coupled with their organization into higher order structures through DNA directed self-assembly, represent a new way of generating customizable and tunable optical nanomaterials. However the field of DNA directed assembly of nanoparticles is still in its early stage and facing many challenges. Majority of the reports on successful assembly of well-ordered plasmonic nanostructures have been limited to small spherical nanoparticles. Thus a more versatile methodology of surface modification for the anisotropic and larger sized nanoparticles needs to be developed to fully make use of the vast library of available plasmonic nanoparticles. These challenges can be overcome with further development in the synthesis of nanoparticle (size and shape engineering), robust and site-specific surface modification chemistry, and basic structural DNA nanotechnology. Advancements of these capabilities will allow precise spatial and orientation control over various nanoparticles with different shapes and sizes, and facilitate the assembly of more complicated multi-particle systems with high yield.

One of the immediate goals of these DNA directed assembly of plasmonic materials is to investigate these interactions in the single molecule level. There have been recent advancements in highly sensitive, super resolution detection of single chromophores on DNA origami platform, such as TIRF and DNA-PAINT techniques, which have been employed to image different fluorophores fixed at specific distances. These techniques can be employed to investigate the photonic interactions between plasmonic particles and fluorophores or semiconducting quantum dots.

Another major challenge in this field is to figure out a way to interface the bottom-up DNA–nanoparticle structures with the top-down lithographic surface patterning and solid-state devices. Marrying these two approaches, the biomolecular directed bottom-up assembly of nanomaterials can be top-down manipulated and guided in the fabrication of macroscopically ordered functional electronic and photonic devices, which leads to a great opportunity for the advancements in massively parallel fabrication of useful devices and circuits.

Although DNA directed nanoparticle assemblies are usually assembled and stabilized in aqueous buffered conditions, recent successes in integrating the bottom-up DNA-guided self-assembly of plasmonic nanostructures with top-down lithography made a very encouraging step towards the application of DNA-guided plasmonics in solid-state electronic devices.[4,5] Based on its versatility and potential as a scaffolding nanomaterials, DNA will play a vital role in the future development of optical and electronic devices, energy transfer devices, and sensing and diagnostic devices.

Below are few snapshots of future directions of the research carried out in this thesis. DNA origami structures have been used for discrete nanoparticle assembly so far. However 3D DNA origami, a rigid DNA structure, has enormous potential to organize nanomaterials in 3 dimensions. This idea is demonstrated in figure 6.1.a and B. In this figure 3D DNA origami is shown to be the rigid spacer to organize same or different type of metallic nanoparticles and help them crystallize in 3D. DNA Origami directed self assembly can potentially used as a platform which can be used to investigate the distance dependent enhancement of

fluorescence of a single quantum dot by metallic nanoparticle depicted in figure 6.1.C. Controlled bottom up metallization of nanostructures can lead to the formation continuous metallic circuits. Figure 6.1.D shows a way to transform a 1D nanoparticle chain scaffolded with or without DNA origami to a continuous metallic rod like structures.

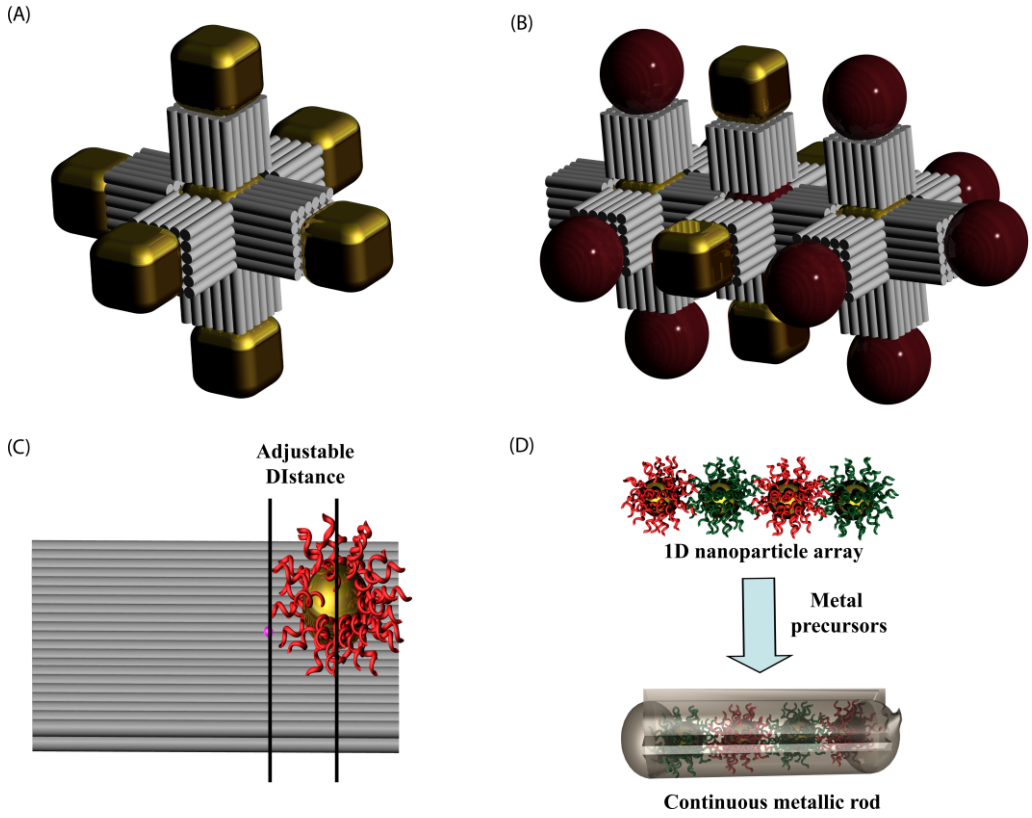

Figure 6.1. (A) 3D DNA origami has been used to crystallize gold or silver nanocubes in 3D. The length of the 3D DNA origami can be varied to change the dimensions of unit cell of the nanoparticle crystals and the interparticle interactions. (B) Binary assembly of spherical nanoparticles and anisotropic nanoparticles in 3D using DNA origami as linker.(C) Using DNA origami platform one can create different distances of nanoparticle and quantum dots. This

constructs can be investigated using single molecule fluorescence measurements. (D) 1D nanoparticle chain can be transformed into a continuous rod depositing more metal precursors on the 1D nanoparticle chain.

DNA functionalization of anisotropic nanoparticle has paved the way to the fabrication of higher E field structures on DNA origami platform. Such a construct of Bowtie triangle antenna is depicted in figure 6.2.a. This antenna structure is known to have a huge E field enhancement called “hot spot” at the junction between two triangles. Using specific DNA hybridization it is possible to place a fluorophore or a quantum dot exactly on the “hot spot”. This can potentially generate high QE enhancement of the fluorophores.

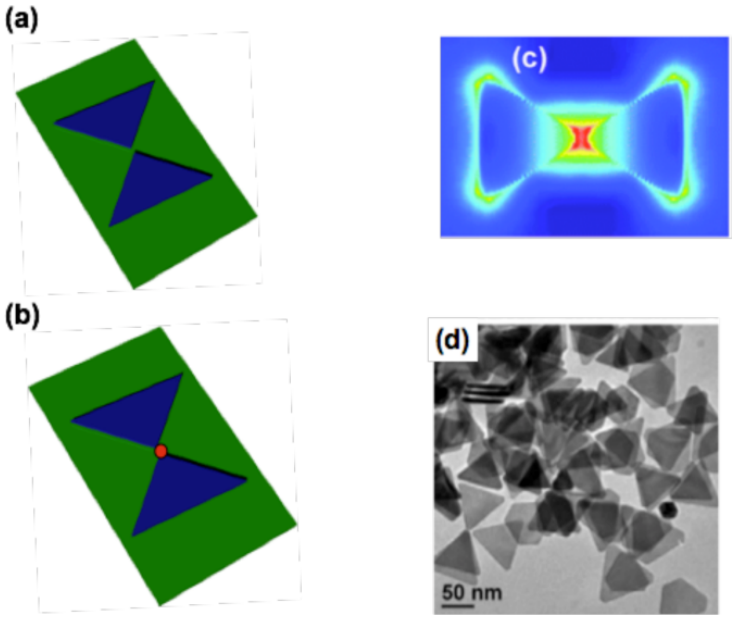

Figure 6.2. (a) Schematic diagram of DNA origami directed assembly of more sophisticated silver or gold nanoprism in discrete dimeric structure called Bowtie antenna structures. (b) Now a quantum dot or a fluorophore (red dot) can be placed in the junction of two nanoprisms. (c) Due to very high E field enhancement in the junction predicted by theoretical calculations, one can expect

to see high QE enhancement of a quantum dot or a fluorophore. (d) The triangle component of the bottom up assembly can be synthesized using known solution phase synthesis protocol. In the figure TEM images of gold nanoprisms has been shown.

6.3. References

(1) Sonnichsen, C.; Reinhard, B. M.; Liphardt, J.; Alivisatos, A. P. *Nat. Biotechnol.* **2005**, 23, 741-745.

(2) Lim, D. K.; Jeon, K. S.; Kim, H. M.; Nam, J. M.; Suh, Y. D. *Nat. Mater.* **2010**, 9, 60-67.

(3) I. H. Stein, C. Steinhauer and P. Tinnefeld, *J. Am. Chem. Soc.,* **2011**, 133, 4193–4195.

(4) Kershner, R. J. *et al. Nature Nanotech.***2009***,* 4**,** 557–561.

(5) Hung, A. M. *et al Nature Nanotech.* **2010**, 5**,** 121–126.

Bibliography

Chapter 1 References

(1) Watson, J. D.; Crick, F. H. C. *Nature.* **1953**, 171, 737-738.

(2) Seeman, N. C. *J. Theor. Biol.* **1982**, 99, 237-247.

(3) Fu, T. J.; Seeman, N. C. *Biochemistry.* **1993**, 32, 3211-3220.

(4) Chen, J. H.; Kallenbach, N. R.; Seeman, N. C. *J. Am. Chem. Soc.* **1989**, 111, 6402-6407.

(5) Chen, J. H.; Seeman, N. C. *Nature.* **1991**, 350, 631-633.

(6) Zhang, Y.; Seeman, N. C. *J. Am. Chem. Soc.* **1994**, 116, 1661-1669.

(7) Li, X. J.; Yang, X. P.; Qi, J.; Seeman, N.C. *J. Am. Chem. Soc.* **1996**, 118, 6131-6140.

(8) LaBean, T. H.; Yan, H.; Kopatsch, J.; Liu, F. R.; Winfree, E.; Reif, J. H.; Seeman, N. C. *J. Am. Chem. Soc.* **2000**, 122, 1848-1860.

(9) Winfree, E.; Liu, F.; Wenzler, L. A.; Seeman, N. C. *Nature.* **1998**, 394, 539-544.

(10) Liu, Y.; Lin, C.; Li, H.; Yan, H. *Angew. Chem. Int. Ed.* **2005**, 44, 4333-4338.

(11) Lin, C.; Liu, Y.; Rinker, S.; Yan, H. *ChemPhysChem.* **2006**, 7, 1641-1647.

(12) Goodman, R. P.; Schaap, I. A. T.; Tardin; C. F.; Erben, C. M.;Berry, R. M.; Schmidt, C. F.; and Turberfield, A. J. *Science.* **2005,** *310*, 1661–1665.

(13) Erben, C. M.; Goodman, R. P.; and Turberfield, A. J. *Angew. Chem., Int. Ed.* **2006,** *45*, 7414–7417.

(14) Shih, W. M.; Quispe, J. D.; Joyce, G. F. *Nature.* **2004,** *427*, 618–621.

(15) He, Y.; Ye, T.; Su, M.; Zhang, C.; Ribbe, A. E.; Jiang, W.; Mao, C. *Nature.* **2008,** *452*, 198–202.

(16) Le, J. D., Pinto, Y.; Seeman, N. C.; Musier-Forsyth, K.; Taton, T. A.; Kiehl,

R. A. *Nano Lett.* **2004,** *4*, 2343–2347.

(17) Zhang, J.; Liu, Y.; Ke, Y.; and Yan, H. *Nano Lett.* **2006,** *6*, 248–251.

(18) Sharma, J.; Chhabra, R.; Liu, Y.; Ke, Y.; Yan, H. *Angew. Chem., Int. Ed.* **2006,** *45*, 730–735.

(19) Sharma, J.; Chhabra, R.; Cheng, A.; Brownell, J.; Liu, Y., Yan, H. *Science.* **2005,** *323*, 112–116.

(20) Lin, C.; Liu, Y.; Yan, H. *Biochemistry.* **2009**, 48, 1663.

(21) Rothemund, P. W. K. *Nature.* **2006**, 440, 297– 302.

(22) Maune, H.T.; Han, S.P.; Barish, R.D.; Bockrath, M.; Goddard, W.A.; Rothemund, P.W.K.; Winfree, E. *Nat. Nanotechnol.* **2010**, 5, 61-66.

(23) Bui, H.; Onodera, C.; Kidwell, C.; Tan, Y.,Graugnard, E.; Kuang, W.; Lee, J.; Knowlton, W. B.; Yurke, B.; Hughes, W. L. *Nano Lett.* **2010**, 10, 3367.

(24) Deng, Z. T.; Samanta, A.; Nangreave, J.; Yan, H.; Liu, Y . *J. Am. Chem. Soc.* 2012, Article ASAP DOI: 10.1021/ja3081023.

(25) Nangreave, J. ;Han, D.; Liu, Y.; Yan, H. *Curr. Opin. Chem. Biol.* **2010**,14, 608-615.

(26) Mirkin, C. A.; Letsinger, R. L.; Mucic, R. C.; Storhoff, J. J. Nature **1996**, 382, 607−609.

(27) Cutler, J. I.; Auyeung, E; Mirkin, C. A. *J. Am. Chem. Soc.*, **2012**, *134*, 1376-1391.

(28) Alivisatos, A. P. *et al. Nature* **1996***,* 382**,** 609–611.

(29) Loweth, C. J.; Caldwell, W. B.; Peng, X.; Alivisatos, A. P.; Schultz, P. G. *Angew. Chem. Int. Ed.* **1999***,* 38**,** 1808–1812.

(30) Mastroianni, A. J.; Claridge, S. A.; Alivisatos; A. P. *J. Am. Chem. Soc.* **2009,** 131**,** 8455–8459.

(31) Mucic, R. C.; Storhoff, J. J.; Mirkin, C. A.; Letsinger, R. L. *J. Am. Chem. Soc.* **1998***,* 120**,** 12674–12675.

(32) Maye, M. M.; Nykypanchuk, D.; Cuisinier, M.; van der Lelie, D.; Gang, O. *Nature Mater.* **2009***,* 8**,** 388–391.

(33) Sharma, J.; Chhabra, R.; Andersen, C. S.; Gothelf, K. V.; Yan, H.; Liu, Y. *J. Am. Chem. Soc.*, **2008**, 130, 7820.

(34) Ding, B.; Deng, Z.; Yan, H.; Cabrini, S.; Zuckermann, R.N.; Bokor, J. *J. Am. Chem. Soc.* **2010**, 132, 3248-3249.

(35) Zhao, Z.; Jacovetty, E. L.; Liu, Y.; Yan, H. *Angew. Chem., Int. Ed.*, **2011**, 50, 2041.

(36) Kershner, R. J. *et al. Nature Nanotech.***2009**, 4**,** 557–561.

(37) Pilo-Pais, M.; Goldberg, S.; Samano, E.; Labean, T. H.; Finkelstein, G. *Nano Lett.* **2011**, 11,3489.

(38) Shen, X. B.; Song, C.; Wang, J. Y.; Shi, D. W.; Wang, Z. A.; Liu,N.; Ding, B. Q. *J. Am. Chem. Soc.* **2012**, 134, 146−149.

(39) Kuzyk, A.; Schreiber, R.; Fan, Z.; Pardatscher, G.; Roller, E.;Högele, A.; Simmel, F.; Govorov, A. O.; Liedl, T. *Nature* **2012**, 483, 311–314.

(40) Acuna, G. P.; Bucher, M.; Stein, I. H.; Steinhauer, C.; Kuzyk, A.; Holzmeister, P.; Schreiber, R.; Moroz, A.; Stefani, F. D.; Liedl, T.*et al ACS Nano* **2012**, 6,3189– 3195.

(41) Rosi, N. L.; Mirkin, C. A. *Chem. Rev.* **2005**, 105, 1547–1562.

(42) Tan, S. J.; Campolongo, M. J.; Luo, D.; Cheng, W. *Nat. Nanotechnol.* **2011**, 6, 268–276.

(43) Principles of Fluorescence Spectroscopy, J. R. Lakowicz, Third edition.

Chapter 2 References

(1) Stewart, M. E.; Anderton, C. R.; Thompson, L. B. ; Maria, J.; Gray, S. K Rogers, J. A.; Nuzzo, R. G. *Chem. Rev.* **2008**, 108, 494 – 521.

(2) Lin, C.; Liu, Y. ; Yan, H. *Biochemistry* **2009**, 48, 1663 – 1674.

(3) Loweth, C. J.; Caldwell, W. B.; Peng, X.; Alivisatos, A. P.; Schultz, P. G.; *Angew. Chem.* **1999**, 111, 1925 – 1929; *Angew. Chem. Int. Ed.* **1999**, 38, 1808 – 1812.

(4) Aldaye, F. A.; Sleiman, H. F.; Angew. *Chem.***2006**, 118, 2262 – 2267; *Angew.Chem. Int. Ed.* **2006**, 45, 2204 – 2209.

(5) Sharma, J.; Chhabra, R.; Andersen, C. S.; Gothelf, K. V.; Yan, H.; Liu, Y. **2008**, 130, 7820 – 7821.

(6) Deng, Z. X. ; Tian, Y.; Lee, S. H.; Ribbe, A. E.; Mao, C. D. *Angew. Chem.* **2005**, 117, 3648 – 3651; *Angew. Chem. Int. Ed.* **2005**, 44, 3582 – 3585.

(7) Beyer, S.; Nickels, P.; P. Simmel, P. *Nano Lett.* **2005**, 5, 719 – 722.

(8) Lee, J. H.; Wernette, D. P.; Yigit, M. V.; Liu, J.; Wang, Z.; Lu, Y. *Angew. Chem.* **2007**, 119, 9164 –9168; *Angew. Chem. Int. Ed.* **2007**, 46, 9006 – 9010.

(9) Niemeyer, C. M.; Brger, W.; Peplies, J. *Angew. Chem.* **1998**, 110, 2391 – 2395; *Angew. Chem. Int. Ed.* **1998**, 37, 2265 – 2268.

(10) Le, J.; Pinto, Y.; Seeman, N. C.; MusierForsyth, K.; Taton, T. A.; Kiehl, R. A.; *Nano Lett.* **2004**, 4, 2343 – 2347.

(11) Zhang, J.; Liu, Y.; Ke, Y.; Yan, H. *Nano Lett.* **2006**, 6, 248 – 251.

(12) Zheng, J. ; Constantinou, P. E.; Micheel, C.; Alivisatos, A. P.; Kiehl, R. A.; Seeman, N. C. *Nano Lett.* **2006**, 6, 1502 – 1504.

(13) Nykypanchuk, D.; Maye, M. M.; Van derLelie, D.; Gang, O. *Nature* **2008**, 451, 549 – 552.

(14) Park, S. Y. et al.,*Nature* **2008**, 451, 553 – 556.

(15) Sharma, J.; Chhabra, R.; Cheng, A.; Brownell, J.; Liu, Y., Yan, H. *Science.* **2005,** *323*, 112–116.

(16) Lee, J.-S.; Lytton-Jean, A. K. R.; Hurst, S. J.; Mirkin, C. A.; *Nano Lett*. **2007**, 7, 2112 – 2115.

(17) Pal, S.; Sharma, J.; Yan, H.; Liu, Y.; *Chem. Commun.* **2009**, 6059 – 6061.

Chapter 3 References

(1) Aldaye, F. A. Palmer, A. L. Sleiman,H. F. *Science*. **2008**, 321, 1795-1799.

(2) Rothemund, P. W. K. *Nature,***2006,** 440, 297-302.

(3) Ke, Y. *et al. J. Am. Chem. Soc.* **2009,** 131, 15903.

(4) Han, D.; Pal, S.; Nangreave, J.; Deng, Z.; Liu, Y.; Yan, H. *Science* **2011**, 332, 342−346.

(5) Deng, Z.; Samanta, A.; Nangreave, J.; Yan, H.; Liu, Y. *J. Am. Chem. Soc.*, 2012, *134* (42), 17424–17427.

(6) Maune, H. T.; Han, S.-p.; Barish, R. D.; Bockrath, M.; Goddard III, W. A.; Rothemund, P. W. K.; Winfree, E. *Nat. Nanotech.* **2009**, 4, 61−66.

(7) Stephanopoulos, N.; Liu, M.; Tong, G. J.; Li, Z.; Liu, Y.; Yan, H.; Francis, M. B. *Nano Lett*. **2010**, 10, 2714–2720.

(8) Numajiri, K.; Yamazaki, T.; Kimura, M.; Kuzuya, A.; Komiyama, M. *J. Am. Chem. Soc.* **2010**, 132, 9937–9939.

(9) B Sacca, B.; Meyer, R.; Erkelenz, M.; Kiko, K. ; Arndt, A.; Schroeder, H.; Rabe, K. S.; Niemeyer, C. M. *Angew. Chem. Int. Ed.* **2010**, 49, 9378 –9383.

(10) Chhabra, R.; Sharma, J. ; Ke, Y.; Liu, Y.; Rinker, S.; Lindsay, S.; Yan, H. *J. Am. Chem. Soc.* **2007**, 129, 10304–10305.

(11) Rinker, S.; Ke, Y.; Liu, Y.; Chhabra, R.; Yan, H. *Nat. Nanotech.* **2008**, 3, 418−422.

(12) Sharma, J.; Chhabra, R.; Andersen, C. S.; Gothelf, K. V.; Yan, H.; Liu, Y. *J. Am. Chem. Soc.* **2008**, 130, 7820–7821.

(13) Ding, B.; Deng, Z.; Yan, H.; Cabrini, S.; Zuckermann, R. N.; Bokor, J. *J. Am. Chem. Soc*. **2010**, 132, 3248–3249.

(14) Hung, A. M.; Micheel, C. M.; Bozano, L. D.; Osterbur, L. W.; Wallraff, G. M.; Cha, J. N. *Nat.Nanotech.* **2010**, 5, 121−126.

(15) Stearns, L. A., Chhabra, R., Sharma, J., Liu, Y.; Petuskey, W. T.; Yan, H.; Chaput, J.C. *Angew. Chem. Int. Ed.* **2009**, 45, 8494−8496.

(16) Kuzuya, A.; Koshi, N.; Kimura, M.; Numajiri, K.; Yamazaki, T.; Ohnishi, T.; Okada, F.; Komiyama, M. *Small.* **2010,** *6*, 2664–2667.

(17) Pal, S.; Deng, Z.; Ding, B.; Yan, H.; Liu, Y. *Angew. Chem. Int. Ed.* **2010***,* 49*,* 2700 –2704.

(18) Pal, S.; Deng, Z.; Wang, H.; Zou, S.; Liu, Y.; Yan, H. *J. Am. Chem. Soc.* 2011, 133, 17606−17609.

(19) Stewart, M. E.; Anderton, C. R.; Thompson, L. B. ; Maria, J.; Gray, S. K.; Rogers, J. A.; Nuzzo, R. G. *Chem. Rev.* **2008**, 108, 494 – 521.

(20) Shen, X. B.; Song, C.; Wang, J. Y.; Shi, D. W.; Wang, Z. A.; Liu,N.; Ding, B. Q. *J. Am. Chem. Soc.* **2012**, 134, 146−149.

(21) Kuzyk, A.; Schreiber, R.; Fan, Z.; Pardatscher, G.; Roller, E.;Högele, A.; Simmel, F.; Govorov, A. O.; Liedl, T. *Nature*. **2012**, 483, 311–314.

(22) Chhabra, R.; Sharma, J.; Wang, H. N.; Zou, S. L.; Lin, S.; Yan, H.; Lindsay, S.; Liu, Y. *Nanotechnology* 2009, 20, 485201-485201.

(23) Yun, C. S.; Javier ,A.; Jennings, T.; Fisher, M.; Hira, S.; Peterson, S.; Hopkins, B.; Reich, N. O.; Strouse, G. F. *J. Am. Chem. Soc.* **2005**, 127, 3115–3119.

(24) Acuna, G. P.; Bucher, M.; Stein, I. H.; Steinhauer, C.; Kuzyk, A.; Holzmeister, P.; Schreiber, R.; Moroz, A.; Stefani, F. D.; Liedl, T.*et al ACS Nano* **2012**, 6, 3189– 3195.

(25) Lakowicz J R 1999 Principles of Fluorescence Spectroscopy 2nd edition (New York: Kluwer Academic Plenum)

(26) Zou, S.; Schatz, G. C. *Chem. Phys. Lett.* **2005**, 403, 62–67.

(27) Zou, S.; Schatz, G. C. *Phys. Rev. B,* **2006***,* 74, 125111.

(28) Busson, M. P.; Rolly, B.; Stout, B.; Bonod, N.; Bidault, S. *Nat. Commun.* **2012**, 3, 962

Chapter 4 References

(1) Burda, C.; Chen, X. B.; Narayanan, R.; El-Sayed, *M. A. Chem. Rev.* **2005**, 105, 1025–1102.

(2) Huang, X. H.; Neretina, S.; El-Sayed, M. A. *Adv. Mater.* **2009**, 21, 4880–4910.

(3) (a) Yu, C.; Irudayaraj, J. *Biophys. J.* **2007**, 93, 3684–3692. (b) Yu, C.; Nakshatri, H; Irudayaraj, J. *Nano Lett.* **2007**, 7 (8), 2300–2306. (c) Wang, L.; Zhu, Y.; Xu, L.; Chen, W.; Kuang, H.; Liu, L.; Agarwal, A.; Xu, C.; Kotov, N. A. *Angew. Chem., Int. Ed.* **2010**, 49 (32), 5472–5475. (d) Dickerson, E. B.; Dreaden, E. C.; Huang, X.; El-Sayed, I. H.; Chu, H.; Pushpanketh, S.; McDonald, J. F.; El-Sayed, M. A. *Cancer Lett.* **2008**,269, 57–66.

(4) Li, Y.; Qian, F.; Xiang, J.; Lieber, C. M. *Mater. Today* **2006**, 9, 18–27.

(5) Lu, W.; Lieber, C. M. J. Phys. D: *Appl. Phys.* **2006**, 39, R387–R406.

(6) Rothemund, P. W. K. *Nature* **2006**, 440, 297–302.

(7) Nangreave, J.; Han, D.; Liu, Y.; Yan, H. *Curr. Opin. Chem. Biol.* **2010**, 14, 608–615.

(8) Shih, W. M.; Lin, C. *Curr. Opin. Struct. Biol.* **2010**, 20, 276–282.

(9) Tan, S. J.; Campolongo, M. J.; Luo, D.; Cheng, W. *Nat. Nanotechnol.* **2011**, 6, 268–276.

(10) Nikoobakht, B.; El-Sayed, M. A. *Chem. Mater.* **2003**,15, 1957–1962.

(11) Jones, M. R.; Macfarlane, R. J.; Lee, B.; Zhang, J. A.; Young, K. L.; Senesi, A. J.; Mirkin, C. A. *Nat. Mater.* **2010**, 9, 913–917.

(12) (a) Purcell, E. M.; PennyPacker, C. R. *Astrophys. J.* **1973**, 186, 705–714. (b) Draine, B. T. *Astrophys. J.* **1988**, 333, 848–872.

(13) Palik, E. D. Handbook of Optical Constants of Solids; Academic Press: New York, **1985**.

(14) Sharma, J.; Chhabra, R.; Anderson, C. S.; Gothelf, K. V.; Yan, H.; Liu, Y. *J. Am. Chem. Soc.* **2008**, 130, 7820–2821.

Chapter 5 References

(1) a) Peyser, L. A.; Vinson, A. E.; Bartko, A. P.; Dickson, R. M. *Science* **2001**, 291, 103 – 106; b) Palmer, R. E.; Pratontep, S.; Boyen, H.-G. *Nat. Mater.* **2003**, 2, 443 – 448; c) Lee, T.-H.; Gonzalez, J. I.; Zheng, J.; Dickson, R. M. *Acc. Chem. Res.* **2005**, 38, 534 – 541; d) Lesniak, W.; Bielinska, A. U.; Sun, K.; Janczak, K. W.; Shi, X.; Baker, Jr., J. R.; Balogh, L. P. *Nano Lett.* **2005**, 5, 2123 – 2130.

(2) Zheng, J.; Dickson, R. M. *J. Am. Chem. Soc.* **2002**, 124, 13982 –13983.

(3) Zhang, J.; Xu, S.; Kemacheva, E. *Adv. Mater.* **2005**, 17, 2336 – 2340.

(4) Branham, M. R.; Douglas, A. D.; Mills, A. J.; Tracy, J. B.; White, P. S.; Murray, R. W. *Langmuir* **2006**, 22, 11376 – 11383.

(5) Yu, J.; Patel, S. A.; Dickson, R. M. *Angew. Chem*. **2007**, 119, 2074 – 2076; *Angew. Chem. Int. Ed.* **2007**, 46, 2028 – 2030.

(6) Nishida, N.; Yao, H.; Ueda, T.; Sasaki, A.; Kimura, K. *Chem. Mater.* **2007**, 19, 2831 – 2841.
(7) Shen, Z.; Duan, H.; Frey, H. *Adv. Mater.* **2007**, 19, 349 – 352.

(8) Narayanan, S. S.; Pal, S. K. *J. Phys. Chem. C* **2008**, 112, 4874 –4879.

(9) Shang, L.; Dong, S. *Chem. Commun.* 2008, 1088 – 1090.

(10) Anson, C. E.; Eichh, AIssac, .; I.; Fenske, D.; Fuhr, O.; Sevillano, P.; Persau, C.; Stalke, D.; Zhang, J. *Angew. Chem*. **2008**,120, 1346 – 1351; *Angew. Chem. Int. Ed.* **2008**, 47, 1326 – 1331.

(11) Yu, J.; Choi, S.; Dickson, R. M. *Angew. Chem.* **2009**, 121, 324 –326; *Angew. Chem. Int. Ed.* **2009**, 48, 318 – 320.

(12) Wu, Z.; Lanni, E.; Chen, W.; Bier, M. E.; Ly, D.; Jin, R. *J. Am. Chem. Soc.* **2009**, 131, 16672–16674.

(13) H. Xu, K. S. Suslick, *Adv. Mater.* **2010**, 22, 1078–1082.

(14) Rao, T. U. B.; Pradeep, T. *Angew. Chem.* **2010**, *122*,4017 – 4021; *Angew. Chem. Int. Ed.* **2010**, 49, 3925 – 3929.

(15) a) Petty, J. T.; Zheng, J.; Hud, N. V.; Dickson, R. M. *J. Am. Chem. Soc.* **2004**, 126, 5207 – 5212; b) Richards, C. I.; Choi, S.; Hsiang, J.-C.; Antoku, Y.; Vosch, T.; Bongiorno, A.; Tzeng, Y.-L.; Dickson, R. M. *J. Am. Chem. Soc.* **2008**, 130, 5038 – 5039; c) Petty, J. T.; Fan, C.; Story, S. P.; Sengupta, B.; Iyer, A. S. J.; Prudowsky, Z.; Dickson, R. M. J. *Phys. Chem. Lett.* **2010**, 1, 2524 – 2529.

(16) a) Sengupta, B.; Ritchie, C. M.; Buckman, J. G.; Johnsen, K. R.; Goodwin, P. M.; Petty, J. T.; *J. Phys. Chem. C* **2008**, 112, 18776 –18782; b) Sengupta, B.; Springer, K.; Buckman, J. G.; Story, S. P.; Henry Abe, O.; Hasan, Z. W.; Prudowsky, Z. D.; Rudisill, S. E.; Degtyareva, N. N.; Petty, J. T. *J. Phys. Chem. C* **2009**, 113, 19518 –19524; c) Gwinn, E. G.; ONeill, P.; Guerrero, A. J.; Bouwmeester, D.; Fygenson, D. K. *Adv. Mater.* **2008**, 20, 279 – 283; d) Guo, W.; Yuan, J. ; Wang, E. *Chem. Commun.* **2009**, 3395 – 3397;e) ONeill, P. R.; Velazquez, L. R.; Dunn, D. G.; Gwinn, E. G.; Fygenson, D. K. *J. Phys. Chem. C* **2009**, 113, 4229 – 4233; f) Sharma, J.; Yeh, H.-C.; Yoo, H.; Werner, J. H.; Martinez, J. S. *Chem.Commun.* **2010**, 46, 3280 – 3282; g) Guo, W.; Yuan, J.; Dong, Q.; Wang, E. *J. Am. Chem. Soc.* **2010**, 132, 932 – 934; h) Molotsky, T.; Tamarin, T.; Moshe, A. B.; Markovich, G; Kotlyar, A. B. *J. Phys.Chem. C* **2010**, 114, 15951 – 15954.

(17) a) Braun, E.; Eichen, Y.; Sivan, U.; Ben-Yoseph, G. *Nature* **1998**,391, 775 – 778; b) Richter, J.; Seidel, R.; Kirsch, R.; Mertig, M.; Pompe, W.; Plaschke,

J.; Schackert, H. K. *Adv. Mater.* **2000**, 12, 507 –510; c) Weizmann, Y.; Patolsky, F.; Popov, I.; Willner, I. *Nano Lett.* **2004**, 4, 787 – 792; d) Berti, L.; Alessandrini, A.; Facci, P.; *J. Am.Chem. Soc.* **2005**, 127, 11216 – 11217; e) Fischler, M.; Simon, U.; Nir, H.; Eichen, Y.; Burley, G. A.; Gierlich, J.; Gramlich, P. M. E.; Carell, T. *Small* **2007**, 3, 1049 – 1055; f) Wirges, C. T.; Timper, J.; Fischler, M.; Sologubenko, A. S.; Mayer, J.; Simon, U.; Carell, T. *Angew. Chem.* **2009**, 121, 225 – 229; *Angew. Chem. Int. Ed.* **2009**,48, 219 – 223.

(18) P. W. K. Rothemund, *Nature* **2006**, 440, 297 – 302.

(19) a) Sharma, J.; Chhabra, R.; Andersen, C. S.; Gothelf, K. V.; Yan, H.; Liu, Y. *J. Am. Chem. Soc.* **2008**, 130, 7820 – 7821; b) Pal, S.; Deng, Z.; Ding, B.; Yan, H.; Liu, Y. *Angew. Chem.* **2010**, 122, 2760;*Angew. Chem. Int. Ed.* **2010**, 49, 2700 – 2704; c) Hung, A. M.; Micheel, C. M.; Bozano, L. D.; Osterbur, L. W.; Wallraff, G. M.; Cha, J. N. *Nat. Nanotechnol.* **2010**, 5, 121 – 126; d) Bui, H.; Onodera, C.; Kidwell, C.; Tan, Y.,Graugnard, E.; Kuang,W.; Lee, J.; Knowlton, W. B.; Yurke, B.; Hughes, W. L. *Nano Lett.* **2010**, 10, 3367; e) Maune, H. T.; Han, S.-p.; Barish, R. D.; Bockrath, M.; Goddard III, W. A.; Rothemund, P. W. K.; Winfree, E. *Nat. Nanotechnol.* **2009**, 4, 61 – 66; f) Numajiri, K.; Yamazaki, T.; Kimura, M.; Kuzuya, A.; Komiyama, M. *J. Am. Chem. Soc.* **2010**, 132, 9937 – 9939; g) Sacca, B.; Meyer, R.; Erkelenz, M.; Kiko, K. ; Arndt, A.; Schroeder, H.; Rabe, K. S.; Niemeyer, C. M. *Angew. Chem.* **2010**, 122, 9568; *Angew. Chem. Int. Ed.* **2010**, 49, 9378 – 9383; h) Voigt, N. V.; Tørring, T.; Rotaru, A.; Jacobsen, M. F.; Ravnsbæk, J. B.; Subramani, R.; Mamdouh, W.; Kjems, J ; Mokhir, A.; Besenbacher, F.; Gothelf, K. V. *Nat. Nanotechnol.* **2010**, 5, 200 –203; i) Sannohe, Y.; Endo, M.; Katsuda, Y.; Hidaka, K.; Sugiyama, H. *J. Am. Chem. Soc.* **2010**, 132, 16311 – 16313.

(20) Burley, G. A.; Gierlich, J.; Mofid, M. R.; Nir, H.; Tal, S.; Eichen, Y.; Carell, T. *J. Am. Chem. Soc.* 2006, 128, 1398 – 1399.

Chapter 6 References

(1) Sonnichsen, C.; Reinhard, B. M.; Liphardt, J.; Alivisatos, A. P. *Nat. Biotechnol.* **2005**, 23, 741-745.

(2) Lim, D. K.; Jeon, K. S.; Kim, H. M.; Nam, J. M.; Suh, Y. D. *Nat.Mater.* **2010**, 9, 60-67.

(3) I. H. Stein, C. Steinhauer and P. Tinnefeld, *J. Am. Chem. Soc.,* **2011**, 133, 4193–4195.

(4) Kershner, R. J. *et al. Nature Nanotech.***2009***,* 4**,** 557–561.

(5) Hung, A. M. *et al Nature Nanotech.* **2010**, 5**,** 121–126.

APPENDIX A

SUPPLEMENTAL INFORMATION FOR CHAPTER 2

Supplemental information for

DNA Origami Directed Self-assembly of Discrete Silver Nanoparticle Architectures

Suchetan Pal, Zhengtao Deng, Hao Yan, Yan Liu
Department of Chemistry and Biochemistry and the Biodesign Institute
Arizona State University, Tempe, AZ 85287

1. Experimental methods and materials:

Materials:

Silver nanoparticles (diameter 20 ± 3 nm) were purchased from Ted Pella Inc (catalog number 15705-5sc, Batch 12466). The size and distribution were analyzed by TEM imaging and was found to be 21 ± 3 nm. M13mp18 single stranded DNA was purchased from New England Biolabs and was used as received. All oligonucleotides used for the experiments were obtained from Integrated DNA Technologies. (±)-α-Lipoic acid, N-hydroxysuccinimide (NHS), N,N′-dicyclohexylcarbodiimide (DCC) and Tris(carboxyethyl) phosphine hydrochloride (TCEP) were purchased from Sigma-Aldrich and used without further purification. Bis(p-sulfonatophenyl)phenylphosphine dihydrate dipotassium salt (BSPP) was purchased from Strem Chemicals Inc. All DNA sequences were ordered from Integrated DNA Technology Inc (www.idtdna.com) and purified by denaturing PAGE gel electrophoresis.

1) The ps-9, ps-6 and ps-3 strands each contains 9, 6, or 3 phosphorothioate (ps) linkage groups marked as a * between the bases close to the 5’ end, and they share a 56 base long recognition sequence.

ps-9 5’ -C*A*T* G*C*G* G*G*C* TAA AAA TTT TTG TTT AGC TAT ATT

TAA TAT GAT ATT CAA GAG GAA GGT TAT CTC CT-3’

ps-6 5’-C*A*T* G*C*G* TAA AAA TTT TTG TTT AGC TAT ATT TAA TAT GAT

ATT CAA GAG GAA GGT TAT CTC CT-3’

ps-3 5’-C*A*T* TAA AAA TTT TTG TTT AGC TAT ATT TAA TAT GAT ATT CAA GAG

GAA GGT TAT CTC CT - 3'

2) The complimentary strand to the recognition domain is modified with an amino-group at the 5’ end, which then is further reacted with lipoic acid to gain two thiol groups at the 5’-end. Bidentate interaction between the lipoic acid

modified DNA with AuNP surface is a stable linkage that allows a 1:1 conjugate of DNA-AuNP to be isolated and hybridized with the ps-9 modified AgNPs to form the bimetallic satellite structure.

Comp: 5' - /5AmMC6/TTT TTT TAG GAG ATA ACC TTC CTC TTG AAT ATC ATA TTA AAT ATA GCT AAA CAA AAA TTT TTA TTT AAA TTT TTT TTT TTT TTT TTT TTT TTT TTT TTT T - 3'

The length of this strand is extended to 100mer by adding 31T and 7T at the 3' and 5' ends, in order to make the 1:1 AuNP:DNA conjugate easier to be separated with the bare AuNP and the 1:2 conjugate by agarose gel electrophoresis.

3) A pair of ps-po-DNAs that each contains 9-ps groups on the 5' end, a 6 base linker (A6) and 9-base recognition sequence that are complementary to each other. These are used to prepare the two sets of AgNPs that carry DNA sequences complimentary to each other to form the large aggregation through DNA hybridization, and thermal melting will recover the uniform dispersed AgNPs.

Ps-9-A 5'-A*T*A* A*G*C* C*A*T* AAA AAA ATC GCG CGC-3'

Ps-9-A' 5'-A*T*A* A*G*C* C*A*T* AAA AAA GCG CGC GAT-3'

Experimental methods

Materials:

Silver nanoparticles (diameter 20 ± 5 nm given by the manufacturer) were purchased from Ted Pella Inc (catalog number 15705-5sc). The size and distribution were analyzed by TEM imaging and was found to be 32 ± 5 nm. All oligonucleotides used for the experiments were obtained from Integrated DNA Technologies. (±)-α-Lipoic acid, N-hydroxysuccinimide (NHS), N,N´-dicyclohexylcarbodiimide (DCC) and Tris(carboxyethyl) phosphine hydrochloride (TCEP) were purchased from Sigma-Aldrich and used without further purification. Bis(p-sulfonatophenyl)phenylphosphine dihydrate dipotassium salt (BSPP) was purchased from Strem Chemicals Inc. Conjugation of ps-DNA with 32 nanometer silver nanoparticle: The silver colloid obtained from the company was concentrated 10 times by centrifugation (10,000 rpm, 20 min) and redispersion in nanopure water. To the 100 μL of silver nanoparticle solution, appropriate aliquots of ps-DNA, SDS solution and 0.1 M pH 7.4 phosphate buffer (PB) solution were added such that their final concentrations were 10 μM, 0.01% and 10 mM. The anoparticle solution was kept for gentle shaking overnight. Then 4 M NaCl was added by small aliquotes over 24 hours to raise the final NaCl concentration to 500 mM. The solution was incubated overnight. Then the excess of Oligonucleotides were removed by centrifugation (10,000 rpm, 20 min) and redispered to a buffer solution that contains 10 mM PB, 500 mM NaCl and 0.01% SDS. This centrifugation and redispersion procedure was repeated three times. Estimation of number of ps-DNA on each AgNP:The approximated surface coverage of ps-DNA on AgNP was calculated by measuring the concentration of AgNPs and the DNA concentrations before and after the

surface attachment. The concentration of the AgNps was calculated from the particle density given by the manufacturer ($4x10^{10}$/ml, OD ~ 0.706 at 407 nm, BB-international via Ted Pella) and OD measurement, assuming no change to the extinction coefficient of the particle when it is conjugated with DNA. The ps-DNA concentration before and after the attachment was calculated from the OD at 260 nm of the DNA solution before mixed with the AgNps and the supernatant after the incubation. From these, the number of ps-DNA per AgNP was estimated to be ~ 3900 and the surface area per ps-DNA is ~ 0.8 nm2 or ~ 200 pmol/cm2. As compared to the reported surface density of thiol-modifed DNA on AgNPs, this surface area per DNA molecule is in the reported ranges1. From the surface area per DNA molecule, the phosphorothiolated portion of the ps9-DNA seems lying tangential on the AgNP surface with the phosphothioate backbone attached on the surface and the bases more likely perpendicular to the surface.

TEM Images:

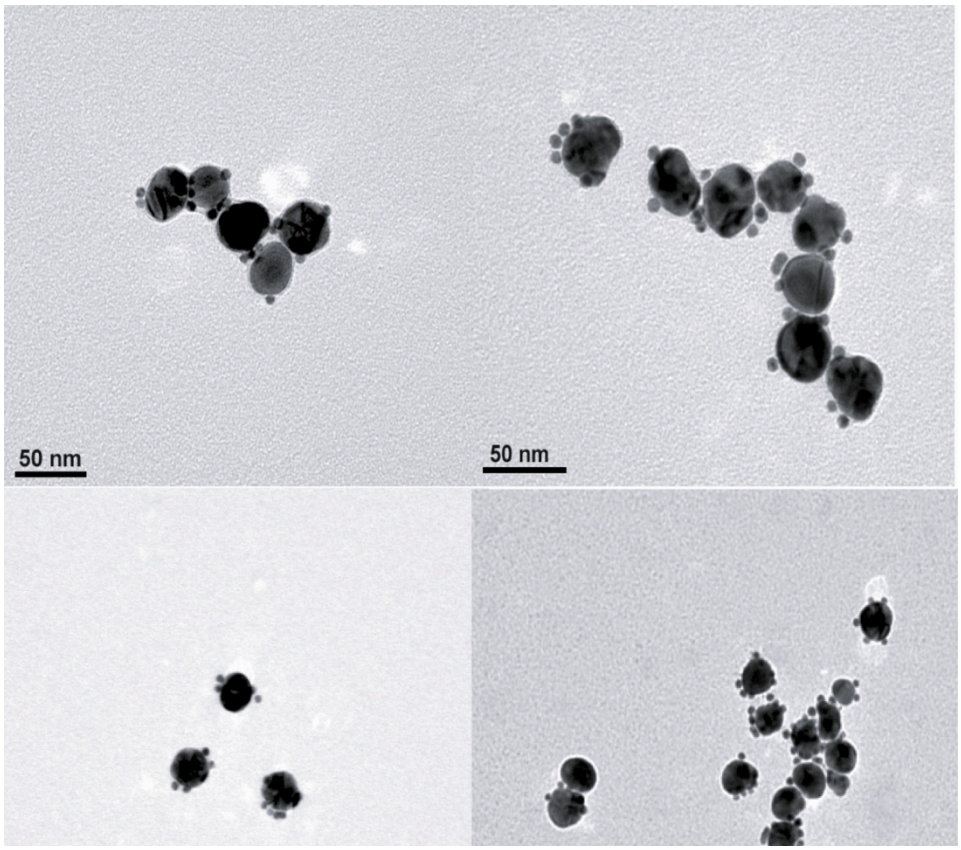

Figure S1. Zoom-out images of Ag core-Au satellite .

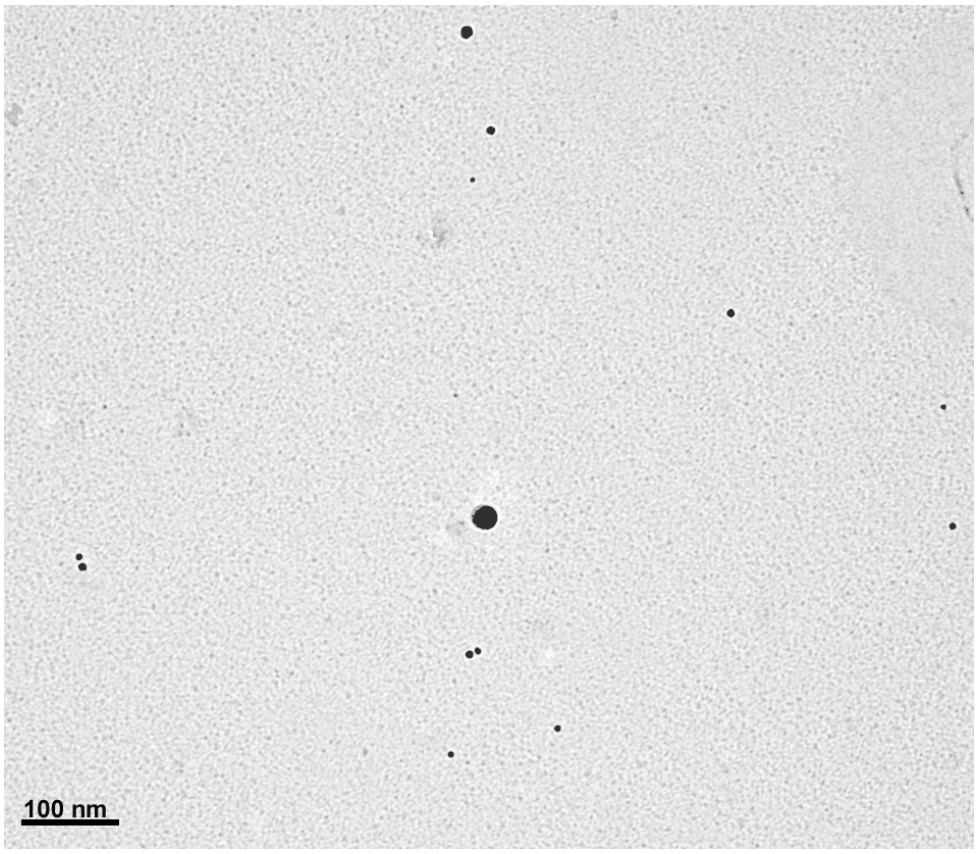

Figure S2. Negative control where the AgNP is modified with ps-DNA not complimentary to DNA attached to the AuNP. Therefore no formation of Ag core-Au satellite structure is observed.

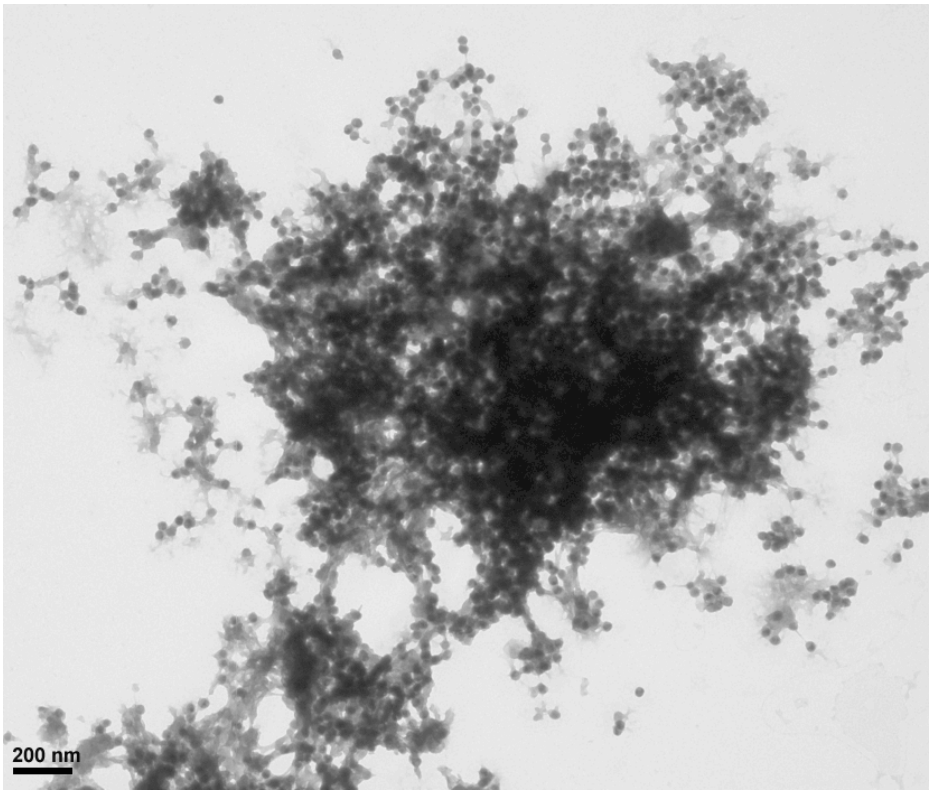

Figure S3. Negative control where the AgNP is modified with ps-DNA not complimentary to DNA attached to the AuNP. Therefore no formation of Ag core-Au satellite structure is observed.

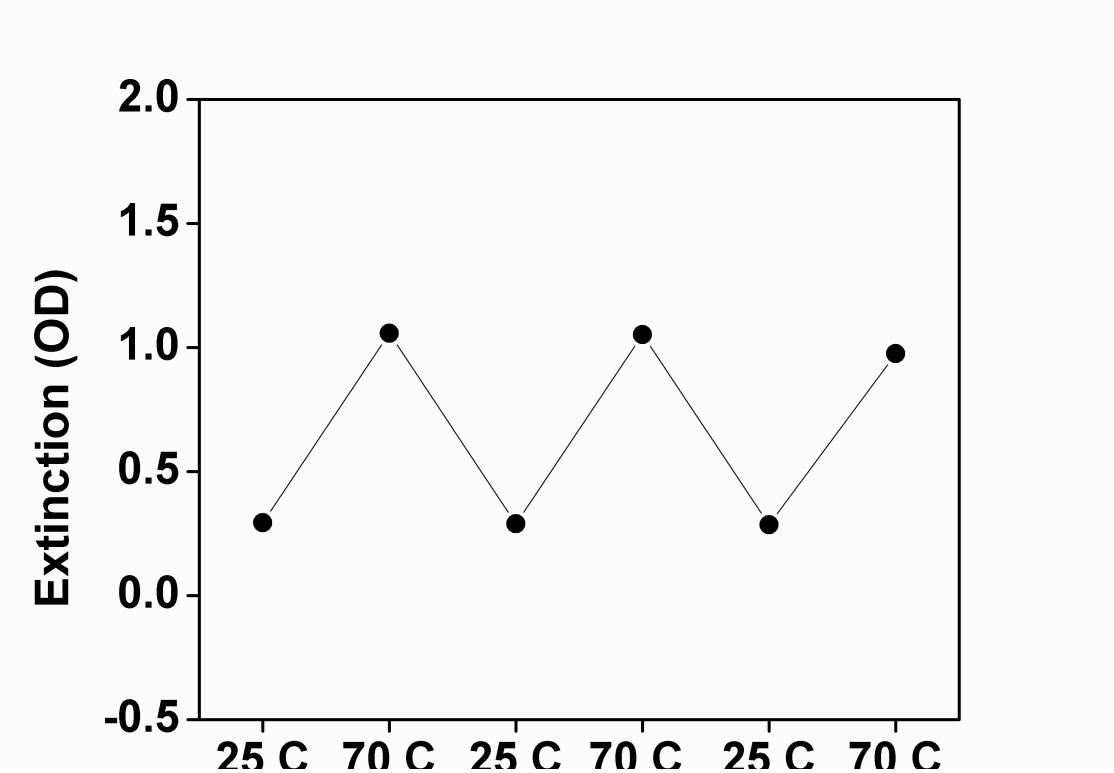

Figure S4: The absorption profile of AgNPs at 412 nm when the temperature is cycled between 25 oC (aggregated state) and 70 o C (separated state). AgNP aggregation was induced by hybridization of two complimentary strands of DNA attached to the surface of two sets of AgNps. The plot shows excellent reversibility, strongly support the mechanism of the aggregation is due to DNA hybridization.

Supporting Information

DNA-Origami-Directed Self-Assembly of Discrete Silver-Nanoparticle Architectures

Suchetan Pal, Zhengtao Deng, Baoquan Ding, Hao Yan,* and Yan Liu*

Department of Chemistry and Biochemistry and

The Biodesign Institute, Arizona State University

Tempe, AZ 85287 (USA)

Fax: (+1) 480-727-2378

E-mail: yan_liu@asu.edu; hao.yan@asu.edu

anie_201000330_sm_miscellaneous_information.pdfPreparation of triangular shaped DNA origami structure:

Preparation of triangular shaped DNA origami structure: To synthesize the triangular origami, 5 nM of single stranded M13mp18 DNA (7,249 nucleotide long) is mixed with 5 times concentration of staple strands (unpurified) following the design outlined by Rothemund (see reference 22 in main text) in 1xTAE-Mg^{2+} (40 mM Tris, 20 mM Acetic acid, 2 mM EDTA and 12.5 mM Magnesium acetate, pH 8.0). To generate the binding sites on the origami, a number of staple strands at selected positions on the origami surface were replaced by the capture strands that extend the corresponding staple strands at the 5'-end by 15 Adenosine. The resulting solution was cooled from 95 ^{o}C to 4 ^{o}C to form the triangular shaped DNA origami structure. In order to get rid of excess staple strands the resultant solution was loaded onto 1% agarose gel using 1xTAE-Mg^{2+} as running buffer under constant voltage of 80 V for 2 hours. The band corresponding to the origami structures was cut out, crushed and subjected to Freeze and Squeeze™ gel extraction (spin columns from Bio-Rad Laboratories). The efficiency of the purification is calculated to be 70-80 %.

The formation of discrete DNA origami structures was found to be more effective at lower M13 DNA concentration. At higher M13 concentration staple strands joining two arms can cross-link more than one origami leading to higher order structures confirmed by agarose gel analysis (Figure S1).

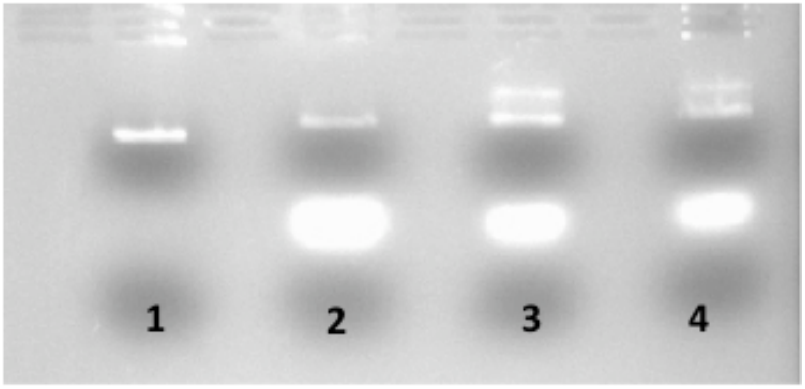

Figure S1: Optimization of annealing conditions for triangular DNA origami: Lane 1- M13; lane 2-4 are origami annealed with: 2) 5 nM M13, in 0.5xTAE-Mg^{2+}; 3) 10 nM M13, in 0.5xTAE-Mg^{2}; and 4) 10 nM M13 in 1xTAE-Mg^{2}. In lane 3 and 4 the slower moving bands are due to cross-linked origami formation due to higher M13 concentration.

TEM imaging of origami triangles:

The TEM sample was prepared by dropping 2 μL of the purified sample solution on carbon coated grid (400 mesh, Ted Pella). Before depositing the sample, the grids were negatively glow discharged using Emitech K100X machine. After 1 minute, the sample was wicked from the grid by touching its edge with a piece of filter paper. To remove the excess salt, touching with a drop of water washed the grid and excess water was wicked away by touching with a filter paper. For staining, the grid was touched with a drop of 0.7 % uranyl formate solution and excess solution was wicked away with a filter paper. Again the grid was touched with the second drop of uranyl formate solution for 20 seconds, and the excess solution was removed with a filter paper. The grid was kept at room temperature to evaporate extra solution. Low-resolution TEM

studies were conducted by using a Philips CM12 transmission electron microscope, operated at 80 kV in the bright field mode.

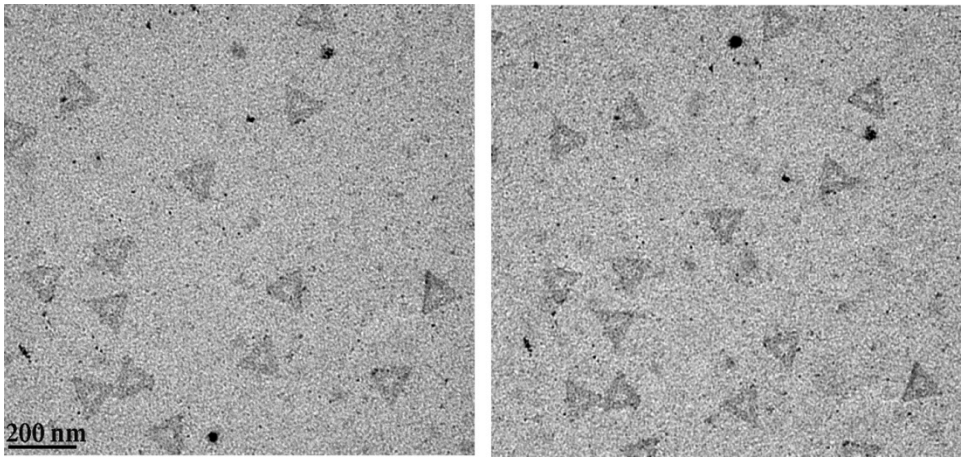

Figure S2: Transmission Electron Microscope (TEM) images of triangular shaped DNA origami structure. The sample was negatively stained with 0.7% Uranyl Formate solution.

Preparation of DNA modified AgNPs:

The silver colloid (1mL) was concentrated 10 times by centrifugation (8,000 rpm, 40 min) and re-dispersed in 1xTBE buffer. To the 100 μL of silver nanoparticle solution, phosphorothioated DNA (9PS-T15) was added so that the final concentration of DNA becomes 8 μM. The nanoparticle solution was kept with gentle shaking overnight on shaker. Then 4 M NaCl was added by small aliquots over 24 hours to raise the final NaCl concentration to 350 mM. The solution was incubated overnight. Then the excess of oligonucleotides was removed by centrifugation (8,000 rpm, 40 min) and re-dispersed to a buffer solution that contains 1xTBE, with 350 mM NaCl. This centrifugation and re-

dispersion procedure was repeated three times to get rid of the excess unattached DNA. The concentration of AgNPs was determined by measuring the absorbance at 400 nm using the extinction coefficient provided by the manufacturer (7.1 X 10^8).

Fabrication of dimer and trimer [(i)-(iv)]:

To 1 μL of 1 nM triangular shaped DNA origami solution, 8 μL (12 μL for trimer) of 0.25 nM 9PS-T15 functionalized AgNP solution (in TBE 1xTBE, 350 mM NaCl buffer) was added. Additional 9 μL of 1x TAE-Mg (13 μL for trimer) buffer was added to make the solution dilute enough to reduce cross-linking. Then the solution was cooled from 45 °C to 4 °C overnight. The resultant dimer and trimer structures were subjected to TEM and STEM imaging for analysis.

Preparation of 1:1 conjugation of DNA with 5 nm AuNP:

a. Activation of Lipoic acid to synthesize NHS ester of lipoic acid. DCC (2.10 g) was mixed with lipoic acid (2.06 g) in THF (10 mL) followed by the addition of NHS (1.15 g, 10 mM). The reaction mixture was filtered after stirring continuously for 72 hrs. The filtrate was evaporated to get a crystalline solid. NHS ester of lipoic acid was further purified by re-crystallization from Toluene.

b. Conjugation of lipoic acid with amine modified oligonucleotides. An ester of lipoic acid prepared as described above was added in excess to 5'-amine modified oligonucleotides (76 mer) in a solution of 70% acetonitrile and 30% water (pH ~ 8). The reaction mixture was kept overnight at room temperature.

Lipoic acid conjugated oligonucleotides were purified by micro-spin G25 columns and used for the next step.

c. Phosphination and concentration of AuNPs. AuNPs (5 nm, Ted Pella Inc.) were stabilized with adsorption of BSPP. Phosphine coating increases the negative charge on the particle surface therefore, stabilizes the AuNPs in high electrolyte concentrations at a higher particle density. BSPP (15 mg) was added to the colloidal nanoparticles solution (50 mL, particle density 5.7x1012/mL) and the mixture was shaken overnight at room temperature. Sodium Chloride (solid) was added slowly to this mixture while stirring until the color changed from deep burgundy to light purple. The resulting mixture was centrifuged at 3000 rpm for 30 min and the supernatant was carefully removed with a pipette. AuNPs were then resuspensed in 1 mL solution of BSPP (2.5 mM). Upon mixing with 1 mL methanol, the mixture was centrifuged, the supernatant was removed and the AuNPs were resuspended in 1 mL BSPP solution (2.5 mM). The concentration of the AuNPs was estimated from the optical absorbance at ~ 520 nm.

d. Preparation of AuNP-DNA conjugates with discrete number of DNA. The lipoic acid modified DNAs is incubated with equimolar ratio of phosphinated AuNPs in 0.5xTBE buffer (89 mM Tris, 89 mM boric acid, 2 mM EDTA, pH 8.0) containing 50 mM NaCl overnight at room temperature. AuNP-DNA conjugates with discrete numbers of oligonucleotides were separated by 3% agarose gel (running buffer 0.5% TBE, loading buffer 50% glycerol, 15 V/cm, 25 μL load volume). The band with 1:1 ratio of AuNP/DNA was electroeluted into the glass fiber filter membrane, backed by dialysis membrane (MWCO 10000). AuNP-

DNA conjugates were recovered using a 0.45 μm centrifugal filter device. Concentration of these AuNP-DNA conjugates was estimated from the optical absorbance at ~ 520 nm.

e. Coating of AuNP/DNA conjugates with short oligonucleotides. The AuNP-DNA conjugates were further stabilized by adding thiolated T5 ssDNA ([HS-T5]/[AuNP]=100, in 0.5x TBE, with 50 mM NaCl) and incubated for 12 hrs at room temperature. Short thymine oligomers on the AuNP surface provide additional stability against the high electrolyte concentration required for DNA self-assembly.

f. Self-assembly of DNA origami nanoarrays. Triangular shaped origami nanoarrays were formed according to Rothemund (Rothemund, P. W. R. *Nature* **2006,** 440, 297-302), except one staple strand at the selected position for the AuNP was replaced with the 1:1 DNA-AuNP conjugate, and three staple strands at the selected position for the AgNP were replaced with the corresponding capture strands. A molar ratio of 1:3 between the long viral ssDNA and the short unmodified helper strands (unpurified) was used, whereas the lipoic acid modified helper strands in 1:1 conjugates with AuNP were used in 1:1 ratios to that of the viral DNA (5 nM). Origami nanoarrays were self-assembled in 1x TBE buffer with 0.5 M NaCl by cooling slowly from 65 °C to room temperature.

g. Fabrication of hetero-metallic 20 nm AgNP, 5 nm AuNP dimer. To the triangular origami modified with one 5 nm AuNP (1μL, 1nM), equivalent amount of 9PS-T15 functionalized AgNP solution (4 μL, 0.25 nM in 1xTBE, 350 mM NaCl buffer) was added. Additional 5 μL of 1x TAE-Mg buffer was added to

make the solution dilute enough to reduce cross-linking. Then the solution was cooled from 45^{O} C to 4^{O} C overnight.

Other characterization methods

High-angle annular dark-field scanning transmission electron microscopy (HAADF-STEM), high-resolution transmission electron microscopy (HRTEM), and energy-dispersive X-ray spectroscopy (EDS) were performed on a JEOL JEM 2010F electron microscope operating at 200 kV. The advantages for STEM imaging of DNA origami samples are: 1) more efficient than a conventional TEM; 2) allowing high contrast imaging of DNA origami samples without requiring staining.

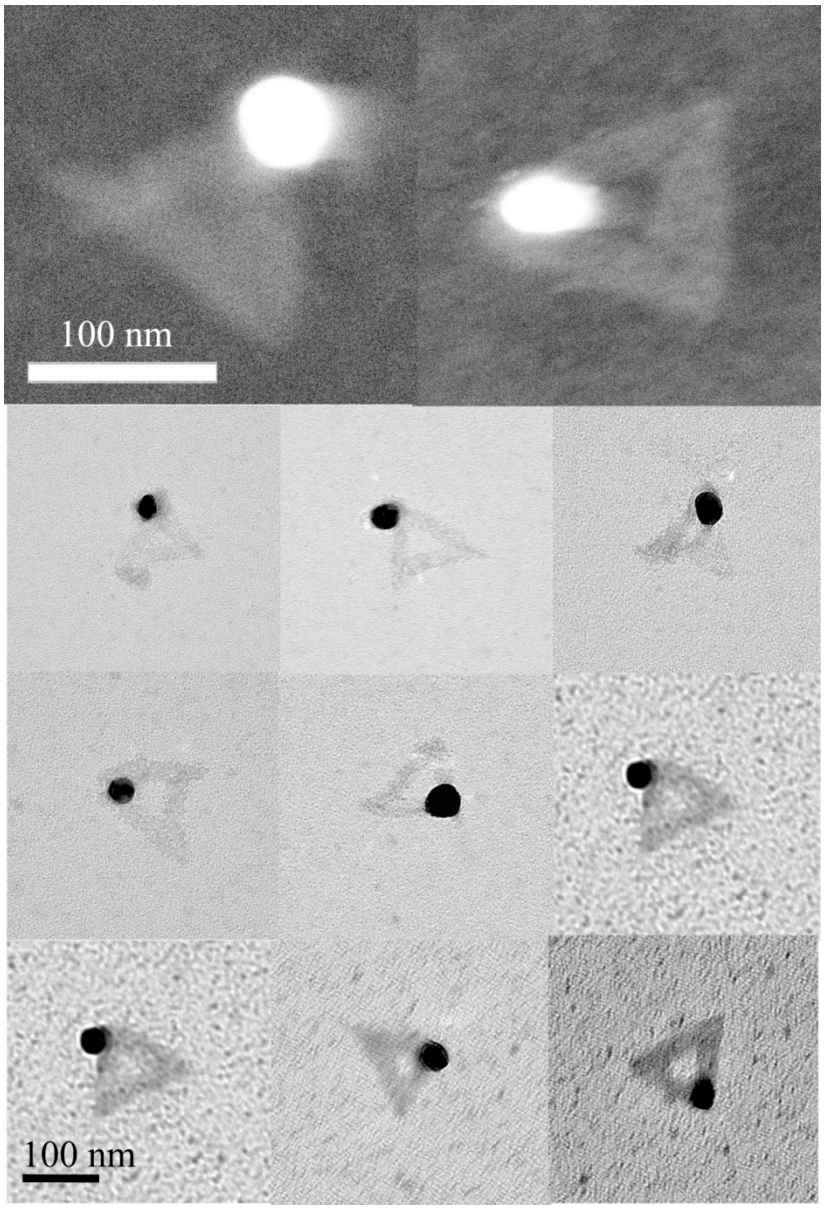

Figure S3: Additional zoom-in STEM (First row) and TEM (Bottom three rows) images of triangular shaped DNA origami with one silver particle. For TEM imaging, the sample was negatively stained with 0.7% Uranyl formate solution. For STEM imaging, the sample was not stained.

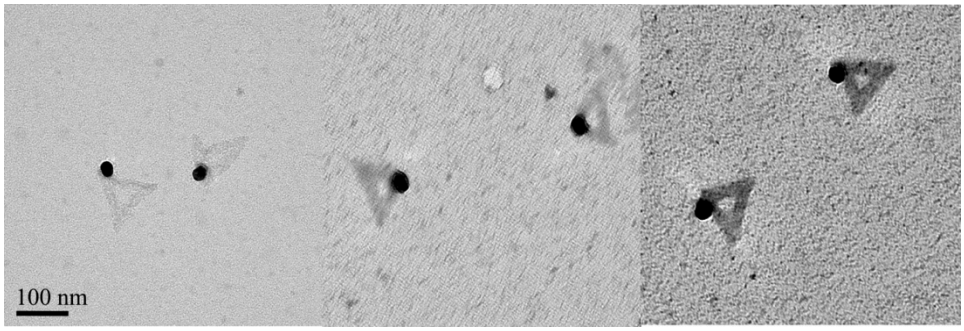

Figure S4: Zoom-out TEM images of triangular shaped DNA origami with one silver particle. For TEM imaging, the sample was negatively stained with 0.7% Uranyl formate solution.

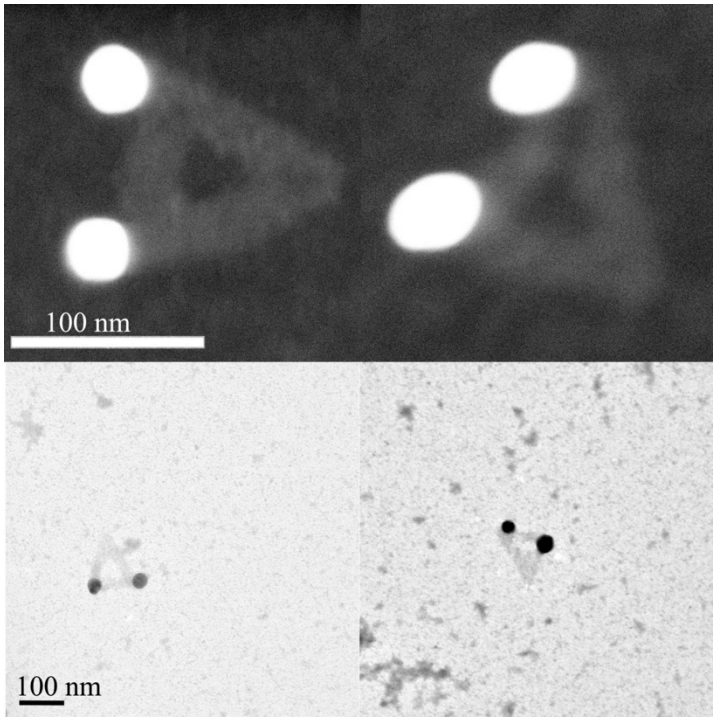

Figure S5: Additional STEM (top row) and TEM images (bottom row) of design (i), AgNP dimers with distance span the full side of the triangular origami. For TEM imaging, the sample was negatively stained with 0.7% Uranyl formate solution. For STEM imaging, the sample was not stained.

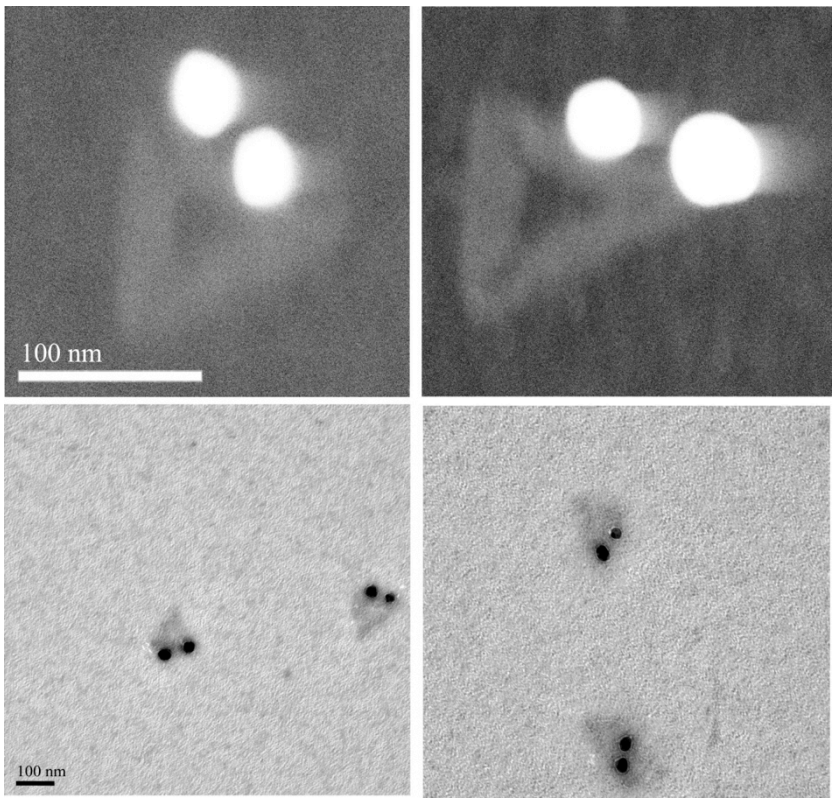

Figure S6: Additional STEM (top row) and TEM (bottom row) images of design (ii), AgNP dimers with distance span half of the side of the triangular origami. For TEM imaging, the sample was negatively stained with 0.7% Uranyl formate solution. For STEM imaging, the sample was not stained.

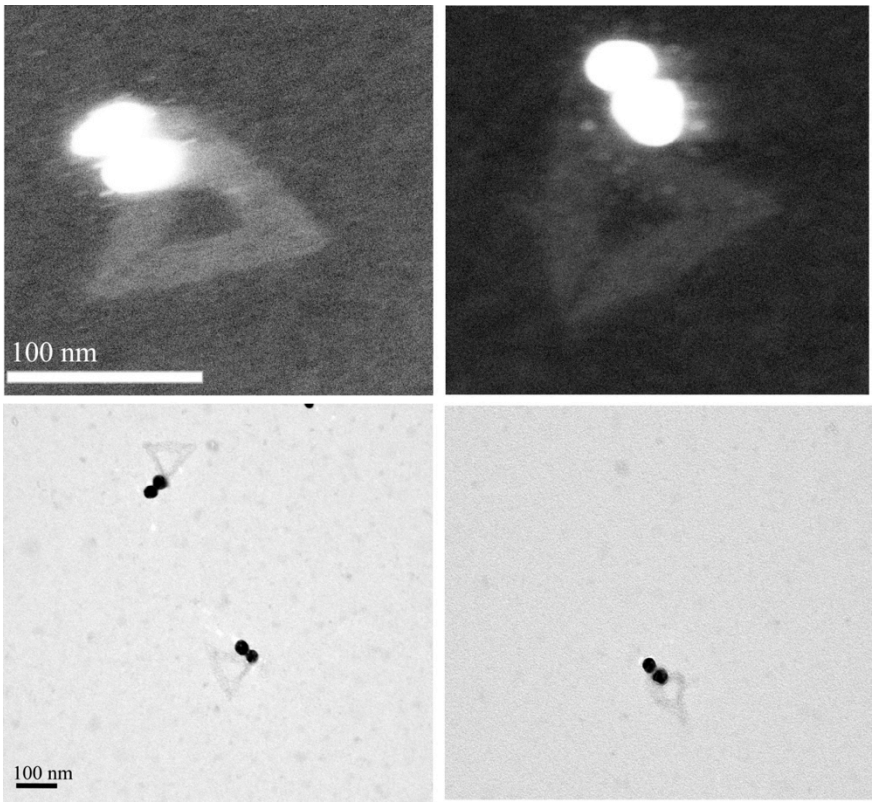

Figure S7: Additional STEM (top row) and TEM (bottom row) images of design (iii) AgNP dimers with a short distance. For TEM imaging, the sample was negatively stained with 0.7% Uranyl formate solution. For STEM imaging, the sample was not stained.

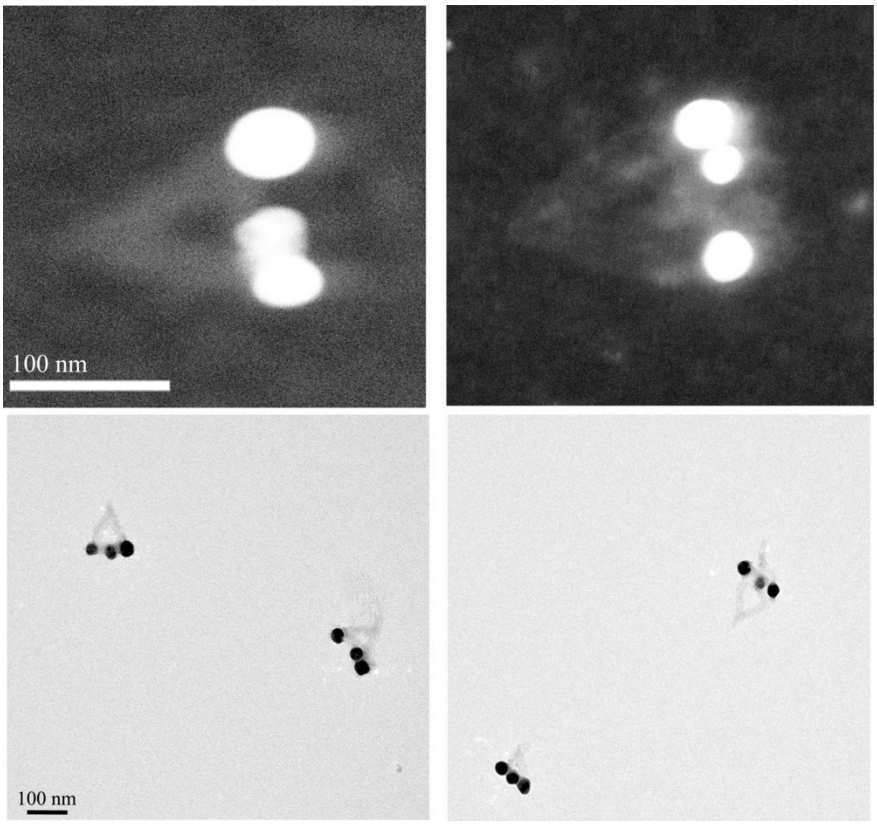

Figure S8: Additional STEM (top row) and TEM (bottom row) images of (iv), AgNP trimers. For TEM imaging, the sample was negatively stained with 0.7% Uranyl formate solution. For STEM imaging, the sample was not stained.

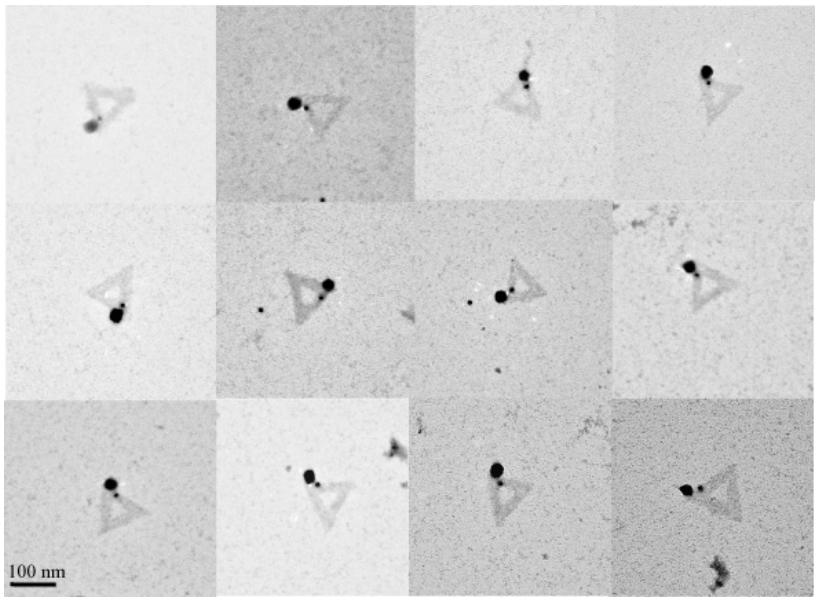

Figure S9: Additional TEM images of hetero dimers of AuNP (5nm) and AgNP (20 nm). For TEM imaging, the sample was negatively stained with 0.7% Uranyl formate solution.

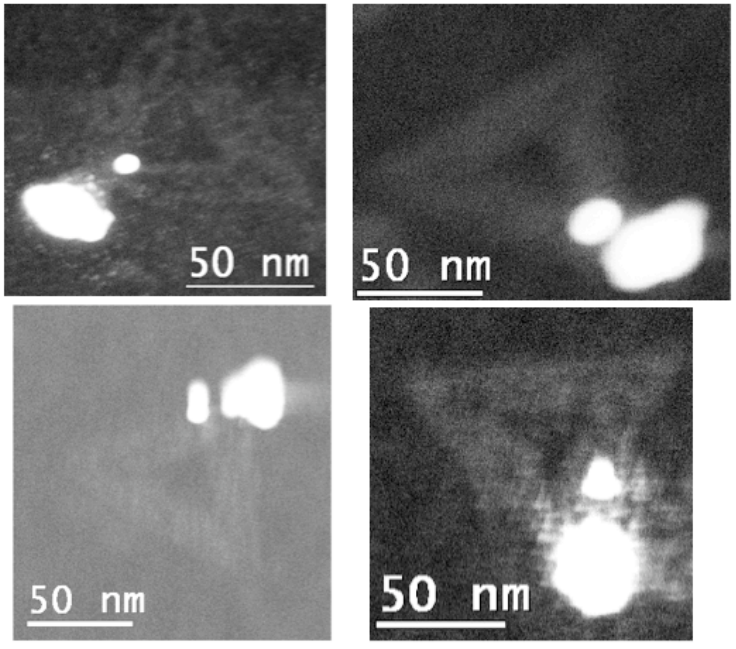

Figure S10: Additional STEM images of hetero dimers of AuNP (5nm) and AgNP (20 nm). For TEM imaging, the sample was not stained.

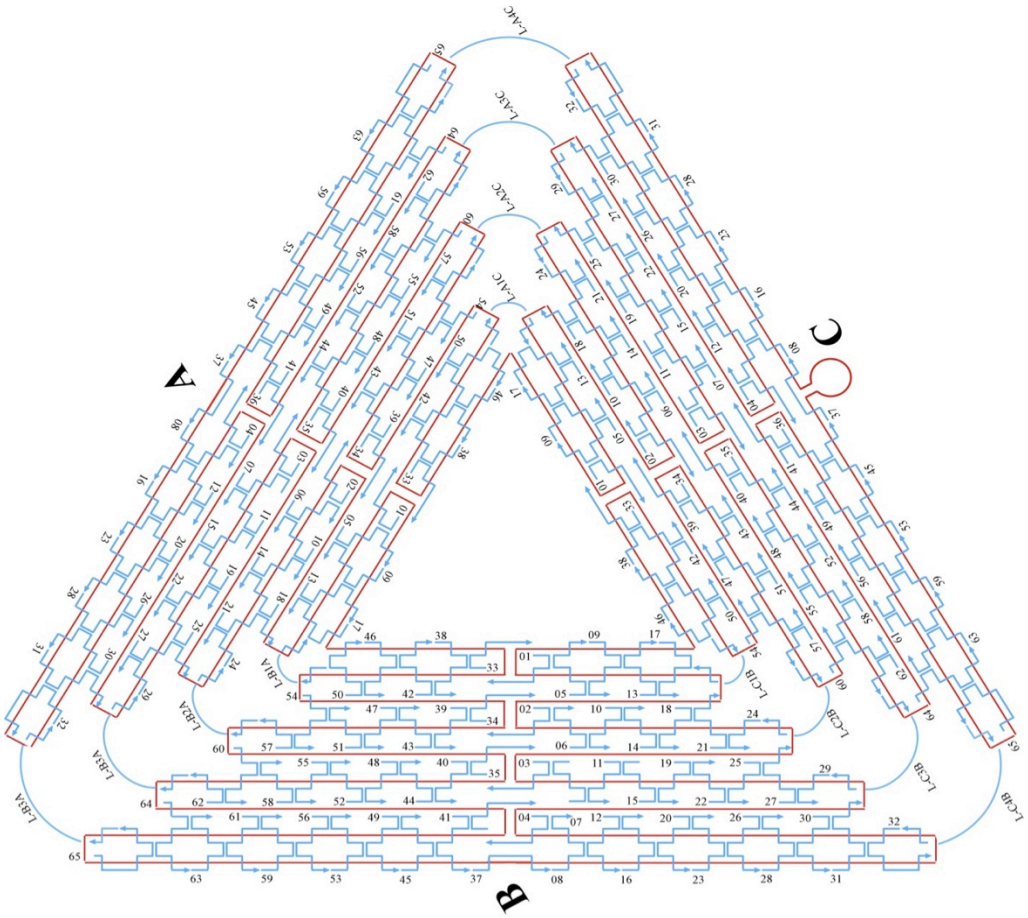

Schematic of origami triangle: showing internal features with helper strands marked with numbers. The viral ssDNA is colored in red and the helper strands are in blue and each individually numbered.

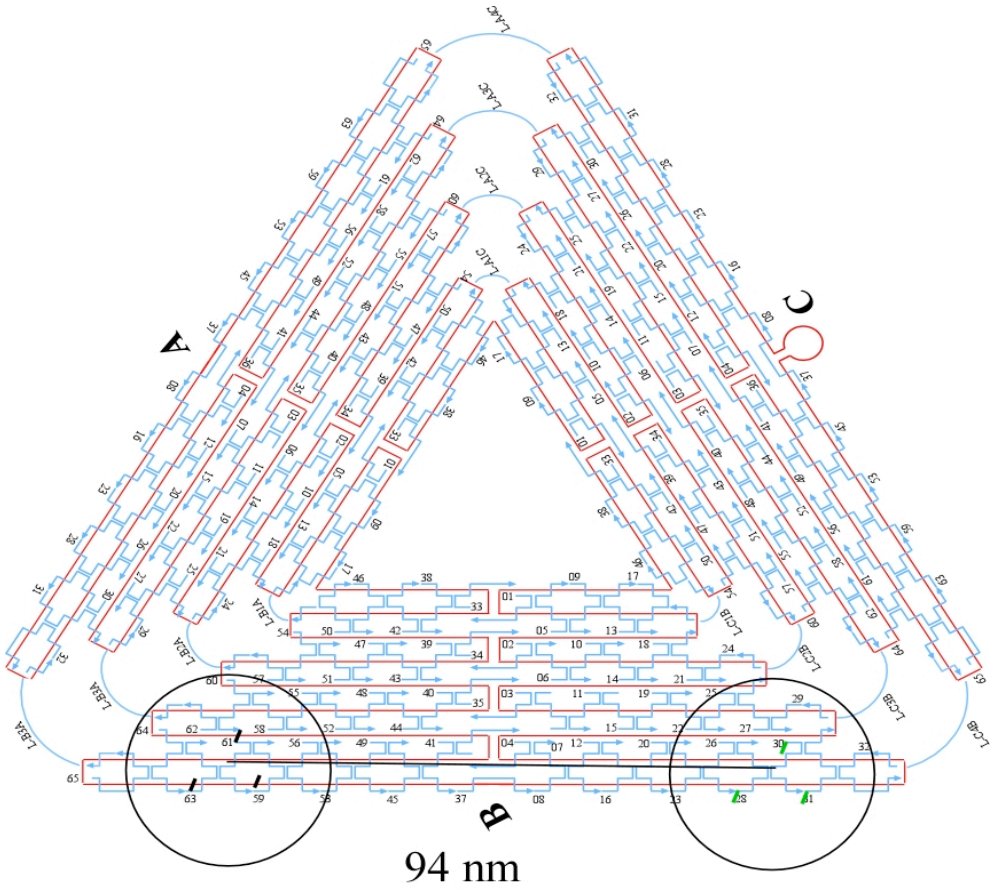

Schematic of design (i), AgNP dimers with distance spanning the full side of the triangular origami. Totally 6 staples strands were selected to extend 15 nucleotides on the 5’ ends as the capture strands, which are marked with short bars, black on the left and green on the right.

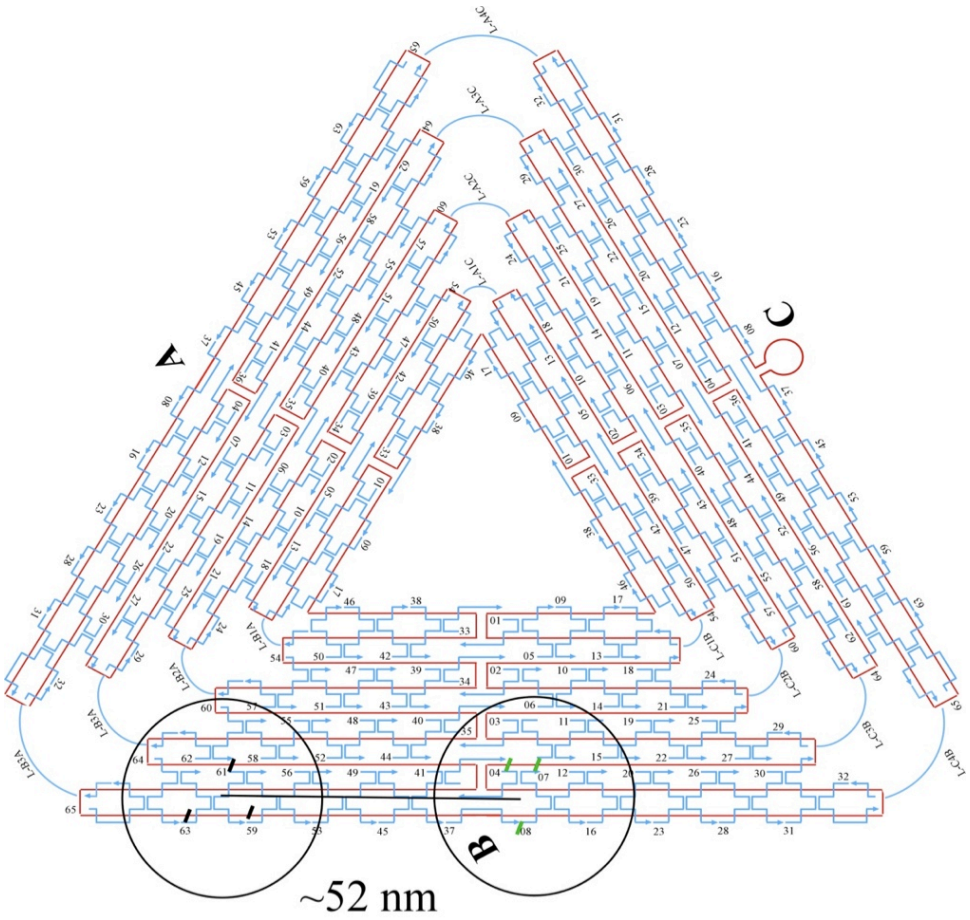

Schematic design of (ii) AgNP dimers with distance spanning half of the side of the triangular origami.

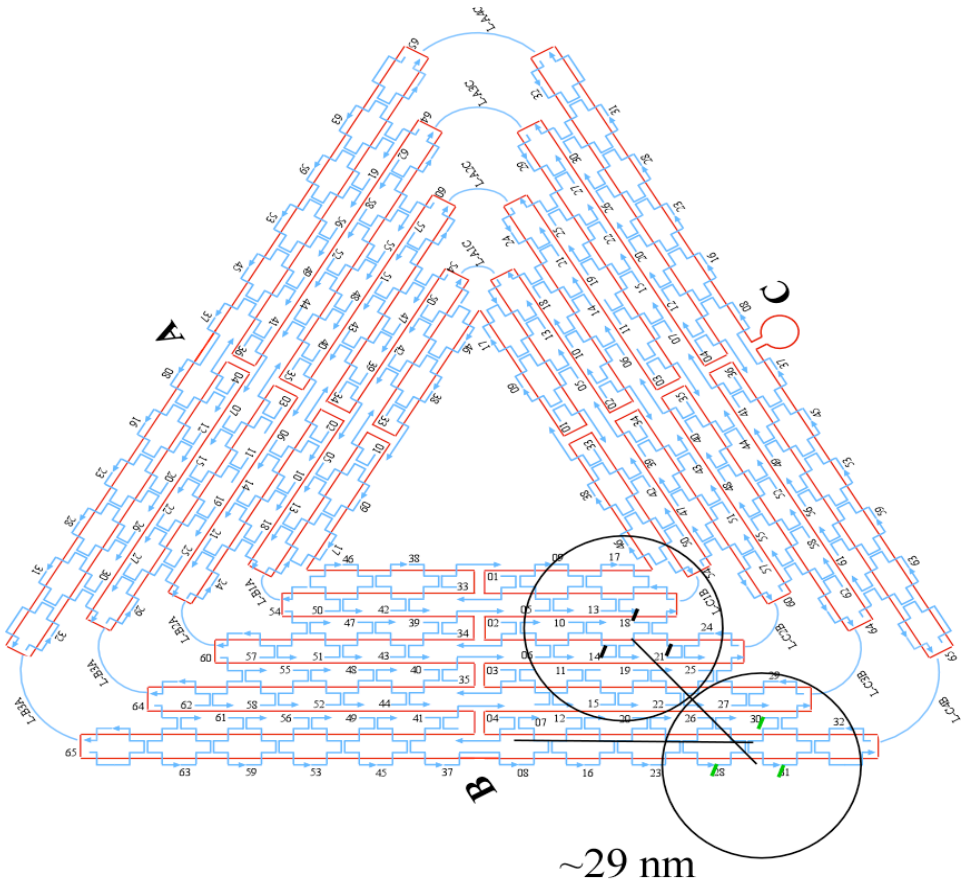

Schematic design of (iii) AgNP dimers with a short distance.

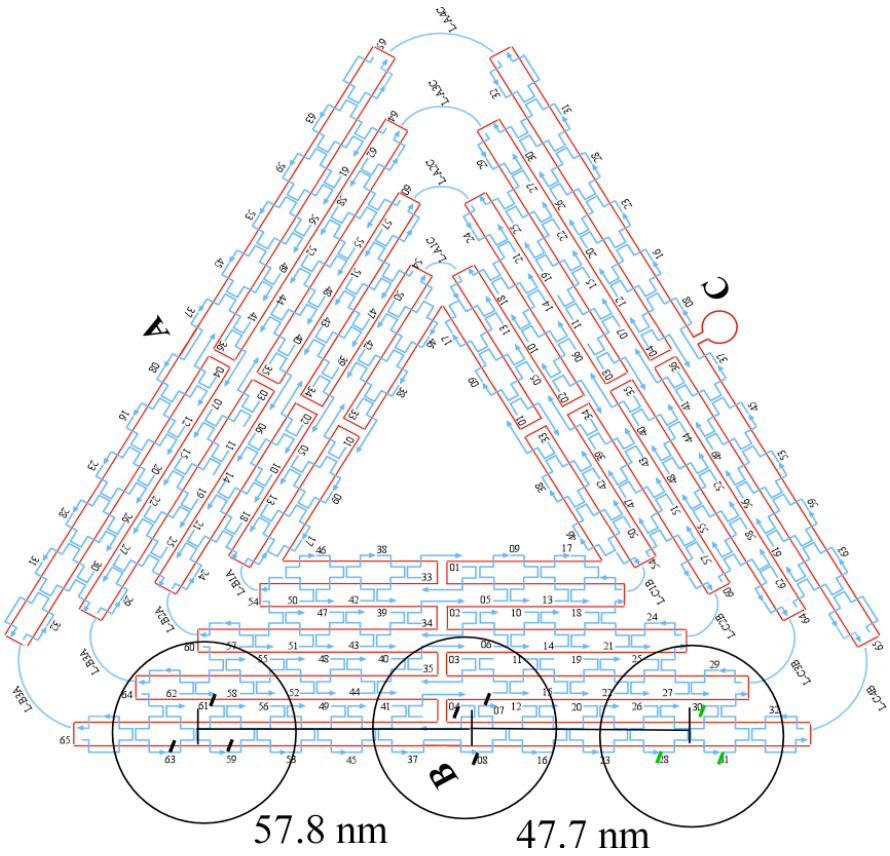

Schematic design of (iv) AgNP trimers.

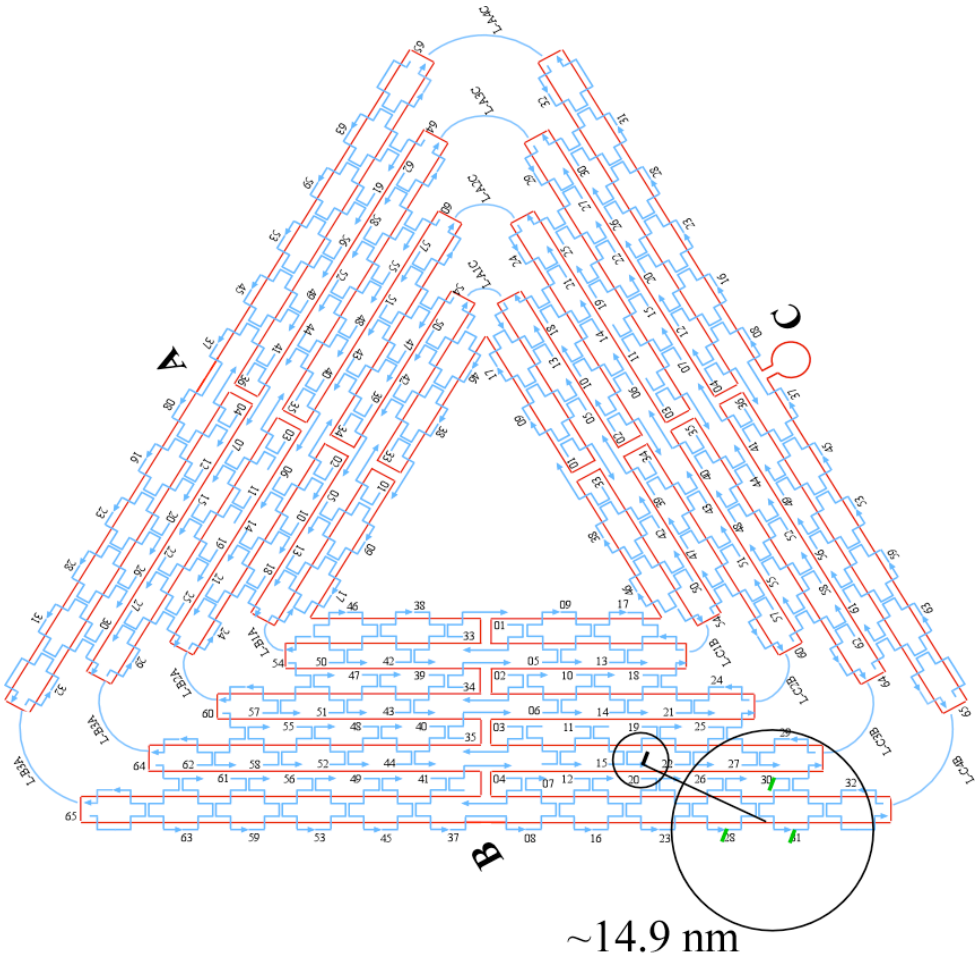

Schematic design of AuNP-AgNP hetero dimer.

DNA Sequences:

A01, CGGGGTTTCCTCAAGAGAAGGATTTTGAATTA,

A02, AGCGTCATGTCTCTGAATTTACCGACTACCTT,

A03, TTCATAATCCCCTTATTAGCGTTTTTCTTACC,

A04, ATGGTTTATGTCACAATCAATAGATATTAAAC,

A05, TTTGATGATTAAGAGGCTGAGACTTGCTCAGTACCAGGCG,

A06, CCGGAACCCAGAATGGAAAGCGCAACATGGCT,

A07, AAAGACAACATTTTCGGTCATAGCCAAAATCA,

A08, GACGGGAGAATTAACTCGGAATAAGTTTATTTCCAGCGCC,

A09, GATAAGTGCCGTCGAGCTGAAACATGAAAGTATACAGGAG,

A10, TGTACTGGAAATCCTCATTAAAGCAGAGCCAC,

A11, CACCGGAAAGCGCGTTTTCATCGGAAGGGCGA,

A12, CATTCAACAAACGCAAAGACACCAGAACACCCTGAACAAA,

A13, TTTAACGGTTCGGAACCTATTATTAGGGTTGATATAAGTA,

A14, CTCAGAGCATATTCACAAACAAATTAATAAGT,

A15, GGAGGGAATTTAGCGTCAGACTGTCCGCCTCC,

A16, GTCAGAGGGTAATTGATGGCAACATATAAAAGCGATTGAG,

A17, TAGCCCGGAATAGGTGAATGCCCCCTGCCTATGGTCAGTG,

A18, CCTTGAGTCAGACGATTGGCCTTGCGCCACCC,

A19, TCAGAACCCAGAATCAAGTTTGCCGGTAAATA,

A20, TTGACGGAAATACATACATAAAGGGCGCTAATATCAGAGA,

A21, CAGAGCCAGGAGGTTGAGGCAGGTAACAGTGCCCG,

A22, ATTAAAGGCCGTAATCAGTAGCGAGCCACCCT,

A23, GATAACCCACAAGAATGTTAGCAAACGTAGAAAATTATTC,

A24, GCCGCCAGCATTGACACCACCCTC,

A25, AGAGCCGCACCATCGATAGCAGCATGAATTAT,

A26, CACCGTCACCTTATTACGCAGTATTGAGTTAAGCCCAATA,

A27, AGCCATTTAAACGTCACCAATGAACACCAGAACCA,

A28, ATAAGAGCAAGAAACATGGCATGATTAAGACTCCGACTTG,

A29, CCATTAGCAAGGCCGGGGGAATTA,

A30, GAGCCAGCGAATACCCAAAAGAACATGAAATAGCAATAGC,

A31, TATCTTACCGAAGCCCAAACGCAATAATAACGAAAATCACCAG,

A32, CAGAAGGAAACCGAGGTTTTTAAGAAAAGTAAGCAGATAGCCG,

A33, CCTTTTTTCATTTAACAATTTCATAGGATTAG,

A34, TTTAACCTATCATAGGTCTGAGAGTTCCAGTA,

A35, AGTATAAAATATGCGTTATACAAAGCCATCTT,

A36, CAAGTACCTCATTCCAAGAACGGGAAATTCAT,

A37, AGAGAATAACATAAAAACAGGGAAGCGCATTA,

A38, AAAACAAAATTAATTAAATGGAAACAGTACATTAGTGAAT,

A39, TTATCAAACCGGCTTAGGTTGGGTAAGCCTGT,

A40, TTAGTATCGCCAACGCTCAACAGTCGGCTGTC,

A41, TTTCCTTAGCACTCATCGAGAACAATAGCAGCCTTTACAG,

A42, AGAGTCAAAAATCAATATATGTGATGAAACAAACATCAAG,

A43, ACTAGAAATATATAACTATATGTACGCTGAGA,

A44, TCAATAATAGGGCTTAATTGAGAATCATAATT,

A45, AACGTCAAAAATGAAAAGCAAGCCGTTTTTATGAAACCAA,

A46, GAGCAAAAGAAGATGAGTGAATAACCTTGCTTATAGCTTA,

A47, GATTAAGAAATGCTGATGCAAATCAGAATAAA,

A48, CACCGGAATCGCCATATTTAACAAAATTTACG,

A49, AGCATGTATTTCATCGTAGGAATCAAACGATTTTTTGTTT,

A50, ACATAGCGCTGTAAATCGTCGCTATTCATTTCAATTACCT,

A51, GTTAAATACAATCGCAAGACAAAGCCTTGAAA,

A52, CCCATCCTCGCCAACATGTAATTTAATAAGGC,

A53, TCCCAATCCAAATAAGATTACCGCGCCCAATAAATAATAT,

A54, TCCCTTAGAATAACGCGAGAAAACTTTTACCGACC,

A55, GTGTGATAAGGCAGAGGCATTTTCAGTCCTGA,

A56, ACAAGAAAGCAAGCAAATCAGATAACAGCCATATTATTTA,

A57, GTTTGAAATTCAAATATATTTTAG,

A58, AATAGATAGAGCCAGTAATAAGAGATTTAATG,

A59, GCCAGTTACAAAATAATAGAAGGCTTATCCGGTTATCAAC,

A60, TTCTGACCTAAAATATAAAGTACCGACTGCAGAAC,

A61, GCGCCTGTTATTCTAAGAACGCGATTCCAGAGCCTAATTT,

A62, TCAGCTAAAAAAGGTAAAGTAATT,

A63, ACGCTAACGAGCGTCTGGCGTTTTAGCGAACCCAACATGT,

A64, ACGACAATAAATCCCGACTTGCGGGAGATCCTGAATCTTACCA,

A65, TGCTATTTTGCACCCAGCTACAATTTTGTTTTGAAGCCTTAAA,

B01, TCATATGTGTAATCGTAAAACTAGTCATTTTC,

B02, GTGAGAAAATGTGTAGGTAAAGATACAACTTT,

B03, GGCATCAAATTTGGGGCGCGAGCTAGTTAAAG,

B04, TTCGAGCTAAGACTTCAAATATCGGGAACGAG,

B05, ACAGTCAAAGAGAATCGATGAACGACCCCGGTTGATAATC,

B06, ATAGTAGTATGCAATGCCTGAGTAGGCCGGAG,

B07, AACCAGACGTTTAGCTATATTTTCTTCTACTA,

B08, GAATACCACATTCAACTTAAGAGGAAGCCCGATCAAAGCG,

B09, AGAAAAGCCCCAAAAAGAGTCTGGAGCAAACAATCACCAT,

B10, CAATATGACCCTCATATATTTTAAAGCATTAA,

B11, CATCCAATAAATGGTCAATAACCTCGGAAGCA,

B12, AACTCCAAGATTGCATCAAAAAGATAATGCAGATACATAA,

B13, CGTTCTAGTCAGGTCATTGCCTGACAGGAAGATTGTATAA,

B14, CAGGCAAGATAAAAATTTTTAGAATATTCAAC,

B15, GATTAGAGATTAGATACATTTCGCAAATCATA,

B16, CGCCAAAAGGAATTACAGTCAGAAGCAAAGCGCAGGTCAG,

B17, GCAAATATTTAAATTGAGATCTACAAAGGCTACTGATAAA,

B18, TTAATGCCTTATTTCAACGCAAGGGCAAAGAA,

B19, TTAGCAAATAGATTTAGTTTGACCAGTACCTT,

B20, TAATTGCTTTACCCTGACTATTATGAGGCATAGTAAGAGC,

B21, ATAAAGCCTTTGCGGGAGAAGCCTGGAGAGGGTAG,

B22, TAAGAGGTCAATTCTGCGAACGAGATTAAGCA,

B23, AACACTATCATAACCCATCAAAAATCAGGTCTCCTTTTGA,

B24, ATGACCCTGTAATACTTCAGAGCA,

B25, TAAAGCTATATAACAGTTGATTCCCATTTTTG,

B26, CGGATGGCACGAGAATGACCATAATCGTTTACCAGACGAC,

B27, TAATTGCTTGGAAGTTTCATTCCAAATCGGTTGTA,

B28, GATAAAAACCAAAATATTAAACAGTTCAGAAATTAGAGCT,

B29, ACTAAAGTACGGTGTCGAATATAA,

B30, TGCTGTAGATCCCCCTCAAATGCTGCGAGAGGCTTTTGCA,

B31, AAAGAAGTTTTGCCAGCATAAATATTCATTGACTCAACATGTT,

B32, AATACTGCGGAATCGTAGGGGGTAATAGTAAAATGTTTAGACT,

B33, AGGGATAGCTCAGAGCCACCACCCCATGTCAA,

B34, CAACAGTTTATGGGATTTTGCTAATCAAAAGG,

B35, GCCGCTTTGCTGAGGCTTGCAGGGGAAAAGGT,

B36, GCGCAGACTCCATGTTACTTAGCCCGTTTTAA,

B37, ACAGGTAGAAAGATTCATCAGTTGAGATTTAG,

B38, CCTCAGAACCGCCACCCAAGCCCAATAGGAACGTAAATGA,

B39, ATTTTCTGTCAGCGGAGTGAGAATACCGATAT,

B40, ATTCGGTCTGCGGGATCGTCACCCGAAATCCG,

B41, CGACCTGCGGTCAATCATAAGGGAACGGAACAACATTATT,

B42, AGACGTTACCATGTACCGTAACACCCCTCAGAACCGCCAC,

B43, CACGCATAAGAAAGGAACAACTAAGTCTTTCC,

B44, ATTGTGTCTCAGCAGCGAAAGACACCATCGCC,

B45, TTAATAAAACGAACTAACCGAACTGACCAACTCCTGATAA,

B46, AGGTTTAGTACCGCCATGAGTTTCGTCACCAGGATCTAAA,

B47, GTTTTGTCAGGAATTGCGAATAATCCGACAAT,

B48, GACAACAAGCATCGGAACGAGGGTGAGATTTG,

B49, TATCATCGTTGAAAGAGGACAGATGGAAGAAAAATCTACG,

B50, AGCGTAACTACAAACTACAACGCCTATCACCGTACTCAGG,

B51, TAGTTGCGAATTTTTTCACGTTGATCATAGTT,

B52, GTACAACGAGCAACGGCTACAGAGGATACCGA,

B53, ACCAGTCAGGACGTTGGAACGGTGTACAGACCGAAACAAA,

B54, ACAGACAGCCCAAATCTCCAAAAAAAAATTTCTTA,

B55, AACAGCTTGCTTTGAGGACTAAAGCGATTATA,

B56, CCAAGCGCAGGCGCATAGGCTGGCAGAACTGGCTCATTAT,

B57, CGAGGTGAGGCTCCAAAAGGAGCC,

B58, ACCCCCAGACTTTTTCATGAGGAACTTGCTTT,

B59, ACCTTATGCGATTTTATGACCTTCATCAAGAGCATCTTTG,

B60, CGGTTTATCAGGTTTCCATTAAACGGGAATACACT,

B61, AAAACACTTAATCTTGACAAGAACTTAATCATTGTGAATT,

B62, GGCAAAAGTAAAATACGTAATGCC,

B63, TGGTTTAATTTCAACTCGGATATTCATTACCCACGAAAGA,

B64, ACCAACCTAAAAAATCAACGTAACAAATAAATTGGGCTTGAGA,

B65, CCTGACGAGAAACACCAGAACGAGTAGGCTGCTCATTCAGTGA,

Link-A1C, TTAATTAATTTTTTACCATATCAAA,

Link-A2C, TTAATTTCATCTTAGACTTTACAA,

Link-A3C, CTGTCCAGACGTATACCGAACGA,

Link-A4C, TCAAGATTAGTGTAGCAATACT,

Link-B1A, TGTAGCATTCCTTTTATAAACAGTT,

Link-B2A, TTTAATTGTATTTCCACCAGAGCC,

Link-B3A, ACTACGAAGGCTTAGCACCATTA,

Link-B4A, ATAAGGCTTGCAACAAAGTTAC,

Link-C1B, GTGGGAACAAATTTCTATTTTTGAG,

Link-C2B, CGGTGCGGGCCTTCCAAAAACATT,

Link-C3B, ATGAGTGAGCTTTTAAATATGCA,

Link-C4B, ACTATTAAAGAGGATAGCGTCC,

Loop, GCGCTTAATGCGCCGCTACAGGGC,

C01, TCGGGAGATATACAGTAACAGTACAAATAATT,

C02, CCTGATTAAAGGAGCGGAATTATCTCGGCCTC,

C03, GCAAATCACCTCAATCAATATCTGCAGGTCGA,

C04, CGACCAGTACATTGGCAGATTCACCTGATTGC,

C05, TGGCAATTTTTAACGTCAGATGAAAACAATAACGGATTCG,

C06, AAGGAATTACAAAGAAACCACCAGTCAGATGA,

C07, GGACATTCACCTCAAATATCAAACACAGTTGA,

C08, TTGACGAGCACGTATACTGAAATGGATTATTTAATAAAAG,

C09, CCTGATTGCTTTGAATTGCGTAGATTTTCAGGCATCAATA,

C10, TAATCCTGATTATCATTTTGCGGAGAGGAAGG,

C11, TTATCTAAAGCATCACCTTGCTGATGGCCAAC,

C12, AGAGATAGTTTGACGCTCAATCGTACGTGCTTTCCTCGTT,

C13, GATTATACACAGAAATAAAGAAATACCAAGTTACAAAATC,

C14, TAGGAGCATAAAAGTTTGAGTAACATTGTTTG,

C15, TGACCTGACAAATGAAAAATCTAAAATATCTT,

C16, AGAATCAGAGCGGGAGATGGAAATACCTACATAACCCTTC,

C17, GCGCAGAGGCGAATTAATTATTTGCACGTAAATTCTGAAT,

C18, AATGGAAGCGAACGTTATTAATTTCTAACAAC,

C19, TAATAGATCGCTGAGAGCCAGCAGAAGCGTAA,

C20, GAATACGTAACAGGAAAAACGCTCCTAAACAGGAGGCCGA,

C21, TCAATAGATATTAAATCCTTTGCCGGTTAGAACCT,

C22, CAATATTTGCCTGCAACAGTGCCATAGAGCCG,

C23, TTAAAGGGATTTTAGATACCGCCAGCCATTGCGGCACAGA,

C24, ACAATTCGACAACTCGTAATACAT,

C25, TTGAGGATGGTCAGTATTAACACCTTGAATGG,

C26, CTATTAGTATATCCAGAACAATATCAGGAACGGTACGCCA,

C27, CGCGAACTAAAACAGAGGTGAGGCTTAGAAGTATT,

C28, GAATCCTGAGAAGTGTATCGGCCTTGCTGGTACTTTAATG,

C29, ACCACCAGCAGAAGATGATAGCCC,

C30, TAAAACATTAGAAGAACTCAAACTTTTTATAATCAGTGAG,

C31, GCCACCGAGTAAAAGAACATCACTTGCCTGAGCGCCATTAAAA,

C32, TCTTTGATTAGTAATAGTCTGTCCATCACGCAAATTAACCGTT,

C33, CGCGTCTGATAGGAACGCCATCAACTTTTACA,

C34, AGGAAGATGGGGACGACGACAGTAATCATATT,

C35, CTCTAGAGCAAGCTTGCATGCCTGGTCAGTTG,

C36, CCTTCACCGTGAGACGGGCAACAGCAGTCACA,

C37, CGAGAAAGGAAGGGAAGCGTACTATGGTTGCT,

C38, GCTCATTTTTTAACCAGCCTTCCTGTAGCCAGGCATCTGC,

C39, CAGTTTGACGCACTCCAGCCAGCTAAACGACG,

C40, GCCAGTGCGATCCCCGGGTACCGAGTTTTTCT,

C41, TTTCACCAGCCTGGCCCTGAGAGAAAGCCGGCGAACGTGG,

C42, GTAACCGTCTTTCATCAACATTAAAATTTTTGTTAAATCA,

C43, ACGTTGTATTCCGGCACCGCTTCTGGCGCATC,

C44, CCAGGGTGGCTCGAATTCGTAATCCAGTCACG,

C45, TAGAGCTTGACGGGGAGTTGCAGCAAGCGGTCATTGGGCG,

C46, GTTAAAATTCGCATTAATGTGAGCGAGTAACACACGTTGG,

C47, TGTAGATGGGTGCCGGAAACCAGGAACGCCAG,

C48, GGTTTTCCATGGTCATAGCTGTTTGAGAGGCG,

C49, GTTTGCGTCACGCTGGTTTGCCCCAAGGGAGCCCCCGATT,

C50, GGATAGGTACCCGTCGGATTCTCCTAAACGTTAATATTTT,

C51, AGTTGGGTCAAAGCGCCATTCGCCCCGTAATG,

C52, CGCGCGGGCCTGTGTGAAATTGTTGGCGATTA,

C53, CTAAATCGGAACCCTAAGCAGGCGAAAATCCTTCGGCCAA,

C54, CGGCGGATTGAATTCAGGCTGCGCAACGGGGGATG,

C55, TGCTGCAAATCCGCTCACAATTCCCAGCTGCA,

C56, TTAATGAAGTTTGATGGTGGTTCCGAGGTGCCGTAAAGCA,

C57, TGGCGAAATGTTGGGAAGGGCGAT,

C58, TGTCGTGCACACAACATACGAGCCACGCCAGC,

C59, CAAGTTTTTTGGGGTCGAAATCGGCAAAATCCGGGAAACC,

C60, TCTTCGCTATTGGAAGCATAAAGTGTATGCCCGCT,

C61, TTCCAGTCCTTATAAATCAAAAGAGAACCATCACCCAAAT,

C62, GCGCTCACAAGCCTGGGGTGCCTA,

C63, CGATGGCCCACTACGTATAGCCCGAGATAGGGATTGCGTT,

C64, AACTCACATTATTGAGTGTTGTTCCAGAAACCGTCTATCAGGG,

C65, ACGTGGACTCCAACGTCAAAGGGCGAATTTGGAACAAGAGTCC,

For following designs we have replaced strands with mentioned sequences:

STRUCTURE (i):

B59 capture:

AAAAAAAAAAAAAAAGCCAGTTACAAAATAATAGAAGGCTTATCCGG

TTATCAAC

B61 capture:

AAAAAAAAAAAAAAAAAAACACTTAATCTTGACAAGAACTTAATCAT

TGTGAATT

B63 capture:

AAAAAAAAAAAAAAATGGTTTAATTTCAACTCGGATATTCATTACCCA

CGAAAGA

B28 capture:

AAAAAAAAAAAAAAA

GATAAAAACCAAAATATTAAACAGTTCAGAAATTAGAGCT

B30 capture:

AAAAAAAAAAAAAAA

TGCTGTAGATCCCCCTCAAATGCTGCGAGAGGCTTTTGCA

B31 capture:

AAAAAAAAAAAAAAA

AAAGAAGTTTTGCCAGCATAAATATTCATTGACTCAACATGTT

STRUCTURE (ii):

B28 capture:

AAAAAAAAAAAAAAA

GATAAAAACCAAAATATTAAACAGTTCAGAAATTAGAGCT

B30 capture:

AAAAAAAAAAAAAAA

TGCTGTAGATCCCCCTCAAATGCTGCGAGAGGCTTTTGCA

B31 capture:

AAAAAAAAAAAAAAA

AAAGAAGTTTTGCCAGCATAAATATTCATTGACTCAACATGTT

B04 capture:

AAAAAAAAAAAAAAA

TTCGAGCTAAGACTTCAAATATCGGGAACGAG

B07 capture:

AAAAAAAAAAAAAAA AACCAGACGTTTAGCTATATTTTCTTCTACTA

B08 capture:

AAAAAAAAAAAAAAA

GAATACCACATTCAACTTAAGAGGAAGCCCGATCAAAGCG

STRUCTURE (iii):

B28 capture:

AAAAAAAAAAAAAAA

GATAAAAACCAAAATATTAAACAGTTCAGAAATTAGAGCT

B30 capture:

AAAAAAAAAAAAAAA

TGCTGTAGATCCCCCTCAAATGCTGCGAGAGGCTTTTGCA

B31 capture:

AAAAAAAAAAAAAAA

AAAGAAGTTTTGCCAGCATAAATATTCATTGACTCAACATGTT

B18 capture:

AAAAAAAAAAAAAAA CCTTGAGTCAGACGATTGGCCTTGCGCCACCC

B14 capture:

AAAAAAAAAAAAAAA CTCAGAGCATATTCACAAACAAATTAATAAGT

B21 capture:

AAAAAAAAAAAAAAA

CAGAGCCAGGAGGTTGAGGCAGGTAACAGTGCCCG

STRUCTURE (iv):

B59 capture:

AAAAAAAAAAAAAAAGCCAGTTACAAAATAATAGAAGGCTTATCCGG

TTATCAAC

B61 capture:

AAAAAAAAAAAAAAAAAAACACTTAATCTTGACAAGAACTTAATCAT

TGTGAATT

B63 capture:

AAAAAAAAAAAAAAATGGTTTAATTTCAACTCGGATATTCATTACCCA

CGAAAGA

B28 capture:

AAAAAAAAAAAAAAA

GATAAAAACCAAAATATTAAACAGTTCAGAAATTAGAGCT

B30 capture:

AAAAAAAAAAAAAAA

TGCTGTAGATCCCCCTCAAATGCTGCGAGAGGCTTTTGCA

B31 capture:

AAAAAAAAAAAAAAA

AAAGAAGTTTTGCCAGCATAAATATTCATTGACTCAACATGTT

B04 capture:

AAAAAAAAAAAAAAA

TTCGAGCTAAGACTTCAAATATCGGGAACGAG

B07 capture:

AAAAAAAAAAAAAAA AACCAGACGTTTAGCTATATTTTCTTCTACTA

B08 capture:

AAAAAAAAAAAAAAA

GAATACCACATTCAACTTAAGAGGAAGCCCGATCAAAGCG

20 nm AgNP-5 nm AuNP hetero dimer:

B28 capture:

AAAAAAAAAAAAAAA

GATAAAAACCAAAATATTAAACAGTTCAGAAATTAGAGCT

B30 capture:

AAAAAAAAAAAAAAA

TGCTGTAGATCCCCCTCAAATGCTGCGAGAGGCTTTTGCA

B31 capture:

AAAAAAAAAAAAAAA

AAAGAAGTTTTGCCAGCATAAATATTCATTGACTCAACATGTT

B(18+19) Au:

NH_2C_6-

GGGTTTTTAATGCCTTATTTCAACGCAAGGGCAAAGAATTAGCAAATA

GATTTAGTTTGACCAGTACCTTAAAAAA

APPENDIX B

SUPPLEMENTAL INFORMATION FOR CHAPTER 3

Supplemental Information for

Quantum Efficiency Modification of Organic Fluorophores Using

Gold Nanoparticles on DNA Origami Scaffolds

Theoretical Calculations:

We simulate the energy transfer between a dye molecule and nearby metal nanoparticles using a coupled dipole method similar to the method described in the reference. "Distance-dependent interactions between gold nanoparticles and fluorescent molecules with DNA as tunable spacers" Rahul Chhabra, Jaswinder Sharma, Haining Wang, Shengli Zou, Su Lin, Hao Yan, Stuart Lindsay, Yan Liu, ***Nanotechnology*** (2009) 20(48) 485201].

The excitation rate of the molecule at the excitation frequency is proportional to the enhanced local electric field $|E|^2$ at the position of the dye molecule due to the presence of nearby metal nanoparticles. At the emission frequency, the energy transfer between the dye molecule and the metal nanoparticle depends on the size and composition of the metal nanoparticle, the distance between the dye and the surface of metal nanoparticle. The quantum yield of the dye molecule will also have an effect to the energy transfer. For a dye molecule molecule with radiative and non-radiative rate constants, k_r and k_{nr}, its quantum yield, η,

$$\eta = \frac{k_r}{k_r + k_{nr}} \qquad (1)$$

when one or more metal nanoparticles are placed near a dye molecule, the energy transfer between the dye molecule and the nanoparticles will change the radiative decay rate of the dye molecule. We represent the new radiative rate constant of the dye molecule as k_t. Please note that part of the radiated energy from the dye molecule will be re-absorbed by the metal nanoparticle and become non-radiative, and only part will be emitted eventually. The modified quantum yield η',

$$\eta' = \frac{k_r'}{k_t + k_{nr}} = \frac{f_r \times k_r}{f_t \times k + k_{nr}} \qquad (2)$$

where k_r' is the radiative rate constant of the total system including the dye molecule and metal nanoparticles.

Since the total energy is conserved, the enhancement or quenching factor of the fluorescence of the dye molecule due to the presence of nearby metal nanoparticles becomes

$$\frac{\eta'}{\eta} = \frac{f_r \times (k_r + k_{nr})}{f_t \times k_r + k_{nr}} = \frac{f_r}{f_t \times \eta + 1 - \eta} \qquad (3)$$

If including the enhancement at the excitation frequency, the measured fluorescence signal relative to the original one can be calculated using

$$\frac{I'}{I_0} = \frac{|E|^2 f_r}{f_t \times \eta + 1 - \eta} \qquad (4),$$

where I_0 and I' are the fluorescence intensities of an isolated dye molecule and a dye molecule surrounded with metal nanoparticle, respectively. $|E|^2$ is the enhanced local electric field at the position of the dye molecule at the excitation frequency due the nearby metal nanoparticles.

In the coupled dipole method, we illuminate only the dye molecule and leave the metal nanoparticles in the dark. $f_r = \frac{k_r'}{k_r}$ is the enhancement of the radiative rate constant of the system due to the presence of nearby metal nanoparticles relative to an isolated dye molecule, which is proportional to the enhanced electric field $|E|^2$ of nearby metal nanoparticle at the position of the dye molecule.[Kerker, M.; Wang, D. S.; Chew, H. *Appl. Opt.* **1980**, *19*, 3373.].

$f_t = \frac{k_t}{k_r}$ is the enhancement factor of the radiative constant of the dye molecule itself, which is partially re-absorbed by the nearby metal nanoparticle and becomes non-radiative decay. f_t can be calculated by subtracting the extinction cross section of the dye molecule and its absorption cross section.

The life time, τ, change of the dye molecule can be calculated using equation

$$\frac{\tau'}{\tau} = \frac{k_r + k_{nr}}{k_t + k_{nr}} = \frac{k_r + k_{nr}}{f_t \times k_r + k_{nr}} = \frac{1}{f_t \times \eta + 1 - \eta} \quad (5)$$

Fluorescence measurements:

Fluorescence decay kinetics was measured using the time-correlated single-photon counting (TCSPC) technique. The excitation source was a fiber supercontinuum laser based on a passive modelocked fiber laser and a high-nonlinearity photonic crystal fiber supercontinuum generator (Fianium SC450). The laser provides 6-ps pulses at a repetition rate variable between 0.1 – 40 MHz. The laser output was sent through an Acousto-Optical Tunable Filer (Fianium AOTF) to obtain excitation pulses at desired wavelength of 525 nm. Fluorescence emission was collected at 90° and detected using a double-grating monochromator (Jobin-Yvon, Gemini-180) and a microchannel plate photomultiplier tube (Hamamatsu R3809U-50). The polarization of the emission was 54.7° relative to that of the excitation. Data acquisition was done using a single photon counting card (Becker-Hickl, SPC-830). The IRF had a FWHM of 50 ps, measured from the scattering of sample at the excitation wavelength. The

excitation repetition rate was 20 MHz. The data was fitted with a sum of exponential decay model globally or at a single wavelength using ASUFIT.

All steady state fluorescence spectra were measured by a Nanolog fluorometer (Horiba Jobin Yvon, L-format, equipped with a CW 450W Xenon light source, thermoelectrically cooled R928 PMT), with a 3 mm path length quartz cell (Hellma). We have used 8 nm excitation and 8 nm emission slit widths and a 550 nm long pass filter was in the emission side to cutoff the scattering from the gold nanoparticles.

Supplemental figures:

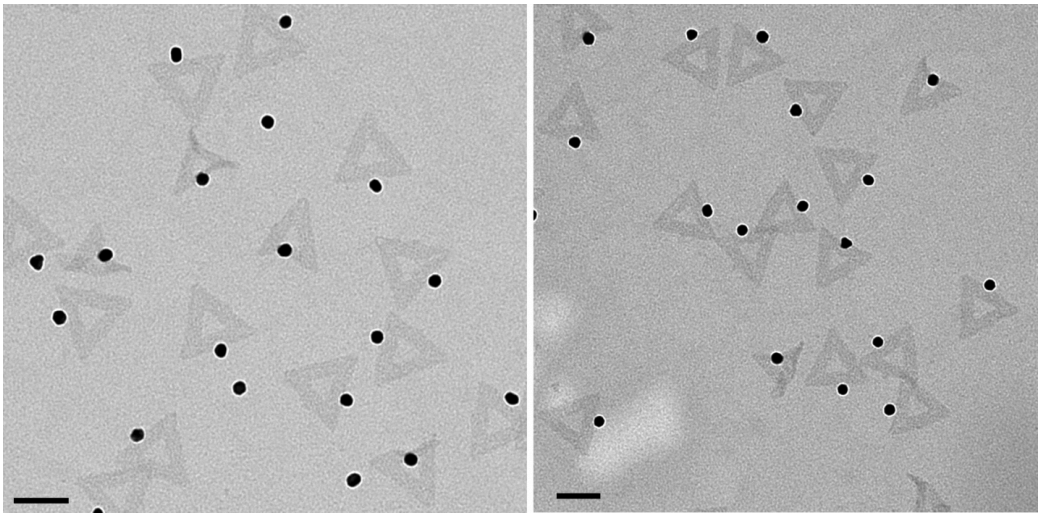

Figure S1: Zoom out TEM images of monomeric constructs with particle dye distance 12.8 nm. Scale bar is 100 nm.

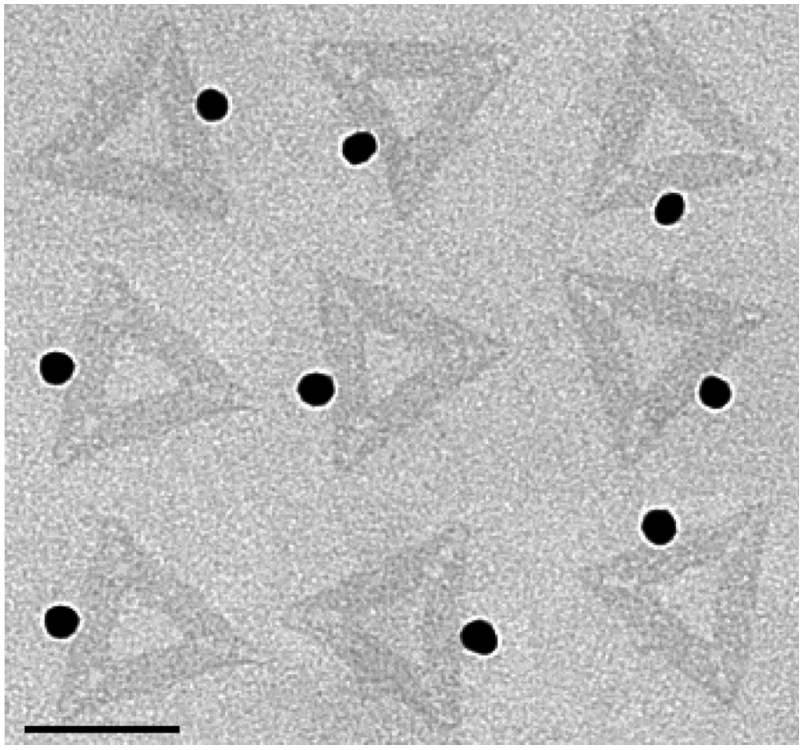

Figure S2: Zoom in TEM images of monomeric constructs with particle dye distance 12.8 nm. Scale bar is 100 nm

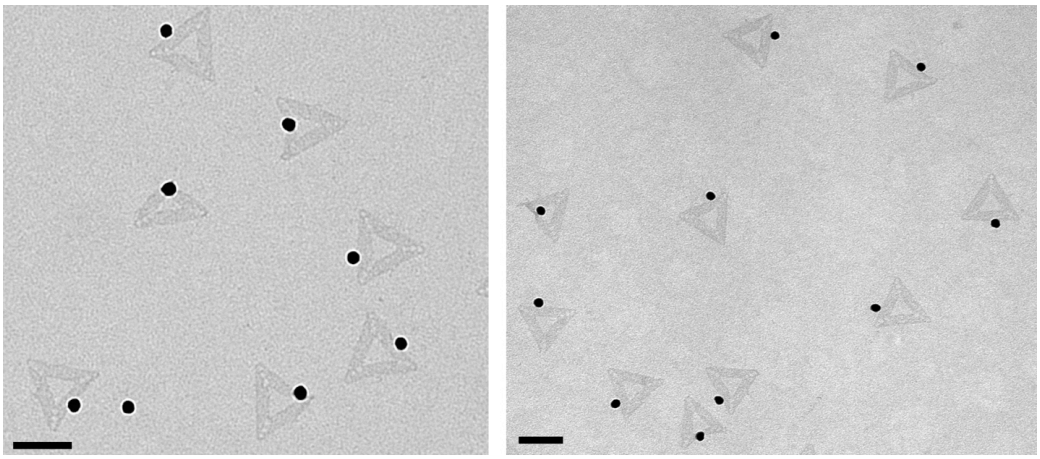

Figure S3: Zoom out TEM images of monomeric constructs with particle dye distance 17.2 nm. Scale bar is 100 nm

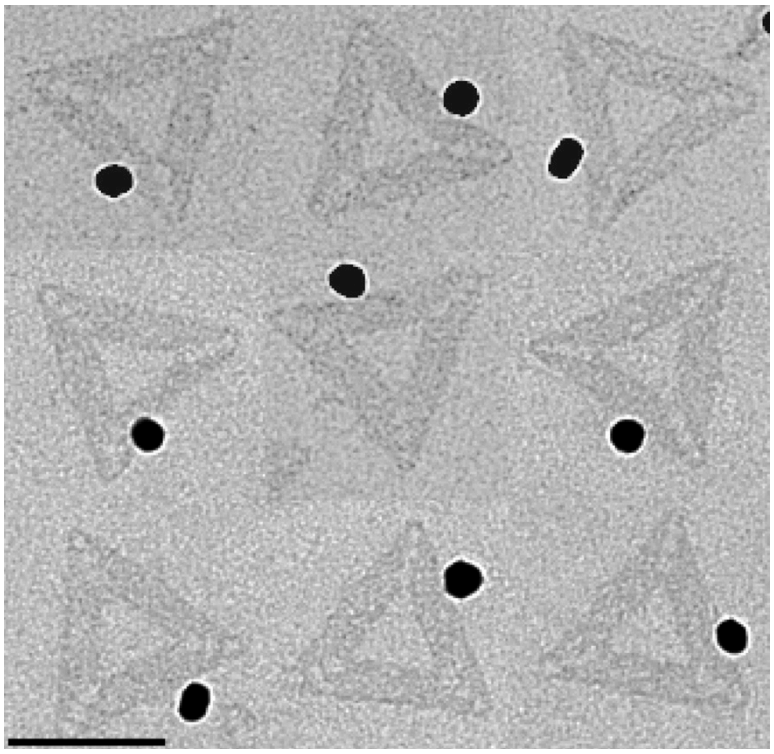

Figure S4: Zoom in TEM images of monomeric constructs with particle dye distance 17.2 nm. Scale bar is 100 nm.

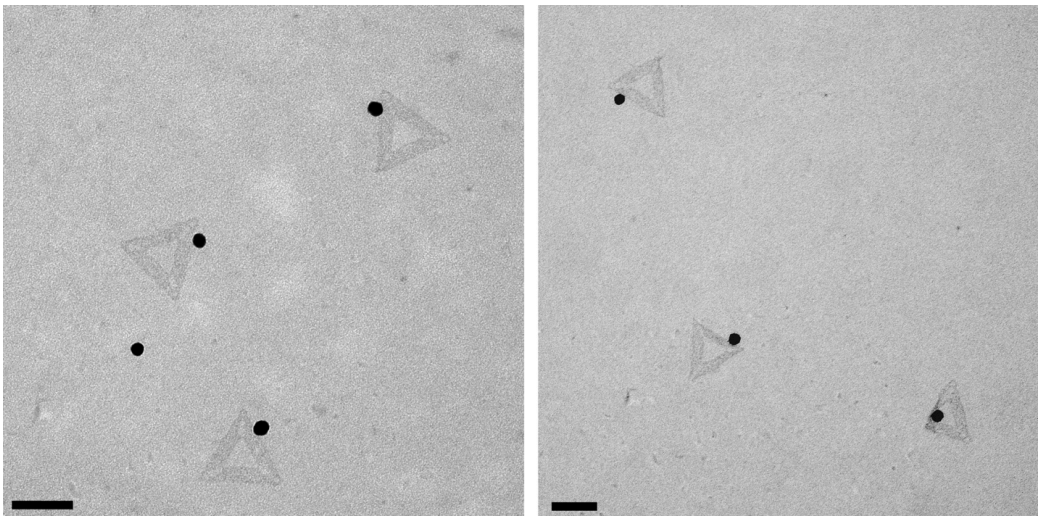

Figure S5: Zoom out TEM images of monomeric constructs with particle dye distance 21.7 nm. Scale bar is 100 nm.

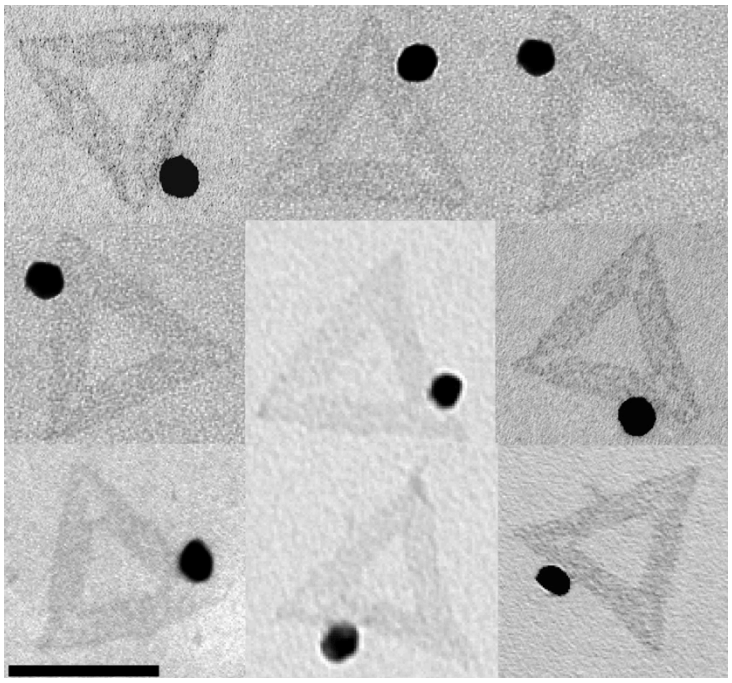

Figure S6: Zoom in TEM images of monomeric constructs with particle dye distance 21.7 nm. Scale bar is 100 nm.

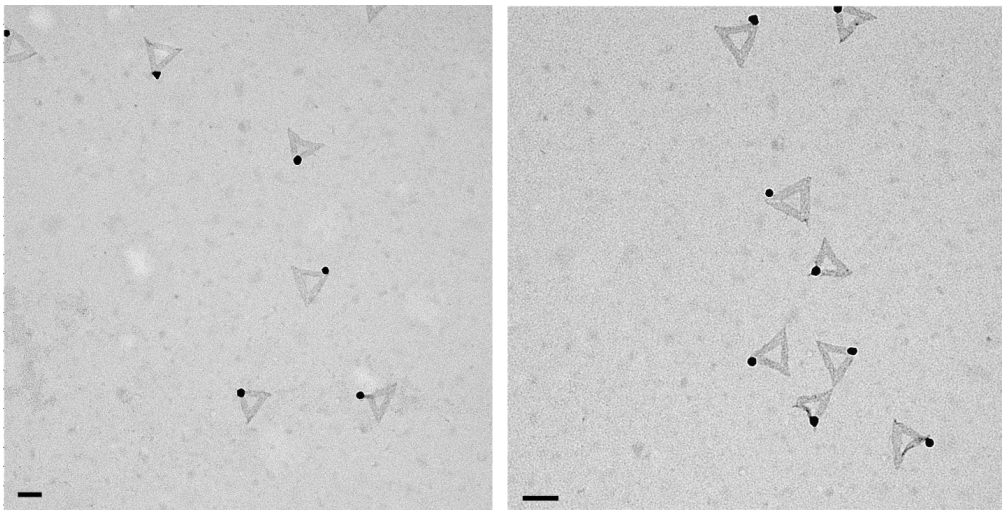

Figure S7: Zoom out TEM images of monomeric constructs with particle dye distance 26.5 nm. Scale bar is 100 nm.

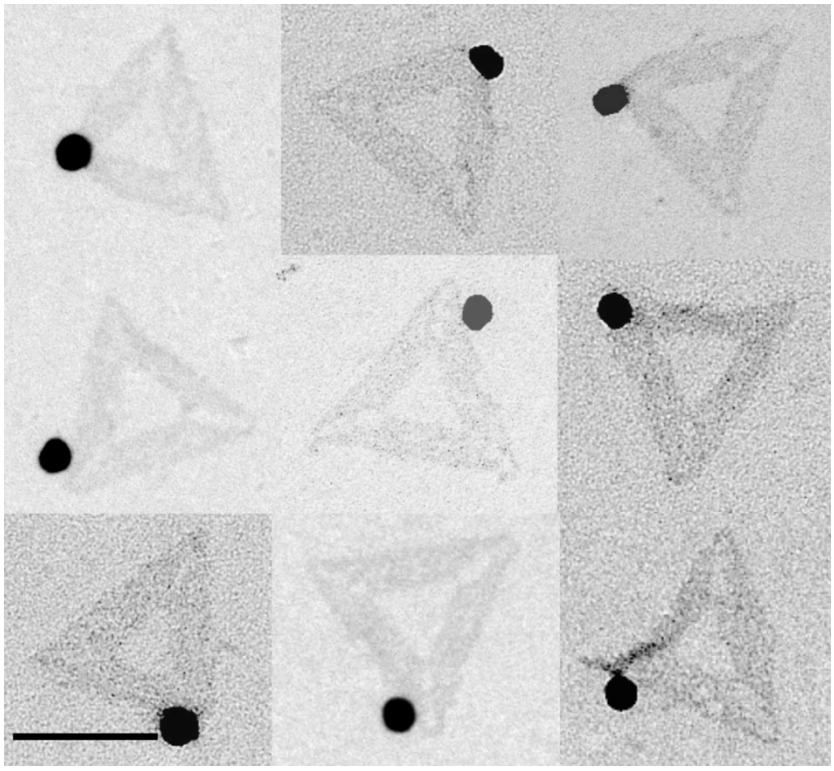

Figure S8: Zoom in TEM images of monomeric constructs with particle dye distance 26.5 nm. Scale bar is 100 nm.

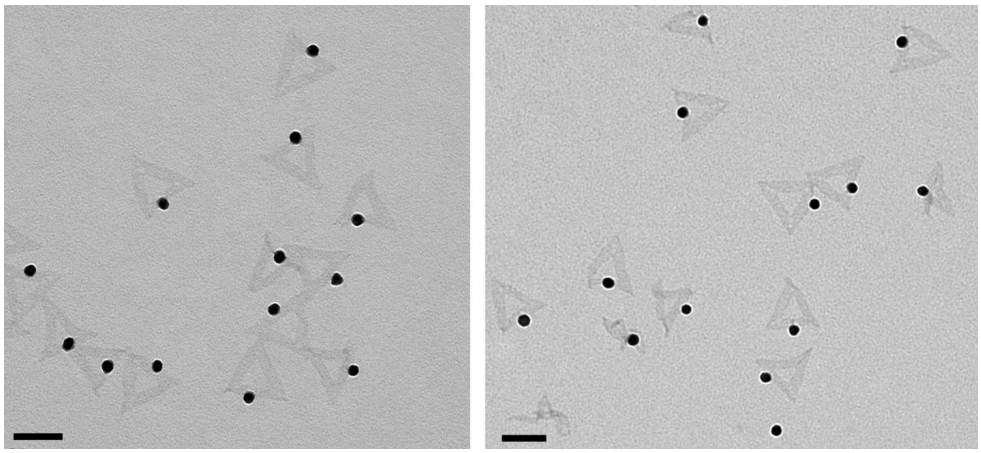

Figure S9: Zoom out TEM images of monomeric constructs with particle dye distance 53.6 nm. Scale bar is 100 nm.

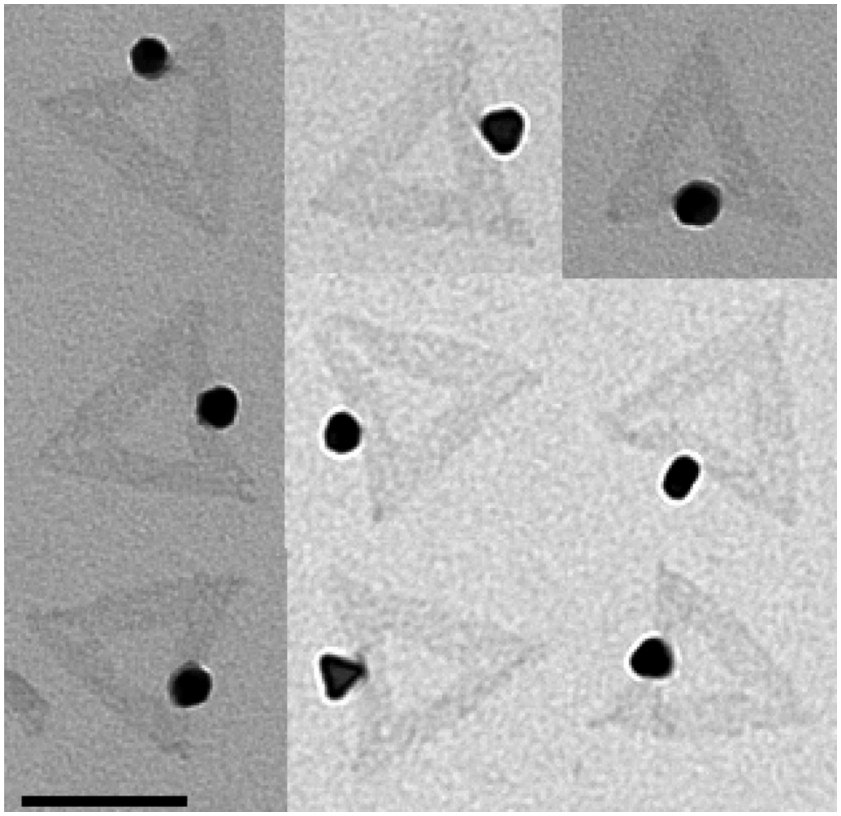

Figure S10: Zoom in TEM images of monomer constructs with particle dye distance 53.6 nm. Scale bar is 100 nm.

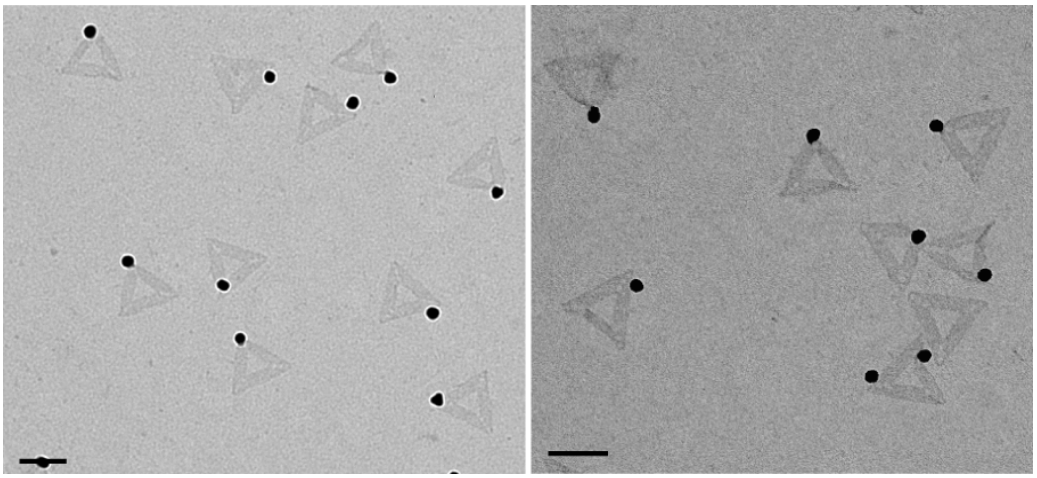

Figure S11: Zoom out TEM images of monomer constructs with particle dye distance 83 nm. Scale bar is 100 nm.

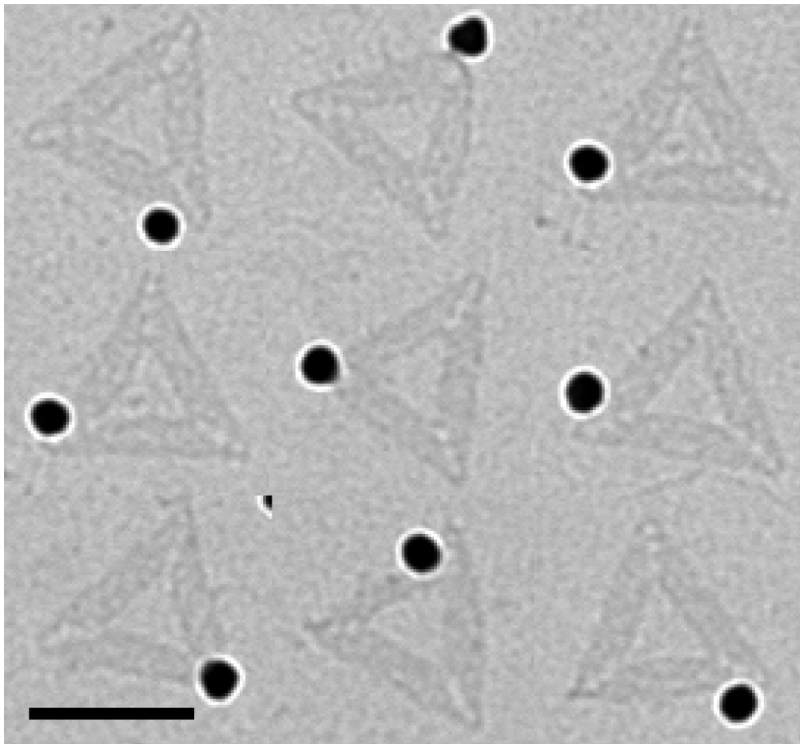

Figure S12: Zoom in TEM images of monomer constructs with particle dye distance 83 nm. Scale bar is 100 nm.

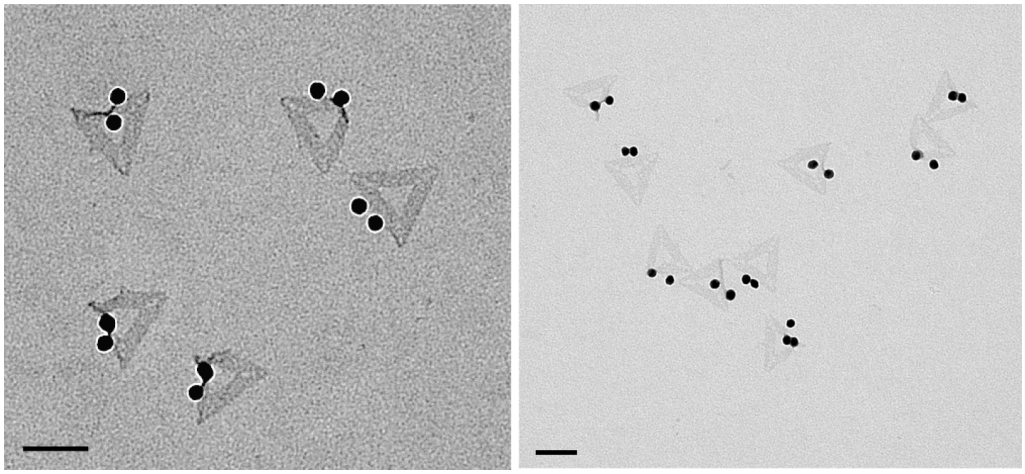

Figure S13: Zoom out TEM images of dimeric constructs with gap distance of ~26 nm in between two 20 nm AuNPs. Scale bar is 100 nm.

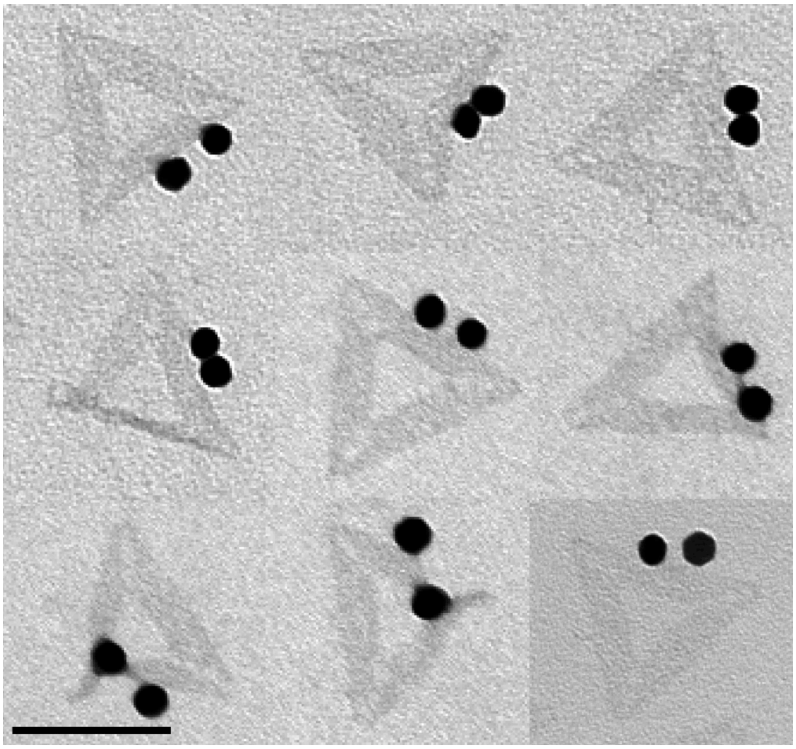

Figure S14: Zoom in TEM images of dimeric constructs with gap distance of ~26 nm in between two 20 nm AuNPs. Scale bar is 100 nm.

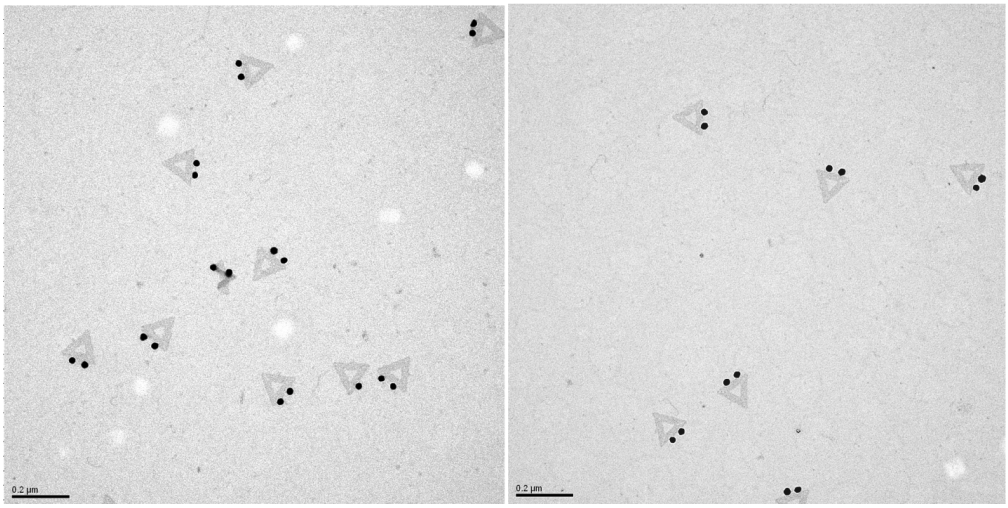

Figure S15: Zoom out TEM images of dimeric constructs with gap distance of ~35 nm in between two 20 nm AuNPs. Scale bar is 100 nm.

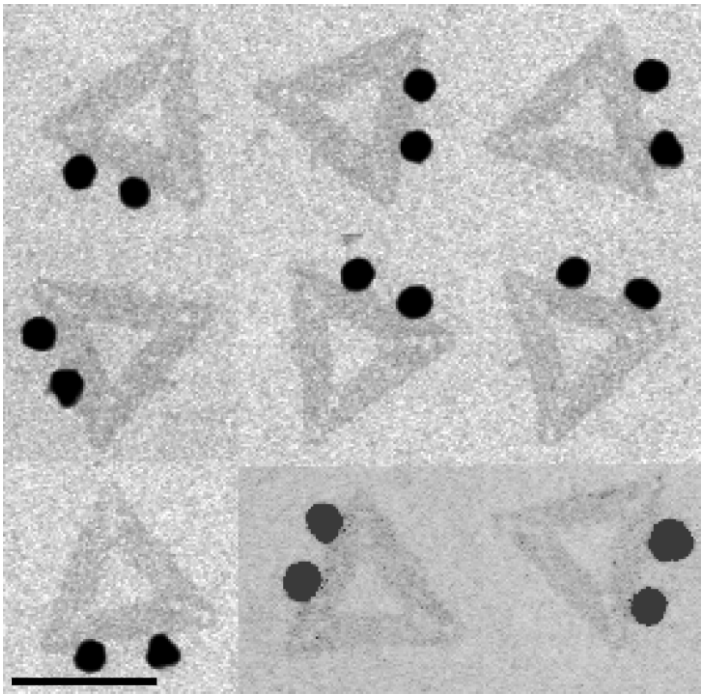

Figure S16: Zoom in TEM images of dimeric constructs with gap distance of ~35 nm in between two 20 nm AuNPs. Scale bar is 100 nm.

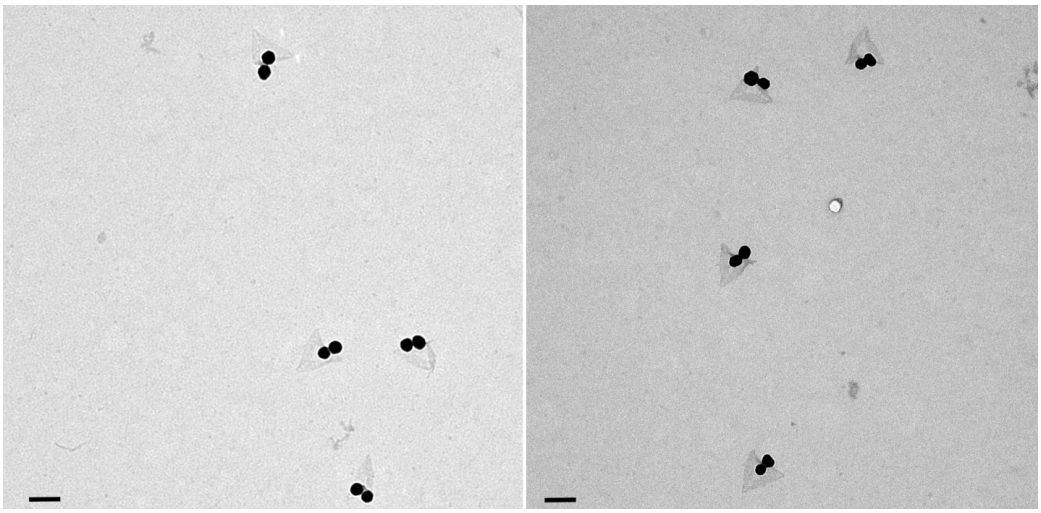

Figure S17: Zoom out TEM images of dimeric constructs with gap distance of ~20 nm in between two 30 nm AuNPs. Scale bar is 100 nm.

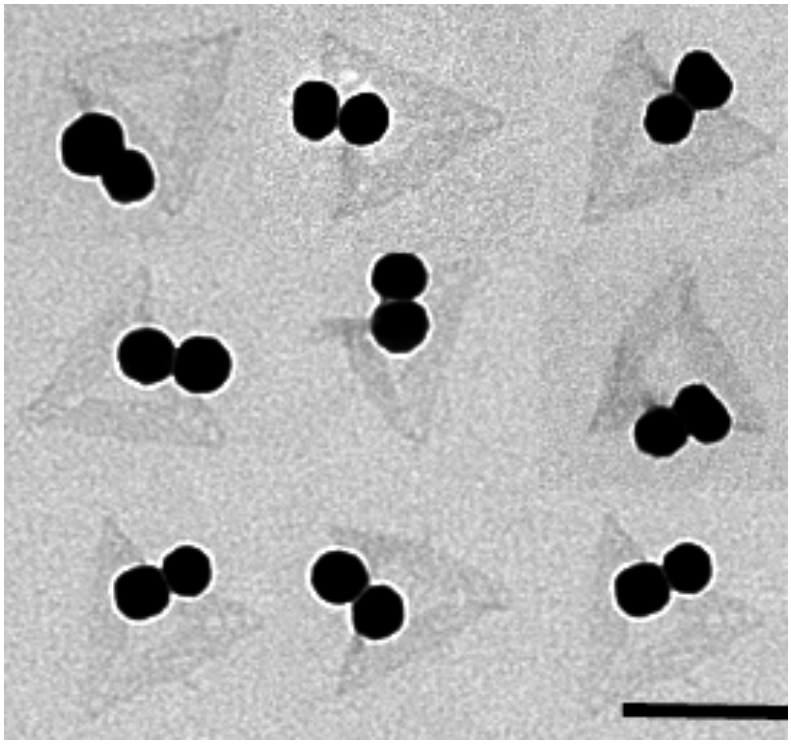

Figure S18: Zoom in TEM images of dimeric constructs with gap distance of ~20 nm in between two 30 nm AuNPs. Scale bar is 100 nm.

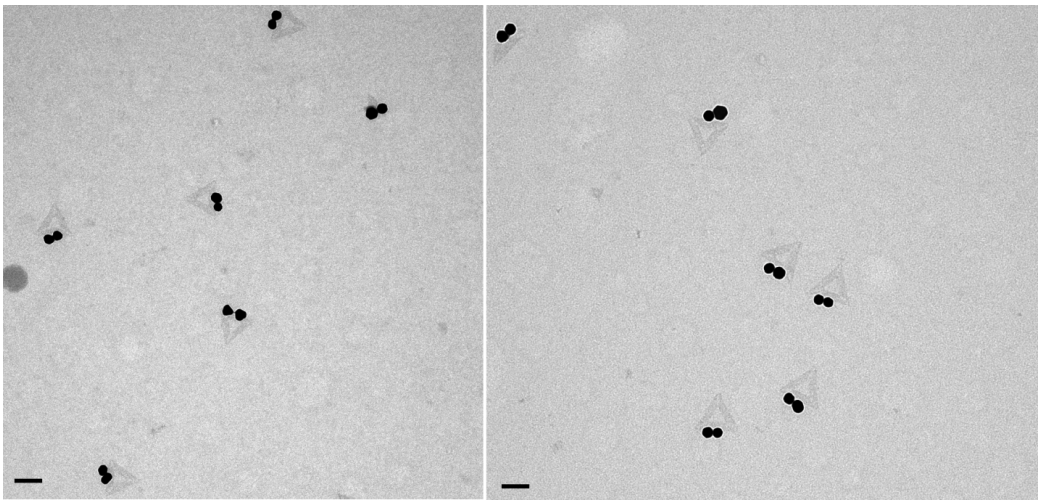

Figure S19: Zoom out TEM images of dimeric constructs with gap distance of ~35 nm in between two 30 nm AuNPs. Scale bar is 100 nm.

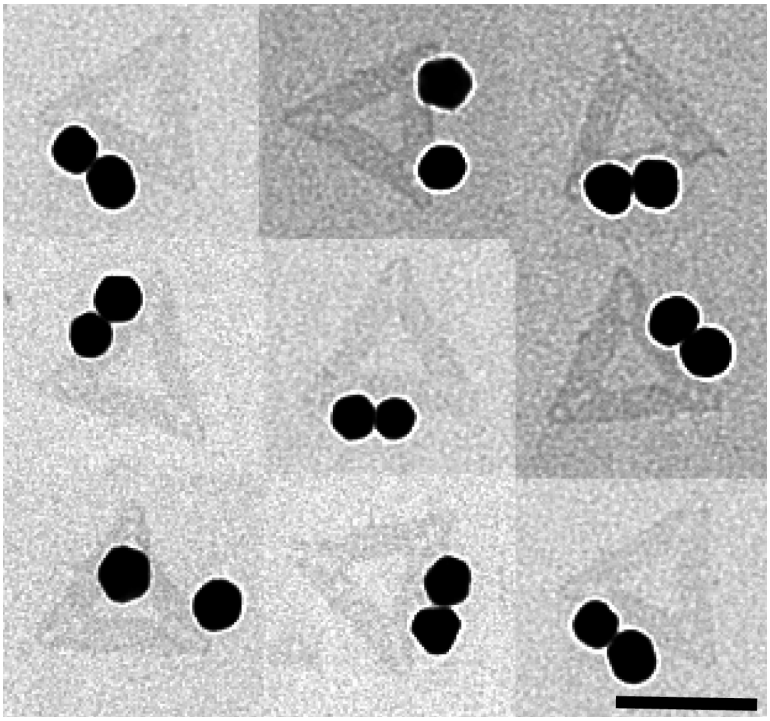

Figure S20: Zoom in TEM images of dimeric constructs with gap distance of ~35 nm in between two 30 nm AuNPs. Scale bar is 100 nm.

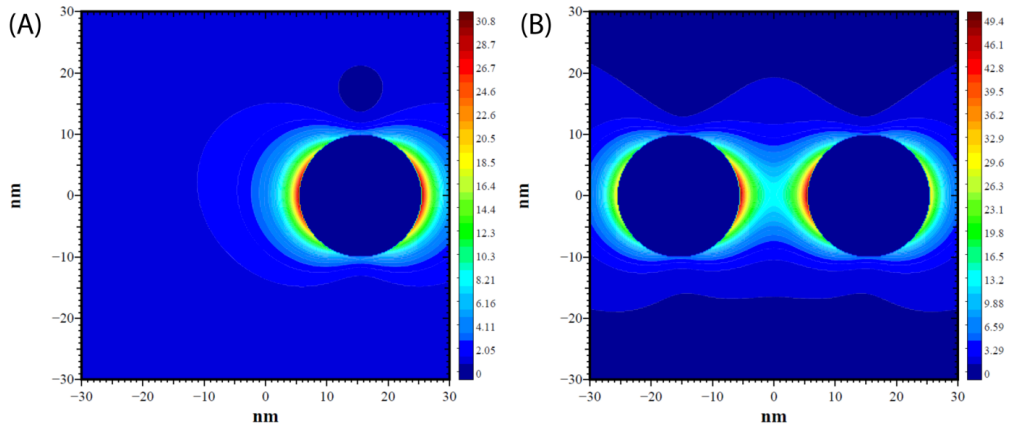

Figure S21: E field enhancement contour of 20 nm AuNP (A) and 20 nm AuNP dimer with 31 nm gap distance (B) with excitation of 525 nm calculated using FTDT calculations. For monomer structures E field is 18.5 times higher at 15.5 nm distance from the surface compared to free space. On the other hand for dimeric structures E field is 169 times higher at 15.5 nm distance from the surface in between two particles.

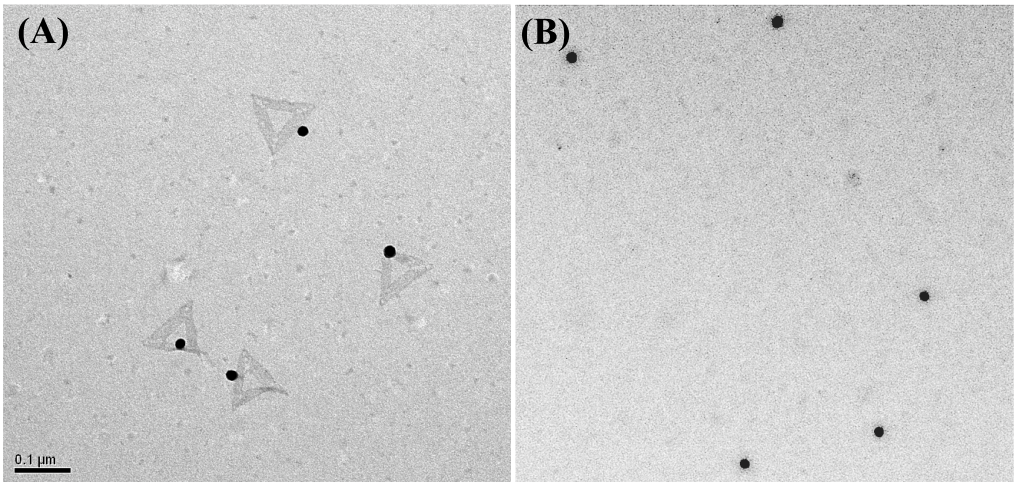

Figure S22: Negatively stained TEM images of sample (A) and control after heating and gradual cooling (B). Scale bar 100 nm.

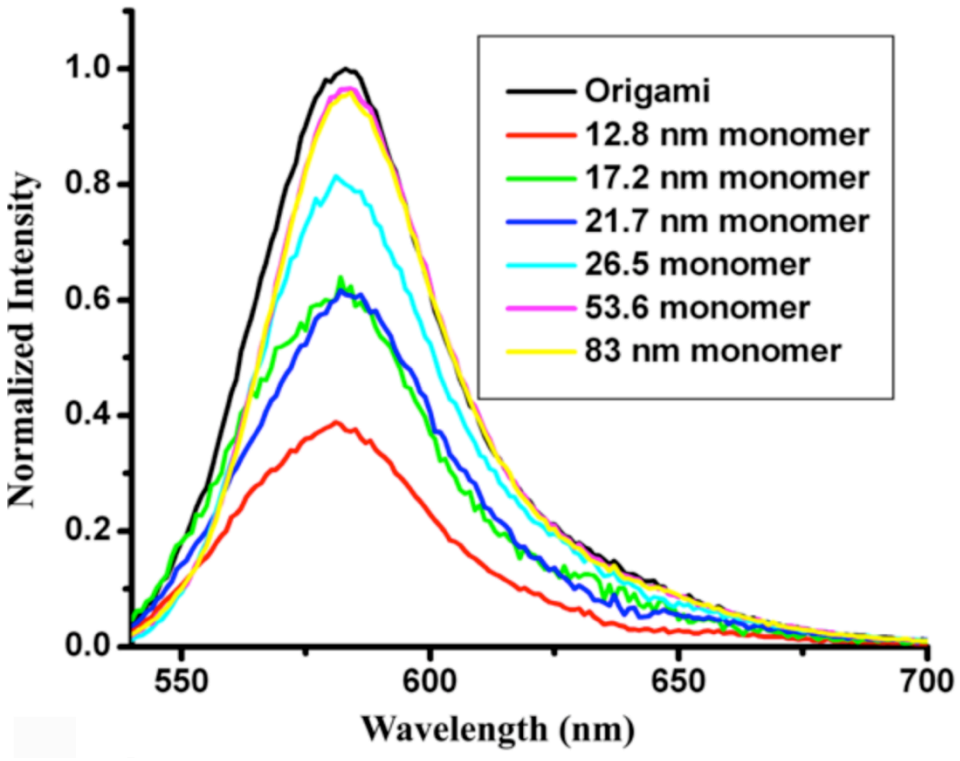

Figure S23: Normalized fluorescence emission spectra of different monomer structures with respect to the control that is origami without the AuNP. All the constructs were excited at 525 nm with the same excitation and emission slit widths.

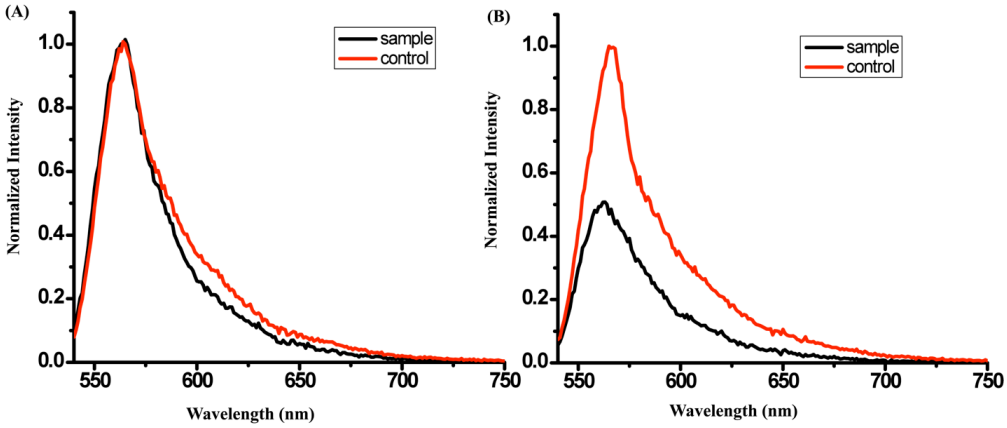

Figure S23: (A) Fluorescence emission spectra of sample (black) and control (red) of 26 nm gap 20 nm AuNP dimer. (B) Fluorescence emission spectra of sample (black) and control (red) of 40 nm gap 20 nm AuNP dimer.

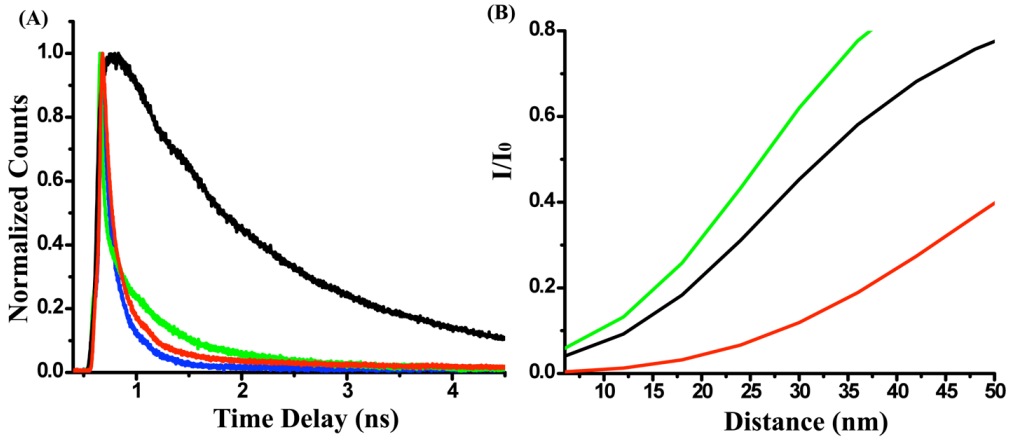

Figure S24: (A) Lifetime decay curve for dsCy3 (black), 35 nm gap 30 nm AuNP dimer (green), 23 nm gap 30 nm AuNP dimer (red) and the instrument response function (blue). (B) The predicted lifetime ratio for average orientation (black), perpendicular orientation (red) and parallel orientation (green).

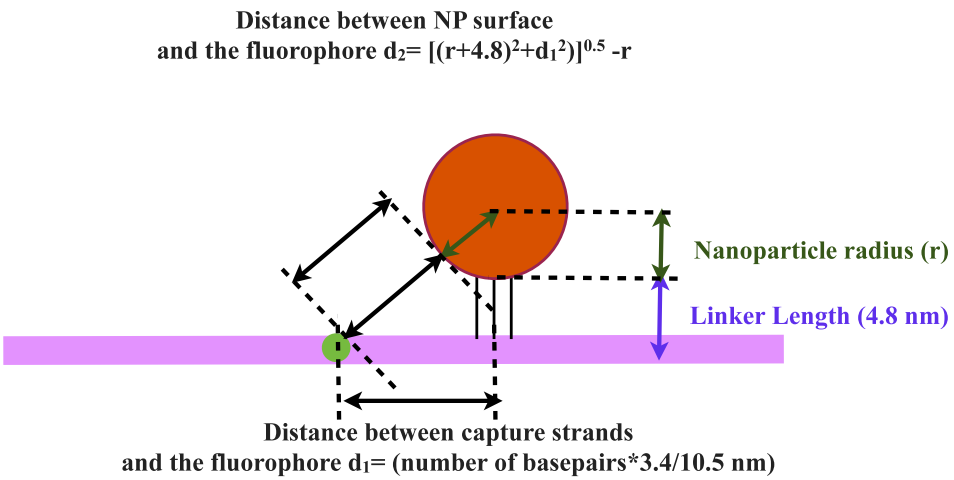

Figure S25: Scheme of calculated distance of the dye from the fluorophore. For the dimer the distance of the dye from both the particles were measured and added up to determine the gap distance.

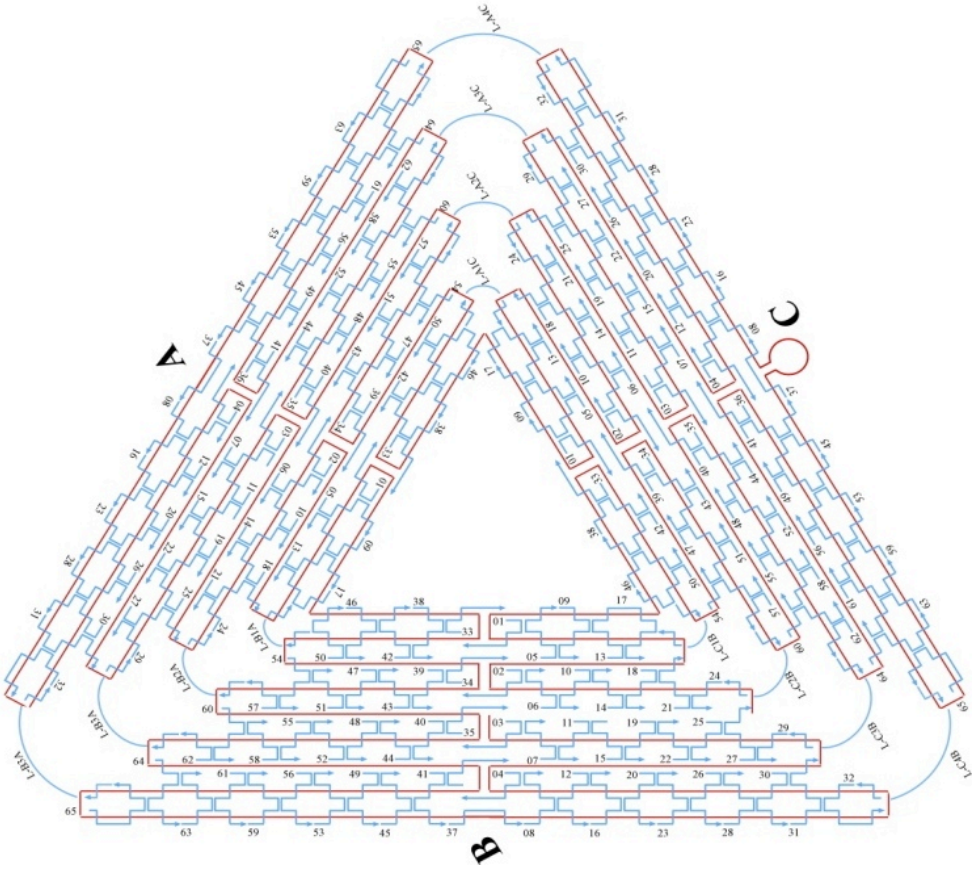

Figure S26: Numbering scheme of triangular origami staple strands.

Sequences of unmodified staple strands are the same as appendix A page 155.

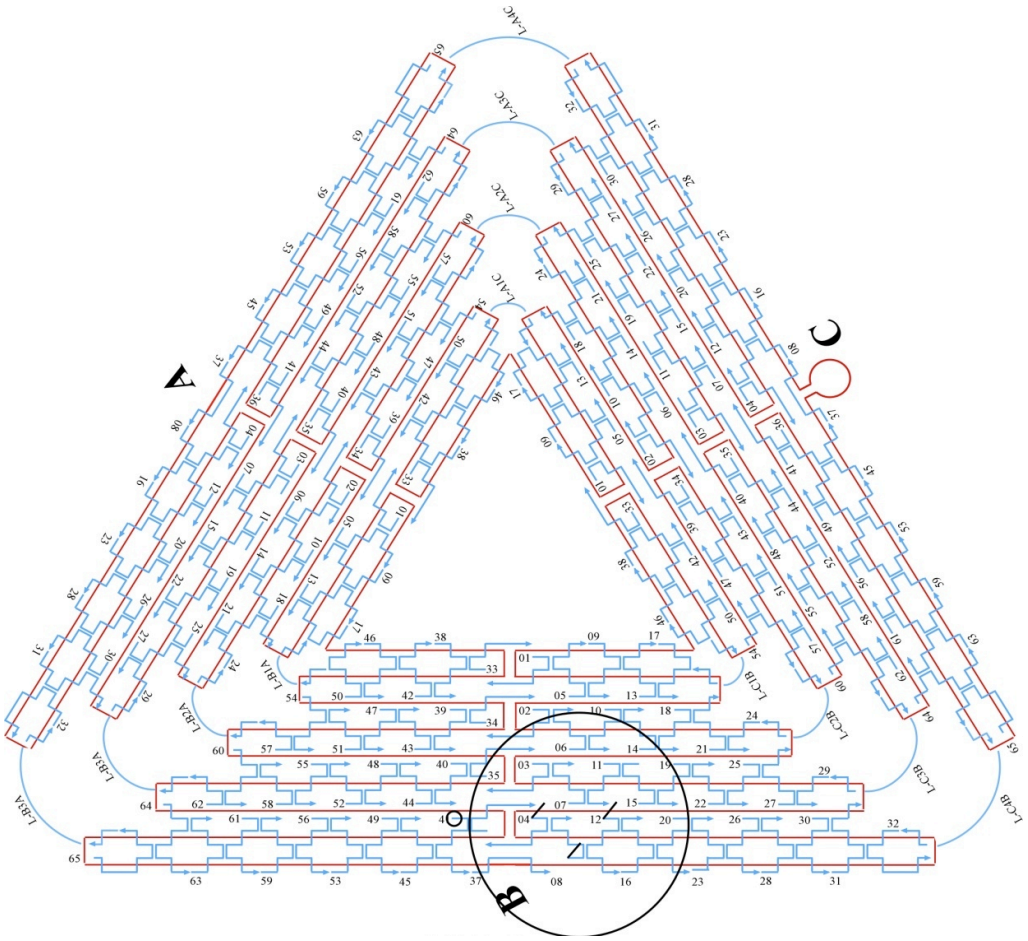

Figure S27: Schematic representation of 12.8 nm monomer. Small circle represents the position of the fluorophore.

B12, agc tat cga atc cag ggt ta

CTCCAAGATTGCATCAAAAAGATAATGCAGATACATAA

B04, agc tat cga atc cag ggt ta

TTCGAGCTAAGACTTCAAATATCGGGAACGAG

B08, agc tat cga atc cag ggt ta

CATTCAACTTAAGAGGAAGCCCGATCAAAGCG

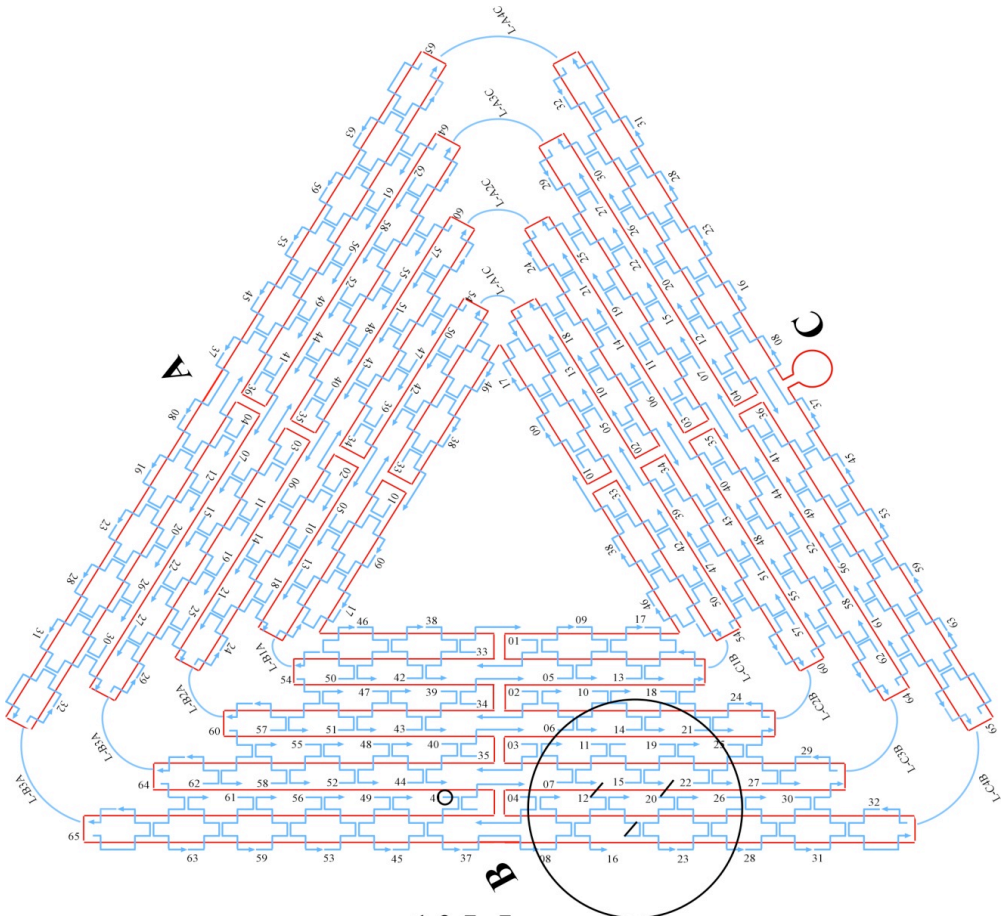

Figure S28: Schematic representation of 17.2 nm monomer. Small circle represents the position of the fluorophore.

B12, agc tat cga atc cag ggt ta

CTCCAAGATTGCATCAAAAAGATAATGCAGATACATAA

B20, agc tat cga atc cag ggt ta

TAATTGCTTTACCCTGACTATTATGAGGCATAGTAAGAGC,

B16, agc tat cga atc cag ggt ta

GGAATTACAGTCAGAAGCAAAGCGCAGGTCAG

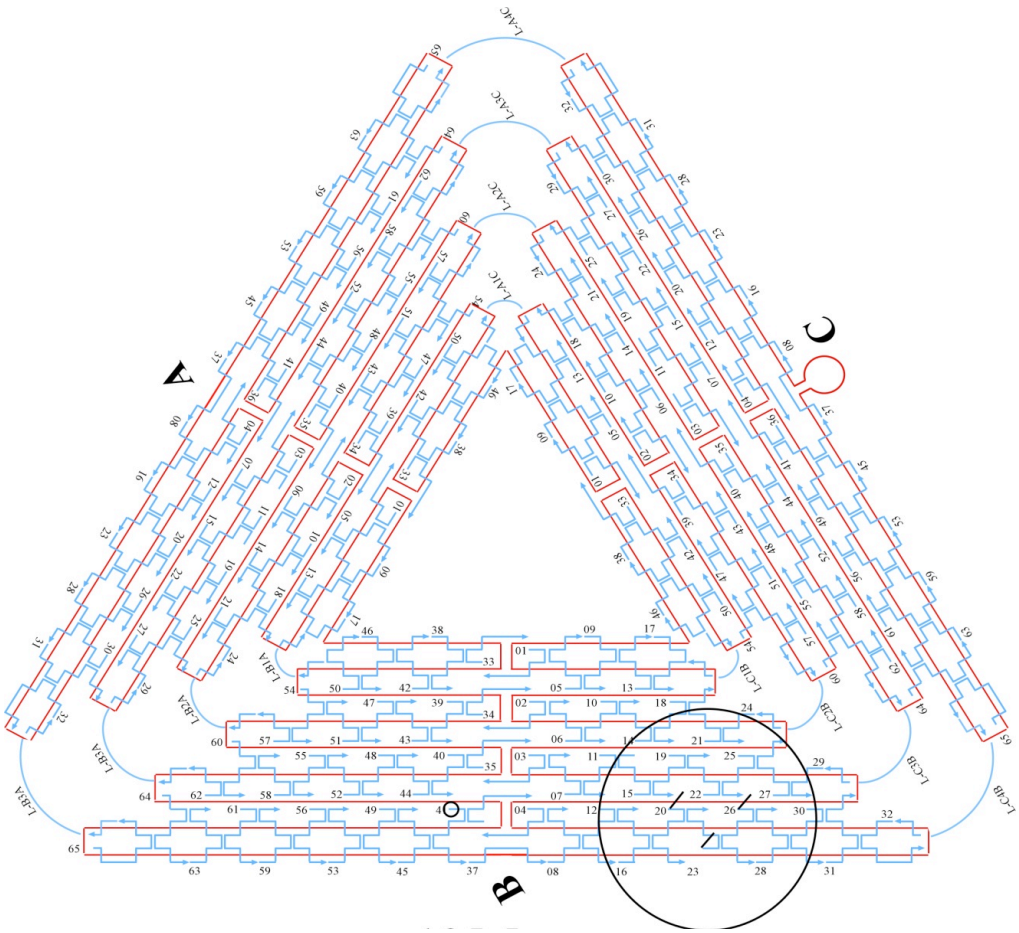

Figure S29: Schematic representation of 21.7 nm monomer. Small circle represents the position of the fluorophore.

B20, agc tat cga atc cag ggt ta

TAATTGCTTTACCCTGACTATTATGAGGCATAGTAAGAGC,

B26, agc tat cga atc cag ggt ta

CGGATGGCACGAGAATGACCATAATCGTTTACCAGACGAC,

B23. agc tat cga atc cag ggt ta

CATAACCCATCAAAAATCAGGTCTCCTTTTGA

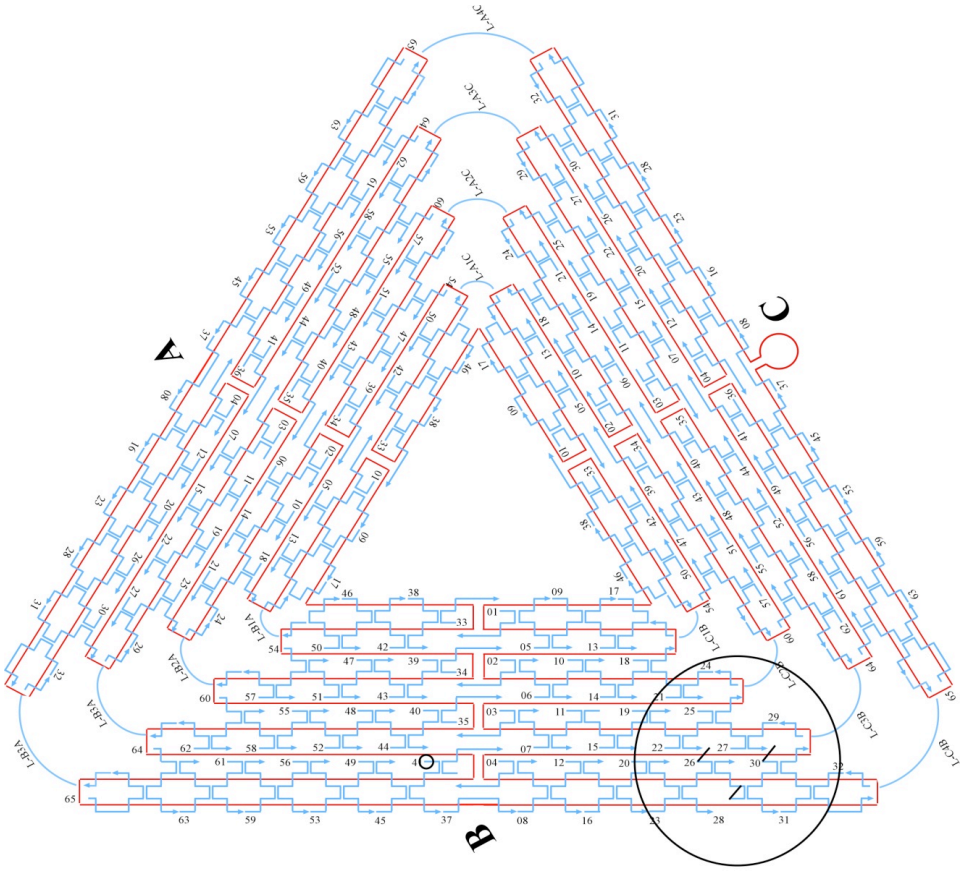

Figure S30: Schematic representation of 26.5 nm monomer. Small circle represents the position of the fluorophore.

B30, agc tat cga atc cag ggt ta

TGCTGTAGATCCCCCTCAAATGCTGCGAGAGGCTTTTGCA,

B26, agc tat cga atc cag ggt ta

CGGATGGCACGAGAATGACCATAATCGTTTACCAGACGAC,

B28. agc tat cga atc cag ggt ta

CCAAAATATTAAACAGTTCAGAAATTAGAGCT

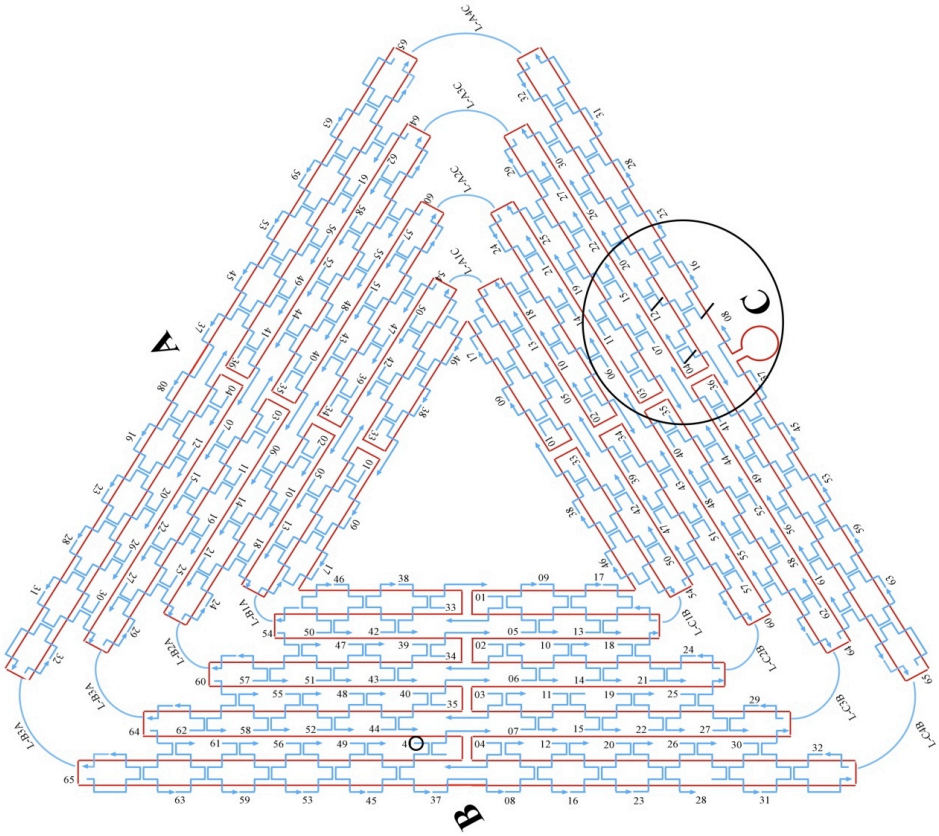

Figure S31: Schematic representation of 53.5nm monomer. Small circle represents the position of the fluorophore.

C04 agc tat cga atc cag ggt ta

CGACCAGTACATTGGCAGATTCACCTGATTGC

C08 agc tat cga atc cag ggt ta

CACGTATACTGAAATGGATTATTTAATAAAAG

C12 agc tat cga atc cag ggt ta

AGAGATAGTTTGACGCTCAATCGTACGTGCTTTCCTCGTT

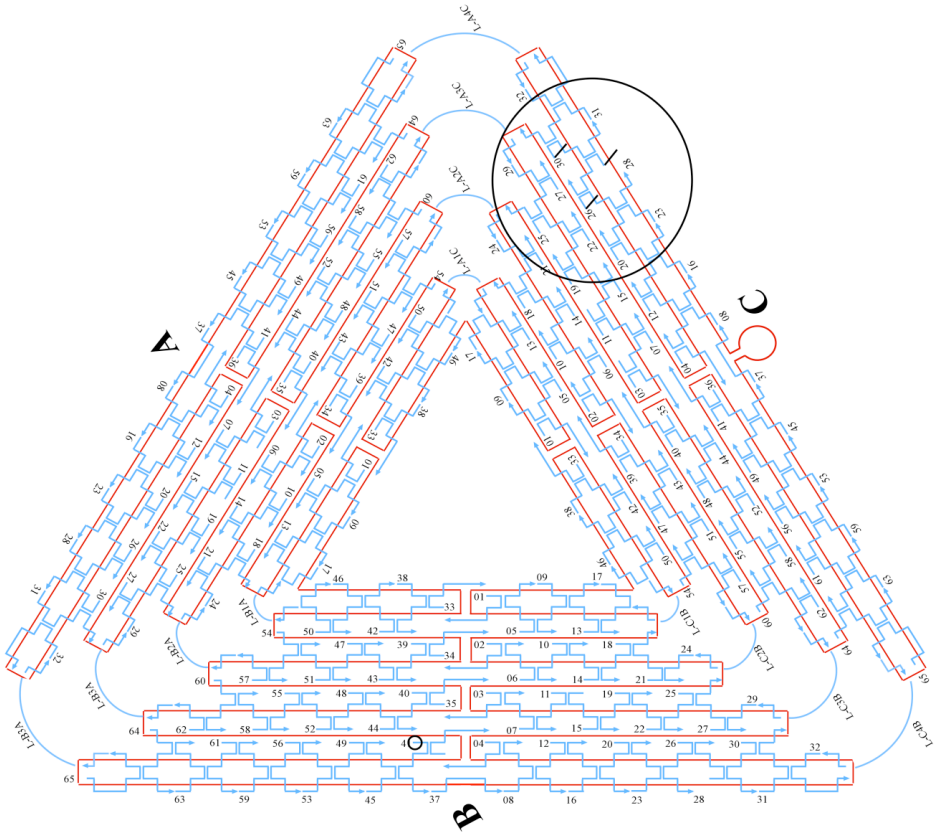

Figure S32: Schematic representation of 12.8 nm monomer. Small circle represents the position of the fluorophore.

C30 S1, agc tat cga atc cag ggt ta T AAA ACA TTA GAA GAA CTC AAA CTT TTT ATA AT C AGT GAG ,

C26 S1, agc tat cga atc cag ggt ta C TAT TAG TAT ATC CAG AAC AAT ATC AGG AAC GGT ACG CCA ,

C28 S1. agc tat cga atc cag ggt ta A GAA GTG TAT CGG CCT TGC TGG TAC TTT AAT G

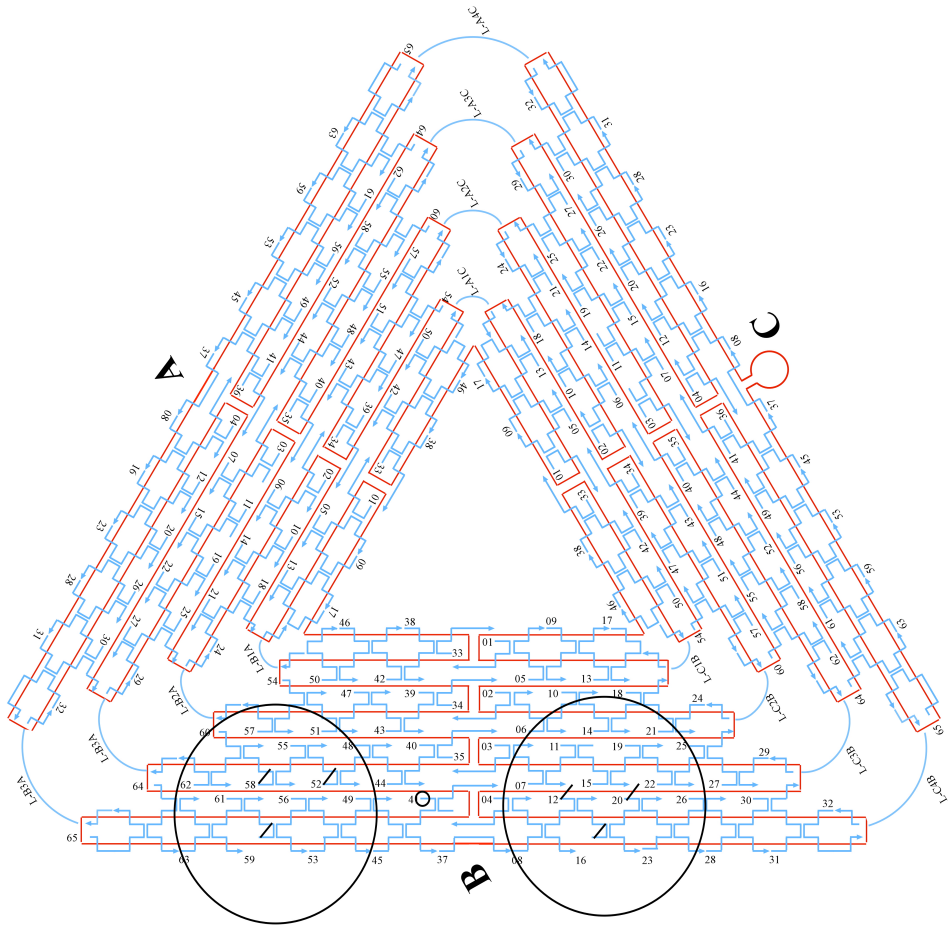

Figure S33: Schematic representation of 40 nm gap dimer with 20 nm particle. Small circle represents the position of the fluorophore.

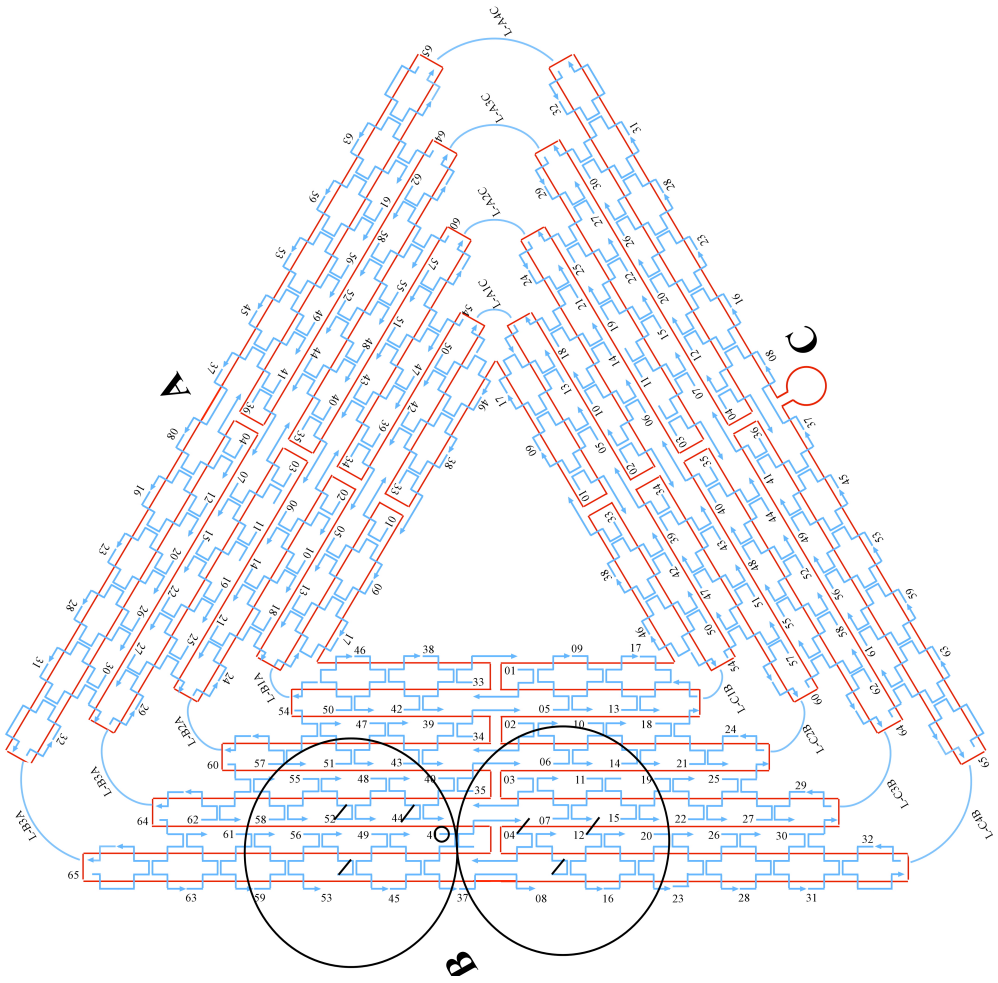

Figure S34: Schematic representation of 35 nm gap dimer with 30 nm particle. Small circle represents the position of the fluorophore.

B12 S1, agc tat cga atc cag ggt ta

AACTCCAAGATTGCATCAAAAAGATAATGCAGATACATAA

B04 S1, agc tat cga atc cag ggt ta

TTCGAGCTAAGACTTCAAATATCGGGAACGAG

B08 S1, agc tat cga atc cag ggt ta

CATTCAACTTAAGAGGAAGCCCGATCAAAGCG

B 44 S1 agc tat cga atc cag ggt ta

ATTGTGTCTCAGCAGCGAAAGACACCATCGCC

B 52 S1 agc tat cga atc cag ggt ta

GTACAACGAGCAACGGCTACAGAGGATACCGA

B 53 S1 agc tat cga atc cag ggt ta

ACCAGTCAGGACGTTGGAACGGTGTACAGACCGAAACAAA

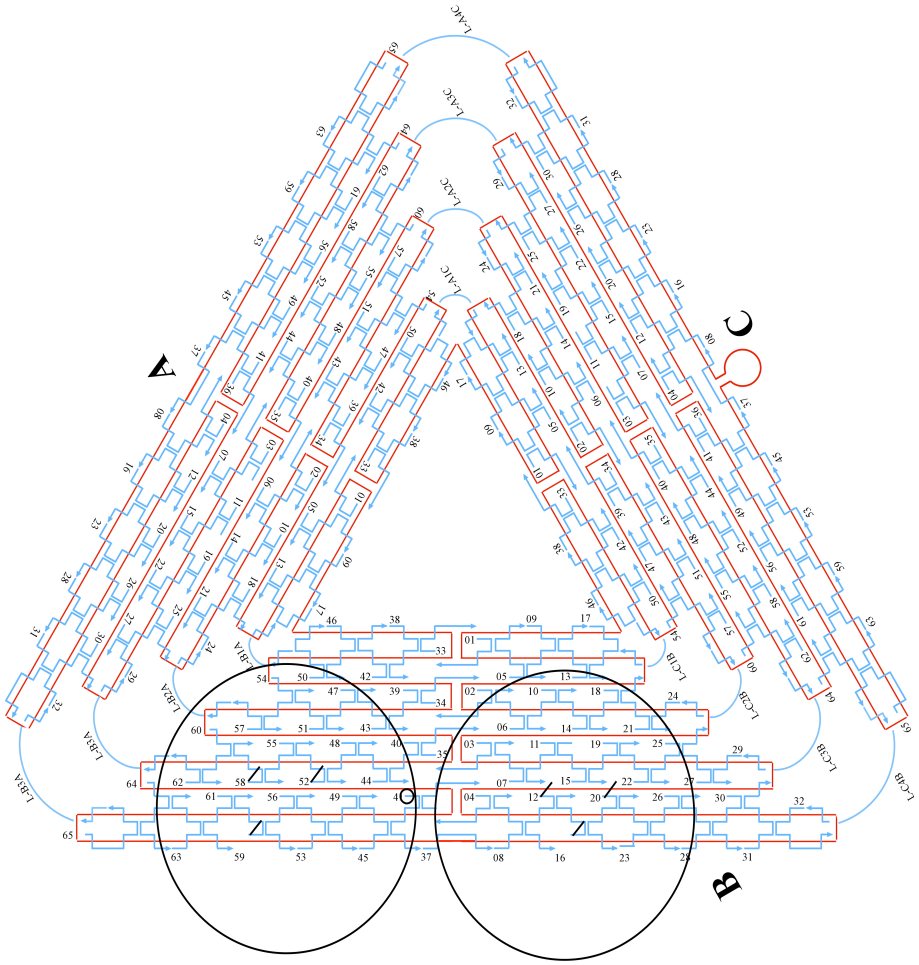

Figure S35: Schematic representation of 26 nm gap dimer with 20 nm particle. Small circle represents the position of the fluorophore.

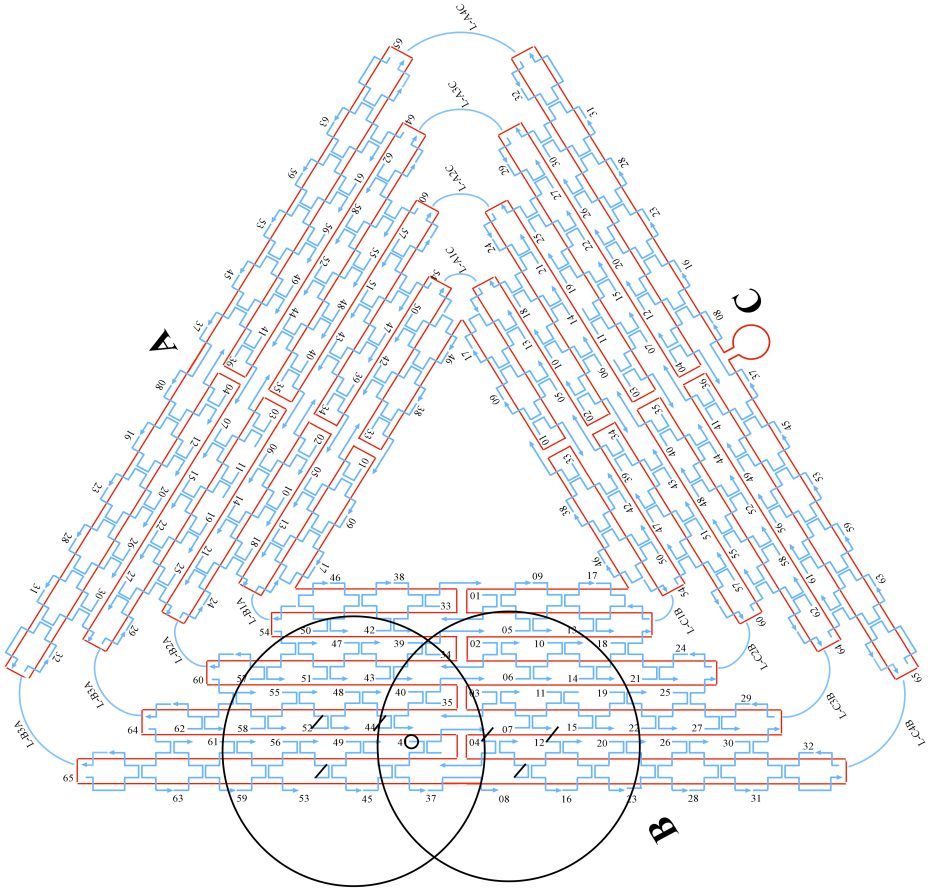

Figure S36: Schematic representation of 23 nm gap dimer with 30 nm particle. Small circle represents the position of the fluorophore.

B52 S1 agc tat cga atc cag ggt ta GTAC AAC GAG CAA CGG CTA CAG AGG ATA CCG A

B58 S1 agc tat cga atc cag ggt ta A CCC CCA GACTTT TTC ATG AGG AACTTG CTT T

B59 S1 agc tat cga atc cag ggt ta CGATTTTATGACCTTCATCAAGAGCATCTTTG

B20 S1, agc tat cga atc cag ggt ta TAATTGCTTTACCCTGACTATTATGAGGCATAGTAAGAGC,

B12 S1, agc tat cga atc cag ggt ta

AACTCCAAGATTGCATCAAAAAGATAATGCAGATACATAA

B16 S1 agc tat cga atc cag ggt ta

GGAATTACAGTCAGAAGCAAAGCGCAGGTCAG

APPENDIX C

SUPPLEMENTAL INFORMATION FOR CHAPTER 4

Supplemental Information for

DNA Origami Directed Self-assembly of Anisotropic Plasmonic Nanostructures

Suchetan Pal,[1,2] Zhengtao Deng,[1] Haining Wang,[3] Shengli Zou,[3] Yan Liu,[1,2*] Hao Yan[1,2*]

[1]The Biodesign Institute, [2]Department of Chemistry and Biochemistry, Arizona State University, Tempe, Arizona 85287

[3]Department of Chemistry, University of Central Florida, Orlando, Florida 32816

A. Experimental Methods

1. Preparation of DNA origami structure:

To assemble the triangular shaped DNA origami, 3 nM of single stranded M13mp18 DNA (NEB, 7,249 nt long) is mixed with the staple strands (unpurified) and the five capture strands (IDTDNA, detailed sequences later) in 1:5:5 molar ratio, following the design outlined by Rothemund (*Nature* **2006,** 440, 297-302) in 1xTAE-Mg^{2+} (40 mM Tris, 20 mM Acetic acid, 2 mM EDTA and 12.5 mM Magnesium acetate, pH 8.0). To generate the binding sites for the AuNRs on the origami, a number of staple strands (5 capture probes arranged in a line for each AuNP) at selected positions on the origami surface were extended at the 5'-end by A_{15} or a random sequence. The resulting solution was cooled from 95^{o}C to 4^{o}C to form the DNA origami structure. Then it was purified by using Microcon centrifugal filtration device (100 kD MWCO filters, Millipore, Bedford, MA) to get rid of the excess staple strands.

2. Preparation of 1:1 conjugation of DNA with 10 nm AuNP (following the previously published method in reference 12 in main text)

a. Activation of Lipoic acid to synthesize NHS ester of lipoic acid. N,N'-Dicyclohexylcarbodiimide **(**DCC, 2.10 g, 10 mmole) was mixed with lipoic acid (2.06 g, 10 mmole) in Tetrahydrofuran (THF,10 mL) followed by the addition of N-hydroxysuccinimide (NHS, 1.15 g, 10 mmole). The reaction mixture was filtered (using filter paper) after stirring continuously for 72 hrs. The filtrate was evaporated to get a crystalline solid. NHS ester of lipoic acid was further purified

by re-crystallization from Toluene.

b. Conjugation of lipoic acid with amine modified oligonucleotides. The NHS ester of lipoic acid prepared as described above was added in excess to 5'-amine modified oligonucleotide (76 mer) in a solution of 70% acetonitrile and 30% water (pH ~ 8). The reaction mixture was kept overnight at room temperature. The lipoic acid conjugated oligonucleotide was purified by micro-spin G25 columns (GE Healthcare) and used for the next step.

c. Phosphination and concentration of AuNPs. AuNPs (10 nm, Ted Pella Inc.) were stabilized with adsorption of Bisp-sulfonatophenyl-phosphene dihydrate dipotassium salt (BSPP, Strem Chemicals). Phosphine coating increases the negative charge on the particle surface therefore, stabilizes the AuNPs in high electrolyte concentrations at a higher particle density. BSPP (15 mg) was added to the colloidal nanoparticles solution (50 mL, particle density $5.7x10^{12}$/mL) and the mixture was shaken overnight at room temperature. Sodium Chloride (solid) was added slowly to this mixture while stirring until the color changed from deep burgundy to light purple. The resulting mixture was centrifuged at 3000 rpm for 30 min and the supernatant was carefully removed with a pipette. AuNPs were then resuspensed in 1 mL solution of BSPP (2.5 mM). Upon mixing with 1 mL methanol, the mixture was centrifuged, the supernatant was removed and the AuNPs were resuspended in 1 mL BSPP solution (2.5 mM). The concentration of the AuNPs was estimated from the optical absorbance at ~ 520 nm.

d. Preparation of AuNP-DNA conjugates with discrete number of DNA. The lipoic acid modified DNAs is incubated with equimolar ratio of phosphinated

AuNPs in 1xTBE buffer (89 mM Tris, 89 mM boric acid, 2 mM EDTA, pH 8.0) containing 50 mM NaCl overnight at room temperature. AuNP-DNA conjugates with discrete numbers of oligonucleotides were separated by 3% agarose gel (running buffer 0.5xTBE, loading buffer 50% glycerol, 15 V/cm, 25 μL load volume). The band with 1:1 ratio of AuNP/DNA was electroeluted into the glass fiber filter membrane, backed by dialysis membrane (MWCO 10000). AuNP-DNA conjugates were recovered using a 0.45 μm pore size centrifugal filter device. Concentration of these AuNP-DNA conjugates was estimated from the optical absorbance at ~ 520 nm.

e. Coating of the AuNP/DNA conjugates with short oligonucleotides. The AuNP-DNA conjugates were further stabilized by adding thiolated T5 ssDNA ([HS-T5]/[AuNP]=100, in 0.5x TBE, with 50 mM NaCl) and incubated for 12 hrs at room temperature. Short thymine oligomers on the AuNP surface provide additional stability against the high electrolyte concentration required for DNA self-assembly.

3. **Synthesis of AuNRs:** The synthesis of AuNRs was carried out using the silver-assisted growth procedure adapted from literature (reference 17 in main text).

a. AuNP Seed synthesis: First, 60 μL of 10 mM ice cold $NaBH_4$ solution was added to 1 mL of 2.5 mM $HAuCl_4$ solution in 100 mM CTAB and vortexed vigorously. The solution color was immediately changed to yellowish brown.

The resultant solution consisted of AuNP seeds, which would act as nucleation points for the AuNR growth.

b. AuNR synthesis: To a 1 mL of 10 mM $HAuCl_4$ solution in 100 mM CTAB solution, 250 µL of 1 mM $AgNO_3$ solution was added. After gentle mixing, 70 µL of 79 mM ascorbic acid solution was added and mixed thoroughly. To this mixture 12 µL of the previously prepared AuNP seed solution was added. The mixture was kept undisturbed for several hours. The solution became purple colored indicating formation of AuNR.

c. **AuNR purification and overgrowth:** 500 µL AuNRs solution was centrifuged (15 min, 7000 rpm), the supernatant was discarded and the pellet was suspended in 500 µL nanopure water. The solution was centrifuged again, and the collected pellet was resuspended in 10 mM CTAB solution. The extinction coefficient was assumed to be $0.9x10^9$ $M^{-1}cm^{-1}$ at 788 nm. To a 0.9 nM solution of AuNRs in 10 mM CTAB, ascorbic acid and $HAuCl_4$ solution was added to make the final concentration 1 mM and 0.005 mM, respectively. This created a thin layer of Au on the AuNR surface to enhance the affinity of thiolated DNA to the AuNR surface. 500 µL of AuNRs solution was washed twice by centrifugation and resuspension in nanopure water. Concentration was measured using UV-Vis spectra.

4. Preparation of DNA functionalized AuNRs:

a. Preparation of the Thiolated DNA: The S-S bond in the thiolated DNA obtained from IDT DNA was reduced by adding 40 µL of 200 mM TCEP

(tris(2-carboxyethyl)phosphine) aqueous solution to 40 μL of 1 mM DNA solution and incubated overnight. The unreacted TCEP was removed using G25 spin column (GE Healthcare).

b. **Coating of DNA on AuNR**: The purified DNA was added to 300 μL of AuNR solution (OD ~1) in water containing 0.01% sodium dodecyl sulfate (SDS) and incubated overnight. Then 10xTBE solution was added to bring the buffer concentration to 1xTBE. After several hours, a 5 M NaCl solution was slowly added to bring the final [NaCl] to 500 mM over 24 hours. Then the solution was allowed to sit at room temperature overnight. The excess DNA was removed by repeated centrifugation (6000 rpm, 15 min) and re-suspension 1XTBE buffer for 3 times. The concentration of AuNR was measured using UV-Vis spectroscopy.

5. Immobilization of AuNRs on DNA origami and gel electrophoresis purification:

To 3 nM DNA origami solution in 0.5xTAE-Mg containing the number of capture strands at desired positions, the DNA functionalized AuNR solution was added with a molar ratio of 1:2. The final NaCl concentration was raised to 300 mM by adding 5M NaCl solution. The mixture was then cycled between 45 ^{o}C and 30 ^{o}C for 60 hours to ensure hybridization of DNA on the AuNRs with the capture strands on the DNA origami. Then the resultant mixture was run into 1% agarose gel for 40 minutes at 80 V constant voltage. The desired band was cut out, extracted using freeze-n-squeeze column (Biorad) and concentrated by

centrifugation and redispersion in 0.5xTAE-Mg buffer at 4000 rpm for 20 minutes.

6. Immobilization of AuNRs on DNA origami with AuNP:

a. Self-assembly of DNA origami with one AuNP. Triangular shaped origami was assembled as described above in **1**, except one staple strand at the selected position for the AuNP was replaced with the 1:1 DNA-AuNP conjugate (note: two staple strands were joined together in order to make the strand long enough for easy separation of the 1:1 DNA-AuNP conjugate, see sequence details later), and five staple strands at the selected positions for the AgNR were replaced with the corresponding capture strands with A_{15} extensions. The molar ratio of the M13 ssDNA, the 1:1 DNA-AuNP conjugate, the other staple strands (unpurified), and the capture probes was 1:1:5:5. The mixture solution was annealed in 1xTBE buffer with 0.5 M NaCl by cooling slowly from 65 °C to 4 °C. In order to get rid of excess staple strands, and to exchange the buffer, the resultant solution was purified by Microcon filtration device (100 kD MWCO) and washed with 0.5xTAE-Mg.

b. Assembly of AuNR-AuNP hetero dimer. To the triangular origami modified with one 10 nm AuNP at a particular position, two equivalent amount of T_{15} functionalized AuNR solution in 0.3xTAE-Mg buffer was added. The mixture was then cycled between 45 ^{o}C and 30 ^{o}C for 60 hours to ensure perfect hybridization of AuNRs with the capture strands on the DNA origami. Then the resultant mixture was loaded into 1% agarose gel and run for 40 minutes at

80 V constant voltage. The desired band was cut out, extracted using freeze-n-squeeze column (Biorad) and concentrated by centrifugation and re-dispersion in 0.5xTAE-Mg buffer at 4000 rpm for 20 minutes.

7. TEM imaging of the origami triangles with or without the AuNP/AuNR:

The TEM sample was prepared by dropping 2 μL of the purified sample solution on carbon-coated grid (400 mesh, Ted Pella) that were negatively glow discharged using Emitech K100X machine. After 1 minute, the sample drop was wicked from the grid by touching its edge with a piece of filter paper. The grid was washed by touching it with a drop of water to remove the excess salt, and the excess water was wicked away by touching with a filter paper. For staining, the grid was touched with a drop of 0.7 % uranyl formate solution for 2 seconds and excess solution was wicked away with a filter paper. Again the grid was touched with the second drop of uranyl formate solution for 12 seconds, and the excess solution was removed with a filter paper. The grid was kept at room temperature to allow drying. Low-resolution TEM studies were conducted by using a Philips CM12 transmission electron microscope, operated at 80 kV in the bright field mode. High-angle annular dark-field scanning transmission electron microscopy (HAADF-STEM), high-resolution transmission electron microscopy (HRTEM), and energy-dispersive X-ray spectroscopy (EDS) were performed on a JEOL JEM 2010F electron microscope operating at 200 keV.

8. Theoretical simulations:

Theoretical simulations by discrete dipole approximation (DDA) method [E. M. Purcell and C. R. PennyPacker, Astrophys. J., 1973, 186, 705; B. T. Draine, Astrophys. J., 1988, 333, 848] were carried out for the optical spectra of Au nanorod dimers. In the simulation, we set both the length and diameter of the Au rod the same as those in the experiments. The distances between two rods in the dimer were also from the experimental data. We considered size distribution and random orientation of single rod and dimer in the solution. The dielectric constants of Au are from Palik's handbook [E. D. Palik, Handbook of Optical Constants of Solids, Academic Press, New York, 1985]. Fig. 2(E) shows the extinction spectrum of two parallel Au rods with 180° angle and 6 nm distance in comparison with that of single Au rod. The resonance peak appears at 790 nm for the single rod and 808 nm for the dimer, which shows a red-shift of 18 nm. The shift is slightly larger than that of 9 nm obtained in experiment. The difference might be from the smaller size distribution in the simulations in which only three different lengths and three diameters (total of 9 different sizes for the single rod) were carried out. When the in-rod angle is 60° and distance is 5 nm shows, the resonance peak red shifted 5 nm to 795, which is close to the experimentally measured 6 nm shift. Fig. 2(E) shows the extinction spectrum of Au nanorod dimer of 0° angle and 8 nm distance. The resonance wavelength is at 780 nm with a blue-shift of 10 nm in comparison to that of the single rod. When the two rods in the dimer were arranged in a 90° angle and separated with a 16 nm distance, the resonance peak of the dimer appears at 787 nm, which is close to that of single

rod but has a slight blue shift. All the peaks around 520 nm don't change much in comparison with that of single rod.

9. Additional figures.

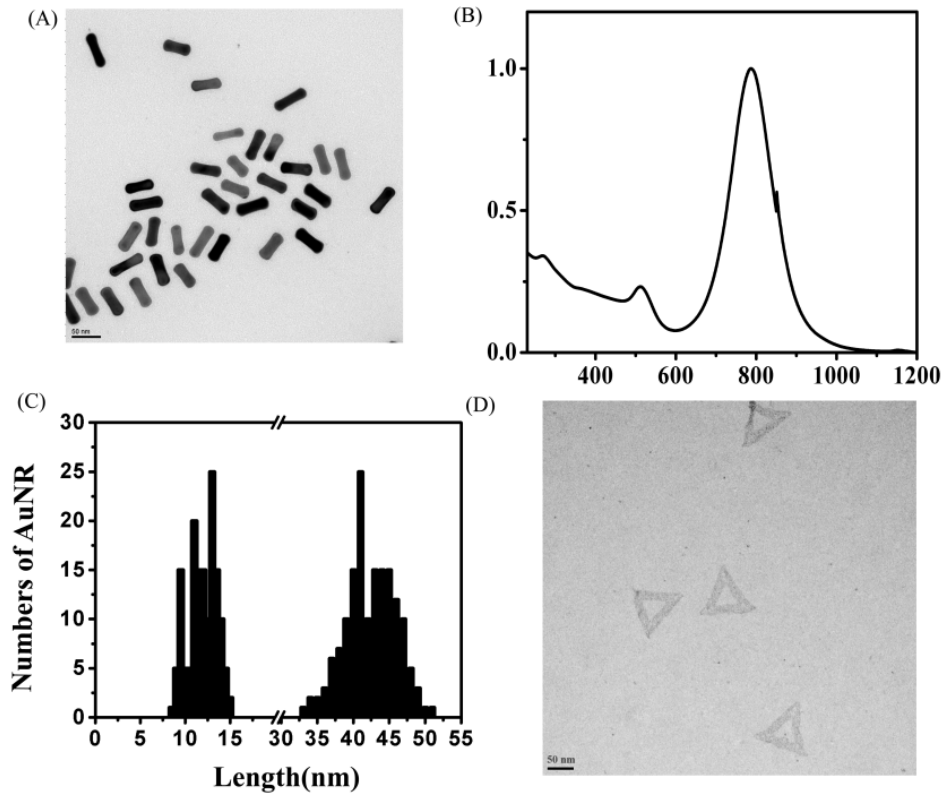

Figure S1: Bottom up components of the different constructs. **(A)** AuNRs, with average length 42.5±6.5 nm and length 12±3.5 nm. They were functionalized with the appropriate DNA (thiolated T_{15} or a 12 nt random sequence) for hybridization with the probes on DNA origami. **(B)** A typical UV-Vis-NIR spectra of DNA functionalized AuNRs. The three distinct peaks at ~ 788 nm, ~ 520 nm, and ~260 nm correspond to longitudinal surface plasmon resonance peak (LSPR), transverse surface plasmon resonance peak (TSPR), and the DNA absorbance peak, respectively. (**C**) Width and length distribution histogram of the AuNRs

measured from TEM images. **(D)** Negative stained TEM images of the triangular DNA origami. Each arm of the origami is ~110 nm.

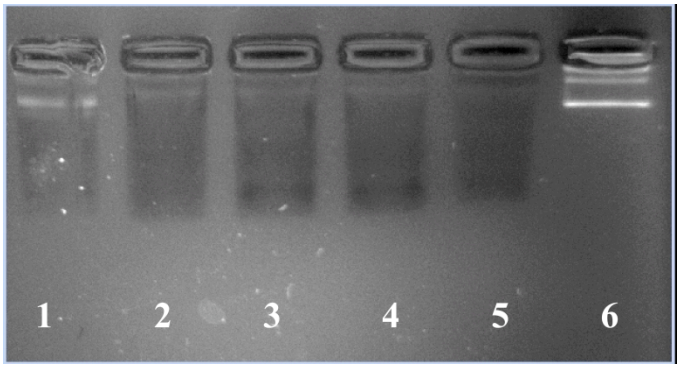

Figure S2: 1% Ethedium Bromide stained agarose purification gel images of different designs. Lane 6 is origami only. Lane 1: monomer construct,lane2-6 different dimeric constructs (i)-(iv). Clearly monomeric construct has lower gel mobility than bare origami. Dimeric constructs runs slower than monomeric construct. The corresponding bands were excised and extracted for TEM imaging and UV-Vis measurements.

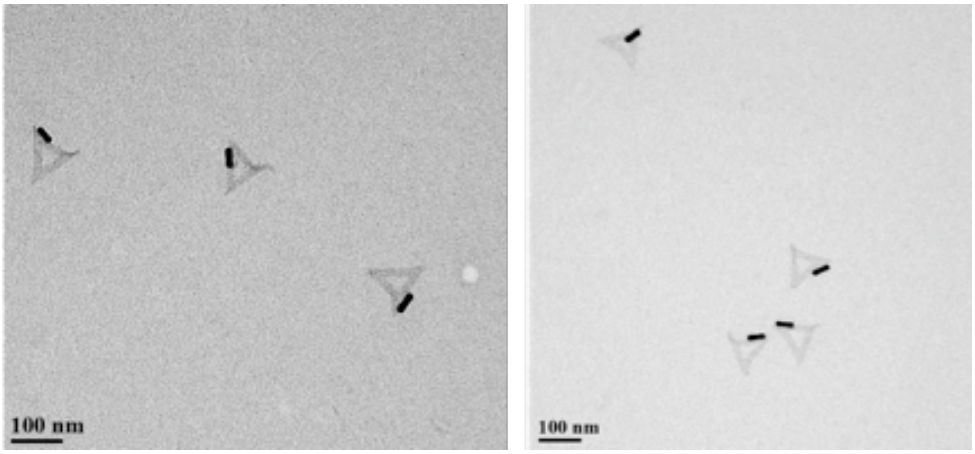

Figure S3: Zoom out TEM images of negatively stained gel purified triangular origami with one AuNR immobilized on it. In the design the capture strands were located along one edge of the triangle. The yield of the desired structure was very high >80%.

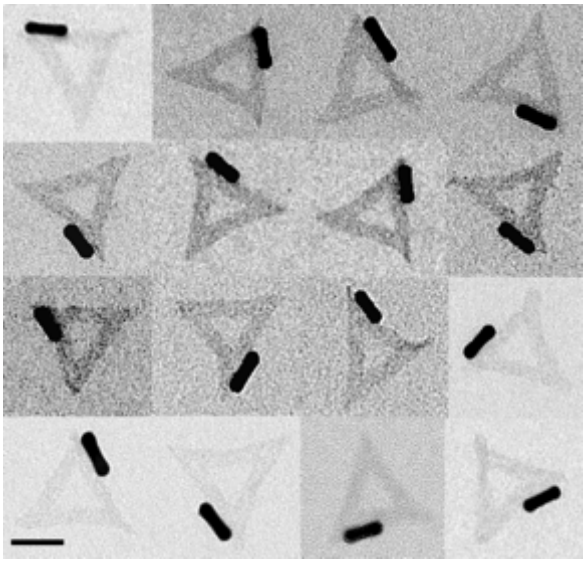

Figure S4: Zoom in TEM images of negatively stained gel purified triangular origami with one AuNR immobilized on it. The AuNR seems aligned very well along one edge of the triangle. Scale bar is 50 nm.

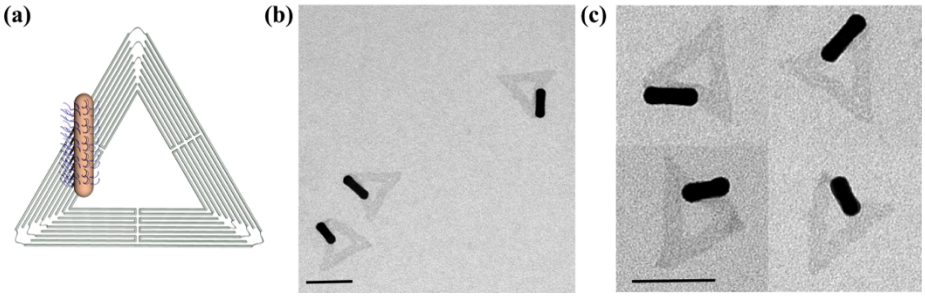

Figure S5: Zoom in TEM images of negatively stained gel purified triangular origami with one AuNR immobilized on it. In this design, the capture strands were located perpendicular to one edge of the triangle. Scale bar is 100 nm.

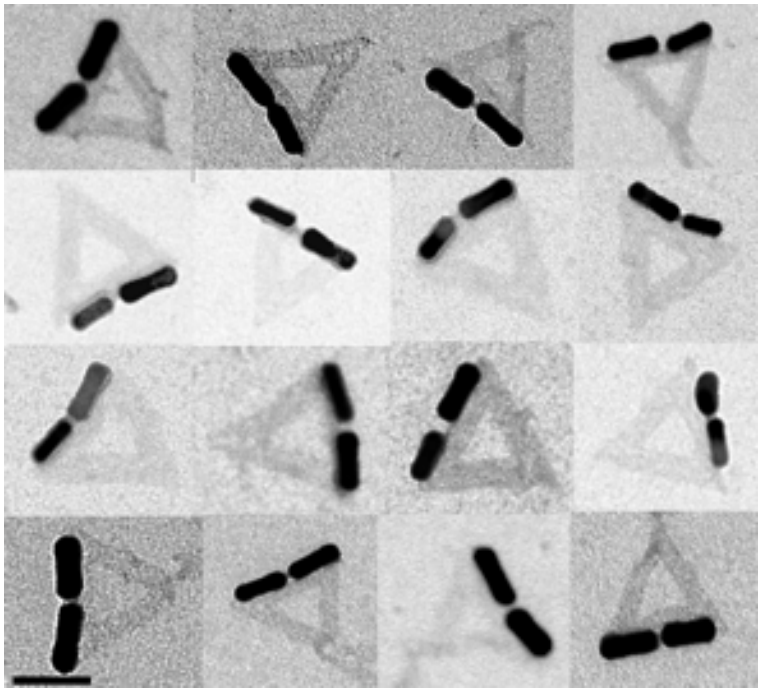

Figure S6: Zoom in TEM images of negatively stained gel purified triangular origami with two AuNRs aligned end-to end along one edge of the triangle with an 180^{o} between the two AuNRs. Scale bar is 100 nm.

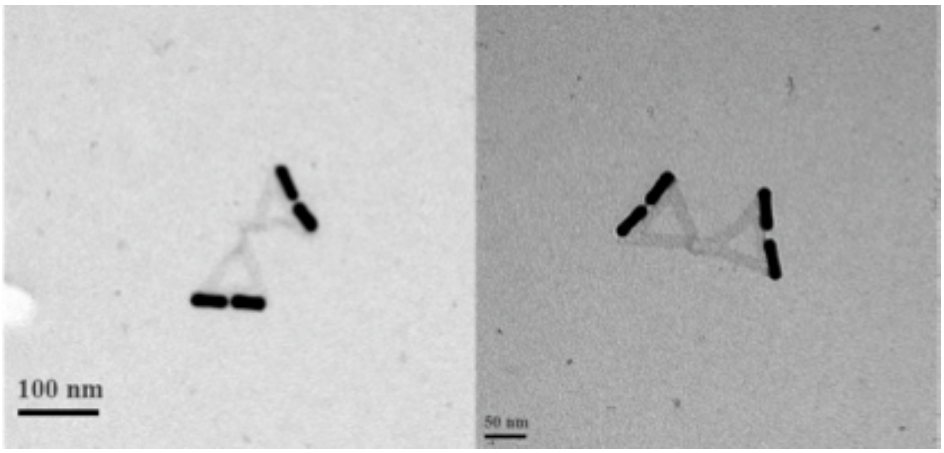

Figure S7: Zoom out TEM images of negatively stained gel purified triangular origami with two AuNR aligned end-to end along one edge of the triangle with an 180^{o} between the two AuNRs. Sometime dimerization of the origami was observed, mainly through helix end base-stacking or staple strand cross-linking.

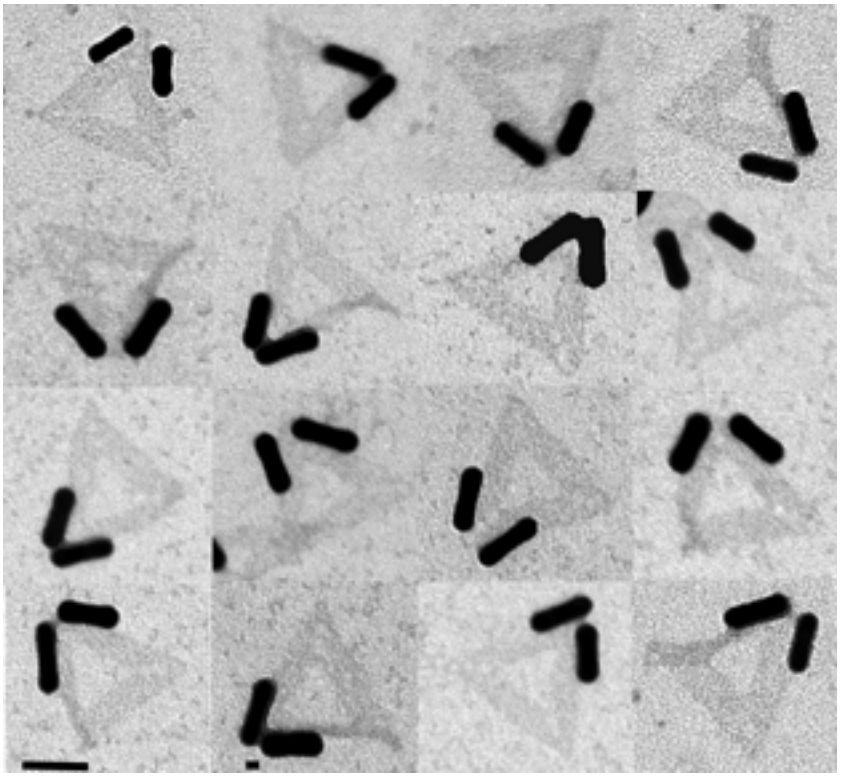

Figure S8: Zoom in TEM images of negatively stained gel purified triangular origami with two AuNRs having a 60^{o} between them.

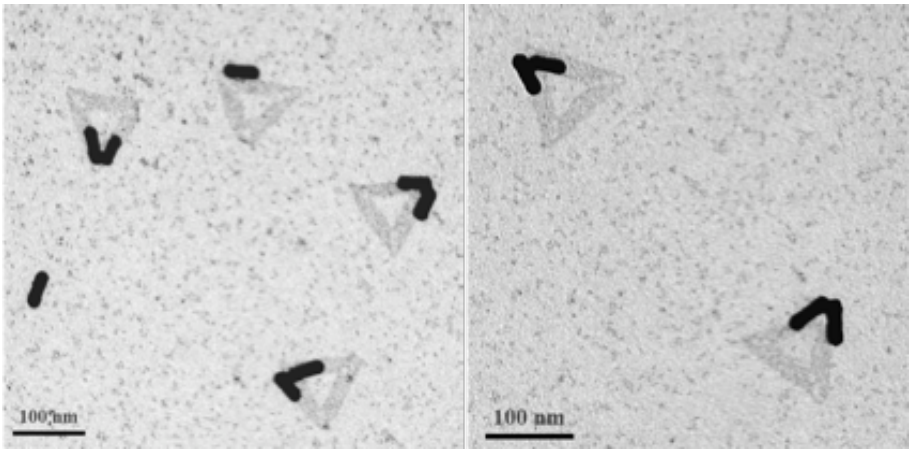

Figure S9: Zoom out TEM images of negatively stained gel purified triangular origami with two AuNR having 60^{o} in between them.

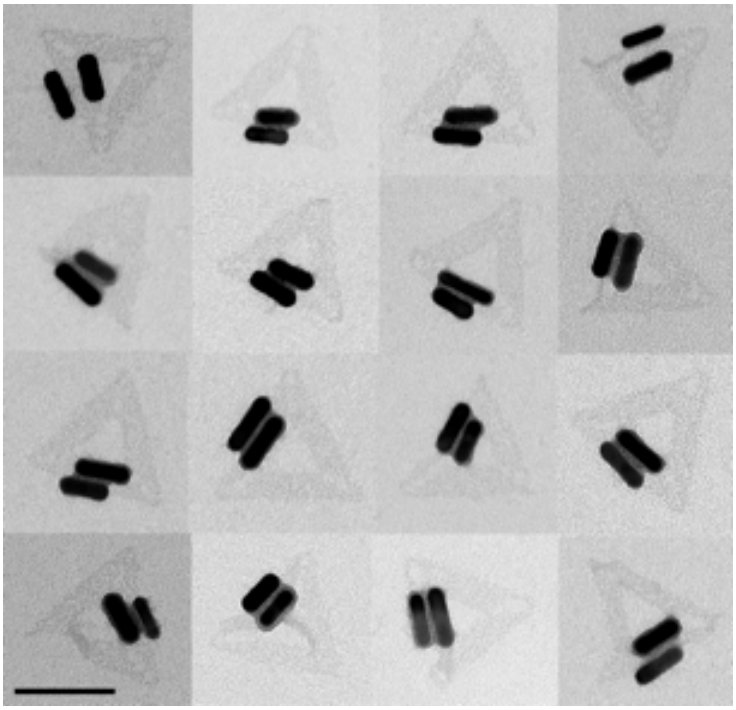

Figure S10: Zoom in TEM images of negatively stained gel purified triangular origami with two AuNRs aligned side by side having 0^{o} in between them. Scale bar is 100 nm.

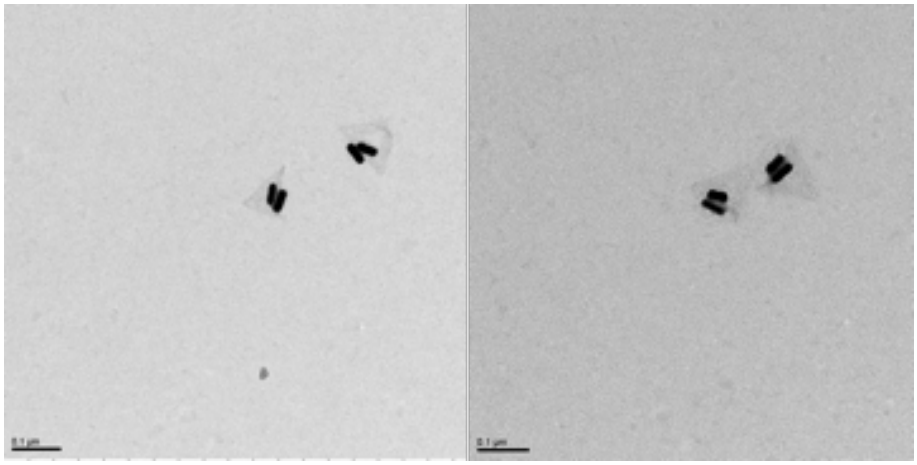

Figure S11: Zoom out TEM images of negatively stained gel purified triangular origami with two AuNRs aligned side by side having 0^{o} in between them.

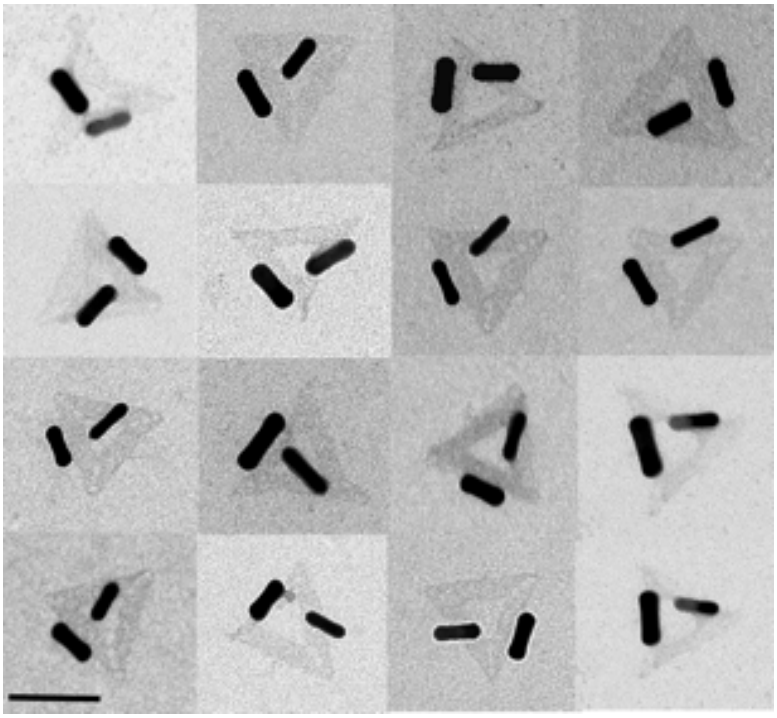

Figure S12: Zoom in negatively stained TEM images of gel purified triangular origami with two AuNR having 90^{o} in between them. Scale bar is 100 nm.

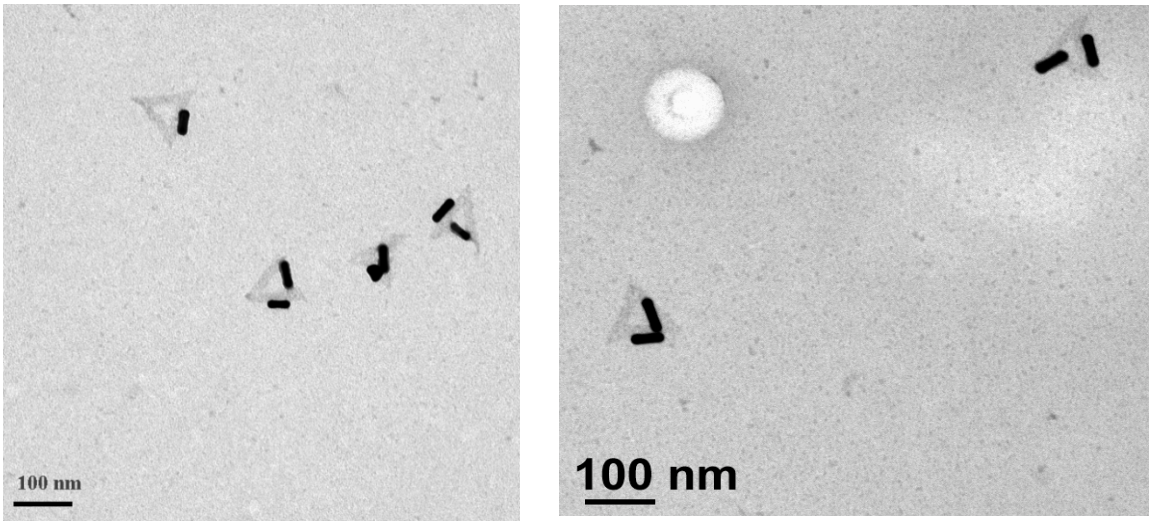

Figure S13: Zoom out TEM images of negatively stained gel purified triangular origami with two AuNRs having 90^{o} in between them.

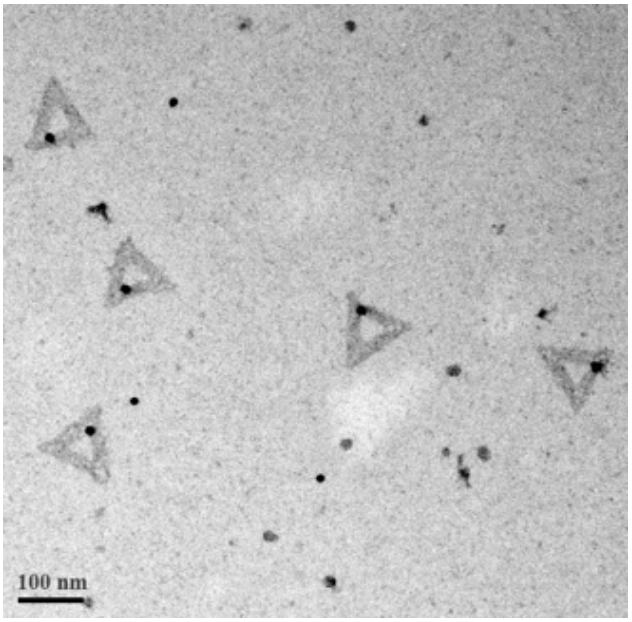

Figure S14: Zoom out TEM images of negatively stained gel purified triangular origami with one 10 nm AuNP preoccupying an end on position (with respect to the AuNR which is not yet attached).

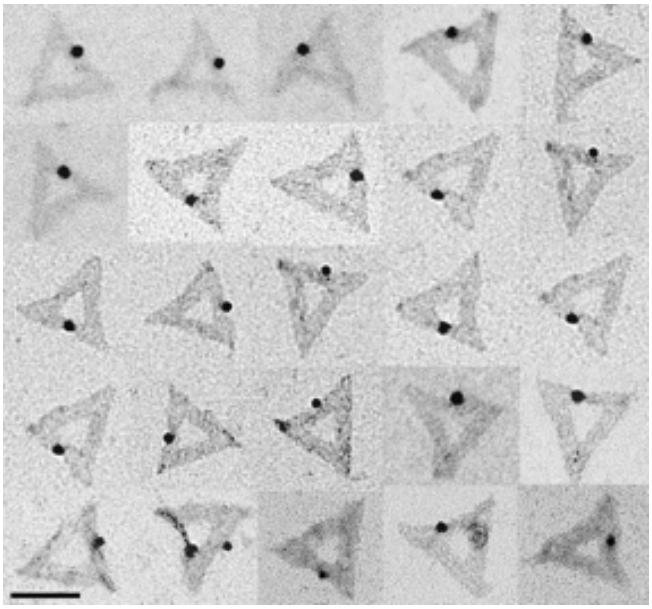

Figure S15: Zoom in negatively stained TEM images of gel purified triangular origami with one 10 nm AuNP preoccupying the end on position. Scale bar is 100 nm.

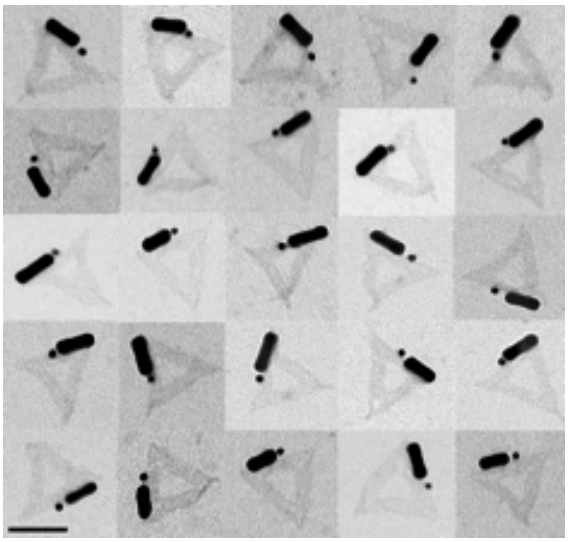

Figure S16: Zoom in TEM images of negatively stained gel purified triangular origami with one AuNR and one AuNP, where the AuNP occupies the end on position. Scale bar is 100 nm.

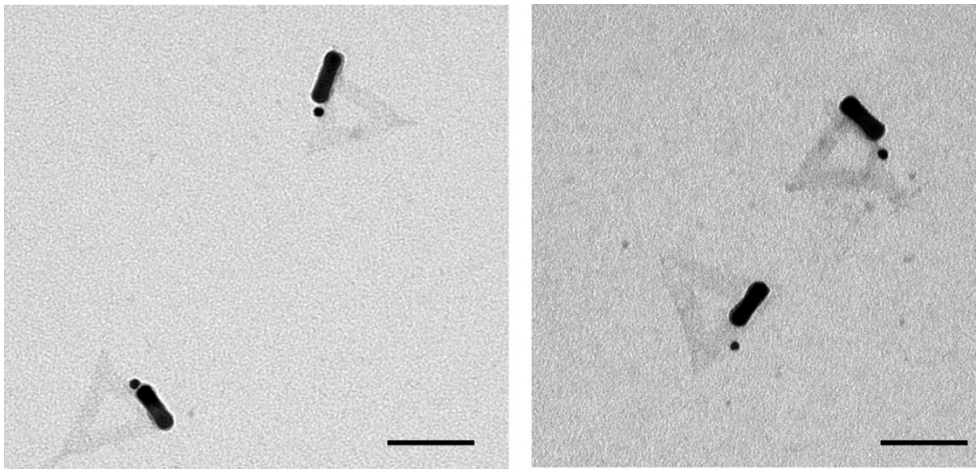

Figure S17: Zoom out TEM images of negatively stained gel purified triangular origami with one AuNR and one AuNP that occupies the end on position respect to the AuNR. Scale bars are 100 nm.

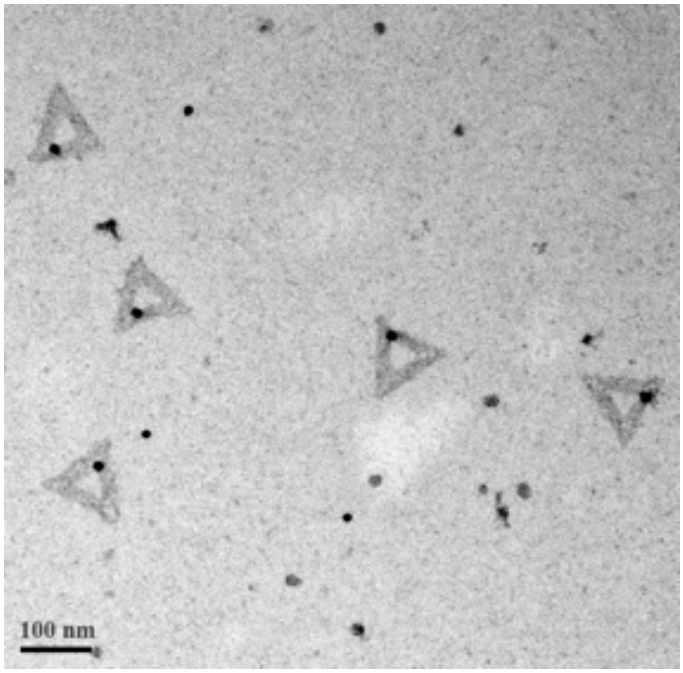

Figure S18: Zoom out TEM images of negatively stained gel purified triangular origami with one 10 nm AuNP preoccupying the side on position (with respect to the AuNR not yet attached).

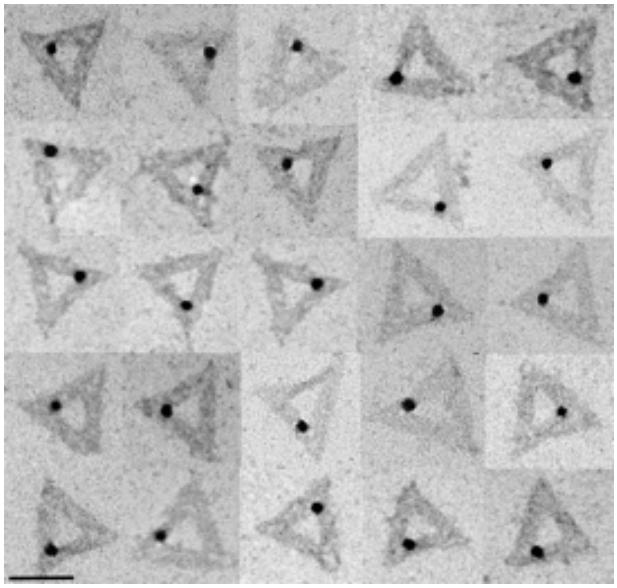

Figure S19: Zoom in TEM images of negatively stained gel purified triangular origami with one 10 nm AuNP preoccupying the side on position. Scale bar is 100 nm.

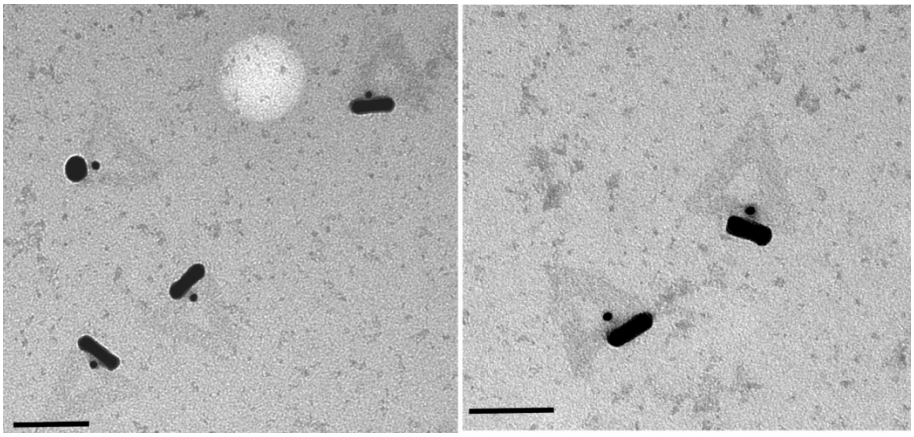

Figure S20: Zoom in TEM images of negatively stained gel purified triangular origami with one AuNR and one AuNP that occupies the side on position with respect to the AuNR. Scale bar is 100 nm.

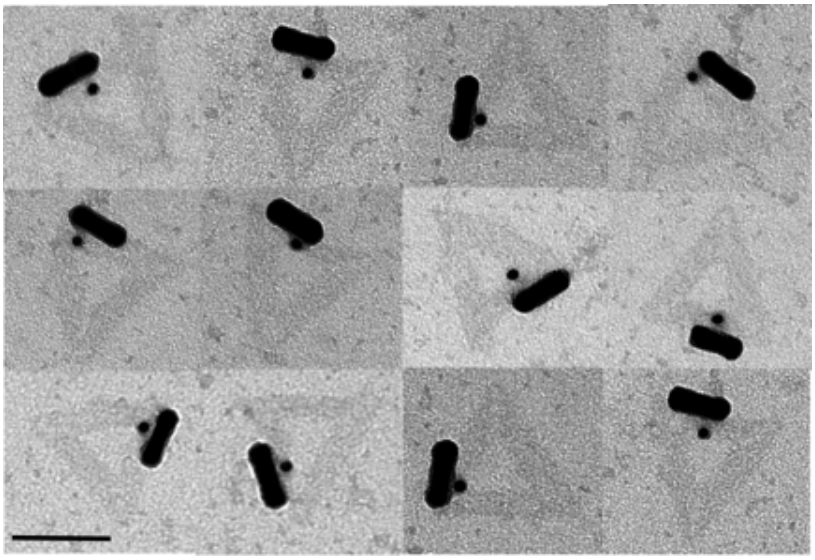

Figure S21: Zoom out TEM images of negatively stained gel purified triangular origami with one AuNR and one AuNP that occupies the side on position.

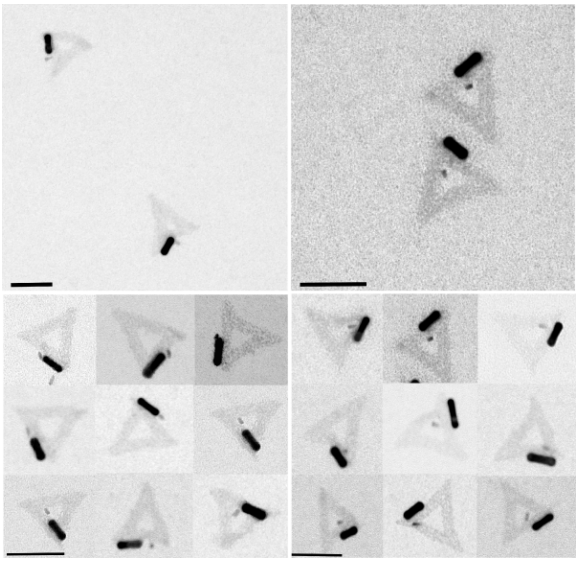

Figure S21-a: Left panel: TEM images of negatively stained gel purified triangular origami with one AuNR and one quantum dot that occupies the side on position. Right panel: TEM images of negatively stained gel purified triangular origami with one AuNR and one quantum dot that occupies the end on position.Scales bars are100 nm.

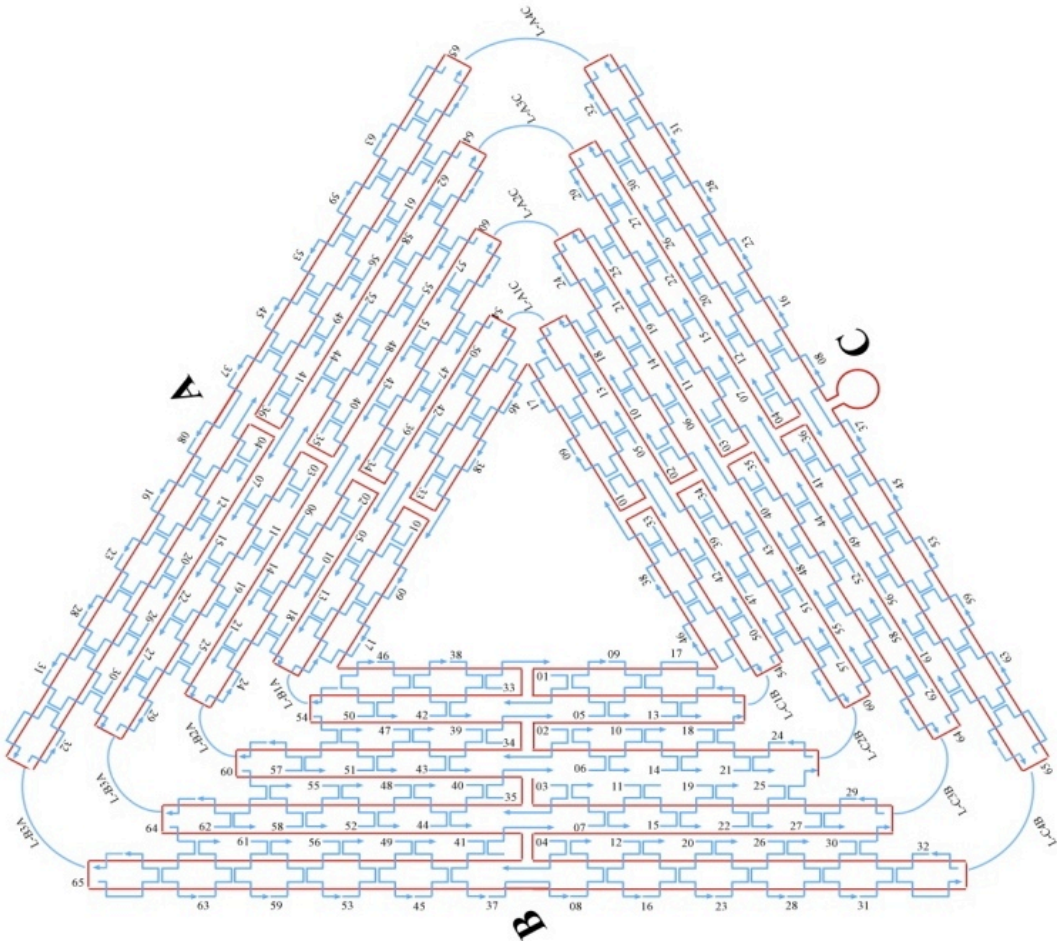

Figure S22: Numbering scheme of triangular origami staple strands.

DNA Sequences:

Sequences of unmodified staple strands are the same as appendix A page 155.

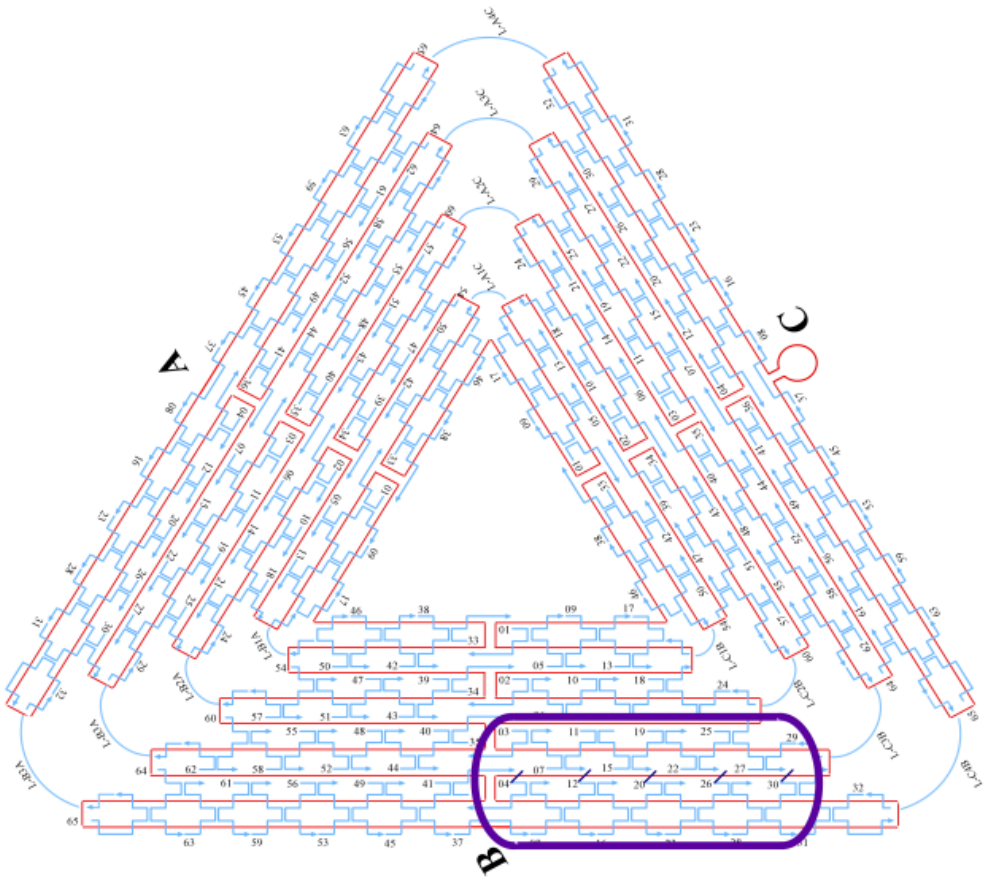

Figure S23: Detailed design and Numbering scheme of triangular origami with one AuNR that is aligned one edge of the triangle.

Capture strand sequences:

B04, AAAAAAAAAAAAAAATTCGAGCTAAGACTTCAAATATCGGGAACGAG,

B12,

AAAAAAAAAAAAAAAAACTCCAAGATTGCATCAAAAAGATAATGCAGATACATAA

B20,

AAAAAAAAAAAAAAATAATTGCTTTACCCTGACTATTATGAGGCATAGTAAGAGC,

B26,

AAAAAAAAAAAAAAACGGATGGCACGAGAATGACCATAATCGTTTACCAGACGAC,

B30,

AAAAAAAAAAAAAAATGCTGTAGATCCCCCTCAAATGCTGCGAGAGGCTTTTGCA.

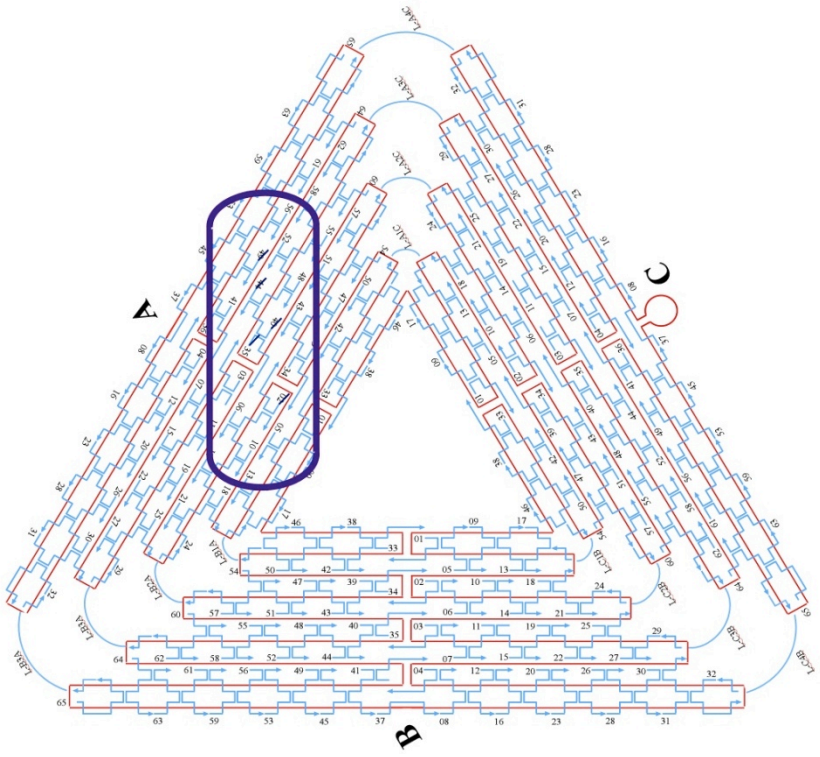

FigureS24: Detailed design and Numbering scheme of triangular origami with one AuNRs aligned at an angle of 30 degree with respect to an arm.

Capture strand sequences:

A02 AGC TAT CGA ATC AGCGTCATGTCTCTGAATTTACCGACTACCTT

A35 AGC TAT CGA ATCAGTATAAAATATGCGTTATACAAAGCCATCTT

A40 AGC TAT CGA ATC TTAGTATCGCCAACGCTCAACAGTCGGCTGTC

A44 AGC TAT CGA ATCTCAATAATAGGGCTTAATTGAGAATCATAATT

A49 AGC TAT CGA ATC AGCATGTATTTCATCGTAGGAATCAAACGATTTTTTGTTT

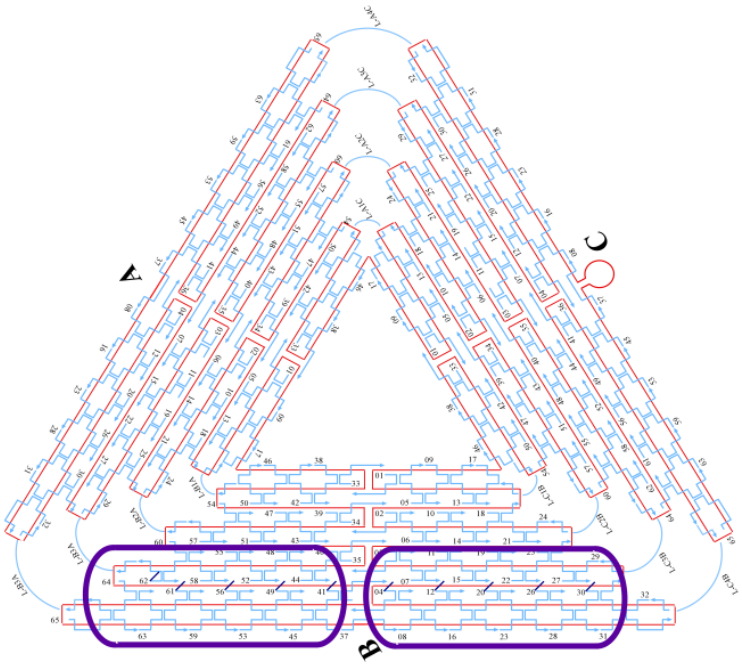

FigureS25: Detailed design and Numbering scheme of triangular origami with two AuNRs aligned end to end along one edge of the triangle that have a 180^{o} angle between them.

Capture strand sequences:

B04, AAAAAAAAAAAAAAATTCGAGCTAAGACTTCAAATATCGGGAACGAG,

B12,

AAAAAAAAAAAAAAAAACTCCAAGATTGCATCAAAAAGATAATGCAGATACATAA

B20,

AAAAAAAAAAAAAAATAATTGCTTTACCCTGACTATTATGAGGCATAGTAAGAGC,

B26,

AAAAAAAAAAAAAAACGGATGGCACGAGAATGACCATAATCGTTTACCAGACGAC,

B30,

AAAAAAAAAAAAAAATGCTGTAGATCCCCCTCAAATGCTGCGAGAGGCTTTTGCA,

B41,AGC TAT CGA ATCCGACCTGCGGTCAATCATAAGGGAACGGAACAACATTATT

B49, AGC TAT CGA ATCTATCATCGTTGAAAGAGGACAGATGGAAGAAAAATCTACG

B56, AGC TAT CGA ATCCCAAGCGCAGGCGCATAGGCTGGCAGAACTGGCTCATTAT

B61, AGC TAT CGA ATCAAAACACTTAATCTTGACAAGAACTTAATCATTGTGAATT,

B62, AGC TAT CGA ATCGGCAAAAGTAAAATACGTAATGCC

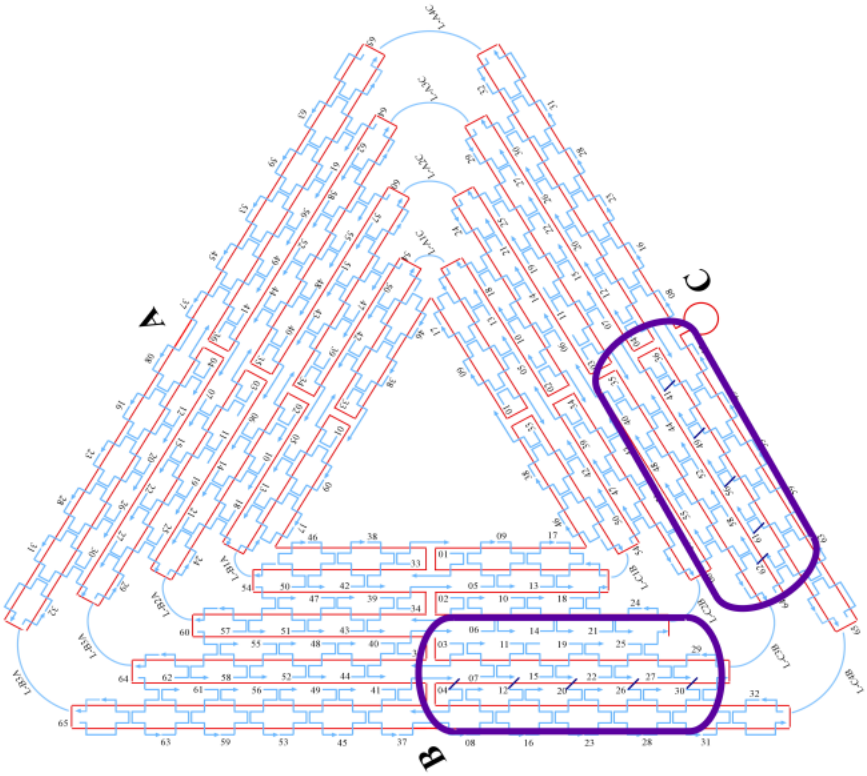

FigureS26: Detailed design and Numbering scheme of triangular origami with two AuNRs having 60^{o} angle.

Capture strand sequences:

B04, AAAAAAAAAAAAAAATTCGAGCTAAGACTTCAAATATCGGGAACGAG,

B12,

AAAAAAAAAAAAAAAAACTCCAAGATTGCATCAAAAAGATAATGCAGATACATAA

B20,

AAAAAAAAAAAAAAATAATTGCTTTACCCTGACTATTATGAGGCATAGTAAGAGC,

B26,

AAAAAAAAAAAAAAACGGATGGCACGAGAATGACCATAATCGTTTACCAGACGAC,

B30,

AAAAAAAAAAAAAAATGCTGTAGATCCCCCTCAAATGCTGCGAGAGGCTTTTGCA,

C41, AGC TAT CGA ATCTTTCACCAGCCTGGCCCTGAGAGAAAGCCGGCGAACGTGG,

C49, AGC TAT CGA ATCTTGTTTGCGTCACGCTGGTTTGCCCCAAGGGAGCCCCCGATT

C56, AGC TAT CGA

ATCTTTTAATGAAGTTTGATGGTGGTTCCGAGGTGCCGTAAAGCA,

C61, AGC TAT CGA ATCTTCCAGTCCTTATAAATCAAAAGAGAACCATCACCCAAAT,

C62, AGC TAT CGA ATCGCGCTCACAAGCCTGGGGTGCCTA,

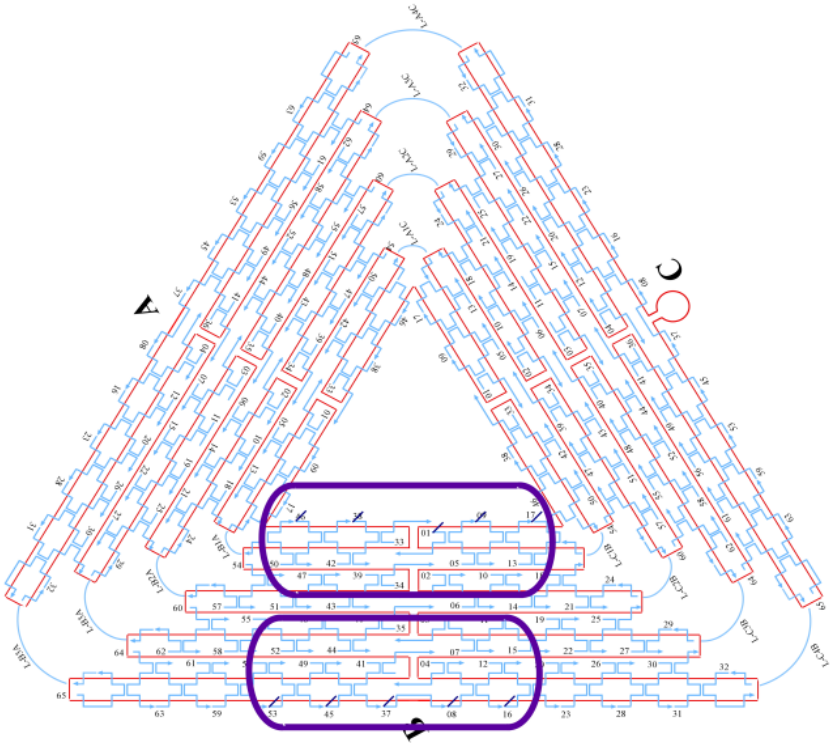

Figure S27: Detailed design and Numbering scheme of triangular origami with two AuNRs aligned side by side with a 0^{o} angle.

Capture strand sequences:

B53, AAAAAAAAAAAAAAA

ACCAGTCAGGACGTTGGAACGGTGTACAGACCGAAACAAA

B45,

AAAAAAAAAAAAAAATTAATAAAACGAACTAACCGAACTGACCAACTCCTGATAA,

B37, AAAAAAAAAAAAAAA ACAGGTAGAAAGATTCATCAGTTGAGATTTAG

B08,

AAAAAAAAAAAAAAAGAATACCACATTCAACTTAAGAGGAAGCCCGATCAAAGCG

B16,

AAAAAAAAAAAAAAACGCCAAAAGGAATTACAGTCAGAAGCAAAGCGCAGGTCAG

B46, AGC TAT CGA ATCAGGTTTAGTACCGCCATGAGTTTCGTCACCAGGATCTAAA

B38, AGC TAT CGA ATCCCTCAGAACCGCCACCCAAGCCCAATAGGAACGTAAATGA

B01, AGC TAT CGA ATCTCATATGTGTAATCGTAAAACTAGTCATTTTC

B09, AGC TAT CGA ATCAGAAAAGCCCCAAAAAGAGTCTGGAGCAAACAATCACCAT

B17, AGC TAT CGA ATCGCAAATATTTAAATTGAGATCTACAAAGGCTACTGATAAA

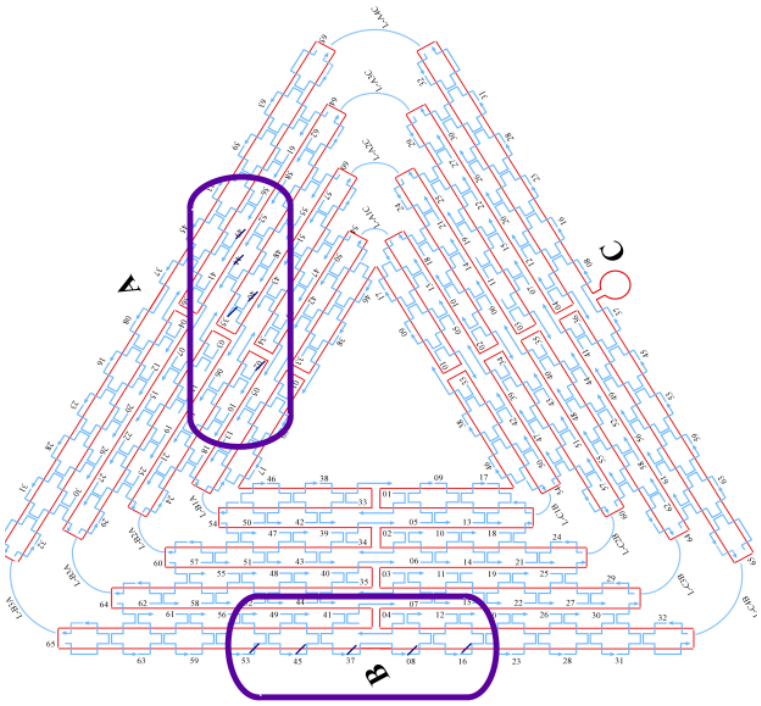

Figure S28: Detailed design and Numbering scheme of triangular origami with two AuNRs forming a 90^{o} angle.

Capture strand sequences:

B53, AAAAAAAAAAAAAAA

ACCAGTCAGGACGTTGGAACGGTGTACAGACCGAAACAAA

B45,

AAAAAAAAAAAAAAATTAATAAAACGAACTAACCGAACTGACCAACTCCTGATAA,

B37, AAAAAAAAAAAAAAA ACAGGTAGAAAGATTCATCAGTTGAGATTTAG

B08,

AAAAAAAAAAAAAAAGAATACCACATTCAACTTAAGAGGAAGCCCGATCAAAGCG

B16,

AAAAAAAAAAAAAAACGCCAAAAGGAATTACAGTCAGAAGCAAAGCGCAGGTCAG

A02 AGC TAT CGA ATC AGCGTCATGTCTCTGAATTTACCGACTACCTT

A35 AGC TAT CGA ATCAGTATAAAATATGCGTTATACAAAGCCATCTT

A40 AGC TAT CGA ATC TTAGTATCGCCAACGCTCAACAGTCGGCTGTC

A44 AGC TAT CGA ATCTCAATAATAGGGCTTAATTGAGAATCATAATT

A49 AGC TAT CGA ATC AGCATGTATTTCATCGTAGGAATCAAACGATTTTTTGTTT

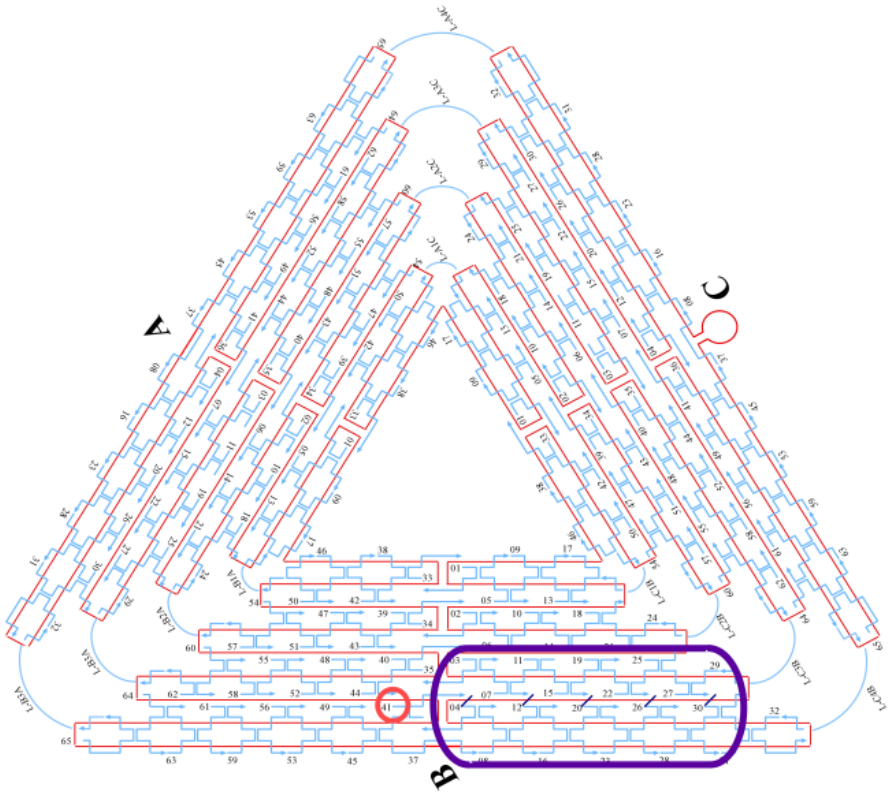

Figure S29: Detailed design and Numbering scheme of triangular origami with end-on AuNR-AuNP hetero-dimer.

Capture strand sequences:

B04, AAAAAAAAAAAAAAATTCGAGCTAAGACTTCAAATATCGGGAACGAG,

B12,

AAAAAAAAAAAAAAAAACTCCAAGATTGCATCAAAAAGATAATGCAGATACATAA

B20,

AAAAAAAAAAAAAAATAATTGCTTTACCCTGACTATTATGAGGCATAGTAAGAGC,

B26,

AAAAAAAAAAAAAAACGGATGGCACGAGAATGACCATAATCGTTTACCAGACGAC,

B30,

AAAAAAAAAAAAAAATGCTGTAGATCCCCCTCAAATGCTGCGAGAGGCTTTTGCA,

B41+37, NH2-

CGACCTGCGGTCAATCATAAGGGAACGGAACAACATTATTACAGGTAGAAAGATTCA

TCAGTTGAGATTTA

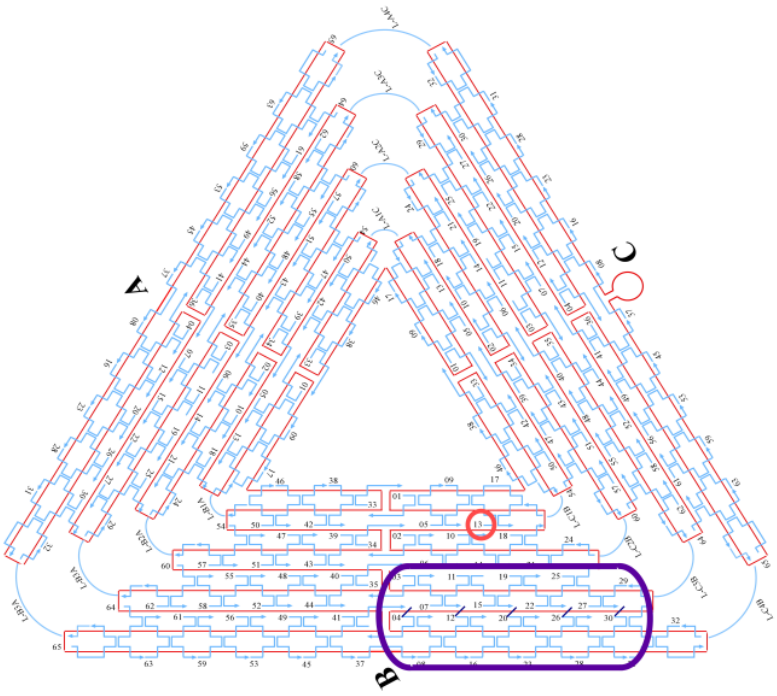

Figure S30: Detailed design and Numbering scheme of triangular origami with side-on AuNR-AuNP hetero-dimer.

Capture strand sequences:

B04, AAAAAAAAAAAAAAATTCGAGCTAAGACTTCAAATATCGGGAACGAG,

B12,

AAAAAAAAAAAAAAAAACTCCAAGATTGCATCAAAAAGATAATGCAGATACATAA

B20,

AAAAAAAAAAAAAAATAATTGCTTTACCCTGACTATTATGAGGCATAGTAAGAGC,

B26,

AAAAAAAAAAAAAAACGGATGGCACGAGAATGACCATAATCGTTTACCAGACGAC,

B30,

AAAAAAAAAAAAAAATGCTGTAGATCCCCCTCAAATGCTGCGAGAGGCTTTTGCA,

B13+17,

GTCCATCGTACGTTCTAGTCAGGTCATTGCCTGACAGGAAGATTGTATAAGCAAATAT

TTAAATTGAGATCTACAAAGGCTACTGATAAA

Thiolated strands:

C1', TTTTTTTTTTTTTTT AGC GA-SH

C2', GATTCGATAGCTTATGCTGC-SH

APPENDIX D

SUPPLEMENTAL INFORMATION FOR CHAPTER 5

Supporting Information

Site specific synthesis and *in-situ* immobilization of fluorescent silver nanoclusters on DNA nanoscaffolds using Tollens' reaction

Suchetan Pal, Reji Varghese, Zhengtao Deng, Zhao Zhao, Ashok Kumar, Hao Yan* and Yan Liu*

Department of Chemistry and Biochemistry and

The Biodesign Institute, Arizona State University

Tempe, AZ 85287 (USA)

Fax: (+1) 480-727-2378

E-mail: yan_liu@asu.edu; hao.yan@asu.edu

Materials

All the DNA strands were purchased from IDT DNA Inc. (www.idtdna.com). Azide modified sugar (6-Azido-6-deoxy-D-galactose), Tris[(1-benzyl-1H-1,2,3-triazol-4-yl)methyl]amine, silver nitrate, and Cu(I)Br were purchased from Sigma-Aldrich. Solvents needed for the organic synthesis were purchased from Sigma-Aldrich and low water content solvents needed for the DNA synthesis were purchased from Honeywell Burdick and Jackson (http://www51.honeywell.com/sm/specialtychemicals/bandj-global/). M13mp18 single stranded DNA was purchased from New England Biolabs and was used as received. Alkyne modified phosphoramidite were purchased from Glen Research (http://www.glenresearch.com/index.php) or Base Click (http://www.baseclick.eu/). All other chemicals and reagents for the DNA synthesis were purchased from Glen Research (http://www.glenresearch.com/index.php).

Methods:

1. Alkyne modified DNA synthesis, purification and characterization:

DNA synthesis: Alkyne modified DNAs were synthesized on an ABI 394 DNA/RNA synthesizer *via* standard phosphoramidite protocols using CPGs (1μ mol) with a coupling time of 10 minutes and concentration of 0.1 M for the modified phosphoramidite. After preparation, the trityl-off oligonucleotides were cleaved off the resin and was deprotected by treatment with concentrated NH_4OH (28 %) at room temperature for 24 h and are subsequently purified by High

Performance Liquid Chromatography (HPLC).

Reverse phase HPLC: The modified oligonucleotides were purified using a ZORBAX SB-C18 reverse phase column on an Agilent Technologies 1200 series HPLC system that is equipped with diode array detector and automated fraction collector. The oligonucleotides after purification were lyophilized and quantified by measuring their absorbance at 260 nm.

MALDI-TOF analyses: The purity and the success synthesis of the modified DNA strands were examined by MALDI-TOF analyses, which were carried out on Applied Biosystem Voyager System 4320 using 3-hydroxypicolinic acid as the matrix with an accelerating voltage of 25 kV.

2. Synthesis of sugar modified DNA using "Click" reaction

Alkyne modified DNA (0.5 mM, 200 μL in nanopure water) and 6-azido-6-deoxy-D-galactose (100 mM in 25 μL DMSO/t-Butanol 3:1) were placed in a 1.5 mL vial. In a separate vial Cu(I)Br solution (100 mM in 25 μL DMSO/t-Butanol 3:1) with tris(1-benzyl-1H-1,2,3-tetrazol-4-yl)methyl]amine (ligand) (100 mM, 50 μL water) was mixed in a vortex. The whole solution of Cu(I)Br and the ligand was then added to the DNA solution. The reaction mixture was shaken at room temperature for 4 hours. After the completion of the reaction, the solvent was evaporated to near dryness. Sodium acetate solution (0.3 M, 100 μL) was added to replace the bound Cu^{+} from the DNA backbone and the suspension was left standing for 1 hour with occasional vortexing.[1] The solution was filtered (Spin-X centrifuge tube filters cellulose acetate membrane, pore size 0.45 μm) and the

product (sugar modified DNA oligonucleotide) was subsequently purified using reverse phase HPLC, lyophilized and characterized by MALDI-TOF spectroscopy.

3. Preparation of triangular DNA origami

To assemble triangular DNA origami with one sugar modified arm, the 5' end of 65 out of the 205 helper strands were extended by 15 bases that contain the complementary sequence to the sugar modified strand. 5 nM of M13 (7249 nucleotide long) with 5 fold excess of staple strands and 650 fold excess of sugar modified strands were mixed in 0.5 × TAE-Mg^{2+} (20 mM Tris, 10 mM Acetic acid, 1 mM EDTA and 6.25 mM Magnesium acetate, pH 8.0). The resulting solution was cooled from 90^{o} C to 4^{o} C to form the triangular origami. In order to get rid of excess staple strands and the excess sugar modified strands, the resultant solution was purified using 1 % agarose gel with 1× TAE-Mg^{2+} as the running buffer under constant voltage of 80 V for 2 hours. The band corresponding to the origami structures was cut off from the gel carefully and crushed. The origami structures were obtained using a freeze and squeeze gel extraction spin columns (Bio-Rad Laboratories). The efficiency of the purification is calculated to be 70-80%. For triangular origami the formation of discrete origami structures were found to be more effective using lower M13 DNA concentration in the annealing step. Otherwise at higher M13 concentration, staple strands joining two arms may crosslink more than one origami leading to higher order structures like dimmers indicated by agarose gel analysis.

4. Synthesis of Ag-NCs and its immobilization on triangular origami

Tollens reagent was prepared by dissolving 16.9 mg of $AgNO_3$ in 1 mL of 1×TAE-Mg^{2+} buffer. The resulting milky white turbid solution was subsequently dissolved by the addition of ammonia solution (28 %) drop by drop until get a clear solution. Tollens' reagent such prepared was filtered (with 0.2μm syringe filter) before addition to the free DNA or origami solutions. The pH of the solution was maintained at ~ 9. The treatment of Tollens' reagent with free **DNA1**-**DNA3** or the preassembled origami structure under dark for 48 hours at room temperature resulted in the formation of fluorescent Ag-NCs. In the case of DNA origami, 3.9 μL of Tollens' reagent (1 mM) was added to a solution of purified origami (100 μL, ~3 nM) in 1xTAE-Mg buffer. In the case of free DNA1-DNA3 in solution, 1 μL of Tollen's reagent (100 mM) was added to a solution of DNA strands (100 μL, 5μM) in 1xTAE-Mg buffer.

5. Structural and spectral characterization of the Ag-NCs:

A. Transmission Electron Microscope (TEM) imaging and analysis: The carbon coated copper grids (400 mesh, Ted Pella) were first glow discharged using Emitech K100× machine in order to increase its hydrophilicity. Then 2 μL of the purified sample solution was dropped on the pretreated grid to bind on the surface. After 1 minute, the unbound sample was wicked from the grid by touching its edge with a piece of filter paper. To remove the excess salt, the grid was touched with a drop of water and the excess water was wicked away by a

filter paper. For negative staining, the grid was touched with a drop of 0.7 % uranyl formate solution for a few seconds and excess solution was wicked away with a filter paper. Again the grid was touched with a second drop of the uranyl formate solution for 20 seconds, and the excess solution was removed with a filter paper. The grid was kept at room temperature to evaporate excess solution. Low-resolution TEM studies were conducted by using a Philips CM12 transmission electron microscope, operated at 80 kV in the bright field mode. High-resolution transmission electron microscopy (HRTEM), high angle annular dark field scanning transmission electron microscopy (HAADF-STEM), and energy dispersive X-ray spectroscopy (EDS) were performed on a JEOL JEM 2010F electron microscope operating at 200 kV.

B. Atomic Force Microscope (AFM) imaging and analysis: Freshly cleaved mica surface was treated with 1×TAE-Mg^{2+} solution prior to sample deposition. 2 μL sample of origami solution was left to adsorb on mica surface for 3 minutes, then 400 μL 1×TAE-Mg^{2+} solution was added to the liquid cell. The sample was scanned in liquid on a Pico-Plus AFM (Molecular Imaging, Agilent Technologies) in tapping mode with NP-S tips (Veeco, Inc.). The AFM images were analyzed using SPIP software.

C. Fluorescence spectra analyses: Steady state photoluminescence (PL) and photoluminescence excitation (PLE) spectra were measured at room temperature using a NanoLog spectrometer manufactured by HORIBA Jobin Yvon equipped with a thermoelectrically cooled PMT (R928 in the range 200 nm to 850 nm) and CW 450W Xenon lamp.

D. Time-correlated single photon counting (TCSPC) for fluorescence lifetime measurement: The excitation source was a titanium sapphire (Ti:S) laser (Spectra-Physics, Tsunami), which provides 130-fs pulses at 80 MHz. The laser output was sent through a frequency doubler and pulse selector (Spectra Physics, Model 3980) to obtain excitation. Fluorescence emission was collected at 90° geometry and detected using a double-grating monochromator (Jobin-Yvon, Gemini-180) and a microchannel plate photomultiplier tube (Hamamatsu R3809U-50). Data acquisition was done using a single photon counting card (Becker-Hickl, SPC-830). The instrument response function (IRF) was 35-45 ps at FWHM. Data analysis was carried out using local written software ASUFIT (URL: www.public.asu.edu/~laserweb/asufit/asufit.html). Data was fit with a sum of exponential decay model.

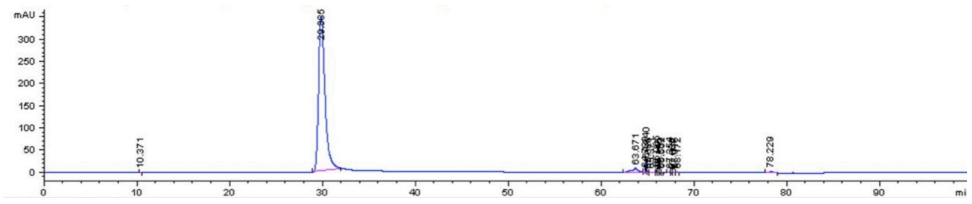

Figure S1. Analytical HPLC trace of **DNA1**.

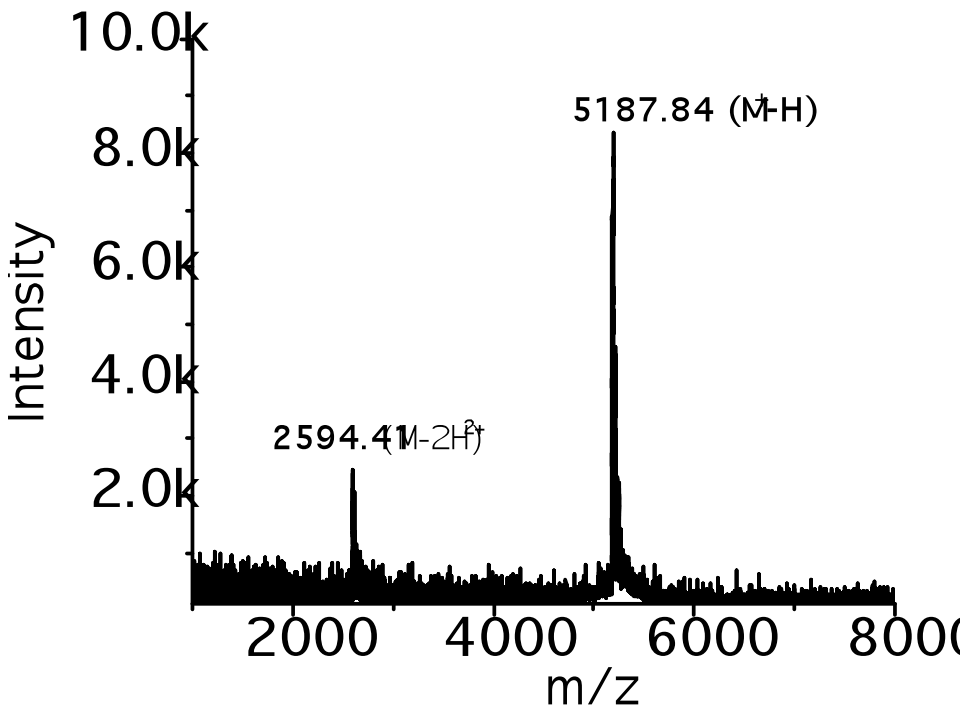

Figure S2. MALDI-TOF mass spectrometry of **DNA1,** the expected molecular mass is 5186.2.

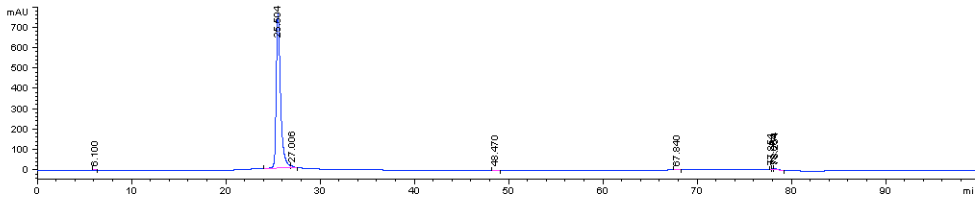

Figure S3. Analytical HPLC trace of **DNA2**.

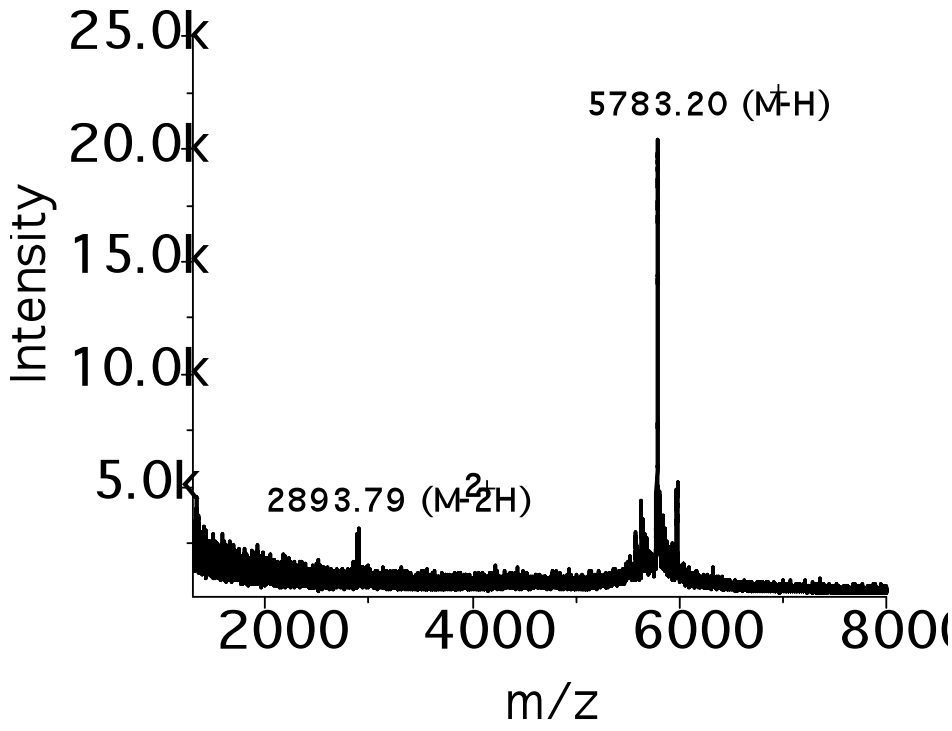

Figure S4. MALDI-TOF spectrum of **DNA2,** the expected molecular mass is 5781.9.

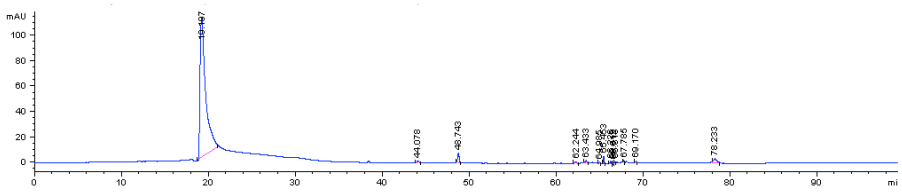

Figure S5. Analytical HPLC trace of **DNA3**.

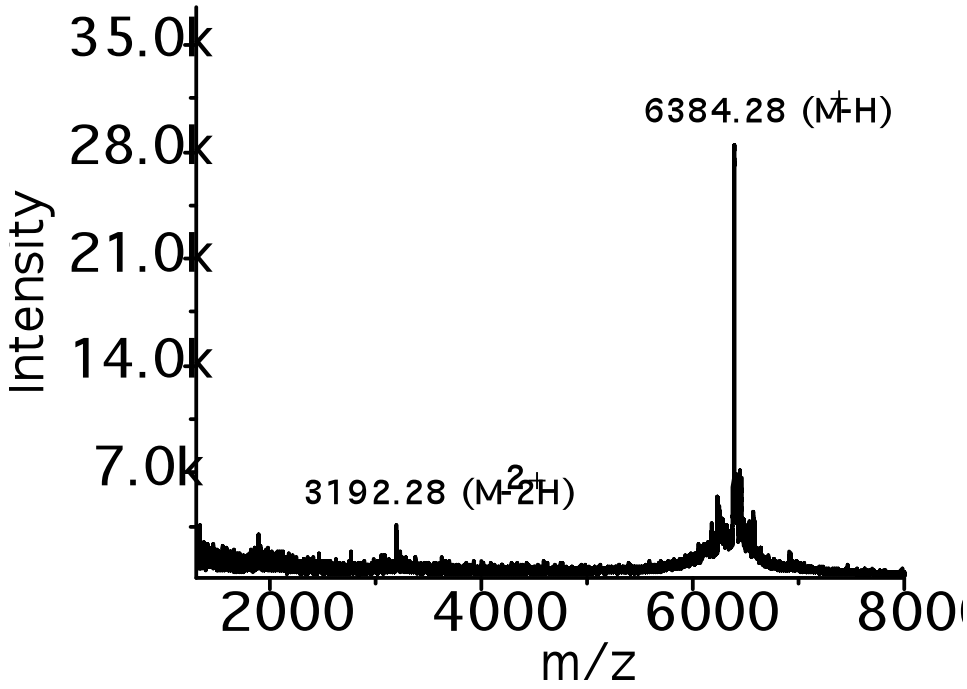

Figure S6. MALDI-TOF spectrum of **DNA3,** the expected molecular mass is 6381.8.

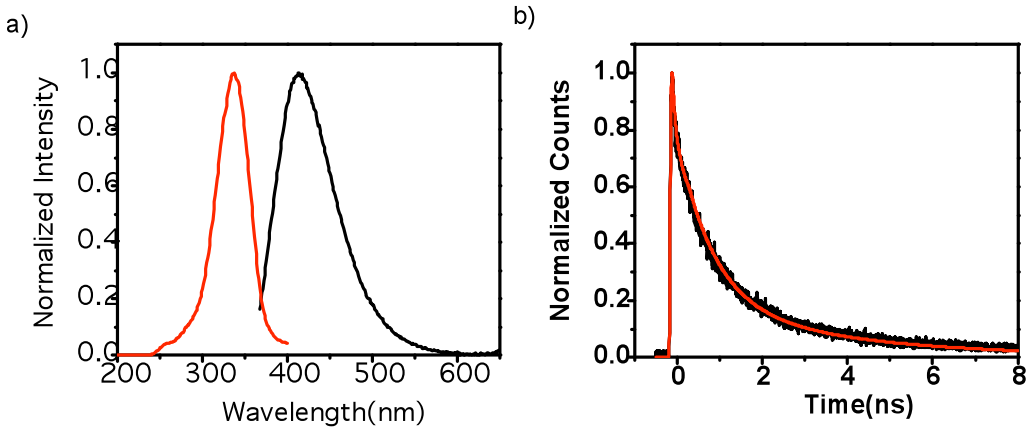

Figure S7: a) Excitation (red) and emission (black) spectrum of Ag-NCs obtained using **DNA1** to react with Tollens' reagent that show peaks at 327 nm and 411 nm, respectively. b) The corresponding life-time decay profile exhibited a tri-exponential decay with lifetimes of 3.6 ns (12 %), 0.8 ns (37 %) and 0.1 ns (51%).

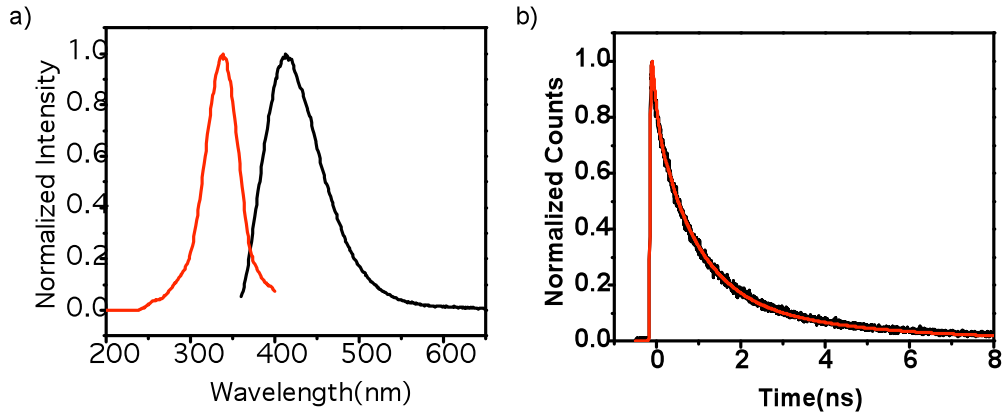

Figure S8: a) Excitation (red) and emission (black) spectrum of Ag-NCs obtained using **DNA2** to react with Tollens' reagent that show peaks at 337 nm and 411 nm, respectively. b) The corresponding life-time decay profile which exhibited a tri-exponential decay with lifetimes of 3.7 ns (12 %), 0.9 ns (42 %) and 0.1 ns (47 %).

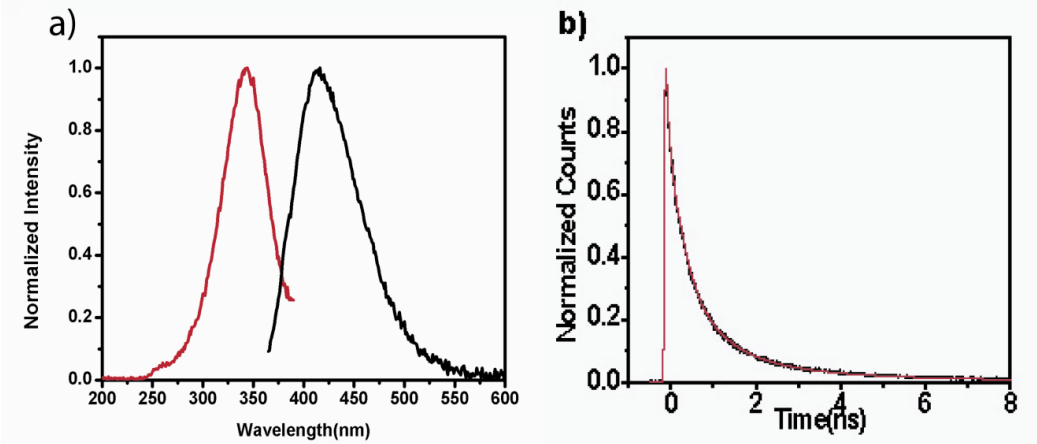

Figure S9: a) Excitation (red) and emission (black) spectrum of Ag-NCs obtained using **DNA3** to react with Tollens' reagent that show peaks at 337 nm and 420 nm, respectively. b) The corresponding life-time decay profile which exhibited a multi-exponential decay with lifetimes of 3.8 ns (4 %), 0.9 ns (21 %), 0.3 ns (31 %) and 0.1 ns (44 %).

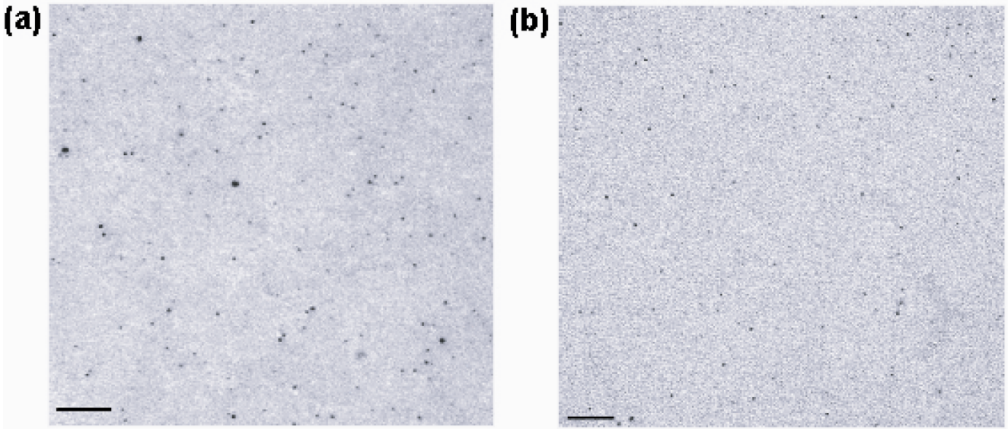

Figure S10: TEM images of Ag-NCs synthesized from **DNA1** (a) and **DNA2** (b). Scale bar is 50 nm.

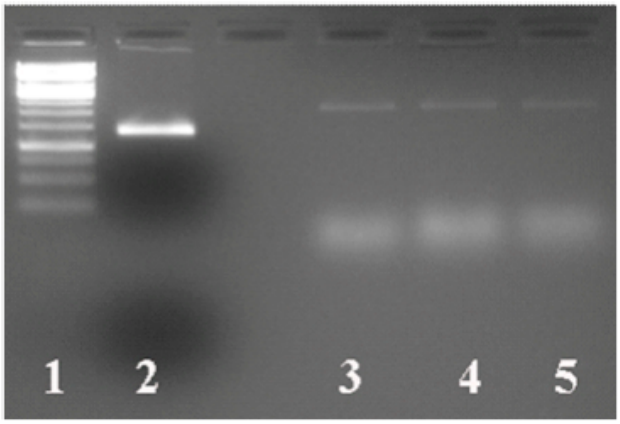

Figure S11: Gel image of agarose gel electrophoresis of the triangular origami samples, gel concentration 1% in 1× TAE-Mg buffer. Lane 1: 1 kb DNA ladder, lane 2: M13mp18 single stranded DNA, and Lane 3, 4, 5, contains the triangular-origami structure carrying **DNA1**, **DNA2**, or **DNA3** at one arm of the triangle, respectively. The thin bands running slower than the M13 single stranded DNA were cut from the gel very carefully, crushed and the DNA origami were extracted from the gel using a 'Freeze-and-Squeeze' gel extraction spin columns, and used for the further studies.

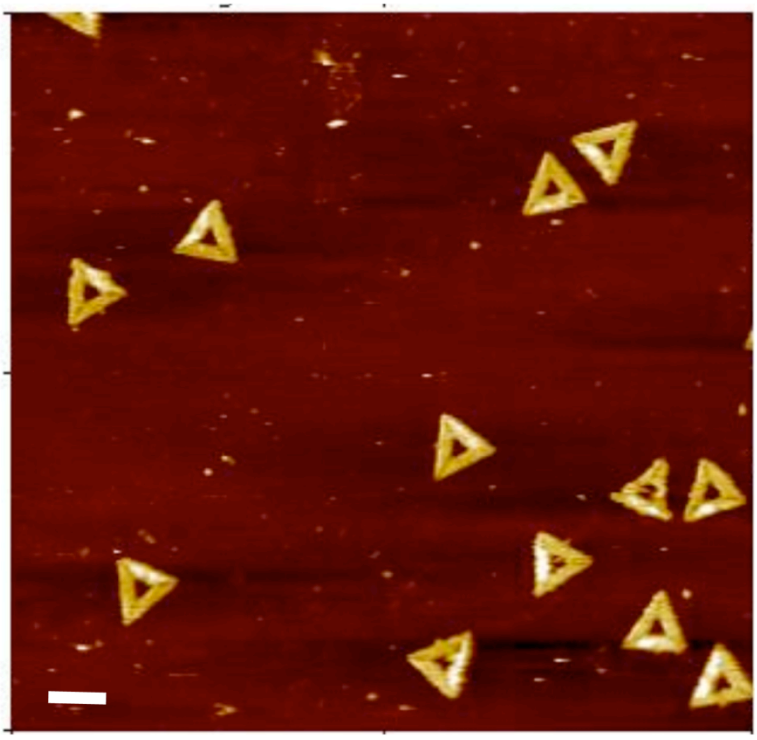

Figure S12: Additional tapping mode AFM images of triangular origami with **DNA3** as the probe before Tollens' reaction. A clear bright stripe is visible in one arm of the triangle which contains the probe strands. Scale bar is 100 nm and z-scale range is 10 nm.

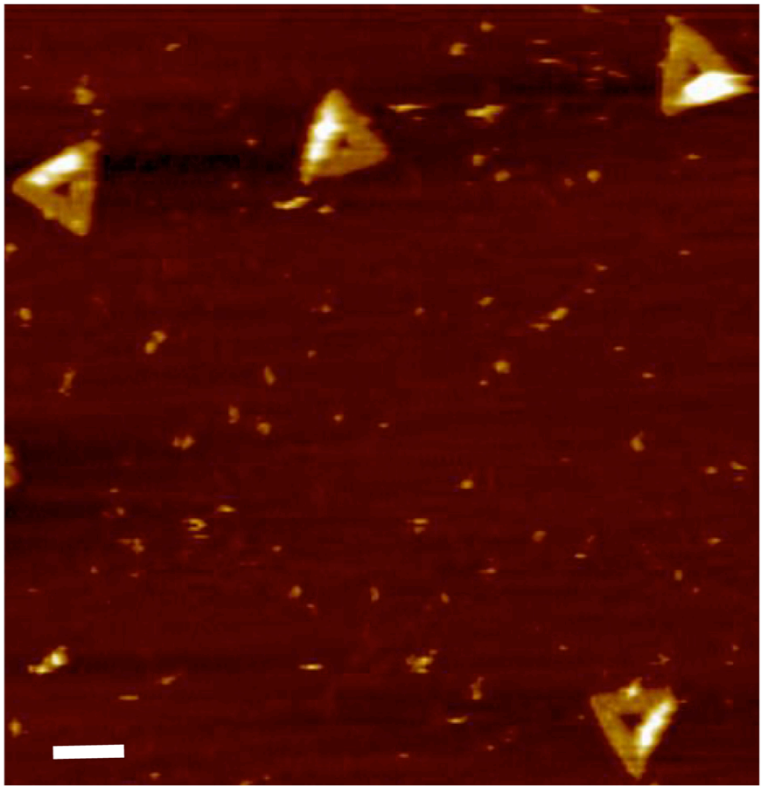

Figure S13: Additional tapping mode AFM images of triangular origami with **DNA3** as the probe after the treatment with Tollens' reagent. A bright stripe is clearly seen in one arm of the triangle, which is due to the site specific immobilization of Ag-NCs at this arm Scale bar is 100 nm and z-scale range is 10 nm.

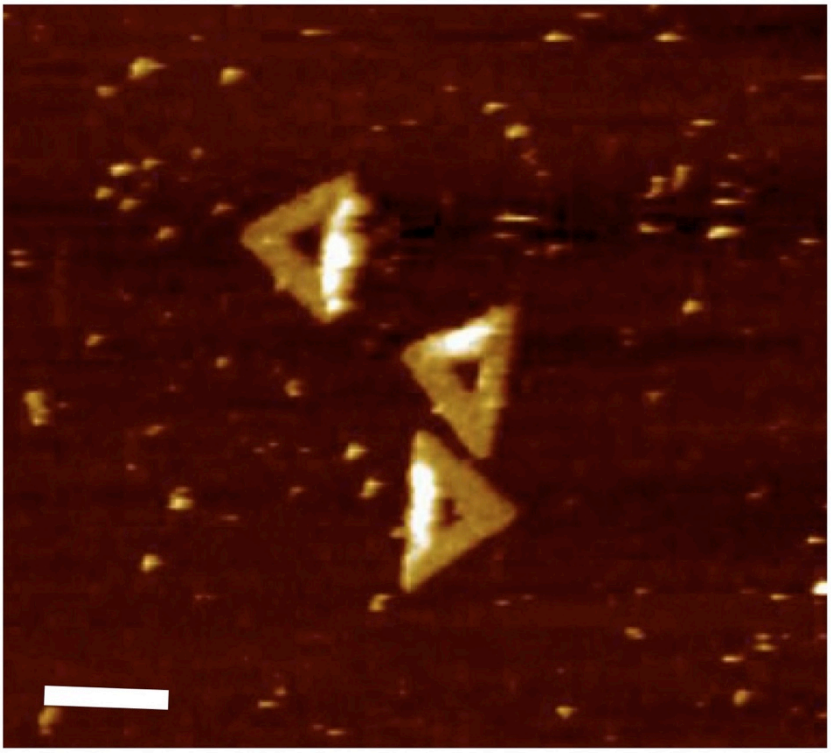

Figure S14: Additional tapping mode AFM images of triangular origami with **DNA2** as the probe after the treatment with Tollens' reagent. In this case also, the bright stripe at one arm of the triangle clearly reveals the site specific immobilization of Ag-NCs. Scan area is 1 μm × 1 μm and z-scale range is 10 nm.

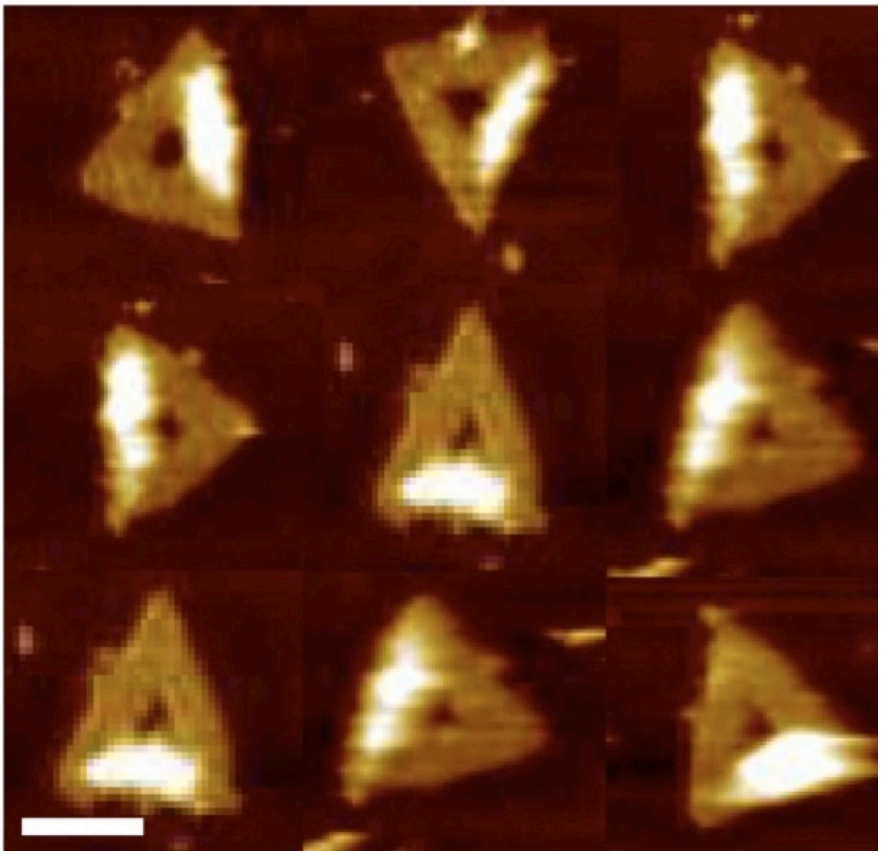

Figure S15: Additional zoom-in AFM images of triangular origami with **DNA3** as probe after treatment with Tollens' reagent. The scale bar corresponds to 100 nm.

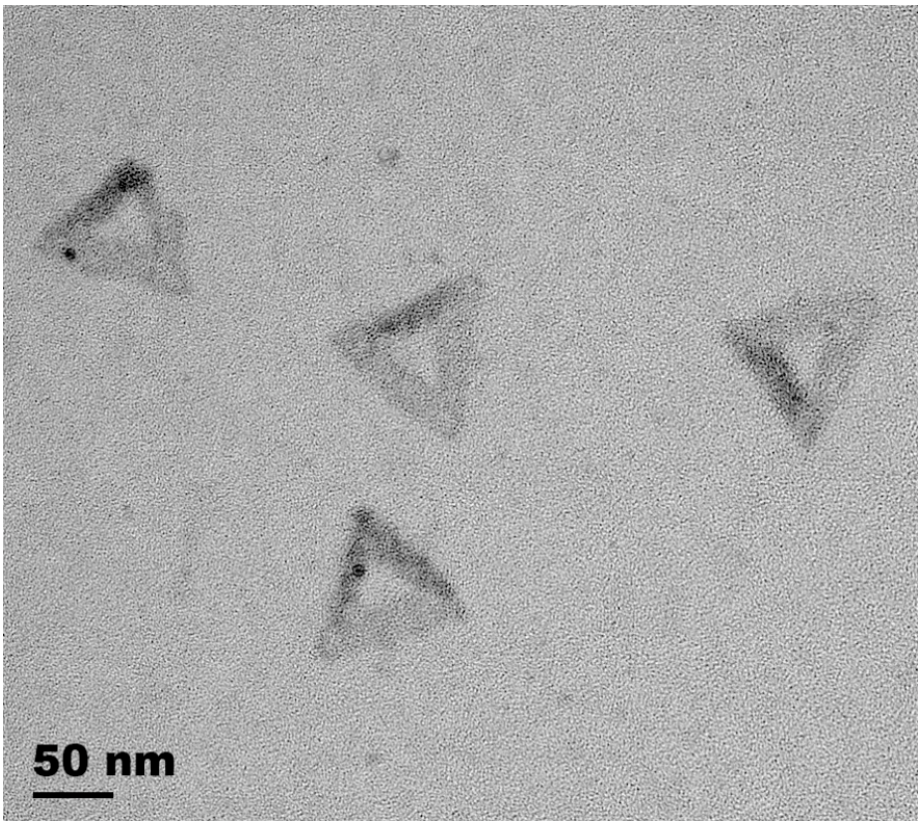

F**igure S16:** Additional TEM images showing site specific localization of Ag-NCs at one arm of the triangular origami.

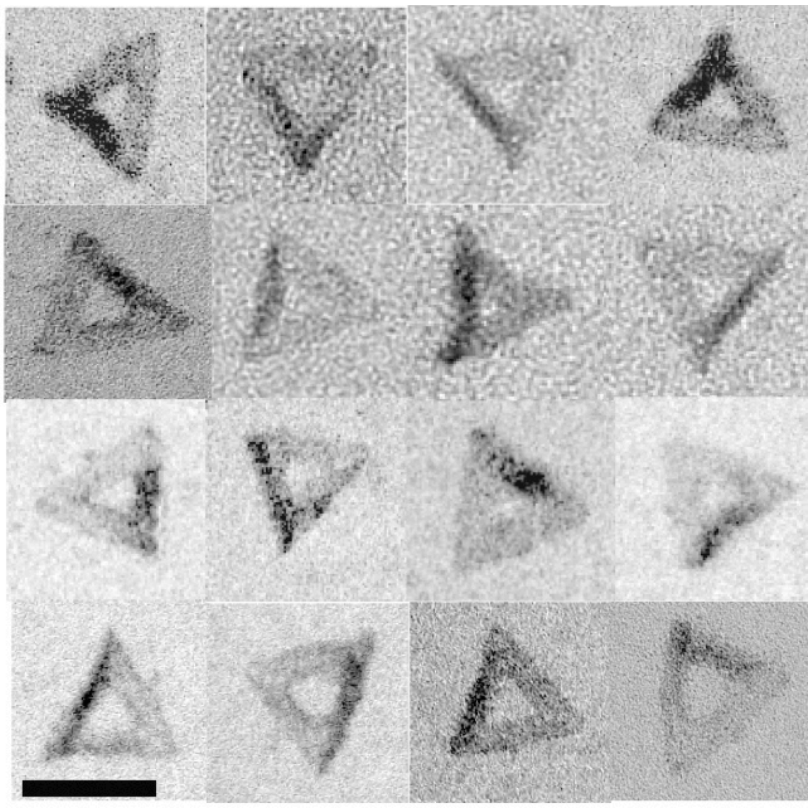

Figure S17: Additional zoom-in TEM images showing site specific localization of Ag-NCs on one arm of the triangular shaped origami. Scale bar corresponds to 100 nm.

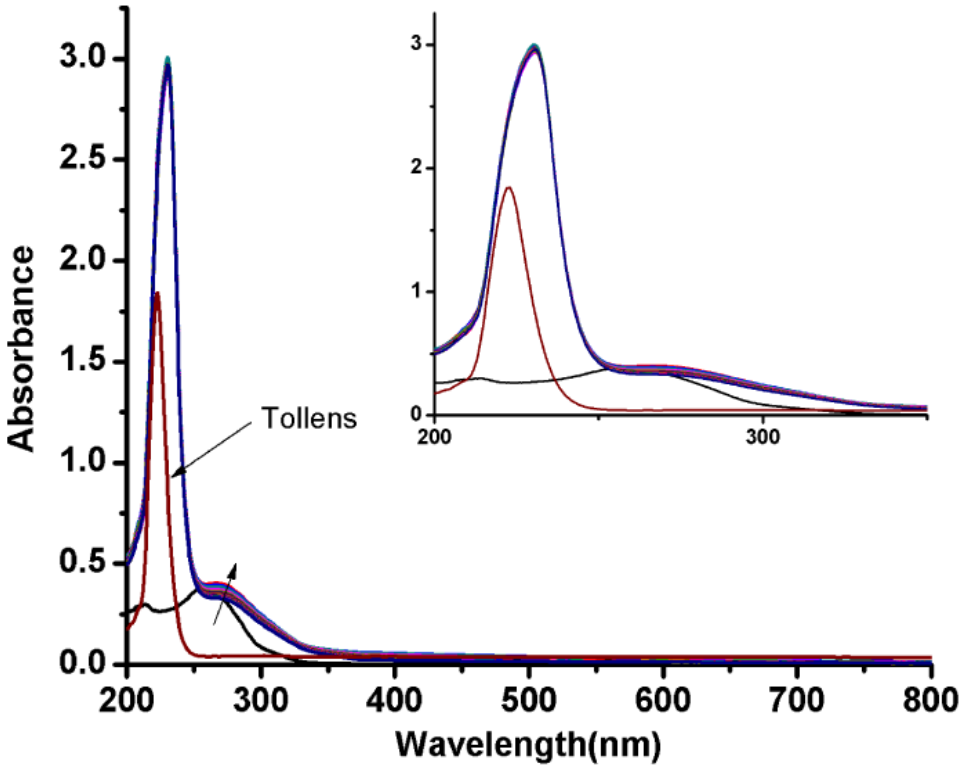

Figure S18: UV-Vis absorption spectrum of starting **DNA3** (black), and spectra taken in 30 minutes interval (for 10 hours) after the addition of 200 fold Ag^{+}. The red shift of the DNA absorbance peak from 260 nm to 275 nm is due to complexation with Ag^{+}

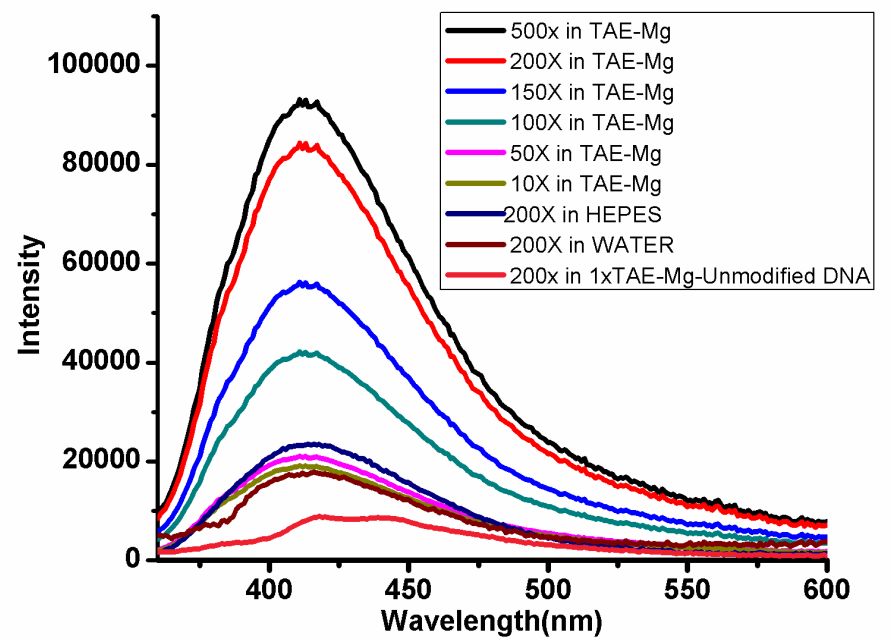

Figure S19: Fluorescence emission spectra of **DNA3** (5 μM) solutions in different buffer conditions and Ag^+/DNA ratio, after incubation for 12 hours. The samples were excited at 340 nm. (please order the data description according to the order of intensity) The data shown here indicates that: 1) the fluorescence intensity of the Ag-NC obtained is proportional to the molar ratio of Ag^+ to sugar modified DNA, but reaches saturation at ~200:1. Further increase of the Ag^+ concentration upto 500:1 did not significantly increase the Fluorescence intensity of the Ag-NC obtained; 2) without TAE buffer, i.e. when the reaction was carried out in water or in HEPES buffer, although the Ag^+ is 200 fold, the Ag-NC formation is minimal comparable to the results with lowest Ag^+ concentration in Tris buffer; 3) Without the sugar modified DNA as the nucleation site, the fluorescent Ag-NC does not form.

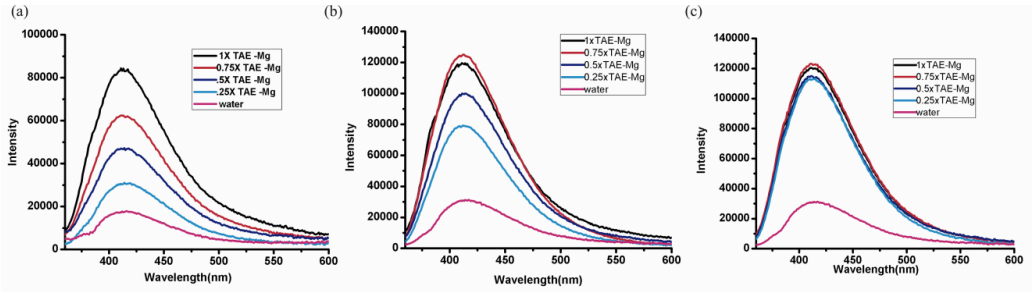

Figure S20: Fluorescence emission spectra of **DNA3** (5 μM) solutions in different TAE-Mg^{2+} buffer concentrations at fixed Ag^{+}/DNA ratio = 200; after (a)12 hrs (b) 48 hrs, and (c) 96 hrs. Samples were excited at 340 nm. Apparently the formation kinetics of the Ag-NC is proportional to the concentration of TAE buffer used: the higher the TEA buffer concentration is, the faster the reaction reaches equilibrium. But it does not affect the final equilibrium, which is presumably determined by the molar ratio of the Ag^{+} to the sugar modified DNA. The reaction in water is not only slow but does not go as far as in Tris buffer. This may be due to lack of reductive species in the mixture for the further growth of the Ag nucleus.

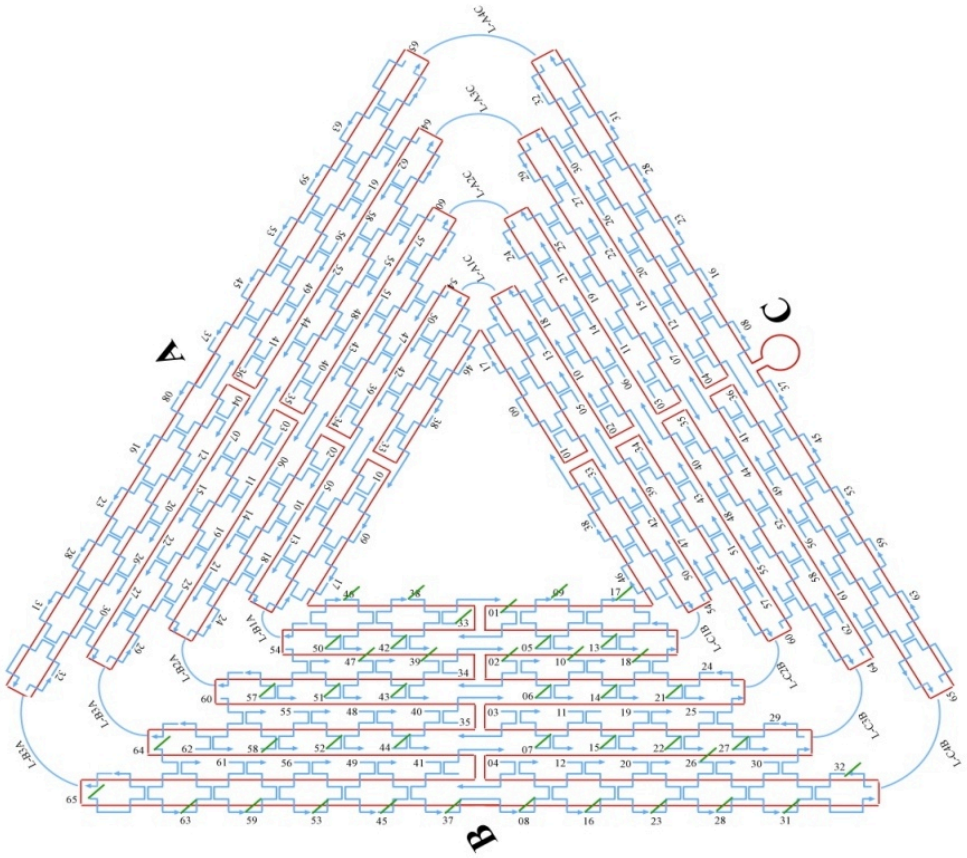

Figure S21: Schematic representation of Teiangular origami with staple strand numbered individually.

DNA SEQUENCES USED FOR ORIGAMI SYNTHESIS

(Probe sequences are highlighted in color)

A05, TTTGATGATTAAGAGGCTGAGACTTGCTCAGTACCAGGCG,

A06, CCGGAACCCAGAATGGAAAGCGCAACATGGCT,

A07, AAAGACAACATTTTCGGTCATAGCCAAAATCA,

A08, GACGGGAGAATTAACTCGGAATAAGTTTATTTCCAGCGCC,

A09, GATAAGTGCCGTCGAGCTGAAACATGAAAGTATACAGGAG,

A10, TGTACTGGAAATCCTCATTAAAGCAGAGCCAC,

A11, CACCGGAAAGCGCGTTTTCATCGGAAGGGCGA,

A12, CATTCAACAAACGCAAAGACACCAGAACACCCTGAACAAA,

A13, TTTAACGGTTCGGAACCTATTATTAGGGTTGATATAAGTA,

A14, CTCAGAGCATATTCACAAACAAATTAATAAGT,

A15, GGAGGGAATTTAGCGTCAGACTGTCCGCCTCC,

A16, GTCAGAGGGTAATTGATGGCAACATATAAAAGCGATTGAG,

A17, TAGCCCGGAATAGGTGAATGCCCCCTGCCTATGGTCAGTG,

A18, CCTTGAGTCAGACGATTGGCCTTGCGCCACCC,

A19, TCAGAACCCAGAATCAAGTTTGCCGGTAAATA,

A20, TTGACGGAAATACATACATAAAGGGCGCTAATATCAGAGA,

A21, CAGAGCCAGGAGGTTGAGGCAGGTAACAGTGCCCG,

A22, ATTAAAGGCCGTAATCAGTAGCGAGCCACCCT,

A23, GATAACCCACAAGAATGTTAGCAAACGTAGAAAATTATTC,

A24, GCCGCCAGCATTGACACCACCCTC,

A25, AGAGCCGCACCATCGATAGCAGCATGAATTAT,

A26, CACCGTCACCTTATTACGCAGTATTGAGTTAAGCCCAATA,

A27, AGCCATTTAAACGTCACCAATGAACACCAGAACCA,

A28, ATAAGAGCAAGAAACATGGCATGATTAAGACTCCGACTTG,

A29, CCATTAGCAAGGCCGGGGGAATTA,

A30, GAGCCAGCGAATACCCAAAAGAACATGAAATAGCAATAGC,

A31, TATCTTACCGAAGCCCAAACGCAATAATAACGAAAATCACCAG,

A32, CAGAAGGAAACCGAGGTTTTTAAGAAAAGTAAGCAGATAGCCG,

A33, CCTTTTTTCATTTAACAATTTCATAGGATTAG,

A34, TTTAACCTATCATAGGTCTGAGAGTTCCAGTA,

A35, AGTATAAAATATGCGTTATACAAAGCCATCTT,

A36, CAAGTACCTCATTCCAAGAACGGGAAATTCAT,

A37, AGAGAATAACATAAAAACAGGGAAGCGCATTA,

A38, AAAACAAAATTAATTAAATGGAAACAGTACATTAGTGAAT,

A39, TTATCAAACCGGCTTAGGTTGGGTAAGCCTGT,

A40, TTAGTATCGCCAACGCTCAACAGTCGGCTGTC,

A41, TTTCCTTAGCACTCATCGAGAACAATAGCAGCCTTTACAG,

A42, AGAGTCAAAAATCAATATATGTGATGAAACAAACATCAAG,

A43, ACTAGAAATATATAACTATATGTACGCTGAGA,

A44, TCAATAATAGGGCTTAATTGAGAATCATAATT,

A45, AACGTCAAAAATGAAAAGCAAGCCGTTTTTATGAAACCAA,

A46, GAGCAAAAGAAGATGAGTGAATAACCTTGCTTATAGCTTA,

A47, GATTAAGAAATGCTGATGCAAATCAGAATAAA,

A48, CACCGGAATCGCCATATTTAACAAAATTTACG,

A49, AGCATGTATTTCATCGTAGGAATCAAACGATTTTTTGTTT,

A50, ACATAGCGCTGTAAATCGTCGCTATTCATTTCAATTACCT,

A51, GTTAAATACAATCGCAAGACAAAGCCTTGAAA,

A52, CCCATCCTCGCCAACATGTAATTTAATAAGGC,

A53, TCCCAATCCAAATAAGATTACCGCGCCCAATAAATAATAT,

A54, TCCCTTAGAATAACGCGAGAAAACTTTTACCGACC,

A55, GTGTGATAAGGCAGAGGCATTTTCAGTCCTGA,

A56, ACAAGAAAGCAAGCAAATCAGATAACAGCCATATTATTTA,

A57, GTTTGAAATTCAAATATATTTTAG,

A58, AATAGATAGAGCCAGTAATAAGAGATTTAATG,

A59, GCCAGTTACAAAATAATAGAAGGCTTATCCGGTTATCAAC,

A60, TTCTGACCTAAAATATAAAGTACCGACTGCAGAAC,

A61, GCGCCTGTTATTCTAAGAACGCGATTCCAGAGCCTAATTT,

A62, TCAGCTAAAAAAGGTAAAGTAATT,

A63, ACGCTAACGAGCGTCTGGCGTTTTAGCGAACCCAACATGT,

A64, ACGACAATAAATCCCGACTTGCGGGAGATCCTGAATCTTACCA,

A65, TGCTATTTTGCACCCAGCTACAATTTTGTTTTGAAGCCTTAAA,

B01, TCATATGTGTAATCGTAAAACTAGTCATTTTC

TCAGGAACAGCCAACG,

B02, GTGAGAAAATGTGTAGGTAAAGATACAACTTT

TCAGGAACAGCCAACG,

B03, GGCATCAAATTTGGGGCGCGAGCTAGTTAAAG

TCAGGAACAGCCAACG,

B04, TTCGAGCTAAGACTTCAAATATCGGGAACGAG

TCAGGAACAGCCAACG,

B05, ACAGTCAAAGAGAATCGATGAACGACCCCGGTTGATAATC

TCAGGAACAGCCAACG,

B06, ATAGTAGTATGCAATGCCTGAGTAGGCCGGAG

TCAGGAACAGCCAACG,

B07, AACCAGACGTTTAGCTATATTTTCTTCTACTA

TCAGGAACAGCCAACG,

B08, GAATACCACATTCAACTTAAGAGGAAGCCCGATCAAAGCG

TCAGGAACAGCCAACG,

B09, AGAAAAGCCCCAAAAAGAGTCTGGAGCAAACAATCACCAT

TCAGGAACAGCCAACG,

B10, CAATATGACCCTCATATATTTTAAAGCATTAA

TCAGGAACAGCCAACG,

B11, CATCCAATAAATGGTCAATAACCTCGGAAGCA

TCAGGAACAGCCAACG,

B12, AACTCCAAGATTGCATCAAAAAGATAATGCAGATACATAA

TCAGGAACAGCCAACG,

B13, CGTTCTAGTCAGGTCATTGCCTGACAGGAAGATTGTATAA

TCAGGAACAGCCAACG,

B14, CAGGCAAGATAAAAATTTTTAGAATATTCAAC

TCAGGAACAGCCAACG,

B15, GATTAGAGATTAGATACATTTCGCAAATCATA

TCAGGAACAGCCAACG,

B16, CGCCAAAAGGAATTACAGTCAGAAGCAAAGCGCAGGTCAG

TCAGGAACAGCCAACG,

B17, GCAAATATTTAAATTGAGATCTACAAAGGCTACTGATAAA

TCAGGAACAGCCAACG,

B18, TTAATGCCTTATTTCAACGCAAGGGCAAAGAA

TCAGGAACAGCCAACG,

B19, TTAGCAAATAGATTTAGTTTGACCAGTACCTT

TCAGGAACAGCCAACG,

B20, TAATTGCTTTACCCTGACTATTATGAGGCATAGTAAGAGC

TCAGGAACAGCCAACG,

B21, ATAAAGCCTTTGCGGGAGAAGCCTGGAGAGGGTAG

TCAGGAACAGCCAACG,

B22, TAAGAGGTCAATTCTGCGAACGAGATTAAGCA

TCAGGAACAGCCAACG,

B23, AACACTATCATAACCCATCAAAAATCAGGTCTCCTTTTGA

TCAGGAACAGCCAACG,

B24, ATGACCCTGTAATACTTCAGAGCA **TCAGGAACAGCCAACG**,

B25, TAAAGCTATATAACAGTTGATTCCCATTTTTG

TCAGGAACAGCCAACG,

B26, CGGATGGCACGAGAATGACCATAATCGTTTACCAGACGAC

TCAGGAACAGCCAACG,

B27, TAATTGCTTGGAAGTTTCATTCCAAATCGGTTGTA

TCAGGAACAGCCAACG,

B28, GATAAAAACCAAAATATTAAACAGTTCAGAAATTAGAGCT

TCAGGAACAGCCAACG,

B29, ACTAAAGTACGGTGTCGAATATAA **TCAGGAACAGCCAACG**,

B30, TGCTGTAGATCCCCCTCAAATGCTGCGAGAGGCTTTTGCA

TCAGGAACAGCCAACG ,

B31, AAAGAAGTTTTGCCAGCATAAATATTCATTGACTCAACATGTT

TCAGGAACAGCCAACG,

B32, AATACTGCGGAATCGTAGGGGGTAATAGTAAAATGTTTAGACT

TCAGGAACAGCCAACG,

B33, AGGGATAGCTCAGAGCCACCACCCCATGTCAA

TCAGGAACAGCCAACG,

B34, CAACAGTTTATGGGATTTTGCTAATCAAAAGG

TCAGGAACAGCCAACG,

B35, GCCGCTTTGCTGAGGCTTGCAGGGGAAAAGGT

TCAGGAACAGCCAACG,

B36, GCGCAGACTCCATGTTACTTAGCCCGTTTTAA

TCAGGAACAGCCAACG,

B37, ACAGGTAGAAAGATTCATCAGTTGAGATTTAG

TCAGGAACAGCCAACG,

B38, CCTCAGAACCGCCACCCAAGCCCAATAGGAACGTAAATGA

TCAGGAACAGCCAACG,

B39, ATTTTCTGTCAGCGGAGTGAGAATACCGATAT

TCAGGAACAGCCAACG,

B40, ATTCGGTCTGCGGGATCGTCACCCGAAATCCG

TCAGGAACAGCCAACG,

B41, CGACCTGCGGTCAATCATAAGGGAACGGAACAACATTATT

TCAGGAACAGCCAACG,

B42, AGACGTTACCATGTACCGTAACACCCCTCAGAACCGCCAC

TCAGGAACAGCCAACG,

B43, CACGCATAAGAAAGGAACAACTAAGTCTTTCC

TCAGGAACAGCCAACG,

B44, ATTGTGTCTCAGCAGCGAAAGACACCATCGCC

TCAGGAACAGCCAACG,

B45, TTAATAAAACGAACTAACCGAACTGACCAACTCCTGATAA

TCAGGAACAGCCAACG,

B46, AGGTTTAGTACCGCCATGAGTTTCGTCACCAGGATCTAAA

TCAGGAACAGCCAACG,

B47, GTTTTGTCAGGAATTGCGAATAATCCGACAAT

TCAGGAACAGCCAACG,

B48, GACAACAAGCATCGGAACGAGGGTGAGATTTG

TCAGGAACAGCCAACG,

B49, TATCATCGTTGAAAGAGGACAGATGGAAGAAAAATCTACG

TCAGGAACAGCCAACG,

B50, AGCGTAACTACAAACTACAACGCCTATCACCGTACTCAGG

TCAGGAACAGCCAACG,

B51, TAGTTGCGAATTTTTTCACGTTGATCATAGTT

TCAGGAACAGCCAACG,

B52, GTACAACGAGCAACGGCTACAGAGGATACCGA

TCAGGAACAGCCAACG,

B53, ACCAGTCAGGACGTTGGAACGGTGTACAGACCGAAACAAA

TCAGGAACAGCCAACG,

B54, ACAGACAGCCCAAATCTCCAAAAAAAAATTTCTTA

TCAGGAACAGCCAACG,

B55, AACAGCTTGCTTTGAGGACTAAAGCGATTATA

TCAGGAACAGCCAACG,

B56, CCAAGCGCAGGCGCATAGGCTGGCAGAACTGGCTCATTAT

TCAGGAACAGCCAACG,

B57, CGAGGTGAGGCTCCAAAAGGAGCC **TCAGGAACAGCCAACG**,

B58, ACCCCCAGACTTTTTCATGAGGAACTTGCTTT

CGTTGTTGAGTCACC,

B59, ACCTTATGCGATTTTATGACCTTCATCAAGAGCATCTTTG

TCAGGAACAGCCAACG,

B60, CGGTTTATCAGGTTTCCATTAAACGGGAATACACT

TCAGGAACAGCCAACG,

B61, AAAACACTTAATCTTGACAAGAACTTAATCATTGTGAATT

TCAGGAACAGCCAACG,

B62, GGCAAAAGTAAAATACGTAATGCC **TCAGGAACAGCCAACG**,

B63, TGGTTTAATTTCAACTCGGATATTCATTACCCACGAAAGA

TCAGGAACAGCCAACG,

B64, ACCAACCTAAAAAATCAACGTAACAAATAAATTGGGCTTGAGA

TCAGGAACAGCCAACG,

B65, CCTGACGAGAAACACCAGAACGAGTAGGCTGCTCATTCAGTGA

TCAGGAACAGCCAACG,

Link-A1C, TTAATTAATTTTTTACCATATCAAA,

Link-A2C, TTAATTTCATCTTAGACTTTACAA,

Link-A3C, CTGTCCAGACGTATACCGAACGA,

Link-A4C, TCAAGATTAGTGTAGCAATACT,

Link-B1A, TGTAGCATTCCTTTTATAAACAGTT,

Link-B2A, TTTAATTGTATTTCCACCAGAGCC,

Link-B3A, ACTACGAAGGCTTAGCACCATTA,

Link-B4A, ATAAGGCTTGCAACAAAGTTAC,

Link-C1B, GTGGGAACAAATTTCTATTTTTGAG,

Link-C2B, CGGTGCGGGCCTTCCAAAAACATT,

Link-C3B, ATGAGTGAGCTTTTAAATATGCA,

Link-C4B, ACTATTAAAGAGGATAGCGTCC,

Loop, GCGCTTAATGCGCCGCTACAGGGC,

C01, TCGGGAGATATACAGTAACAGTACAAATAATT,

C02, CCTGATTAAAGGAGCGGAATTATCTCGGCCTC,

C03, GCAAATCACCTCAATCAATATCTGCAGGTCGA,

C04, CGACCAGTACATTGGCAGATTCACCTGATTGC,

C05, TGGCAATTTTTAACGTCAGATGAAAACAATAACGGATTCG,

C06, AAGGAATTACAAAGAAACCACCAGTCAGATGA,

C07, GGACATTCACCTCAAATATCAAACACAGTTGA,

C08, TTGACGAGCACGTATACTGAAATGGATTATTTAATAAAAG,

C09, CCTGATTGCTTTGAATTGCGTAGATTTTCAGGCATCAATA,

C10, TAATCCTGATTATCATTTTGCGGAGAGGAAGG,

C11, TTATCTAAAGCATCACCTTGCTGATGGCCAAC,

C12, AGAGATAGTTTGACGCTCAATCGTACGTGCTTTCCTCGTT,

C13, GATTATACACAGAAATAAAGAAATACCAAGTTACAAAATC,

C14, TAGGAGCATAAAAGTTTGAGTAACATTGTTTG,

C15, TGACCTGACAAATGAAAAATCTAAAATATCTT,

C16, AGAATCAGAGCGGGAGATGGAAATACCTACATAACCCTTC,

C17, GCGCAGAGGCGAATTAATTATTTGCACGTAAATTCTGAAT,

C18, AATGGAAGCGAACGTTATTAATTTCTAACAAC,

C19, TAATAGATCGCTGAGAGCCAGCAGAAGCGTAA,

C20, GAATACGTAACAGGAAAAACGCTCCTAAACAGGAGGCCGA,

C21, TCAATAGATATTAAATCCTTTGCCGGTTAGAACCT,

C22, CAATATTTGCCTGCAACAGTGCCATAGAGCCG,

C23, TTAAAGGGATTTTAGATACCGCCAGCCATTGCGGCACAGA,

C24, ACAATTCGACAACTCGTAATACAT,

C25, TTGAGGATGGTCAGTATTAACACCTTGAATGG,

C26, CTATTAGTATATCCAGAACAATATCAGGAACGGTACGCCA,

C27, CGCGAACTAAAACAGAGGTGAGGCTTAGAAGTATT,

C28, GAATCCTGAGAAGTGTATCGGCCTTGCTGGTACTTTAATG,

C29, ACCACCAGCAGAAGATGATAGCCC,

C30, TAAAACATTAGAAGAACTCAAACTTTTTATAATCAGTGAG,

C31, GCCACCGAGTAAAAGAACATCACTTGCCTGAGCGCCATTAAAA,

C32, TCTTTGATTAGTAATAGTCTGTCCATCACGCAAATTAACCGTT,

C33, CGCGTCTGATAGGAACGCCATCAACTTTTACA,

C34, AGGAAGATGGGGACGACGACAGTAATCATATT,

C35, CTCTAGAGCAAGCTTGCATGCCTGGTCAGTTG,

C36, CCTTCACCGTGAGACGGGCAACAGCAGTCACA,

C37, CGAGAAAGGAAGGGAAGCGTACTATGGTTGCT,

C38, GCTCATTTTTTAACCAGCCTTCCTGTAGCCAGGCATCTGC,

C39, CAGTTTGACGCACTCCAGCCAGCTAAACGACG,

C40, GCCAGTGCGATCCCCGGGTACCGAGTTTTTCT,

C41, TTTCACCAGCCTGGCCCTGAGAGAAAGCCGGCGAACGTGG,

C42, GTAACCGTCTTTCATCAACATTAAAATTTTTGTTAAATCA,

C43, ACGTTGTATTCCGGCACCGCTTCTGGCGCATC,

C44, CCAGGGTGGCTCGAATTCGTAATCCAGTCACG,

C45, TAGAGCTTGACGGGGAGTTGCAGCAAGCGGTCATTGGGCG,

C46, GTTAAAATTCGCATTAATGTGAGCGAGTAACACACGTTGG,

C47, TGTAGATGGGTGCCGGAAACCAGGAACGCCAG,

C48, GGTTTTCCATGGTCATAGCTGTTTGAGAGGCG,

C49, GTTTGCGTCACGCTGGTTTGCCCCAAGGGAGCCCCCGATT,

C50, GGATAGGTACCCGTCGGATTCTCCTAAACGTTAATATTTT,

C51, AGTTGGGTCAAAGCGCCATTCGCCCCGTAATG,

C52, CGCGCGGGCCTGTGTGAAATTGTTGGCGATTA,

C53, CTAAATCGGAACCCTAAGCAGGCGAAAATCCTTCGGCCAA,

C54, CGGCGGATTGAATTCAGGCTGCGCAACGGGGGATG,

C55, TGCTGCAAATCCGCTCACAATTCCCAGCTGCA,

C56, TTAATGAAGTTTGATGGTGGTTCCGAGGTGCCGTAAAGCA,

C57, TGGCGAAATGTTGGGAAGGGCGAT,

C58, TGTCGTGCACACAACATACGAGCCACGCCAGC,

C59, CAAGTTTTTTGGGGTCGAAATCGGCAAAATCCGGGAAACC,

C60, TCTTCGCTATTGGAAGCATAAAGTGTATGCCCGCT,

C61, TTCCAGTCCTTATAAATCAAAAGAGAACCATCACCCAAAT,

C62, GCGCTCACAAGCCTGGGGTGCCTA,

C63, CGATGGCCCACTACGTATAGCCCGAGATAGGGATTGCGTT,

C64, AACTCACATTATTGAGTGTTGTTCCAGAAACCGTCTATCAGGG,

C65, ACGTGGACTCCAACGTCAAAGGGCGAATTTGGAACAAGAGTCC,

References

1. C. T. Wirges, J. Timper, M. Fischler, A. S. Sologubenko, J. Mayer, U. Simon, T. Carell, *Angew. Chem. Int. Ed.* **2009**, *48*, 219 –223.
2. L Berti, A. Alessandrini, P. Facci, *J. Am. Chem. Soc.* **2005**, *127*, 11216–11217.

APPENDIX F

CO-AUTHOR APPROVAL

I verify that the following co-authors have approved of my use of our publications in my dissertation.

Yan Liu (Arizona State University)

Hao Yan (Arizona State University)

Zhengtao Deng (Arizona State University)

Reji Varghese (Arizona State University)

Baoquan Ding (Arizona State University)

Zhao Zhao (Arizona State University)

Jaswinder Sharma (Arizona State University)

Shengli Zou (University of Central Florida)

Haining Wang (University of Central Florida)